

Combination nanovaccines against respiratory pathogens

by

Sean Michael Kelly

A dissertation submitted to the graduate faculty
in partial fulfillment of the requirements for the degree of

DOCTOR OF PHILOSOPHY

Major: Chemical Engineering

Program of Study Committee:
Balaji Narasimhan, Co-major Professor
Michael J. Wannemuehler, Co-major Professor
Bryan Bellaire
Ian Schneider
Kaitlin Bratlie

The student author, whose presentation of the scholarship herein was approved by the program of study committee, is solely responsible for the content of this dissertation. The Graduate College will ensure this dissertation is globally accessible and will not permit alterations after a degree is conferred.

Iowa State University

Ames, Iowa

2019

Copyright © Sean Michael Kelly, 2019. All rights reserved.

TABLE OF CONTENTS

LIST OF TABLES	vii
LIST OF FIGURES.....	viii
ACKNOWLEDGEMENTS	x
ABSTRACT	xii
CHAPTER 1. LITERATURE REVIEW	1
1.1 Immune Response to Respiratory Pathogens	1
1.1.1 Physiochemical Barrier of the Lungs.....	2
1.1.2 Dendritic Cells.....	3
1.1.3 Macrophages	5
1.1.4 Adaptive Immune Response	8
1.1.5 Cell-Mediated Immunity	12
1.1.6 Humoral Immunity.....	13
1.2 Pneumonic Plague	15
1.2.1 Introduction	15
1.2.2 History of Plague Weaponization	17
1.2.3 Pneumonic Plague Pathogenesis	19
1.2.4 Pneumonic Plague Mechanisms of Action	21
1.2.5 Current Vaccine Strategies against Pneumonic Plague.....	29
1.2.6 Summary	36
1.3 Inhalation Anthrax.....	37
1.3.1 Introduction	37
1.3.2 History of Anthrax Weaponization.....	38
1.3.3 Inhalation Anthrax Pathogenesis	39
1.3.4 Inhalation Anthrax Mechanisms of Action	42
1.3.5 Current Vaccine Strategies against Inhalation Anthrax.....	46
1.3.6 Summary	55
1.4 Bovine Respiratory Syncytial Virus.....	56
1.4.1 Introduction - BRSV	56
1.4.2 BRSV Pathogenesis	57
1.4.3 BRSV Mechanisms of Action	58
1.4.4 Current Vaccination Strategies against BRSV	60
1.4.5 Summary	61
1.5 Vaccine Adjuvants	62
1.5.1 Traditional Adjuvants	62
1.5.2 Current FDA-approved Adjuvants	64
1.6 Next-Generation Adjuvants	65
1.6.1 Cyclic Dinucleotides.....	66
1.6.2 Polymeric Nanoparticles as Adjuvants.....	68
1.6.3 Polyester Nanoparticle Adjuvants	71
1.6.4 Polyanhydride Nanovaccines.....	74

1.7 Conclusions	77
1.8 Tables	79
1.9 Figures	85
CHAPTER 2. RESEARCH OBJECTIVES AND THESIS ORGANIZATION	94
CHAPTER 3. SINGLE-DOSE COMBINATION NANOVACCINE INDUCES BOTH RAPID AND LONG-LIVED PROTECTION AGAINST PNEUMONIC PLAGUE.....	96
Abstract	97
3.1 Introduction	98
3.2 Material and Methods	101
3.2.1 Materials	101
3.2.2 Polyanhydride Synthesis	102
3.2.3 Nanoparticle Synthesis	102
3.2.4 Protein Release and Encapsulation Efficiency	103
3.2.5 Animals	103
3.2.6 Immunization and Serum Collection	104
3.2.7 ELISA	104
3.2.8 ELISPOT	105
3.2.9 Peptide Microarray Printing and Analysis	106
3.2.10 Lethal Challenge	108
3.2.11 Statistical Analyses	109
3.3 Results	109
3.3.1 F1-V Nanovaccine Characterization	109
3.3.2 Combination Nanovaccine Induces Rapid Protective Immunity	110
3.3.3 Combination Nanovaccine Enhances Long-lived Protective Immunity	111
3.3.4 Combination Nanovaccine Provides Broad Antibody IgG Recognition to F1-V Linear Epitopes	112
3.3.5 Combination Nanovaccine Induces Long-lived Plasma Cells	113
3.4 Discussion	114
3.5 Acknowledgements	119
3.6 Author Contributions	119
3.7 Conflict of Interest Statement	120
3.8 Figures	120
CHAPTER 4. SINGLE-DOSE COMBINATION NANOVACCINE INDUCES BOTH RAPID AND LONG-LIVED TOXIN NEUTRALIZING ANTIBODY RESPONSES AGAINST BACILLUS ANTHRACIS TOXIN.....	133
Abstract	133
4.1 Introduction	134
4.2 Methods and Materials	138
4.2.1 Materials	138
4.2.2 Polymer Synthesis	138
4.2.3 Particle Synthesis	138
4.2.4 Animals	139

4.2.5 Vaccinations	139
4.2.6 Serum Antibody	140
4.2.7 Cell Culture	141
4.2.8 Toxin Neutralization Assay	141
4.2.9 Statistical Analysis	142
4.3 Results	142
4.3.1 Polyanhydride Nanoparticle Characterization	142
4.3.2 Polyanhydride Nanovaccine Elicits High and Long Lasting Anti-PA Antibody Responses	142
4.3.3 Polyanhydride Nanovaccine Elicits Rapid Toxin Neutralization Antibodies Against the Anthrax Toxin	143
4.3.4 Combination Nanovaccine and Alhydrogel formulation Elicit Similar Long Term Anti-PA Responses	144
4.4 Discussion	145
4.5 Tables	148
4.6 Figures	149
CHAPTER 5. EFFICACY OF MUCOSAL POLYANHYDRIDE NANOVACCINE AGAINST RESPIRATORY SYNCYTIAL VIRUS INFECTION IN THE NEONATAL CALF	
Abstract	153
5.1 Introduction	154
5.2 Materials and Methods	157
5.2.1 Protein Production and Purification	157
5.2.2 Polymer Synthesis and Characterization	159
5.2.3 Nanoparticle Synthesis	159
5.2.4 Protein Release Assay	160
5.2.5 Animals	160
5.2.6 Vaccine Studies	161
5.2.7 BRSV Inoculum and Aerosol Challenge Model	161
5.2.8 Antigen Recall Assays	162
5.2.9 Necropsy and Pathological Evaluation	162
5.2.10 <i>In vitro</i> Analysis of Nanoparticle Immunogenicity in Bovine APC	163
5.2.11 Real-time PCR	163
5.2.12 Virus Isolation	164
5.2.13 ELISAs and Multiplex Cytokine Immunoassay	165
5.2.14 Virus Neutralization Assay	166
5.2.15 Statistics	166
5.2.16 Data Availability	166
5.3 Results	167
5.3.1 <i>In vitro</i> Release Kinetics of BRSV-F/G Nanoparticles	167
5.3.2 Immunogenicity of Recombinant BRSV-F/G is Preserved Following Release from CPTEG:CPH Nanoparticles	167
5.3.3 Amphiphilic CPTEG:CPH Particles Activate Bovine Monocyte- derived Dendritic Cells (moDC)	168

5.3.4 In vivo Immunogenicity and Efficacy of the BRSV-F/G Nanovaccine	169
5.3.5 Reduced Gross and Microscopic Pathology in BRSV-F/G Nanovaccine-Administered calves	170
5.3.6 Reduced Viral Burden and Reduced Virus Shedding in BRSV-F/G Nanovaccine-administered Calves	171
5.3.7 BRSV-specific IgA in the Nasal and BAL Fluid of BRSV-F/G Nanovaccine-administered Calves	172
5.3.8 BRSV-specific Cellular Responses in the Lungs and Peripheral Blood of BRSV-F/G Nanovaccine-administered Calves	173
5.4 Discussion	174
5.5 Tables	179
5.6 Figures	180
 CHAPTER 6. SYNTHESIS AND CHARACTERIZATION OF NOVEL RAPIDLY-DEGRADING POLYANHYDRIDES AS VACCINE ADJUVANTS	192
Abstract	192
6.1 Introduction	193
6.2 Materials and Methods	195
6.2.1 Materials	195
6.2.2 Animals	196
6.2.3 Copolymer Synthesis and Characterization	196
6.2.4 Erosion Kinetics	197
6.2.5 Nanoparticle Synthesis and Characterization	198
6.2.6 Protein Release Kinetics	198
6.2.7 Protein Release Characterization	199
6.2.8 Native PAGE Gel Analysis	199
6.2.9 ELISA	200
6.2.10 Differentiation of Bone Marrow-derived Dendritic Cells (BMDCs)	201
6.2.11 Biocompatibility and Cellular Internalization of CPTEG:SA Nanoparticles	201
6.3 Results	202
6.3.1 CPTEG:SA Copolymer Structural Characterization	203
6.3.2 Erosion Kinetics of Polyanhydride Films	204
6.3.3 CPTEG:SA Nanoparticles Stabilize Protein Payloads and Provide Sustained Release	205
6.3.4 CPTEG:SA Nanoparticles Are Biocompatible and Enhance Cellular Internalization	206
6.4 Discussion	207
6.5 Tables	212
6.6 Figures	213
 CHAPTER 7. CONCLUSIONS AND ONGOING/FUTURE RESEARCH	222
7.1 Conclusions	222
7.2 Ongoing/Future Work	225

7.2.1 Neutralization of IFN γ /TNF α Impacts Pneumonic Plague Challenge Outcome	225
7.3 Figures	227
BIBLIOGRAPHY	228

LIST OF TABLES

Table 1.1. Examples of 1 st generation adjuvants.....	79
Table 1.2. List of Current FDA-approved adjuvants	80
Table 1.3 Examples of polymeric adjuvants currently studied.....	81
Table 1.4. List of various classes of polymers and their respective polymer erosion front width $(D/k)^{1/2}$ and erosion velocity $(Dk)^{1/2}$ (adapted from ²⁷⁰)	82
Table 1.5. Chemical structure of polyester and polyanhydride adjuvants.....	83
Table 1.6. pKa values of various polyester and polyanhydride monomers.....	84
Table 4.1. Summary of toxin neutralization assays	148
Table 5.1. Virus neutralization titers measured in the nasal fluid on day 28 (day 0 before challenge) and day 6 post-challenge	179
Table 6.1. CPTEG:SA copolymer characterization.....	212
Table 6.2. CPTEG:SA copolymer film composition over time.....	212
Table 6.3. Characterization of CPTEG:SA nanoparticles	212

LIST OF FIGURES

Figure 1.1. Host defense against foreign pathogens in the lungs.....	85
Figure 1.2. <i>Yersinia pestis</i> virulence factors.....	86
Figure 1.3. <i>B anthracis</i> virulence factors	87
Figure 1.4. BRSV structure and virulence factors.	88
Figure 1.5. Immune skewing of adjuvants	89
Figure 1.6. Chemical structure of cyclic-diGMP (CDG)	90
Figure 1.7. Stimulator of Interferon Genes (STING) pathway.....	91
Figure 1.8. Sizes of particles/pathogens internalized by antigen presenting cells.....	92
Figure 1.9. Bulk erosion vs. surface erosion	93
Figure 3.1. Characterization of F1-V Nanovaccine.....	120
Figure 3.2. Combination Nanovaccine provides rapid protective immunity against lethal <i>Y. pestis</i> challenge	123
Figure 3.3. Combination Nanovaccine provides long-lived protective immunity against lethal <i>Y. pestis</i> challenge	124
Figure 3.4. Combination Nanovaccine and CDN Vaccine provide broad antibody responses to potentially protective linear epitopes	125
Figure 3.5. Long-lived antibody responses to F1-V originate from long-lived plasma cells in the bone marrow.....	126
Figure 4.1. Characterization of PA Nanovaccine	149
Figure 4.2. Combination Nanovaccine induces antibodies against protective antigen.....	150
Figure 4.3. Combination Nanovaccine elicits rapid toxin neutralizing antibodies against protective antigen.....	151
Figure 4.4. Combination Nanovaccine elicits similar long term toxin neutralizing antibodies against protective antigen compared to alhydrogel	152

Figure 5.1. Recombinant BRSV F and G proteins are stable and immunogenic following encapsulation and release from polyanhydride nanoparticles ...	180
Figure 5.2. Polyanhydride nanoparticles activate bovine APC	182
Figure 5.3. Reduced BRSV-associated gross and microscopic pathology in BRSV-F/G nanovaccine-administered calves.....	185
Figure 5.4. Reduced viral burden in the lungs of BRSV-F/G nanovaccine-administered calves.....	187
Figure 5.5. Increased BRSV-specific IgA in the nasal fluid and BAL fluid of BRSV-F/G nanovaccine-administered calves.....	189
Figure 5.6. Enhanced BRSV-specific T cell responses in the peripheral blood and BAL of BRSV-F/G nanovaccine administered calves.. ..	190
Figure 6.1. CPTEG:SA copolymers demonstrate characteristic polyanhydride physical properties via NMR spectroscopy	213
Figure 6.2. CPTEG:SA copolymers demonstrate characteristic polyanhydride physical properties via DSC and WAXD	214
Figure 6.3. CPTEG:SA copolymers demonstrate chemistry-dependent erosion kinetics	216
Figure 6.4. CPTEG:SA nanoparticles can be fabricated into discrete nanoparticles with narrow size distribution	218
Figure 6.5. CPTEG:SA nanoparticles maintain protein conformational stability following encapsulation and release.....	219
Figure 6.6. CPTEG:SA nanoparticles are biocompatible and exhibit high rates of internalization by antigen presenting cells	221
Figure 7.1. Neutralization of IFN γ /TNF α decreases the protective efficacy of the Combination Nanovaccine 14 days post-immunization	227

ACKNOWLEDGEMENTS

The work reflected in the manuscript was the contribution of many people who I could probably never thank enough. I have learned so much throughout this experience, and could not have done so without the great people who I was surrounded by.

I can confidently say that without my family, I would not be where I am today. Thank you for always believing in me. Thank you for coming to visit me multiple times throughout my PhD studies, for listening when times were tough, and for always making me feel loved and supported. I can't thank you enough.

To my friends and colleagues in both the Chemical Engineering, Microbiology, and Immunology departments, thank you for always supporting me. Your friendship has meant so much, your encouragement helped get me through, and your ideas helped me solve challenging problems. To Sam and Eldon, who visited me multiple times throughout the PhD program, thank you for always being there for me. Your friendship has meant more to me than words can describe.

To Danielle, who was my partner in crime throughout graduate school, it's been real. Thank you for teaching me so many of the skills necessary to complete these chapters. And thank you for being so patient and always encouraging.

I would not have joined this PhD program if Dr. Kipper at Colorado State University had not told me about Balaji's laboratory. I am forever thankful to him for providing me opportunities to work in his lab as an undergraduate, to grow as a researcher, and to continue to support me throughout the PhD process.

To Balaji, thank you so much for this opportunity. I have learned so much from you. Your incredible patience, drive, and sharp thinking have kept challenging me to

never settle, and you have been an incredible example of how to make your ideas a reality through your tireless work ethic and drive. I am also so thankful for how you treated me with respect and always believed in me.

To Dr. Wannemuehler, I also thank you for this opportunity. You shaped how I think about science, challenging me to always consider the value of each experiment, how to think outside the box to find solutions, and how to enjoy the science as a never ending pursuit of learning.

To Dr. Bellaire and all of the other role models that I have been blessed to learn from and follow, I cannot thank you enough. I have learned so much from you about both life and research, and am proud to say you have made me into a better scientist and person. To all of staff that played a role with the experiments described in this work, thank you for all of your help and support. It wouldn't have been possible to do these experiments without your high degree of professionalism.

I would also like to thank my program of study committee for taking the time to read this manuscript and attend my preliminary exam and oral defense presentations, provide me feedback, and invest in my future. I am very grateful.

Lastly, I would like to thank my funding sources for making this work possible. The majority of this work was supported by the National Institutes of Health (R01-AI111466).

ABSTRACT

Evidence of mass pandemic plagues dates back to the earliest recorded history, with the Book of Exodus describing plagues inflicted upon Egypt that devastated citizens and livestock. Since then, countless plagues have been recorded, including the Plague of Athens (430-416 BCE), Justinian's plague (541-542 AD), and the Black Death (1346-1352 AD), which are responsible for the deaths of hundreds of millions of people throughout history^{1,2}.

Among the deadliest pathogens are *Yersinia pestis*, the causative agent of the plague, and *Bacillus anthracis*, the causative agent of anthrax. *Y. pestis* is responsible for Justinian's plague and the Black Death and is estimated to have accounted for over 200 million human deaths throughout history¹, while *B. anthracis* has been suggested to have caused the Plague of Athens, which wiped out 100,000 people, a quarter of the city's population, over a three year period³. Beyond their dark past, both of these pathogens have been used as biological weapons to cause harm to civilians and military personnel, with the most recent being the 9/11 attacks in the United States in 2001, in which 22 citizens were infected with *B. anthracis* spores that were delivered in letters in the mail, resulting in the deaths of five individuals. These pathogens are highly lethal if inhaled, with mortality rates approaching 100% if untreated after only a few days.

Unfortunately, there is no FDA-approved vaccine against *Y. pestis*. There is an FDA-approved AVA vaccine against *B. anthracis*, the AVA vaccine, however it has limitations. The AVA vaccine requires multiple immunizations to achieve purported protective immunity, and hence is insufficient in the event of mass exposure to civilian

populations and warfighters of *B. anthracis*. In addition, the AVA vaccine has been reported to induce injection site reactogenicity due to its aluminum-based alhydrogel adjuvant⁴, and there are concerns of thermal stability with proteins adsorbed to aluminum-based adjuvants^{5,6}.

In addition to these deadly pathogens, human respiratory syncytial virus (RSV) is a devastating disease that is the leading cause of severe acute lower respiratory tract disease in infants and young children worldwide⁷, accounting for up to 70% of hospitalized bronchiolitis cases in industrialized countries⁸. Globally, there are an estimated 33 million new episodes of HRSV-associated disease in children under five years of age with more than 100,000 resultant deaths⁹. Severe RSV infection has been linked with the development and exacerbation of recurrent wheezing and asthma¹⁰, and is a predisposing factor to the development of otitis media¹¹. RSV infection has a devastating, worldwide impact on human health and despite significant efforts, no approved vaccine currently exists for use against the disease in humans. Hence, there is a need to design and develop vaccines against RSV that are capable of providing robust immune responses against this pathogen and reduce the prevalence of this disease.

One final consideration for vaccine design against such dangerous respiratory pathogens is thermal stability. As all World Health Organization prequalified vaccines currently require refrigeration, obviating the cold chain would enable delivery of vaccines to refrigeration-scarce zones around the world, reduce cost, and improve stockpiling capabilities¹². Therefore, it is imperative to develop vaccines that are capable

of eliciting rapid and long-lived protective immunity to both civilian and warfighters, ideally in a single dose, as well as obviate the cold chain.

Polyanhydride nanoparticle-based vaccines (i.e., nanovaccines) are a promising next-generation vaccine platform for safe and effective single-dose vaccines against such pathogens. These materials are safe and biocompatible¹³, have demonstrated adjuvant properties^{14–17}, enable dose sparing¹⁸, and have enhanced shelf stability of labile proteins¹⁹. These characteristics are needed for the next generation of vaccine formulations, which will allow for the production of safe and highly effective vaccines that can be administered in a single dose, have reduced cost and the ability to obviate the cold chain for vaccine stockpiling.

The goal of the work described in this thesis is the design and evaluation of a single dose combination-adjuvant polyanhydride-based nanovaccine formulation that is capable of providing rapid and long-lived protective immunity against multiple respiratory pathogens, including the inhaled forms of *Y. pestis* and *B. anthracis*, pneumonic plague and inhalation anthrax, respectively, as well as against RSV. This was achieved by encapsulating the *Y. pestis* fusion protein F1-V and *B. anthracis* protective antigen (PA) into polyanhydride nanoparticles, which were co-administered with the cyclic di-nucleotide adjuvant cyclic di-guanosine monophosphate, and evaluating the protective efficacy following lethal intranasal (IN) challenge of the respective fully virulent pathogens. For RSV, the RSV-specific post-fusion proteins, F and G, were encapsulated into polyanhydride nanoparticles and administered intranasally in a neonatal calf model in order to evaluate the protective efficacy of IN

RSV challenge. In addition, this report describes the rational design of polyanhydride nanovaccines for enhanced adjuvanticity and shelf stability.

CHAPTER 1. LITERATURE REVIEW

Highly lethal pathogens such as *Y. pestis* and *B. anthracis* utilize many pathogenic factors in order to subvert the immune response and establish infection in the host. However, this depends on the route of infection as well as the virulence factors that the pathogen is capable of expressing. This chapter will begin with an overview of the immune response to foreign pathogens in Section 1.1, highlighting the role of dendritic cells and macrophages in the lungs, as well as the adaptive immune response. Section 1.2 will describe *Y. pestis* pathogenesis, mechanisms of establishing infection, and vaccine strategies. Similarly, Section 1.3 will describe *B. anthracis* pathogenesis, mechanisms of establishing infection, and vaccine strategies. Section 1.4 will describe bovine respiratory syncytial virus mode of infection and vaccine strategies. Section 1.5 will introduce vaccine adjuvants and highlight the need for improved vaccine adjuvants. Section 1.6 will focus on two specific adjuvant platforms, cyclic dinucleotides (CDNs) and polymeric nanoparticle-based adjuvants and highlight the need for combination adjuvant approaches to next-generation vaccines.

1.1 Immune Response to Respiratory Pathogens

The lungs are a vital organ that function by replenishing oxygen to the host while also releasing 'spent' oxygen in the form of carbon dioxide. They are exposed to an impressive 8000-9000 liters of air daily²⁰, which can contain particulate matter as well as microbes that deposit and must be cleared to avoid blockage of gas exchange and potential infection, respectively. The immune response of the lungs is a fine-tuned process used to distinguish self from non-self, eliminate foreign pathogens and

particles, and re-establish homeostasis, all without causing too much inflammation that could prove lethal to the host. This requires the coordination of many specialized cell types that together aim to eliminate the foreign intruder quickly, as well as develop immunological memory in the event of re-exposure.

1.1.1 Physiochemical Barrier of the Lungs

The first line of defense against foreign inhaled pathogens in the lungs are the physiochemical barriers that block initial invasion of the epithelium (Figure 1.1A & 1.1B). This consists of a viscous mucous layer, secreted by mucin-secreting goblet cells, containing antimicrobial peptide β -defensins, the bacterial membrane lysing enzyme lysozyme, the iron-limiting protein lactoferrin, and other proteins responsible for either killing the pathogen, disrupting bacterial aggregation, or blocking interactions with epithelial cells^{21,22}. In addition, the mucous contains secretory IgA and IgG antibodies, proteins secreted by plasmablasts and plasma cells that bind to unique molecular patterns on pathogens and either neutralizes their ability to bind to the epithelium, or (in the case of IgG) opsonizes the pathogen, enhancing its phagocytosis by alveolar macrophages^{21,23}. The majority of the epithelium contains ciliated cells that collectively make up the ‘mucociliary escalator’, which clears mucus from the lungs in an effort to rid the lungs of particulates and pathogens²².

If a pathogen is able to evade this barrage, it must then find a way either into or through the epithelium itself. The lung epithelium itself creates a physical barrier with tight junctions between cells to block pathogen entry²⁴. The lungs also contain sentinel cells, such as dendritic cells (DCs) and macrophages (MØs), which can engulf foreign

invaders via recognition of specific pathogen associated molecular patterns (PAMPs) on the pathogen (Figure 1.1C & 1.1D), or through recognition of opsonized pathogens via Fc receptors, and migrate to the draining lymph nodes to initiate the adaptive immune response against the pathogen²⁰. Recognition of PAMPs by epithelial cells can stimulate secretion of multiple proinflammatory as well as CXC and CC chemokine production that recruit neutrophils to the airway lumen, which ingest and kill pathogens with reactive oxygen species, bactericidal proteins, and degradative enzymes^{25,26}.

1.1.2 Dendritic Cells

DCs were originally identified and named after the Greek word *dendron* (“tree”) for their branched, extended morphology²⁰. DCs are found in virtually every tissue and were realized to be professional antigen presenting cells (APCs) critical for T cell stimulation, displaying the ability to engulf, digest, and present antigen on both MHC I and MHC II to drive adaptive immune responses²⁷. It is now understood that DCs can be divided into more specific subsets and that their role extends beyond infectious disease, including cancer, autoimmunity, and allergic reactions, depending on the tissue location and the cellular phenotype. This review will focus on the role of DCs in infectious disease.

DCs can be divided into three subsets with specialized roles: conventional DCs (cDCs), monocyte-derived DCs (moDCs), and plasmacytoid DCs (pDCs). In addition, cDCs can be further broken down into CD8 α ⁺ and CD103⁺ cDCs or CD11b⁺ cDCs; CD8 α ⁺ and CD103⁺ DCs are nearly functionally identical, however CD8 α ⁺DCs are found in lymphoid tissue while CD103⁺ DCs are found in nonlymphoid tissue²⁷. Recent work

has begun to elucidate the roles that each cell type plays in the immune response, however the exact differences between the aforementioned cell types are difficult to assess because there are conflicting reports of DC subset function and it is difficult to differentiate cDC and moDC phenotype because they both express CD11b²⁷.

cDCs are found in lymphoid (CD8 α ⁺) and non-lymphoid (CD103⁺) tissues, displaying short half-lives of 3-6 days, and are constantly regenerated from bone marrow. Both CD103⁺ and CD11b⁺ cDCs are the main DC subset found in the lungs and are positioned in the bronchus and alveoli²⁰. In the alveoli, CD103⁺ cDCs project long extensions of the cell membrane called pseudopodia between the epithelium and out into the lumen of the lungs, where they continuously 'sample' the environment for foreign pathogens (Figure 1.1C)²⁰. If a foreign pathogen is encountered, CD103⁺ cDCs internalize and degrade it, and then traffic to the draining lymph node, where they can present the antigen to T cells and initiate adaptive immune responses²⁷. CD103⁺ cDCs are capable of biasing CD4⁺ T cells towards either a Th₁ or Th₂ response and also have enhanced ability to cross-present antigen to CD8⁺ T cells, suggesting they enhance cytotoxic T cell (CTL) immunity²⁷. The role of CD11b⁺ cDCs has remained more elusive, due to their overlapping surface marker expression to mDCs, however CD11b⁺ cDCs have shown to preferentially drive a Th₂ and Th₁₇ response against foreign dust mites and fungal pathogens, therefore likely play a role in directing CD4⁺ T cell responses as well as establishing memory T cells²⁷.

moDCs are also found in lymphoid and non-lymphoid tissues, including the lungs, and are derived from differentiated monocytes that influx to inflamed tissue²⁷. They are difficult to differentiate from cDCs due to their similar surface expression

profiles, however their gene expression differs considerably from cDCs²⁷. As it is difficult to discern them from cDCs, their role in immunity is not well understood, however they express MHC II, CD11b, and CD11c, and show the ability to stimulate T cells *in vitro*²⁷.

pDCs are primarily found in circulation and peripheral organs²⁷. During inflammation, these cells traffic into inflamed tissues, where they can recognize intracellular viruses through pattern recognition receptors (PRRs), such as Toll-like receptor TLR-7 and TLR-9²⁸. Compared to cDCs, pDCs have a restricted ability to stimulate T cells, however when activated secrete high amounts of type I interferons following viral infection, which is critical for natural killer (NK) cell activation, cells that are highly cytolytic and secrete interferon- γ (IFN- γ) to drive Th₁ immune responses²⁹. Interestingly, however, they can also express cytokines TGF- β and IL-6, which promote regulatory T cell (T_{reg}) responses, as well as Th₁₇ responses against extracellular pathogens, highlighting their multifaceted role in immunity that needs further clarification²⁸.

1.1.3 Macrophages

MØs are the sentinels of the immune system, found in virtually all tissues and play a host of roles in tissue homeostasis, inflammation, and tissue repair³⁰. In fact, they along with DCs and monocytes make up the mononuclear phagocyte system, a family of functionally related cells, and it is often difficult to differentiate between DCs and MØs in various tissues³¹. Regardless, following pathogen evasion of the initial physical barriers of the host, MØs are the main line of defense, aiding in destroying foreign pathogens through ingesting the invader, presenting it on MHC I and MHC II, and

secreting cytokines to give cues to direct the immune response in a highly specialized manner while also minimizing inflammation, as excessive inflammation is especially destructive in tissues such as the lung, where maintaining lung homeostasis is critical for the exchange of oxygen and carbon dioxide^{31,32}.

MØs have recently been identified to be either tissue resident or monocyte derived. Tissue-resident MØs (tMØs) develop from embryonic precursor cells before birth, and are able to renew their population over the lifetime of an individual³³. Monocyte-derived MØs (moMØs), much like moDCs, are differentiated from monocytes in circulation that are recruited to inflamed tissue³³. moMØs appear to take on functionally similar roles as tMØs, and can even aid in replenishing their population in certain tissues if a population contraction occurs, though this process is not entirely understood³¹. As the functional roles of tMØs and moMØs are very similar, they will further be simply referred to as MØs.

There are three types of MØs in the lung: bronchial MØs, interstitial MØs, and alveolar MØs (AMs). Of note, AMs are currently the most well understood and are critical for controlling pulmonary immune responses toward pathogens, as this is where vital gas exchange occurs. Therefore, the focus of this review will be on AMs in infectious disease.

AMs are located in the alveolar lumen of the lungs, and make up 90-95% of the cellular content in the alveoli air space (Figure 1.1D)²⁰. However, as there are several million alveoli and only roughly one to two million AMs in the lungs, not every alveolar sac contains an AM²⁰. In the alveolar lumen, they attach to alveolar epithelial cells through the integrin $\alpha_v\beta_6$ and sample the luminal environment for signs of pathogens²⁰.

During lung homeostasis, AMs repress inflammation through their interactions with pulmonary DCs, lung T cells, and alveolar epithelial cells. For example, AMs secrete TGF- β and enzymes retinol dehydrogenases 1 and 2, which induces naïve CD4⁺ T cells to differentiate into inducible regulatory T cells (iT_{reg}) following DC stimulation²⁰. iT_{reg} cells have long been linked to tolerance of foreign antigens through suppression of Th₂ airway inflammation.

However, AMs are armed with a host of PRRs, including the TLRs, NOD-like receptors (NLRs), C-type lectin receptors (CLRs), and activation of these receptors, particularly TLR-2, TLR-4, and TLR-9, by their ligands causes a switch from a tolerogenic to inflammatory state through inhibiting the anti-inflammatory IL-10 receptor signaling pathways³⁴. Additionally, activation of AMs via GM-CSF and TNF significantly increases phagocytosis, oxidative burst, and inflammatory cytokine production³⁴. Much like DCs, these cells can rapidly traffic phagocytosed pathogens to local draining lymph nodes, however their role in initiating adaptive immune responses remains unclear because they have very low expression levels of MHC II and other costimulatory molecules necessary to activate T cells²⁰.

Following infection, AMs and alveolar epithelial cells are able to quell inflammation in the lungs through increasing expression of CD200R and CD200L, respectively, whose interaction is known to negatively regulate inflammation²⁰. CD200R expression is also increased with TGF- β stimulation, providing an additional ostensible negative feedback loop for inflammation in the alveoli and thus reduce the extent of inflammation-induced tissue destruction²⁰.

1.1.4 Adaptive Immune Response

The collective of innate immune cells previously described provides a broad and rapid-acting front against the multitude of invading pathogens, however due to many different virulence factors pathogens utilize to bypass this front line of defense, the epithelium requires the aid of additional cell types to effectively halt foreign invasion through developing robust, pathogen-specific immune responses, which is collectively called the adaptive immune response.

The central dogma of initiating adaptive immune responses lies in the ability of DCs and MØs to traffic to the draining lymph nodes and stimulate T cells following detection and phagocytosis of a foreign pathogen³⁵. In the lymph nodes, these cells present foreign peptides derived from the pathogen on MHC I and MHC II to naïve CD8⁺ and CD4⁺ T cells, respectively, who contain highly specific T cell receptors (TCR) on their cell surface that bind to peptide-MHC complexes^{35,36}. There are a multitude of events that determine the fate of both the APC and T cell following this interaction, however there are three main signals that are exchanged between DCs and T cells during their encounter, and these signals are what determine the fate of the stimulated T cell and outcome of the immune response against the encountered pathogen.

The first signal consists of TCR recognition of the peptide-MHC complex. The TCR is surface-bound protein complex that recognizes and binds to specific peptides bound to MHC I or MHC II³⁷. Following binding of the TCR and peptide-MHC complex, the second signal consists of co-stimulation of both the APC and T cells – lack of this interaction results in anergy of T cells³⁸. These interactions include those of the B7/CD28 family and TNFR/TNF family, whose outcomes result in both APC and T cell activation, differentiation, survival, and tolerance³⁸. Most notably, the interaction

between CD28 on T cells and its ligand CD80/86 on APCs is critical for naïve T cell activation and differentiation toward an effector phenotype³⁸. The third activation signal are cytokines secreted by both of these cells that differentiate T cells into specialized effector phenotypes to direct immune responses in inflamed tissues. APCs can secrete a host of cytokines, depending on their mode of activation (i.e., which PRRs were stimulated), and these cytokines ultimately determine the differentiation pathway of the T cell. APCs that secrete type I interferons and IL-12 drive CD4⁺ T cells toward a Th₁ phenotype, as well as CD8⁺ T cells towards a cytotoxic T cell (CTL) phenotype³⁷. Th₁ responses are characterized by Th₁ and CTL cells that secrete pro-inflammatory cytokines IFN- γ and TNF- α , of which IFN- γ activates M ϕ s toward an inflammatory M₁ phenotype, as well as enhanced cytolysis of intracellular pathogens via CTL release of perforin and granzymes (see *Cell-Mediated Immunity* section below)^{36,37,39}. APCs that secrete IL-4 drive T cells towards a Th₂ phenotype, characterized by their secretion of IL-4, IL-5, and IL-13, whose signaling results in enhancing B cell antibody responses against extracellular pathogens (see *Humoral Immunity* section below)^{37,39}.

There are a number of additional T cell phenotypes that have been discovered to date, including IL-9 secreting Th₉ cells, IL-17-secreting Th₁₇ cells, IL-22-secreting Th₂₂ cells, regulatory T cells, natural killer T cells, follicular helper T cells (T_{FH} cells), who play a vital role in immune responses, depending on the context of infection. One of the most important roles of T_{FH} cells is in developing robust high-affinity antibody responses against extracellular pathogens⁴⁰. This is achieved through a well-regulated process of selecting the highest affinity B cell clones and converting them into plasma cells, terminally-differentiated B cells who secrete high levels of antibodies⁴¹.

There are three types of B cells: follicular B cells, marginal zone B cells, and B1 cells. Follicular B cells are the majority population and reside in the secondary lymphoid organs (SLOs), such as the lymph node and spleen⁴². Marginal zone B cells reside in the marginal sinus of the spleen and survey for pathogens in circulation⁴². B1 cells, in contrast, reside in the peritoneal and pleural cavities and mucosal sites, and survey for environmental pathogens⁴². Due to their specialized location, marginal zone B cells and B1 cells predominantly secrete rapid, yet short-lived antibodies against invasive pathogens⁴². Hence, this review will focus on follicular B cells, which are capable of generating high-affinity antibodies, as well as immunologic memory, and will hence be referred to solely as B cells.

Naïve B cells traditionally reside in SLOs, such as the lymph nodes or spleen, and are localized in follicles with a T cell region bordering the follicles⁴¹. Early during infection, pathogen-derived proteins, termed antigens (ANTIbody GENErators), can enter the draining lymph nodes either through direct transport by DCs and MØs or through passive transport⁴³. If these passive antigens are opsonized, they are taken up by subcapsular sinus macrophages (SSMs) via complement receptor 3 (CR3)⁴³. If not opsonized, draining antigens eventually end up being taken up by follicular DCs (FDCs) located in the center of the lymph node follicles⁴³.

Naïve B cells initially express surface-bound antibodies IgM and IgD, which are associated with intracellular signaling surface molecules CD79A and CD79B heterodimer (also called Ig α and Ig β) - this complex is termed the B cell receptor (BCR)⁴⁴. B cells can bind to antigen bound to CR3 on SSMs via their BCR and this receptor-antigen complex is internalized, degraded, followed by B cell migration to the

T/B cell border, where the peptide-MHC II complex is presented to T_{FH} cells⁴³. These B cells will then either migrate to the follicle and contribute to germinal center (GC) formation, a network of FDCs and actively proliferating B cells, or differentiate into short-lived plasmablasts, which migrate to the medullary chords of the SLOs and secrete low-affinity antibodies^{41,43}.

The ability of B cells to differentiate into plasma cells that secrete high-affinity antibody responses is dependent on FDCs and the environment of the follicle. FDCs maintain antigen in non-degradative compartments, and are capable of presenting antigen to B cells for months following infection⁴³. Naïve B cells recognize FDC surface-bound antigen via their BCR, which they then internalize and subsequently migrate to the T/B cell border (termed the 'light zone') and initiate TCR:peptide-MHC II interactions with T_{FH} cells⁴³. This co-stimulation can result in three outcomes. The first two possible outcomes are that some B cells will receive cues to differentiate into low affinity plasmablasts or memory B cells⁴¹. The third is that the B cell enters back into the GC, undergoing a high degree of proliferation in a region called the 'dark zone', of which a process called somatic hypermutation occurs, resulting in mutations (cytosine to uracil) in the V(D)J genes of the antibody immunoglobulin loci^{41,45}. These B cells continually cycle between the light and dark zones of the GC and initiate the same process of stimulation by T_{FH} cells, generating higher affinity B cells and plasmablasts. Following multiple rounds of this process, the B cells of high affinity for antigen are selected for, while low affinity B cells undergo apoptosis, a phenomena termed affinity maturation⁴¹. During affinity maturation, high affinity plasmablasts are capable of exiting the lymph node and migrate to the bone marrow, where they establish a niche and terminally

differentiate into long-lived plasma cells that secrete high quantities of antigen-specific antibodies for extended periods of time⁴⁶.

Plasmablasts and plasma cells are able to secrete five different classes of antibodies, or isotypes, namely IgM, IgD, IgA, IgG, and IgE, each with their own role in preventing infection⁴⁷. As previously mentioned, naïve B cells express surface-bound IgM and IgD, however during affinity maturation, an additional process known as 'class switching' can occur, in which some light zone B cells undergo gene rearrangements and begin to produce higher levels of the other antibody isotypes, each with their own effector functions⁴¹. Therefore, affinity maturation provides the immune response with plasma cells that secrete highly specific antibodies capable of disrupting pathogenesis, as well as memory B cells that can rapidly proliferate and produce high affinity plasma cells upon re-exposure to the same foreign pathogen.

1.1.5 Cell-Mediated Immunity

Cellular-mediated immunity (CMI) is a coordinated immune response to intracellular pathogens that involves phagocytes (DCs and MØs), cytotoxic T lymphocytes (CTLs), NK cells, and the release of specific cytokines that play a role in activating cytotoxic cells and destroying infected cells. Following infection by a foreign pathogen, infected cells will secrete type I interferons, which activate NK cells that destroy infected cells through the release of perforin and granzymes, as well as anti-microbial α -defensins against extracellular bacteria²⁹. These cells also secrete high levels of IFN- γ and TNF- α ²⁹. Simultaneously, DCs and MØs phagocytose pathogens and apoptotic cells, migrate to the draining lymph nodes, present antigen to T cells on

MHC I and MHC II, and secrete IL-12, the cytokine that causes naïve CD4⁺ T cell differentiation toward a Th₁ phenotype and CD8⁺ T cells toward a CTL phenotype³⁵. These Th₁ cells and CTLs then migrate to the site of infection and interact with APCs, secreting cytokines IL-12, IFN- γ , TNF- α , and IL-2³⁹. CTLs demonstrate enhanced cytolytic capacity of intracellular pathogens through secreting perforin and granzymes following binding of peptide-MHC I complexes, which induce apoptosis in infected cells³⁹. Additionally, IFN- γ enhances M ϕ phagocytic ability, nitric oxide production, as well as antigen presentation on MHC I and MHC II³⁷. Thus, CMI allows for the rapid killing of infected cells before they are shed into nearby cells and boosts the clearance of any free or shed pathogens that may be looking for a new host cell.

1.1.6 Humoral Immunity

Humoral immunity is generally viewed as the ability of antibodies, the complement cascade proteins, and antimicrobial peptides to eliminate extracellular pathogens. Early in the response, naïve B cells may become activated in a T-cell-independent manner via activation of PRRs or the crosslinking of the BCR to repeating epitopes, such as those from bacterial cell wall proteins or polysaccharides, and leads to the secretion of low-affinity antibodies by short-lived plasmablasts due to lack of necessary co-stimulation by T cells⁴². However, following affinity maturation, B cells of higher affinity for pathogen-derived antigens develop and leads toward the induction of long-lived plasma cells that secrete high levels of antibodies against pathogen-derived proteins⁴¹.

Antibodies, whether high or low affinity, play numerous roles in immunity to pathogens. Antibodies are capable of binding to and neutralizing secreted proteins and toxins, such as the *B. anthracis* tripartite toxins, blocking their activity by binding directly to active site or indirectly to other epitopes on the protein⁴⁸. Binding of antibodies to soluble antigens can form immune complexes, which activate phagocytes via their Fc receptors, and enhance phagocytosis and subsequent activation of CD4⁺ and CD8⁺ T cells⁴⁹. Antibodies can also bind to pathogen surface proteins and neutralize pathogen function, as is the case with many viruses⁵⁰. For example, hemagglutinin neutralization is largely believed to be the standard correlate for protection against influenza virus. Antibody bound to bacterial surface proteins can initiate the classical complement pathway against bacteria, in which complement molecules C1q, C1r, and C1s binds to the antibodies and leads to the formation of the membrane attack complex (MAC), resulting to cytolysis or opsonophagocytosis of the pathogen⁵¹.

The complement system is also capable of inducing cytolysis through the alternative pathway, in which the molecule C3b binds to the bacteria directly, driving assembly of the MAC⁵¹. Mannose binding lectin or Ficolin are capable of binding to carbohydrates on yeast, bacteria, parasites, and even viruses, and binds to the molecule C4b to initiate complement pathway⁵¹. Therefore, the combined effect of complement and antibody responses against foreign antigens plays a wide role in blocking pathogenesis of the organism through neutralization of its activity, cytolysis, opsonophagocytosis, which further drive adaptive immune responses.

1.2 Pneumonic Plague

1.2.1 Introduction

Pneumonic plague is a disease that has devastated humans throughout their history, most notably for causing the well-known Black Death pandemic, which killed an estimated 20 to 30 million individuals across Europe, wiping out approximately one third of the world's population⁵². Unfortunately, this disease continues to persist and an estimated 1,000-2,000 individuals are reported to contract the disease annually worldwide, with the latest pneumonic plague outbreak occurring in Madagascar recently in 2017⁵³.

Plague is caused by the Gram-negative bacteria *Yersinia pestis* and is part of the family *Enterobacteriaceae*¹. It is one of three species of *Yersinia* that are pathogenic to humans, the other two being *Yersinia pseudotuberculosis* and *Yersinia enterocolitica*, which produce disease in the intestinal tract of the host⁵⁴. *Y. pestis* is responsible for pneumonic, bubonic, and septicemic plague, whose symptoms and severity of disease differ via mode of infection.

Pneumonic plague is a communicable respiratory disease and is typically contracted by inhalation of contaminated aerosols containing *Y. pestis* from other infected hosts, the environment, or potentially as a bioterror weapon⁵⁵. Pneumonic plague's symptoms onset rapidly, and include fever, headache, weakness, chills, nausea, progressing to adult respiratory distress syndrome along with coughing and sputum production, increased chest pain, hypoxia, hemoptysis, which can ultimately result in septicemia⁵². Antibiotic treatment of *Y. pestis* is possible if started early during infection within the first 18-24 hours, with intravenous or oral ciprofloxacin and

doxycycline over a 48 hour course of treatment¹. If untreated after 24-36 hours post-infection, mortality rates approach 90-100%¹.

Bubonic plague is an infection of the lymphatic system and causes the most cases of naturally occurring plague. This disease, also known as secondary pneumonic plague, is a zoonotic disease caused by the bite of infected fleas transmitted from deceased rats, and is believed to have been the cause of the infamous Black Death plague epidemic in the 14th century⁵². Following a blood meal, bacteria are injected into the cutaneous layer of the skin, where they then migrate to regional lymph nodes, resulting in inflammation and swelling of the lymph nodes. Symptoms occur after 2-6 days, with patients experiencing malaise, headache, chills, and fever. As the disease progress, 1-10 cm buboes develop in the skin of patients⁵². *Y. pestis* can spread to the lungs and circulation, resulting in similar symptoms to pneumonic plague and ultimately death⁵². This disease onsets less rapidly and has a lower mortality rate than pneumonic plague and can also be treated with antibiotics, which greatly relieves most symptoms, however the buboes can persist for weeks⁵². It is rare for *Y. pestis* to be transmitted from person to person via aerosol route, hence bubonic plague is not as grave a biological weapon threat as pneumonic plague.

Primary septicemic plague is the rarest of the form of plague, accounting for 10-15% of cases, and is caused following by *Y. pestis* infecting the blood stream usually through an exposed wound, resulting in septicemia without lymphadenopathy, though (as mentioned above) septicemic plague usually results secondarily from pneumonic and bubonic plague⁵². Replication of bacteria in the blood stream initiates a strong inflammatory response and tissue damage, with symptoms including organ failure,

respiratory distress syndrome, and disseminated intravascular coagulopathy resulting in hemorrhaging in the skin and gangrenous necrosis⁵². Additional complications include plague pneumonia, meningitis, endophthalmitis, and splenic abscesses⁵². Septicemic plague can be treated similarly to pneumonic and bubonic plague using antibiotics, however if untreated is almost always fatal. As septicemia usually results secondarily from the other forms of plague, it is not generally regarded as high level of a biological warfare threat as pneumonic plague.

1.2.2 History of Plague Weaponization

The use of *Y. pestis* as a biological weapon dates back to the 14th century, when the Tartars sieged Genoese forces in the city of Caffa and hurled plague-infected cadavers from catapults, causing an epidemic within the city that eventually led the Genoese to retreat from the city⁵². In 1710 AD, Russian forces performed similar actions by catapulting plague-infected cadavers into Swedish cities⁵⁶. During World War II, Japanese forces reportedly dropped fleas containing plague over Chinese and Manchurian civilian populations, which led to 10,000 casualties in the city of Changteh in 1941⁵². The Japanese experimentation during this time with biological warfare agents, including *Y. pestis*, resulted in the deaths of 10,000 prisoners, including 3,000 prisoners of war, some of whom were Americans⁵⁶. Following World War II, the United States and Russia researched the possibility of weaponizing plague, however only Russia succeeded in growing sufficient quantities of the organism for weaponization⁵⁶. The United States terminated its biological weapons program in 1970, but established the United States Army Medical Research Institute of Infectious Diseases (USAMRIID)

to develop vaccines and other defenses against the event of biological weapons use⁵⁶. Following this, 103 nations cosigned the 1972 Convention on the Prohibition of the Development, Production, and Stockpiling of Bacteriological (Biological) and Toxin Weapons and on Their Destruction treaty, which prohibits the stockpiling of biological warfare agents and toxins⁵⁶. However, there are no guidelines for ensuring countries adhere to this agreement or enforcement of violations, and violations of this agreement have been alleged⁵⁶. Following the 9/11 attacks in the United States, the Select Agent Program was created, with *Y. pestis* listed as a Tier 1 select agent, meaning it has the highest risk of mass casualty to civilian populations following exposure.

Due to the prevalence of this disease, significant progress has been made in understanding the pathogenesis of the organism, enabling the design of targeted prophylactic vaccines, however there is no currently licensed vaccine that provides long-lived protective immunity to pneumonic plague. As a licensed vaccine currently does not exist, and due to the high mortality rate and ease of transmission of pneumonic plague, there is a general fear of its use as a biological warfare agent. Therefore, it is imperative to design a vaccine against this pathogen that is able to provide rapid immunity in the event of outbreak and maintain long-lived immunity against subsequent exposure. The next section will focus on pneumonic plague pathogenesis as well as current vaccination strategies, as this route of infection is communicable and believed to be most necessary to vaccinate against.

1.2.3 Pneumonic Plague Pathogenesis

Y. pestis infection has been studied in numerous animal models that purportedly closely resemble that of human hosts, however on the cellular level the exact mechanism of pathogenesis and dissemination is not well understood. It is known that the pathogenesis occurs in a biphasic manner, with an initial 'pre-inflammatory phase' followed by the more severe and lethal 'proinflammatory phase'. The first 36 hours of disease progression is coined the pre-inflammatory phase, as this pathogen replicates rapidly within the lungs, with little immune activity observed¹. During this time, it is hypothesized that *Y. pestis* plays a role in limiting the inflammatory cytokine IL-1 β activity, possibly through upregulating the IL-1 β antagonist receptor IL-1RA, which binds to IL-1 β and suppresses the downstream effects of inflammasome activation¹.

Following this initial pre-inflammatory phase, the proinflammatory phase of disease begins with a spike in the levels of inflammatory cytokines IL-6, IL-17, TNF- α , IFN- γ , and chemokines CXCL1 and CCL2¹. This cytokine spike follows with an influx of neutrophils into lung alveoli, which form packed inflammatory foci and expand throughout the course of infection¹. After 72 hours, the extent of persistent inflammation causes extensive alveolar tissue destruction, leading to edema and hemorrhaging of the lungs and ultimately can be fatal¹. Therefore, pneumonic *Y. pestis* infection is actually a host response-mediated disease, in which the immune response, characterized by hyperresponsive neutrophils, is what furthers severity of disease¹.

Y. pestis is a non-motile, facultative intracellular bacterium. Although both neutrophils and alveolar macrophages are capable of internalizing the pathogen, neutrophils are more effective at killing the internalized pathogen and *Y. pestis* appears to preferentially infect macrophages early during infection, establishing *Y. pestis*

containing vacuoles (YCVs) that attenuate acidification of the vacuole and allow the bacteria to replicate intracellularly^{54,57}. Following internalization, infected macrophages are hypothesized to traffic the bacteria to the draining lymph nodes, where the pathogen subsequently escapes into the extracellular environment, upregulates virulence and antiphagocytic factors such as the Type III secretion system (T3SS) and fraction 1 antigen, respectively, and eventually enter into circulation, causing lethal sepsis (Figure 1.2). Recently, Heine *et al.* showed that although *Y. pestis* was undetectable in the spleen or blood of mice in the first 24 hours following intranasal challenge, bacterial levels greatly increased after 24 hours and were detected in both the lungs and blood, with the counts leveling after 48 hours above the initial challenge dose⁵⁸.

In contradiction to this hypothesis, however, a recent report using a dermal bubonic plague infection model in mice demonstrated that although neutrophils were successful in eliminating bacteria from the infection site, the bacteria were able to disseminate from the dermal layer of the skin into the draining lymph node after only 10 minutes post-infection independently of host cells, which may challenge the 'Trojan horse' model of dissemination to the draining lymph nodes⁵⁹.

Understanding the entire process of how *Y. pestis* establishes infection is critical for designing vaccines against this pathogen. Although much still remains unknown, multiple virulence factors have been found to play a critical role in establishing infection and are likely vaccine candidates.

1.2.4 Pneumonic Plague Mechanisms of Action

Following deposition in the lungs, *Y. pestis* utilizes a wide array of virulence factors that contribute to its ability to evade innate immune responses and establish infection. The following are a few notable examples.

Type III Secretion System

The type III secretion system (T3SS) is a large protein complex that forms a “needle structure” and is inserted within eukaryotic cells, injecting a series of effector proteins known as Yersinia outer proteins (Yops) crucial in disrupting phagocytosis and proinflammatory cytokine secretion by host immune cells⁶⁰. All of the genetic information encoding both the proteins that assemble to form T3SS and Yops are contained within a 70 kb plasmid pYV⁶⁰.

The T3SS contains two domains. The first is termed the “base structure”, which is integral in the membrane of *Y. pestis* and protrudes out of the bacteria. The second domain is called the needle, whose shaft is composed of a single protein YscF that is polymerized to form a long, thin needle structure⁶¹. At the tip of the needle is a tip protein called Low Calcium Response V antigen (LcrV or V antigen), which forms a homopentameric head⁶². This protein assembly is the means by which Yops are able to transport into host cells. T3SS activity and Yop secretion is highly dependent on contact between LcrV with host cells and the concentration of calcium^{63,64}. However, Fields *et al.* demonstrated that Yop secretion can continue even when LcrV is bound by LcrV-specific antigen, suggesting that there may be multiple pathways to secrete Yops⁶⁵. Indeed, Yop secretion can be regulated by a number of proteins, namely YopN, cytosolic TyeA, ScN, YscB, and LcrG⁶⁶.

Once the T3SS of *Y. pestis* is successful in navigating through the extracellular environment of the host and contacts a host cell, it becomes activated and injects Yops into the cytoplasm. There are at least six known Yop proteins, namely YpkA/YopO, YopE, YopT, YopH, YopM, YopJ/YopP, that are injected directly in host cells. The combined effect of Yop translocation is responsible for disrupting actin, a main component of the microfilaments eukaryotic cell's cytoplasm, and also interrupting cell signaling pathways that lead to induction of proinflammatory cytokines⁶⁰. As rearrangement of actin is critical for cells to be able to phagocytose pathogens, disrupting its activity helps attenuate innate immune responses and allows the bacteria to disseminate from the infection site⁶⁶. The following is a list of known Yops and their observed functions:

YpkA/YopO: Anti-phagocytic. Binds to actin, where it is activated via autophosphorylation. Inhibits GDP-GTP exchange of RhoA and Rac1, retaining their inactive state, thus limiting actin stress fiber formation⁶⁰. Additionally phosphorylates Gαq, which also controls actin stress fiber formation, hence both of its functions appear to attenuate cytoskeletal rearrangement and phagocytosis⁶⁰.

YopE: Anti-phagocytic. Non-canonical GTPase activating protein (GAP) that induces G-proteins RhoA, Rac1, and CDC42, which converts GTP to GDP, disrupting cytoskeletal rearrangement, and thus phagocytosis⁶⁰. Additional role potentially includes resealing pores made by T3SS so proinflammatory cytokine leakage cannot occur and induce an inflammatory response⁶⁰.

YopT: Anti-phagocytic. Cleaves phenyl groups of lipid-modified RhoA, Rac1, and Cdc42, causing their detachment from plasma membrane and attenuates downstream actin cytoskeletal signaling pathways⁵⁴. Very similar activity to YopE that may be redundant.

YopH: Anti-phagocytic. Contains a protein tyrosine phosphatase domain that dephosphorylates p130^{Cas}, FAK, and paxillin in epithelial cells and p130^{Cas}, SKAP-HOM and Fyb in macrophages, which attenuates β 1 integrin-mediated phagocytosis⁵⁴.

YopM: Role in pathogenesis unclear. Recently suggested that YopM binds to and antagonizes caspase-1-dependent inflammasome activity, thus disrupting pyroptosis⁶⁷. Also recently shown to be critical for *Y. pestis* virulence through binding and activating PRK1 and PRK2, thus inhibiting the pyrin inflammasome⁶⁸.

YopJ/YopP: Targets MAPK kinases and I κ B kinase- β and inhibits downstream signaling pathways, promoting apoptosis and further inhibition of cytokine expression⁶⁰. Recently shown to suppress chemotactic IL-8 secretion by polymorphonuclear (PMN) cells, suggesting a role in delaying PMN recruitment to sites of infection⁶⁹.

These Yops are the effective means by which *Y. pestis* is able to establish infection following escape into the extracellular environment. Yop secretion occurs early during infection. It has been observed in mice that after approximately 12 hours, 5% of the lung cells were injected, followed by an increase to roughly 50% of lung cells after 24 hours⁷⁰.

Y. pestis appears to preferentially target specific cell types over the course of infection. Pechous *et al.* observed that greater than 96% of the Yop injection events in the lungs of mice occurred in leukocytes as compared to lymphocytes and epithelial/endothelial cells⁷⁰. After 24 hours, approximately 40% of all leukocytes in the lung were injected with YopE, far greater than the other two categories (3% for both)⁷⁰. It was noted that after six hours post-infection, approximately 55% of the infected cells were AMs, while 18% were neutrophils and other cell types. After 12 hours, there was a switch in preference as more than 70% of cell types injected were neutrophils and less than 10% were AMs. After 24 hours, more than 90% of cell types were neutrophils, suggesting that *Y. pestis* is capable of attenuating innate immune responses early during infection by AMs and later following neutrophil influx⁷⁰.

Fraction 1 Antigen

Another key component to the most virulent strains of *Y. pestis* is the ability to encapsulate itself with the surface capsule Fraction 1 (F1) antigen. F1 is encoded by the *caf1* gene on the 100-kb plasmid pFra, whose expression on the cell surface is greatly increased at 35-37°C following release from intracellular compartments, and within hours post-infection^{54,57}. F1 is a polymer composed of repeating units of Caf1 and forms a linear, fimbrial structure that coats the bacteria and has been shown to reduce phagocytosis by MØs through blocking the binding to opsonins to *Y. pestis*' surface, suggesting that F1 is a critical virulence factor able to block the uptake of *Y. pestis* by innate immune cells⁷¹.

Psa

Psa, like F1 antigen, is a homopolymer that forms a capsule-like structure on the surface of *Y. pestis*. It forms an adhesion pilus of 15 kDa and is expressed optimally at 37°C at pH ranges of 5.8-6, conditions similar to that of the phagolysosome^{54,57}. This protein structure is known to bind to β 1-linked galactosyl residues in glycosphingolipids and apoB-containing LDL in human plasma, thus aiding in avoiding recognition by host phagocytic cells⁵⁴. However, Psa has shown to adhere to host cells, though it does not appear to play a role in the invasion of bacteria into host phagocytic cells⁵⁴. Therefore, this protein likely binds to host serum proteins and uses this as a mechanism to avoid host phagocytes.

Ail

Ail is a 17.5 kDa protein that occupies the outer membrane of *Y. pestis*, with four short extracellular loops that extend from the bacterial surface. These loops are believed to play a role in cell adhesion through binding to fibronectin, allowing the bacteria to adhere and enter into host cells⁵⁴. Ail demonstrates virulence in mice, as a 3000-fold increase in the 50% lethal dose of an Ail knockout strain of KIM5 *Y. pestis* was required to achieve the same lethality as the parental strain⁷².

Braun's Lipoprotein

Y. pestis contains Braun's Lipoprotein (Lpp) on its outer membrane. This protein is found in all *Enterobacteriaceae* and is the essential link between the peptidoglycan layers of Gram-negative bacteria with the outer membrane. Sha *et al.* recently

demonstrated that mice infected with a Lpp knockout strain of *Y. pestis* had improved survival rates than that of the parenteral KIM/D27 strain, with bacteria undetectable in the blood and spleen of infected mice, suggesting a critical role of Lpp in establishing infection⁷³. Prior work from this same group showed that Lpp was able to induce TNF- α and IL-6 production in peritoneal exudate macrophages independent of lipopolysaccharide (LPS), and that Lpp and LPS synergistically induced lethal shock in LPS-responsive and LPS-nonresponsive mice, suggesting Lpp contributes an important role in inducing septic shock⁷⁴.

Lipopolysaccharide

Another important component of *Y. pestis* that contributes to virulence is LPS, a lipoglycan composed of lipid A covalently bound to a polysaccharide O antigen⁷⁵. This molecule can be found on virtually all Gram-negative bacteria. LPS is the main culprit that induces toxic shock syndrome in hosts, causing fever, rash, and organ failure due to the massive inflammatory cytokine storm released⁷⁵. LPS is known for triggering the innate immune response through binding to TLR-4, the innate immune receptor that recognizes the conserved sequence of LPS on Gram-negative bacteria⁷⁵. The number and length of the fatty acid side chains of lipid A can vary, depending on the organism, and the number and length of these side chains is critical for the binding and activation of TLR-4⁷⁶. In fact, hexa-acylated lipid A containing 12 to 14 carbons in the fatty acid side chain optimally activates immune responses in humans, while lipid A containing other numbers of chains having reduced responses. Interestingly, it has been observed that *Y. pestis* is able to regulate the structure of lipid A depending on its environment,

with hexa-acylated LPS being produced maximally at 21 to 26°C (flea gut conditions), switching to a nonstimulatory tetra-acylated LPS following exposure to 37°C (host temperature)⁵⁷. The change in LPS expression is appears critical for *Y. pestis* to prevent activation of innate immune cells and secretion of proinflammatory cytokines that would recruit neutrophils to the infection site as well as drive adaptive immune responses.

Plasminogen Activator

In addition to pYV and pFra plasmids, *Y. pestis* can contain another plasmid pPCP1, which is a 9.5-kb plasmid that contains the genes for plasminogen activator Pla⁵⁴. Pla is a membrane-bound protease, containing five surface-exposed loops that contain catalytic activity and activates plasminogen to plasmin; plasmin is an enzyme that dissolves fibrin clots, an important clotting factor in blood, and digests laminin, resulting in the disruption of the host tissue barrier⁵⁴. A recent study by Lathem *et al.* infecting mice with either wild type *Y. pestis* CO92 or an isogenic *Y. pestis* strain lacking Pla revealed that mice infected the Pla-knockout strain had significantly greater survival rates corresponding to a lack of bacterial outgrowth, edema, proinflammatory cytokine production, and polymorphonuclear cell infiltration in the lungs, despite detection of bacteria in the spleen by 72 hours⁷⁷. These results suggest that Pla is critical for bacterial growth within the lungs and can lead to fatal pneumonia, but is not critical for dissemination into other host tissues. Interestingly, the opposite appears to hold true in cases of bubonic plague, where Pla is critical for dissemination but not for outgrowth at the infection site. The authors speculated this may be due to the high vascularization of the lungs, which allow for the escape of a few Pla-knock out organisms into circulation.

An additional role for adhesion activity has been reported for Pla. Zhang *et al.* reported that Pla can bind to the DC surface receptor DEC-205, a C-type lectin receptor that is thought to mediate antigen uptake and presentation⁷⁸. This interaction was found to mediate invasion of AMs and subsequent dissemination.

Recently, Pla has shown to bind to and degrade Fas ligand (FasL)⁷⁹. Following infection, host cells undergo a process apoptosis, or programmed cell death, in order to prevent the replication of bacteria intracellularly. This process is initiated by FasL binding to its cognate receptor Fas, which results in apoptosis through the activation of caspases 3 and 7⁸⁰. Pla has shown to bind to FasL and degrade it, attenuating the ability of cells to undergo apoptosis⁷⁹.

Outermembrane Vesicles

Y. pestis has the ability to release vesicles, termed outermembrane vesicles (OMVs), which contain phospholipids, outermembrane proteins, LPS, and periplasmic contents, some of these including virulent proteins and enzymes. Recently, Eddy *et al.* recently demonstrated that *Y. pestis* is capable of releasing OMVs of approximately 100 nm in diameter containing Ail, Pla, and F1 antigen and OMV secretion was increased at elevated temperature (37°C)⁸¹. The OMVs were able to bind to fibronectin and laminin, displaying catalytic behavior of Pla. These results suggest that *Y. pestis* is capable of enhancing its virulence through secreting these OMVs, which may have antiphagocytic properties and allow for the bacteria to disseminate by degrading host extracellular matrix.

1.2.5 Current Vaccine Strategies against Pneumonic Plague

There currently is no FDA-approved vaccine against *Y. pestis*, however Russia and China have approved the use of a live-attenuated strain⁸². As *Y. pestis* is predominantly an extracellular bacterium, many studies have focused on developing strong humoral immunity against the pathogen, characterized by high antibody titers against specific neutralizing epitopes of the T3SS and opsonizing antibodies against the F1 capsule. As described below, in certain animal models anti-F1 IgG antibody titers have shown to correlate with protection, suggesting a threshold antibody titer is necessary to achieve protective immunity⁸³.

Whole-cell Vaccines

The use of whole-cell vaccines against plague dates back to 1895, when Alexandre Yersin first evaluated the efficacy of both killed and live whole-cell vaccines in small animal models⁸². These vaccines were shown to generate immune responses against bubonic plague in a single formulation, but not to pneumonic plague⁸⁴.

A comparative study using the killed plague vaccine USP and a live-attenuated strain of *Y. pestis* (EV76) showed that EV76 could provide complete protection in Porton outbred mice after a single intramuscular dose⁸⁴. However, the authors noted that all of the EV76-immunized mice developed severe side effects, with paralysis in the injected limb that did not improve throughout the study, sensory and motor dysfunction, and even one death. There were no observed symptoms in mice immunized with USP, even after two doses. In both small animal models and non-human primates, it has been shown that live-attenuated strains of *Y. pestis* develop rapid immunity, however the bacteria is capable of disseminating and proliferating within tissues, and has been

shown capable of proving fatal in these animal models⁸². Therefore, killed whole-cell vaccines are generally regarded to be safer for use in humans and have been studied more thoroughly as a vaccine candidate.

Early studies using killed whole-cell vaccines in mice and guinea pigs demonstrated high levels of protection in mice, however guinea pig protection was suboptimal, with only 10-20% of guinea-pigs surviving after receiving the recommended human dose⁸⁵. However, using a killed EV76 strain of *Y. pestis*, lacking the Ybt iron acquisition system, was capable of improving survival to 69% protection, although results in guinea-pig models varied widely due to guinea-pig genetic heterogeneity⁸². Studies in non-human primates were variable as well, with potency tests on macaques proving unreliable due to low and variable susceptibility of the species. Studies in langurs immunized with the killed USP vaccine demonstrated safe administration and the ability to generate antibody responses and were protected from lethal challenge⁸⁵. Hence, the efficacy of killed whole-cell vaccines varies widely, depending on the animal model.

Early clinical trials before 1944 to evaluate safety and dosage requirements of proven killed plague vaccines previously evaluated in mice and guinea pigs showed that the vaccine could be well tolerated in humans, however only generated antibodies in 50-60% of subjects⁸⁵. Leading into World War II, the United States Subcommittee on Tropical Diseases, National Research Council Committee on Medical Research passed a resolution recommending the use of killed-whole cell vaccines, despite the lack of evidence supporting their efficacy⁸⁵. Hence, military personnel deployed to the battlefield were immunized with a killed whole-cell vaccine, called the USP plague

vaccine. No United States military personnel contracted plague during World War II, though field efficacy could not be evaluated as other factors, such as insecticides, were employed in tandem with vaccination.

Subsequent studies have reported local and systemic adverse reactions to the USP vaccine following boost, with some symptoms reported as strong pain at the injection site, swelling, malaise, headache, weakness, and fever-like symptoms⁸². Additionally, a clinical trial in humans immunized with two doses of the USP vaccine showed that albeit tolerance of the injection and development of antibodies, after only three months post-vaccination, antibody titers had waned to low or undetectable levels⁸⁵. Hence, the current status of killed whole-cell vaccines require multiple immunizations, do not elicit strong immunological memory and, in addition to higher frequency of injection site reactions, is not suitable for mass vaccination of both military and civilian populations in the event of exposure to *Y. pestis* employed as a biological weapon.

Plague Subunit Vaccines

Due to the injection site reactogenicity and concerns of poor immunological memory with whole-cell vaccines, plague subunit vaccines have become attractive vaccine candidates. Of note, *Y. pestis* culture supernatants do not contain any known toxins, hence immune responses against *Y. pestis* are generally directed towards cell surface components of the bacteria, though effector Yops have been evaluated as well.

The F1 antigen is has long been studied as a vaccine candidate as it is believed that generating opsonizing antibodies to the capsule will aid in bacterial clearance by

phagocytic cells. Indeed, it has shown much promise as a vaccine candidate, proving to be protective in both small animal and non-human primate models against fully virulent strains of *Y. pestis* expressing the F1 capsule, however it fails to protect against the bacterial strains that do not express F1⁸⁶. Additionally, F1⁻ strains of *Y. pestis* have been found in rodents and humans that succumbed to the fully virulent, F1⁺ strain⁸⁶. Hence, plague vaccines cannot rely on F1 alone and require additional antigens to provide protective immunity.

V antigen was first identified as a major *Y. pestis* virulence factor by Burrows in 1956, shown to protect mice against lethal challenge with both F1⁺ and F1⁻ strains of *Y. pestis*^{86,87}, thus supporting its use as a vaccine candidate in addition to F1 antigen. It is believed that generating neutralizing antibodies against LcrV attenuates the translocation of Yops into host cells via the T3SS. In fact, Ivanov *et al.* recently demonstrated direct neutralization of the tip of the T3SS was sufficient to block Yop translocation *in vitro* using a monoclonal antibody (MAb) known to bind to LcrV (MAb 7.3)⁸⁸. This same group showed that the Fc domain of MAb 7.3 was not required to block Yop translocation, further supporting the necessity of neutralization rather than opsonophagocytosis. However, Noel *et al.* reported that both MAb 7.3 and polyclonal antibodies opsonizing LcrV were unable to inhibit apoptosis in naïve and IFN- γ -activated MØs infected with using a KIM5 strain of *Y. pestis*, and this was due to *Y. pestis*' ability to continue surviving within the macrophages and blocking acidification of the phagosome⁸⁹. Hence, generating antibody responses against LcrV alone is likely insufficient for protection and requires the use of a co-antigen. Regardless, Overheim *et al.* designed an LcrV variant lacking immunosuppressive residues 271 to 300 (rV10)

and showed that this antigen retains the ability to elicit neutralizing antibodies against the T3SS and protected mice, rats, guinea pigs, and cynomolgus macaques from lethal challenge and displayed reduced immunoregulatory capabilities associated with the full length protein, suggesting its use as a vaccine candidate^{64,90–92}.

Due to the protective capabilities of both F1 and V antigens, most studies have evaluated co-administering the two. Hill *et al.* passively immunized mice with the anti-F1 MAb 7.3 and an anti-LcrV monoclonal antibody F1-04-A-G1, demonstrating synergistic protection when administering both antibodies 48 hours post-challenge, while the individual monoclonal antibodies were insufficient for protection⁹³, supporting the hypothesis that generating antibody responses against both antigens will enhance immunity. Studies in mice immunized intramuscularly with a vaccine formulation containing both F1 and V antigen co-adsorbed to alhydrogel demonstrated that anti-F1 IgG1 antibody titers correlated with protection against subcutaneous challenge, suggesting there may be an anti-F1 antibody threshold required for protection⁸³. Studies in cynomolgus macaques immunized with a high dose (80 µg) of both F1 and V antigens adsorbed to alhydrogel in prime-boost regimen and challenged 8-9 weeks PI showed complete protection against *Y. pestis* CO92⁹⁴. Interestingly, a separate group of cynomolgus macaques immunized with 40 µg of both antigens were also protected from lethal challenge, however one macaque succumbed to infection and was found to have similar anti-V IgG titer to those that survived, supporting the requirement for developing robust antibodies against both antigens.

In an effort to improve vaccine production and reduce cost, a fusion protein containing F1 and V, named F1-V, was developed by USAMRIID and is currently the

most promising plague vaccine candidate⁹⁵. This fusion protein is highly immunogenic and has shown to be completely protective in mice against both F1+ and F1- *Y. pestis* strains, and was more protective than either F1 or V antigen administered alone⁹⁵. Recent studies have shown that the route of immunization and adjuvant use influence immune responses toward F1-V, with subcutaneous immunization eliciting the highest levels of IgG in the lungs and serum⁹⁶. The inclusion of adjuvants dictated the types of immune responses generated, with alum enhancing both serum and mucosal anti-F1-V IgG1 responses (Th₂ response) following subcutaneous immunization.

Quenee *et al.* evaluated clinical grade F1-V efficacy in mice, guinea-pigs, and cynomolgus macaques, showing complete protection against fully virulent *Y. pestis* in all of the animal models⁹². These animals were immunized intramuscularly with F1-V adsorbed to alhydrogel in a prime-boost schedule and challenged with fully virulent *Y. pestis* CO92. The results showed complete protection in mice and guinea pigs, while three out of the four nonhuman primates challenged survived. Additionally, serum collected from the non-human primates passively transferred to mice demonstrated near complete protection in mice from serum of the primates that survived challenge. Mice transferred serum from the one non-human primate that succumbed to challenge had a only two out of five mice survive, however this animal had anti-F1-V antibody titers comparable with those of the primates that survived, supporting previous findings that non-human primate models can have variable protective responses with F1-V.

Additional Considerations Necessary for Protective Plague Vaccines

Despite the plethora of evidence suggesting humoral immunity is required for protection, there is a growing body of evidence to posit that cell-mediated immunity is critical for protective immunity as well. Szaba *et al.* demonstrated the necessity for cell-mediated immunity by showing protection in μ MT mice (deficient in mature B cells) immunized with a live-attenuated strain of *Y. pestis* against lethal challenge with *Y. pestis* D27⁹⁷. Protection was ablated following depletion of CD4⁺ and CD8⁺ T cells. Additionally, immunization led to an increase in TNF- α and IFN- γ producing T cells. Work from this same group later demonstrated that protective immunity against *Y. pestis* D27 could be achieved in mice with the CD8⁺ T cell epitope YopE₆₉₋₇₇ and was dependent on TNF- α for protection, with IFN- γ aiding in CD8⁺ T cell differentiation to CTLs, though perforin activity was dispensable for protection⁹⁸. When immunized mice were challenged with the fully virulent CO92 strain, protection was incomplete but significantly higher than unimmunized mice, supporting the notion for the requirement for proper activation of cell-mediated immunity to aid in protective immunity.

Recently, Mizel *et al.* demonstrated protective efficacy of a fusion protein encompassing the flagellin fused to F1-V⁹⁹. Flagellin is a structural protein in Gram-negative bacterial flagella filaments and is a potent agonist of TLR-5 in neutrophils, NK cells, monocytes, macrophages, endothelial cells, and epithelial cells, which drives cellular immune responses at the site of immunization¹⁰⁰. When flagellin-F1-V was cultured with RAW 264.7 cells (macrophages) *in vitro*, high levels of TNF- α was detectable in the supernatant. BALB/c mice immunized with a prime-boost regimen of this fusion protein were completely protected against *Y. pestis* CO92 lethal challenge,

displaying high anti-F1 and anti-V antibody titers with no detectable levels of bacteria in blood, liver, lungs, or spleen three days post-challenge⁹⁹. Additionally, both young and adult African green monkeys and cynomolgus macaques were immunized in prime-boost regimen with varying doses of flagellin-F1-V, displaying high anti-F1 and anti-V IgG titers that were of the same magnitude as the immunized BALB/c mice, suggesting that these animals could be protected against lethal challenge. Impressively, this vaccine candidate recently completed phase I clinical trials and will hopefully undergo further evaluation¹⁰¹. However, this vaccine candidate requires multiple immunizations, and these reports stress the need for a pneumonic plague vaccine formulation that is able to both prime both the cellular and humoral branches of the immune response.

1.2.6 Summary

Y. pestis is a highly pathogenic organism that causes near complete mortality after 2-4 days if untreated. There currently is no FDA-approved vaccine against pneumonic plague. The most promising vaccine candidates currently being studied utilize the F1 capsule and V antigens, however many (if not all) reports of its efficacy rely on multiple immunizations to achieve protective immunity, particularly against the fully virulent CO92 strain, and rely heavily on generating humoral immunity, which may be insufficient for a genetically heterogeneous human population. Despite such promise with F1/V-based vaccines, there are no reports of a F1/V-based vaccine platform that provides rapid protective immunity, in as little as 14 days PI, which is critical in the event of mass exposure to civilians and warfighters. Therefore, there still remains a critical need for a vaccine platform against pneumonic plague that properly stimulates both the

cell-mediated and humoral branches of the immune system and is capable of providing both rapid and long-lived protective immunity, ideally in a single dose.

1.3 Inhalation Anthrax

1.3.1 Introduction

Anthrax has roots as deep as humanity itself. In fact, many scholars posit that anthrax appeared as early as chapter nine in the Book of Exodus, causing the fifth and sixth plagues inflicted upon Egypt². Anthrax is believed to have plagued ancient Greece and Rome, possibly causing the Plague of Athens (430-427 BCE)². The word “anthrax” derives from the Greek word *anthrakites*, which means “coal-like”, referring to the black eschar that is seen following cutaneous anthrax infections². During the 18th century, anthrax wiped out half of the sheep population in Europe, and later became known as woolsorter’s disease, due to the frequency at which mill workers came into contact with infectious wool, goat hair, or alpaca wool². Beyond its deadly past, anthrax has played a pivotal role in the study of infectious disease and development of vaccines. In fact, during the 1870’s, Robert Koch used anthrax to develop Koch’s postulates, which define the causal relationship between a pathogen and disease². Louis Pasteur furthered this work by immunizing cattle and sheep with the first anthrax vaccine, a live-attenuated organism, and showed that the vaccinated cows survived infection with virulent anthrax^{2,102}. The first instance of anthrax infection in the United States occurred in the 1900’s, when workers in the textile and tanning industries contracted the disease following exposure to goat hair, skin, and wool². However, overall the incidence of anthrax infections decreased in the 20th century, attributed to the development of a live

anthrax spore vaccine by Max Sterne in the 1930s for use in animals, as well as improved work conditions^{2,102}.

1.3.2 History of Anthrax Weaponization

The modern era is when anthrax weaponization began its roots. During World War I, there was evidence that Germany, England, and France started biological weapons programs, including the weaponization of *B. anthracis*¹⁰³. Reports surfaced that the Germans tried shipping cattle and horses infected with various diseases, including anthrax, to the United States and other countries, though this was never verified⁵⁶. During World War II, a Japanese weapons program tested various organisms, including *Y. pestis* and *B. anthracis*, on prisoners and was responsible for the deaths of more than 10,000 people, with at least 3,000 being prisoners of war (including Americans)¹⁰³. The British were also experimenting with *B. anthracis*, and developed a bomb that could deploy aerosolized droplets containing the bacteria, to be inhaled within the blast zone¹⁰³. The weapon was never implemented in the war, however it led to the contamination of Gruinard Island, which remains a restricted zone even today¹⁰³. As mentioned previously, 103 nations cosigned the 1972 Convention on the Prohibition of the Development, Production, and Stockpiling of Bacteriological (Biological) and Toxin Weapons and on Their Destruction treaty, which prohibits the stockpiling of biological warfare agents and toxins.

Despite this, anthrax exposure events have continued and even remain a recent memory for many alive today. In 1979, there was an outbreak of human anthrax in Sverdlovsk, the Soviet Union, in which 96 cases of inhalation anthrax occurred¹⁰⁴. It was

concluded that aerosolized anthrax spores had accidentally been released from a military facility located nearby and caused the outbreak incident. Although it was concluded that this was an accidental release occurrence, it nonetheless highlighted the possibility of mass exposure of civilian populations to biological weapons.

The first intentional anthrax release in the United States occurred in the Fall of 2001 following the 9/11 attacks, when 22 Americans were infected from letters contaminated with anthrax spores. 11 of these cases were determined to be inhalation anthrax, and 11 were either confirmed or suspected to be cutaneous anthrax. Of the 11 cases of inhalation anthrax, five people died¹⁰⁵, though fortunately the survival rate was higher than that reported in the early 1900s (15%), attributed to early diagnosis and quality of treatment². The 11 cases of cutaneous anthrax were observed in postal workers or people who were believed to have handled contaminated mail, and all survived infection². Following these attacks, the Special Agent Program was created with *B. anthracis* listed as a Tier 1 Select Agent, for its high likelihood for mass casualty following exposure to civilian and military populations. Because of *B. anthracis*' prior biological weapons use in the United States, its ability to sporulate, as well as its high lethality in human hosts, there remains a general public fear of its use as another biological weapon. Therefore, much research has gone into understanding the pathogenesis of this organism in order to design improved antibiotics and prophylactics.

1.3.3 Inhalation Anthrax Pathogenesis

Anthrax is an acute disease caused by the bacteria *Bacillus anthracis*. This Gram-positive bacteria has been found on every continent and is able to form

endospores, which endow the spores with resistance against heat, cold, and radiation, allowing them to survive for up to decades and centuries¹⁰⁶. Anthrax spores are capable of being transmitted to the host via three modes - inhalation, gastrointestinal, and cutaneous. Inhalation anthrax occurs through inhalation of spores into the lungs, where they deposit in the upper airways and alveoli¹⁰⁷. This route of infection is the most deadly, with mortality rates of reportedly 86% during the 1979 outbreak in the Soviet Union and 89% in the United States¹⁰⁸.

The exact mode of pathogenesis of this bacterium is still rather unclear. It has long been known that the bacteria are capable of disseminating from the lungs into circulation via the lymphatic system, where they ultimately spread throughout the body. Autopsies from patients that died from the Sverdlovsk outbreak in 1979 revealed bacteremia and toxemia at time of death, with edema and hemorrhaging throughout the body, including the lungs, thoracic lymph nodes, and brain¹⁰⁹. The first proposed mechanism of anthrax pathogenesis was by Joan Ross in 1957, who observed bacillus spores were phagocytosed by alveolar macrophages and trafficked to the draining tracheal bronchial lymph nodes¹¹⁰. This discovery and many after led to the 'Trojan Horse' model of anthrax infection in 2002 by Guidi-Rontani, in which alveolar macrophages provide the route of infection for anthrax¹¹¹. In this model, anthrax spores deposit in the alveoli of the lungs but are unable to germinate in the lumen. Alveolar macrophages, which situate on the apical side of the epithelium, phagocytose anthrax spores and transport the bacillus across the lung epithelium and to the draining lymph node, where spore germination and subsequent infection occurs¹¹¹.

However, recent evidence has cast doubt on the Trojan Horse model (see ¹¹² for detailed review). One of the most compelling issues with this model is that there currently is no direct evidence that bacteremia derives from macrophage-phagocytosed spores. Some reports have shown that although alveolar macrophages are the first to engulf anthrax spores within as little as 10 minutes after infection, pulmonary DCs are also able to phagocytose spores after 30 minutes and traffic to the thoracic lymph nodes directly after, which may lend a new avenue for anthrax pathogenesis¹¹³. Another study reported that epithelial cells and fibroblasts are able to internalize both anthrax spores and vegetative cells *in vitro*, thus suggesting new mode of infection that does not involve a Trojan horse phagocyte at all¹¹⁴. Lastly, recent studies have shown that anthrax spores actually can germinate within the nasal-associated lymphoid tissues (NALT) in the lungs, which has prompted a new model called the 'Jailbreak' model of dissemination, in which anthrax spores germinate within the NALT and produce exotoxins and proteases that disrupt innate immune cell function and permeabilize lung tissue through degrading the extracellular matrix, thus allowing for vegetative bacteria to drain to the draining lymph nodes and subsequently into circulation¹¹².

It is very likely that all of the above modes of action contribute to some degree to disease pathogenesis. Regardless, it is certain that by the time *B. anthracis* enters the lungs, it releases an arsenal of virulence factors upon the host that enable it to overcome host immune defenses, which will be detailed in the next section.

1.3.4 Inhalation Anthrax Mechanisms of Action

B. anthracis belongs to the *Bacillus cereus* group, a small group of six *Bacillus* species who all have very similar chromosomes¹⁰². However, it is the extrachromosomal genetic elements that differentiate *B. anthracis* from other species. In fact, *B. anthracis* itself exhibits very little genetic diversity across strains, however the major differences between strains lie in the plasmids that the bacteria express, with these plasmids providing the virulence factors that differentiate fully virulent, lethal anthrax strains from nonvirulent strains¹⁰².

The main virulence factors associated with *B. anthracis* are displayed on two plasmids. The first plasmid, a 183-kb plasmid pXO1, allows *B. anthracis* to secrete the bipartite exotoxins, lethal toxin (LT) and edema toxin (ET), which have shown to modulate innate cell signaling processes, including oxidative burst in macrophages, chemotaxis, cytokine secretion, and cellular activation¹⁰². It has been revealed that transcription of the toxin genes is located on a pathogenicity island and is regulated by the anthrax toxin activator protein, a pleiotropic regulator protein, and also carbon dioxide and bicarbonate, thus inferring that recognition of the host tissue environment activates toxin secretion¹⁰². There are three proteins that are secreted that make up the two bipartite toxins. They are protective antigen (PA), edema factor (EF), and lethal factor (LF). The second plasmid, pXO2, is a 96-kb plasmid that encodes for poly-γ-D glutamic acid (PGA), a polypeptide capsule that encapsulates the bacteria and blocks phagocytosis of the bacteria¹⁰². Interestingly, expression of PGA is also upregulated by presence of carbon dioxide, further suggesting that bacterial virulence is increased following recognition of the host tissue environment¹⁰².

Protective Antigen

PA is an 83 kDa protein that contains four domains. Its role in pathogenesis involves recognition of host cells and subsequently coordinating the transport of both EF and LF into the cytosol of host cells (Figure 1.3). It does this through the binding of its domain III to the Anthrax Toxin Receptors, of which only two receptors have been identified thus far^{115,116}. Following binding, PA is cleaved at domain I into a 63 kDa active fragment by the cell surface protease furin¹¹⁷, where it then oligomerizes into heptamer and octamer pores on the cell surface¹⁰². These complexes contain binding sites for both LF and EF, which are believed to aid in allowing the LF/EF-PA complexes to become internalized into endosomes, where LF and EF are released through the pore and into the cytosol of the host cell¹⁰². As PA is critical for the delivery of LF and EF into the cell, it has been the most studied target antigen for most current vaccines against anthrax, as it is believed that neutralizing antibodies against PA will ablate toxin efficacy.

Lethal Factor

LF is a 90 kDa protein containing four domains. The most critical is domain III, which contains a zinc-binding catalytic active site, which cleaves the mitogen-activated protein kinase kinase (MAPKK) family of proteins¹⁰². This is detrimental to cells, as the downstream signaling effects of MAPKK cleavage ultimately disrupts inflammatory cytokine production and therefore suppresses innate immune defenses against the pathogen (see ¹¹⁸ for a more detailed review). This outcome of attenuated innate immunity ultimately leads to lack of bacterial clearance, subsequent dissemination into

circulation, of which LF preferentially targets cardiomyocytes and smooth muscle cells, which leads to vascular collapse and finally host death, hence why it is named 'lethal factor'¹⁰².

Edema Factor

EF is also a 90 kDa protein catalyst that converts free ATP to cAMP at a very high rate (2,000 molecules per second)¹⁰². This higher than normal level of cAMP is known to be detrimental to innate immunity, as higher levels suppresses inflammatory cytokine production, enhances anti-inflammatory IL-10 production, suppress receptor-mediated phagocytosis of pathogens by monocytes, macrophages, and neutrophils, and generation of reactive oxygen species that aids in killing internalized pathogens¹¹⁹.

Poly-D-γ-glutamic acid

The PGA capsule of *B. anthracis* plays a vital role in defense of the extracellular pathogen against both humoral and cell-mediated immunity. PGA is a T cell-independent type II antigen, making it weakly immunogenic, and thus generates weak antibody responses, enabling the bacteria to evade immune responses via subverting phagocytosis¹²⁰. Even though it is possible to activate the classical complement pathway of *B. anthracis* spores¹²¹, expression of capsule is also believed to block opsonization by antibodies, and many current efforts have been made to design MAbs against the capsule, which have shown to protect mice against lethal challenge^{122–124}. This suggests that the PGA capsule is essential for bacterial dissemination from the lungs into circulation. Drysdale *et al.* demonstrated this by showing that fully virulent

pXO1⁺ pXO2⁺ *B. anthracis* strain UT500 could be detected in the spleens of BALB/c mice, whereas a strain with the capsule synthesis operon attenuated could not be detected in the spleen and had minimal signs of pathology in lungs and spleen¹²⁵.

Recent studies are beginning to recognize additional roles of PGA in pathogenesis. PGA is not solely expressed on the cell surface. In fact, it is polymerized on the cell surface until it reaches a high molecular mass, where it is then degraded to a lower molecular mass polymer and is released from the bacteria¹²⁶. PGA levels in blood appear in later stages of disease (after 24 hours) in mice, rabbits, and non-human primates and is capable of reaching concentrations as high as 500 µg in mice¹²⁷, correlating with the level of bacteria in circulation^{128–130}. Jang *et al.* demonstrated that co-administering PGA with LT can enhance LT lethality *in vitro* in J774.1 cells as well as in BALB/c mice, though the exact mechanism is unknown¹³¹. Interestingly, Cho *et al.* showed that PGA can activate caspase-1 and induce IL-1β secretion in human THP-1-derived macrophages, suggesting that PGA may contribute to the inflammatory cytokine storm and could explain the enhanced lethality of co-administered PGA and LT¹³². Supporting this theory are reports that PGA has shown to bind to TLR-2, inducing proinflammatory cytokines^{133,134}. However, Ahn *et al.* demonstrated that PGA derived from *Bacillus subtilis* upregulated proinflammatory mRNA, specifically IL-1β, TNF-α, and IL-6 in bone marrow-derived macrophages while simultaneously inhibiting inflammasome activation, suggesting a role for PGA in reducing inflammation. This was conclusively shown by challenging mice with LPS and PGA, in which PGA protected mice against LPS challenge¹²⁵. This is supported by a report showing PGA suppresses Th-17 responses and promotes the differentiation of anti-inflammatory regulatory T

cells¹³⁵. PGA therefore may play a role enhancing innate immune cell death while additionally quelling innate immune responses.

Whether through interaction with TLR-2 or other additional pathways, the immune outcomes of PGA are profound. It was recently shown that immature DCs differentiated from monocytes in the presence of PGA had an attenuated maturation following peptidoglycan stimulation and secreted high levels of IL-8¹³⁶. It has also been shown that PGA stimulation of bone marrow-derived DCs (BMDCs) led to the release of Th₁ cytokines that skew naïve T cells to a Th₁ phenotype¹³⁷, an undesirable immune phenotype against extracellular pathogens. Paradoxically, the authors report this was dependent on TLR-4 signaling. PGA can stimulate natural killer DCs and displays anti-tumor activity¹³³. Despite all of the information currently gathered demonstrating the effects of PGA on various aspects of the immune response, further studies are needed to elucidate the exact mechanism of PGA's enhancement of lethality *in vivo*.

1.3.5 Current Vaccine Strategies against Inhalation Anthrax

Most vaccine strategies, including the current FDA-approved vaccine, center around inclusion of PA as it is believed that neutralizing its ability to heptamerize and translocate LF and EF into the cytosol is critical to prevent dissemination of the bacteria and toxemia associated with mortality¹⁰². Indeed, a number of monoclonal antibodies have been generated that confer toxin neutralizing capacity *in vitro and in vivo*¹³⁵. A recent study demonstrated that anti-PA antibody titer and toxin neutralization titer following prime-boost vaccination did correlate with protection in New Zealand white rabbits challenged intranasally with Ames strain spores¹³⁸. In a similar study with guinea

pigs, it was shown that antibody titer did not correlate with protection, however toxin neutralization titer did correlate following prime-boost vaccination¹³⁹.

Anthrax Vaccine Adsorbed

Currently, the only FDA-approved vaccine against anthrax is the Biothrax Anthrax Vaccine Adsorbed (AVA), which is manufactured by Emergent Biodefense Corporation, formerly BioPort Corporation. Approved in 1970, this vaccine is described as “a sterile, milky-white suspension...made from cell-free filtrates of microaerophilic cultures of an avirulent, non-encapsulated strain of *Bacillus anthracis*.” These cell-free filtrates are adsorbed to aluminum hydroxide in a sodium chloride solution, which is injected intramuscularly (IM). The current vaccine regimen requires three IM doses within the first six months followed by boosters at 12 and 18 months, and yearly boosters following. It is believed that PA is the most immunogenic component of the AVA vaccine, and that anti-PA neutralizing antibodies are the correlate for protection.

AVA has not had a controlled clinical study performed to evaluate its vaccine efficacy against inhalation anthrax due to the lack of infectious occurrences in the modern times, therefore establishing human correlates for protection are difficult. The first study conducted to evaluate a similar PA-based vaccine formulation derived from the F1-NP mutant of the Vollum strain of anthrax in humans was performed between 1955-1959 by Brachman *et al.*⁴. Mill workers during this time were at high risk of anthrax exposure from goat hair, hence workers from four textile mills were immunized with three injections at two-week intervals, followed by another three injections at six-month intervals, with yearly boosters afterward. During the course of this study, 26 cases of

anthrax occurred, with 21 cases of cutaneous anthrax and five of inhalation anthrax. Three of the cases occurred in vaccinated individuals, though only one of these had received a “complete vaccine” consisting of the first three immunizations. Hence, the efficacy was determined to be 92.5 percent, however protective efficacy against inhalation anthrax could not be determined due to the low sample size. Another study performed by the Centers for Disease Control and Prevention between 1962 to 1974 in textile mills found that of 27 cases of cutaneous anthrax identified, none occurred in individuals who received at least the first three immunizations – two cases occurred in individuals who received less than three immunizations⁴. These results suggest that AVA is an effective vaccine candidate against cutaneous anthrax, however it requires multiple immunizations in order to achieve protective immunity. Additionally, its protective efficacy in humans against inhalation anthrax has yet to be demonstrated.

AVA efficacy against inhalation anthrax has been studied in multiple animal models. In mice (A/J, BALB/cJ, and CBA/J strains) immunized three times with the AVA vaccine, protection could not be achieved against cutaneous challenge using the fully virulent V1b strain¹⁴⁰. This is because mouse models are quite difficult to model anthrax immunity due to their high susceptibility to polyglutamic acid capsule positive strains of anthrax – the 100% lethal dose is at most 20 spores in CBA, C57BL/6, and BALB/c mouse strains¹⁴¹. Protection in guinea pigs is very difficult to achieve, as antibodies directed against PA appear to not correlate with protection⁴. However, rabbits and non-human primate models appear to have the most similar disease pathology and immune responses to humans, and anti-PA antibody titer does appear to correlate with protection in rabbits against intranasal challenge with *B. anthracis* Ames strain⁴. Studies

have shown complete protection in rhesus macaques against aerosol challenge with *B. anthracis* Ames strain, even after a single dose of AVA⁴. Despite the variable responses in various animal models, the high levels of protection achieved in rabbits and rhesus macaques supports the purported efficacy of the AVA vaccine. Recently, addition of a B-class CpG DNA adjuvant CPG 7909 (TLR-9 agonist) to the AVA vaccine was evaluated in a phase I clinical trial and shown to be well tolerated, both accelerating and enhancing antibody response to PA by 6-8-fold¹⁴², hence it may be possible to reduce the number of immunizations.

Despite the body of evidence supporting the efficacy of AVA in both human and animal studies, this vaccine platform has a few major limitations. Firstly, the cell-free filtrate used in the AVA vaccine is not well defined¹⁴³, and batch to batch variability could presumably be very high. Second, as mentioned above, protective efficacy in both human and animal models requires multiple immunizations (generally at least three) in order to achieve purported protective antibody titers⁴. From a patient compliance standpoint, the requirement for multiple immunizations is undesirable, and this is highly non-ideal for military personnel who are being deployed, as the first three immunizations occur over the course of six months. The requirement for multiple immunizations is also highly non-ideal in the event of mass exposure of civilian and warfighter populations. In addition to the requirement for multiple immunizations, there have been injection-site reactogenicities reported with aluminum-based vaccines. A large comprehensive review by the Committee to Assess the Safety and Efficacy of the Anthrax Vaccine in 2000 concluded that local events (redness, swelling, nodules) were fairly common in vaccinees, systemic reactions (fever, malaise, myalgia) occurred but were less

common, and immediate-onset health effects that causes brief functional impairment could occur as well⁴. Therefore, it would be desirable to design vaccine formulations that are safer to administer. Lastly, there are concerns of thermal stability with proteins adsorbed to aluminum-based adjuvants^{5,6}, hence there is a need for an anthrax vaccine that can provide rapid and long-lived immunity, ideally in a single dose, and is thermostable.

Additional PA-based Vaccines

In an attempt to improve consistency of vaccine batches, recombinant protective antigen (rPA) has been produced in various bacterial strains and has demonstrated protective in guinea pigs¹⁴⁴, rabbits¹³⁸, and non-human primate¹⁴⁵ models against aerosol challenge. This protection appears to be largely antibody based, as high antibody titer and *in vitro* toxin neutralization seem to determine whether animals are protected or not. Interestingly, rhesus macaques immunized with a single dose of rPA adjuvanted with either aluminum hydroxide, saponin QS-21, or monophosphoryl lipid A (MPL) in squalene/lecithin/Tween 80 emulsion (SLT) were completely protected against the fully virulent Ames strain lethal challenge six weeks PI¹⁴⁵.

Whole-cell Vaccines

Currently, Russia and China have approved the use of an attenuated, live spore anthrax vaccine¹⁴⁶. Despite the difficulties with protecting mice against intranasal lethal challenge of the Ames strain using PA-based vaccines, mice can be protected against Ames strain lethal challenge by using non-encapsulated whole-cell vaccines or

spores¹⁴⁶. In fact, it has recently been reported that two doses of alhydrogel-adjuvanted formalin-inactivated spores adjuvanted from *Bacillus cereus*, an avirulent bacteria, provided BALB/c mice significant protection against aerosolized challenge with the Ames strain, suggesting that generating immune responses against spore antigens may be important for providing protection¹⁴⁷.

Poly-D-γ-glutamic acid Capsule-based Vaccines

In addition to the evidence supporting generating antibodies against PA as well as whole cell and spore antigens, the PGA capsule has become of recent interest as a vaccine candidate. As previously mentioned, fully virulent strains of anthrax are those that are both capsule and toxin positive, and despite the ability to protect non-human primates with the current AVA vaccine in a single shot¹⁴⁵, mice are extremely susceptible to capsulated strains of *B. anthracis*, making vaccine design difficult to evaluate in mice¹⁴⁸. As PGA has been shown to be critical for the dissemination of *B. anthracis* from the lungs into circulation, it is believed that generating opsonizing antibodies against the capsule may enhance bacterial clearance. Indeed, multiple studies have demonstrated protection through passive anti-PGA antibody transfer in mice against the fully virulent Ames strain^{122–124,127,149}. Glinert *et al.* showed that while vaccination with PA was protective against subcutaneous challenge with Ames strain spores, it failed to protect against intravenous (IV) challenge with vegetative Ames strain cells, thus suggesting that neutralizing PA alone is not sufficient for protection in later stages of disease¹⁴⁹.

PGA has shown promise as a vaccine candidate, despite being poorly immunogenic. Due to its low immunogenicity, early attempts included conjugating it with more immunogenic proteins, such as PA¹⁵⁰ and BSA¹⁵¹. Chabot *et al.* demonstrated complete protection in rhesus macaques using PGA conjugated to the outer membrane protein complex (OMPC) of *Neisseria meningitidis* using prime-boost vaccination over 28 days¹⁵². Unfortunately, this vaccine failed to protect New Zealand white rabbits. This is likely due to the necessity for PA to be incorporated into the anthrax vaccine, as PA has already shown to protect rabbits¹³⁸. This hypothesis is further motivated by work from Glinert *et al.*, who showed that despite the inability of PA to protect New Zealand white rabbits against IV challenge with vegetative Ames strain cells, complete protection could be achieved if rabbits were co-immunized with PA plus a secreted protein fraction containing PGA and other secreted proteins from a toxin-null anthrax mutant¹⁴⁹. Therefore, inclusion of multiple antigens can likely aid in improving immune responses against anthrax. It is important to note, however, that the challenge in this study was not intranasal, so it is not certain how mice would be protected from intranasal lethal challenge.

Inclusion of multiple antigens, PA and PGA in particular, is capable of providing protection in mice. Candela *et al.* demonstrated complete protection in OF1 mice, an outbred strain of mice, against subcutaneous challenge of fully virulent *B. anthracis* 9602 following co-immunization with PA and a PGA-peptidoglycan conjugate that was purified from *Bacillus lecheniformis*¹⁵³. Only partial protection was afforded when immunizing mice with either PA or PGA alone. Unfortunately, however, this protection required four vaccinations over the course of 42 days, which is not non-ideal, as well as

the fact that the challenge was subcutaneous and not intranasal. Regardless, the fact that PGA demonstrates protective efficacy in non-human primates following IN lethal challenge as well as enhances immunity when co-immunized with PA suggests there may be promise in improving upon the currently approved AVA vaccine by inducing antibodies that neutralize PA and also opsonize the bacteria directly, thus improving cell-mediated immune responses and subsequently bacterial clearance.

Lethal Factor-based Vaccines

LF may demonstrate the ability to be a successful vaccine candidate. This is supported by the observation that the AVA vaccine does contain trace quantities of LF, humans immunized with the AVA vaccine develop antibody titers against LF^{154,155}, and CD4⁺ T cell responses to LF *ex vivo* were found to be similar in patients immunized with the European-licensed vaccine (anthrax vaccine precipitated, or AVP) to those who survived cutaneous anthrax infection, whereas vaccinees did not generate CD4⁺ T cell responses to PA¹⁵⁶. This CD4⁺ T cell response was found to correlate with domain III of LF. Recent work by Baillie *et al.* demonstrated that both the full length LF and a truncated protein (domain I of LF) fully protected BALB/c mice from intraperitoneal challenge with STI spores of anthrax¹⁵⁷. However, this antigen has yet to show protection in animal models against lethal intranasal challenge with a fully virulent *B. anthracis* strain and needs to be further evaluated.

Additional Anthrax Vaccine Considerations

Despite the numerous studies citing the protective efficacy of both the AVA vaccine and recombinant PA, PA is a highly labile protein, demonstrating loss in toxin neutralization activity after only two minutes stored at elevated temperatures¹⁵⁸.

Therefore, improved anthrax vaccines need to be developed that are able to maintain or improve immune responses to PA while improving shelf stability.

Much focus on anthrax vaccines is towards developing humoral immunity, characterized by robust antibody titers against PA as well as *in vitro* toxin neutralization assays for correlates of protection. However, as mentioned above, it may be important generate immune responses that balance cell-mediated and humoral immunity. For example, Glomski *et al.* questioned the dogma of humoral immunity by demonstrating that mice passively transferred immune serum from formalin-inactivated anthrax spore (FIS)-immunized mice were not protected against subcutaneous challenge with a toxin-attenuated, capsulated spores of *B. anthracis*, however protection in naïve μ MT mice (lacking mature B cells) passively transferred splenocytes from FIS-immunized mice were protected¹⁵⁹. These results, though not evaluated with the Ames strain, suggest that cell-mediated immunity may critically important for protection, especially early during infection in order to target non-vegetative spores.

Based upon the successes of multiple anthrax antigens, it may be important to target antigens other than solely PA, or incorporate additional adjuvants, that are able to improve the breadth of the immune response against anthrax. For example, human individuals who survived cutaneous anthrax infection developed memory CD4⁺ T cells that secrete a diverse cytokine profile, including Th₁, Th₂, and Th₉ cytokines following

restimulation with domain III of LF, whereas CD4⁺ T cells from individuals vaccinated with AVP fail to induce diverse cytokine secretion¹⁶⁰. As PA additionally fails to induce IFN- γ -secreting CD4⁺ T cells in vaccinated individuals¹⁵⁶, additional strategies should be employed to ensure a robust and balanced immune response against anthrax can be achieved.

1.3.6 Summary

B. anthracis is a highly pathogenic organism that causes near complete mortality after only a few days if untreated. Currently, there exists the FDA-approved AVA vaccine against anthrax that likely is capable of protecting humans, however it is limited in that it is not a well-defined formulation, requires multiple immunizations to achieve purported protective immunity, contains reactogenic aluminum, and doesn't provide rapid immunity. In addition, PA is a highly labile protein, whose shelf stability must be improved. Most studies against anthrax rely heavily on generating humoral immunity against PA, though humoral immunity alone may be insufficient, particularly in mouse models. Recently, additional antigens, including LF and PGA, have been evaluated as vaccine candidates in multiple animal models. However, there are no reports of an anthrax vaccine platform that provides rapid protective immunity, in as little as 14 days PI, which is critical in the event of mass exposure to civilians and warfighters. Therefore, there still remains a critical need for a vaccine platform against inhalation anthrax that properly stimulates both cell-mediated and humoral branches of the immune system and is capable of providing both rapid and long-lived protective immunity, ideally in a single dose.

1.4 Bovine Respiratory Syncytial Virus

1.4.1 Introduction

Human respiratory syncytial virus (HRSV) is a leading cause of severe acute lower respiratory tract disease in infants and young children worldwide⁷ and accounts for up to 70% of hospitalized bronchiolitis cases in industrialized countries⁸. Globally, there are an estimated 33 million new episodes of HRSV-associated disease in children under five years of age with more than 100,000 resultant deaths⁹. Severe RSV infection has been linked with the development and exacerbation of recurrent wheezing and asthma¹⁰, and is a predisposing factor to the development of otitis media¹¹. RSV infection has a devastating, worldwide impact on human health and despite significant efforts, no approved vaccine currently exists for use against the disease in humans.

Bovine RSV (BRSV) is closely related to HRSV and a significant cause of morbidity in young cattle. BRSV infection in calves displays many similarities to RSV infection in humans, including similar age dependency and disease pathogenesis, making it an attractive animal model for vaccine studies with HRSV (recently reviewed in ¹⁶¹). Although vaccines have been widely available for BRSV for decades, their efficacy in the field is problematic, and BRSV infection in calves continues to have significant impacts on animal health and the agricultural economy^{162,163}.

BRSV is an enveloped, negative-stranded RNA virus that is a member of the *Pneumovirus* genus (Figure 1.4)¹⁶⁴. This virus is pleomorphic, with either a rounded or filamentous shape. The envelope of the virus contains lipids derived from the host plasma membrane, as well as three virally encoded transmembrane surface glycoproteins, namely the large glycoprotein G, fusion protein F, and small hydrophobic

protein SH, but it is the former two which appear to play a critical role in viral replication¹⁶⁴.

1.4.2 BRSV Pathogenesis

As previously mentioned, the pathogenesis and disease symptoms between humans and cattle are similar. In cattle, BRSV can have massive detrimental effects between autumn and winter seasons, with a high morbidity (60-80%), and upwards of 20% mortality rates¹⁶⁵. This pathogen has been found in cattle from Europe, America, and Asia, and is highly contagious, being transmitted by direct contact via aerosolization¹⁶⁴. Following inhalation of viral-containing aerosols, the virus deposits within both the upper and lower airways of the lungs. The virus preferentially replicates superficially on the ciliated epithelium of the lungs, where it utilizes the surface glycoproteins to attach and fuse with the host cell membrane, enabling the release of the nucleocapside into the cytosol¹⁶⁴. The nucleocapside is a ribonucleoprotein complex that contains one copy of the genome and the machinery that initiates viral transcription and later genome replication. During transcription, the viral RNA-dependent RNA polymerase transcribes messenger RNA and is regulated by the chaperone phosphoprotein while the nucleoprotein protects the genomic RNA from RNase degradation¹⁶⁴. Once enough viral protein is translated into protein, the viral RNA polymerase switches to what is called read through mode, in which viral replication commences. During this step, positive-sense RNA is synthesized, which acts as template to synthesize additional negative-sense RNA. After this is complete, the nucleocapside is assembled within the cytoplasm and coordinates with a matrix protein

M to traffic to the cell membrane which contains virally-produced surface glycoproteins¹⁶⁴. There, the viral particle assembles and viral budding can be observed on the cell surface, after which the virus is released and continues on to infection additional cells.

Interestingly, no cytopathology is observed *in vitro* in epithelial cell cultures infected with either BRSV or HRSV¹⁶⁶, suggesting (much like with *Y. pestis* infection) that the host response to this pathogen is what causes the severity of disease. This is corroborated in the clinical signs and symptoms that develop. Following an incubation period between 2-5 days, microscopic lesions develop in primarily in the cranioventral region of the lungs, with exudative inflammation in the bronchi, alveolar collapse, and a high degree of cellular infiltration to the inflamed tissue¹⁶⁴. Due to the inflammation, necrotic tissue and cellular debris can collect in the epithelium and often obstructs the bronchoalveolar lumen⁷. In addition, viral fusion with host cells results in the synthesis of a small peptide virokinin, which induces the contraction of smooth muscle cells and constricts the lung airways¹⁶⁴. This can result in labored breathing, including polypnea, dyspnea, audible wheezing, and in cattle can result in depression and anorexia¹⁶¹. Therefore, it is critical to understand the molecular basis for how this pathogen interacts with host cells to reduce the severity of this infection.

1.4.3 BRSV Mechanisms of Action

G glycoprotein

The G glycoprotein is a 257-264 amino acid, heavily glycosylated nonglobular type II glycoprotein (depending on the isolate) that resembles cellular mucins and is the

major attachment protein¹⁶⁴. It is synthesized either in a membrane-anchored form or secreted form, with approximately 80% in the secreted form 24 hours post-infection¹⁶⁴. The surface-bound protein forms a trimer and is believed to attach to the cell surface by interacting with heparin-binding domains with glycosaminoglycans on all cell membranes¹⁶⁷; it appears vital to viral pathogenesis *in vivo*, as knocking out this gene attenuates viral replication. It has been hypothesized that the secreted form of the protein acts as a decoy by binding to neutralizing antibodies, however its exact role in disease pathogenesis is not well understood.

F glycoprotein

The RSV F protein is a 574 amino acid protein that is responsible for viral penetration into host cells. It is highly conserved between virus strains, as well as between HRSV and BRSV, demonstrating approximately 80% homology¹⁶⁸. This protein is a type I viral fusion protein that exists in two forms on the viral surface: a metastable pre-fusion form and a stable post-fusion form¹⁶⁹. It is initially synthesized as an inactive precursor called F0, which is cleaved by furin to its active heterodimer form¹⁶⁴. This heterodimer then functions by fusing the viral and cell membranes, resulting in delivery of the nucleocapsid into the cytosol; hence, this protein is also indispensable for viral replication. The F protein is also responsible for the formation of the RSV characteristic syncytia, which are the presence of multinucleated cells formed via fusion of infected cells to healthy host cells found in the lumen and epithelium of infected lung tissue¹⁶⁴.

1.4.4 Current Vaccination Strategies against BRSV

RSV-specific immune responses are directed against a number of viral proteins; however, the fusion (F) and attachment (G) proteins appear to be the most important targets¹⁶⁷. Although still not entirely understood, it is believed that neutralizing IgG and IgA have a role in protection from RSV. Adults repeatedly infected with RSV demonstrate robust levels of IgA in nasal secretions, which has shown to prevent virus replication in the upper airways, regardless of serum Ig levels^{170,171}. Mucosal IgA also plays an important role in reducing the occurrence and severity of RSV infection in infants and children¹⁷². However, in adults, IgA responses can wane¹⁷¹ and the IgG response may be more important in long-term protection.

However, there is still a poor understanding of the immune responses that are most important for protection from RSV disease in the neonate, and even less appreciation for the role of maternal antibody in protection from infection. Some studies suggest that maternal antibody can prevent RSV infection^{173,174}; and systemic, prophylactic administration of Palivizumab, a monoclonal antibody that is specific to the RSV F protein, is effective at reducing RSV-related hospitalization in high-risk infants¹⁶⁵. However, both human infants^{175–177} and calves¹⁷⁸ with maternal antibodies still develop severe RSV disease; and in infants, there is no correlation between titers of virus-specific maternal IgG and prevention of hospitalization with RSV^{176,179}.

The pre-fusion F protein contains antigenic site Ø, and recent evidence suggests that this epitope is the primary target for neutralizing antibodies in humans¹⁸⁰. Vaccine formulations incorporating the pre-fusion form of the F protein are highly efficacious in rodent models^{169,181–183}; and a highly efficacious pre-fusion F vaccine was also recently reported for BRSV¹⁶⁸, suggesting that the antigenic Ø site is conserved and of

immunologic relevance to the calf model as well. In addition, the post-fusion form of the F protein contains two major neutralizing epitopes, antigenic sites II and IV¹⁸⁴. High-affinity, site-II directed neutralizing antibodies are protective in mice and cotton rats^{185,186}. Post-fusion F is also highly stable, making it an appealing candidate for incorporation into a subunit vaccine.

Reports in mice have shown that vaccines that elicit G-protein specific antibody and T cell responses are protective against RSV infection^{187,188}. Bastien *et al.* also demonstrated that immunization with a conserved peptide from the BRSV G protein afforded partial protection against BRSV infection in cattle¹⁸⁸. The F and G protein have also been shown suitable vaccine targets in cattle, as recombinant vector-vaccines targeting the BRSV F^{189,190} and G^{190–192} proteins, and recombinant plasmid-based strategies targeting the G protein^{192,193}, have both been shown to reduce virus shedding and BRSV-associated lung pathology in challenged calves.

1.4.5 Summary

Human respiratory syncytial virus (HRSV) is a leading cause of severe acute lower respiratory tract disease in infants and young children worldwide. Following inhalation of viral-containing aerosols, the virus deposits within both the upper and lower airways of the lungs, where it preferentially replicates superficially on the ciliated epithelium of the lungs, utilizing the surface glycoproteins F and G proteins to release the nucleocapsid into the cytosol that induces viral transcription and replication. Due to their indispensable roles in viral pathogenesis, the post-fusion F glycoprotein and G

glycoprotein are attractive vaccine candidates for generating high titer antibodies that neutralize the binding and fusion of the virus to host cells.

1.5 Vaccine Adjuvants

Vaccination is an effective strategy to combating disease by establishing a strong immune defense against foreign pathogens before the individual is exposed to the organism. In an attempt to move away from whole-cell organisms, which have risk of causing deleterious side effects, many current strategies employ subunit vaccines, which generally consist of antigens derived from the pathogen or produced recombinantly. However, these vaccine antigens are generally weakly immunogenic when administered alone and require the inclusion of additional materials to enhance immune responses to vaccine antigens, termed adjuvants. The following section will describe traditional adjuvants studied and motivate the need for next-generation adjuvants.

1.5.1 Traditional Adjuvants

An adjuvant is any material that has the potential to modulate the immune response. These materials are typically employed with vaccines in order to improve vaccine efficacy through reducing the optimal dose of vaccine, increasing the robustness of the immune response, and/or modulating the phenotypic response of various immune cells¹⁹⁴. Traditionally, adjuvants have been divided into either 1st or 2nd generations.

1st generation adjuvants are simply classified as either delivery systems or immune potentiators (Table 1.1). Examples of delivery systems include alum, MF59, polymeric microparticles, and liposomes¹⁹⁴. MF59, which consists of a squalene oil-in-water emulsion, along with the water insoluble aluminum salts, were classically known to provide a 'depot effect' *in vivo*, in which the antigen is slowly released from the water insoluble adjuvant phase, allowing for controlled release of antigen over time¹⁹⁵. Unlike emulsions, liposomes and polymeric particles act as a delivery vehicle by encapsulating the vaccine constituent, thereby releasing the antigen via triggered release mechanisms¹⁹⁶ and controlled degradation kinetics¹⁹⁷, respectively. Hence 'delivery vehicle' is a broad description of the many routes by which vaccines can be control released from a carrier vessel.

Examples of immune potentiators include monophosphoryl lipid A (MPL), CpG DNA, poly(I:C), cyclic dinucleotides (CDNs), double-stranded RNA, and small molecule potentiators¹⁹⁴. Many of these immune potentiator adjuvants are derived from and exploit known biological signaling pathways in order to modulate the immune response to vaccine formulations. For example, MPL is a detoxified derivative of LPS, the cell wall component of Gram-negative bacteria, and is an agonist for toll-like receptor 4 (TLR-4) on host immune cells¹⁹⁸.

It should be noted that the traditional view of 1st generation adjuvants is not entirely complete, as some delivery systems have also been found to have immunomodulatory capabilities. For example, alum's adjuvant mechanism (through the depot effect) is currently being challenged, as removal of the alum-containing injection site shortly after administration did not alter B and T cell activation or antibody

production *in situ* compared to control mice that retained the injection site, suggesting another mechanism other than the depot effect was driving adaptive immune responses¹⁹⁹. It is now known that alum provides immunomodulatory capabilities, though its exact mechanism of action is still being investigated^{200,201}. Additionally, as will be discussed later in this review, polymeric nano- and microparticles demonstrate immunomodulatory capabilities^{15,17,18,202–206}. Therefore, this broad generalization of adjuvants as solely delivery vehicles is incomplete.

2nd generation adjuvants have expanded upon the concept of 1st generation adjuvants by trying to modulate immune responses through encompassing both features of vaccine delivery as well as immune potentiation (Figure 1.5). Such examples include Complete Freund's adjuvant, and GlaxoSmithKline's FDA-approved AS01b, AS03, and AS04 adjuvants. Complete Freund's adjuvant contains inactivated *Mycobacterium tuberculosis* emulsified in mineral oil; AS01b is a liposomal-based adjuvant containing MPL and the saponin QS-21; AS03 consists of an immune potentiator alpha tocopherol emulsified with MF59; AS04 consists of MPL adsorbed to alum.

1.5.2 Current FDA-approved Adjuvants

The first FDA-approved adjuvant and to date mostly widely used are aluminum-based. These include aluminum phosphate, aluminum hydroxide, potassium aluminum sulfate (alum), or mixed aluminum salts. Its adjuvant properties were demonstrated over ninety years ago by Glenny *et al.*, who showed that alum enhanced antibody responses to diphtheria toxin¹⁹⁵, presumably via the depot effect. Since then, aluminum

has been used extensively in a wide range of vaccine formulations. Alum is a potent inducer of Th₂ immune responses^{48,207}, characterized by robust humoral responses against extracellular pathogens, such as helminths. In contrast to this, adjuvants such as MPL and Complete Freund's adjuvant induce a Th₁ response, characterized by T cells that drive cell-mediated immune responses against intracellular pathogens²⁰⁷

Currently, the list of adjuvants included across all of the current 98 FDA-approved or introduced vaccines is limited to only aluminum salts, MPL, MF59, SD-101, AS01b, AS03, and AS04 (Table 1.2)^{194,208,209}. This list is ever-increasing, considering the vaccines containing SD-101 and AS01b were approved in 2017.

1.6 Next-Generation Adjuvants

Extensive research is underway to increase the pool of adjuvant candidates that are both biocompatible and immunomodulatory, however the small pool of adjuvants currently available limits future vaccine development, and there are still many needs and challenges that traditional adjuvants do not address. These include the need to design vaccine formulations that, while being highly effective, are very safe, have a broad protective age range for the young and elderly, improve patient compliance (i.e., needle-free and single dose), reduce cost through dose sparing, and overcome cold chain challenges for long term storage on the shelf or in harsh conditions. This will require the development of novel next-generation adjuvants and tailoring immune responses through a combinatorial adjuvant approach, in order to increase the robustness and breadth of the immune response. This section will introduce a few novel adjuvants that have recently shown promise as vaccine adjuvants.

1.6.1 Cyclic Dinucleotides

A promising new class of adjuvants is represented by cyclic dinucleotides (CDNs). CDNs are small molecules composed of two purine molecules linked together, with the prototypical CDNs being cyclic di-GMP (CDG), cyclic di-AMP (CDA), and cyclic AMP-GMP (cGAMP). These molecules are found in many bacterial and mammalian cells, and play a host of different roles, depending on the organism. In fact, CDG, composed of two GMP molecules linked by two 3'-5' phosphodiester bonds, has recently been recognized as a universal secondary messenger molecule in Gram-negative bacteria, playing a variety of roles in bacterial development, motility, biofilm formation, and virulence (Figure 1.6)²¹⁰. Despite playing such a critical role in the bacterial life cycle, these molecules are recognized as PAMPs by mammalian host cells. The PRR responsible for recognition of CDNs is a transmembrane endoplasmic protein called STING (STimulator of Interferon Genes) which, as its name suggests, binds to cytosolic CDNs and induces expression cytokines and chemokines, including type I IFNs (Figure 1.7)²¹¹. Found in a variety of organs, including the heart, spleen, kidney, placenta, lung and peripheral leukocytes²¹², STING is able to recognize intracellular bacteria, viruses, and protozoa through its ability to bind directly to a wide variety of CDNs, including CDG, CDA, cGAMP²¹¹. Protozoa and viruses don't express CDNs, however another cytosolic protein called cyclic GMP-AMP synthase (cGAS), was discovered to recognize cytosolic double stranded DNA and synthesize cGAMP, which then can bind to STING and activate type I IFN responses²¹¹.

These molecules have recently been studied as vaccine adjuvants due to their potent adjuvant activity, while CDG is the most characterized CDN adjuvant to date. Karaolis *et al.* first demonstrated CDG's adjuvant potential by co-administering CDG

along with *S. aureus* clumping factor (ClfA) in mice, which produced significantly higher anti-ClfA IgG titers and had enhanced recruitment of activated monocytes and granulocytes to the immunization site²¹³. Human immature DCs cultured with CDG had increased levels of costimulatory markers CD80/CD86, proinflammatory cytokines (including IL-12 and IFN- γ), and chemokine receptor expression. Interestingly, mature DCs activated with CDG enhanced T cell stimulation. Work from this same group also showed that treatment with CDG intranasally alone protected against *Klebsiella pneumoniae* challenge, evidenced by a robust innate immune response in the lungs characterized by enhanced accumulation of neutrophils, activated $\alpha\beta$ T cells, and activated NK cells, which correlated with high expression of chemokines and type I cytokines²¹⁴. Ebensen *et al.* demonstrated that mice immunized with β -gal adjuvanted with CDG displayed a balanced Th₁/Th₂ response characterized by levels of IgG1 and IgG2a in mouse sera, as well as higher levels IFN- γ , IL-2, and IL-4 in *ex vivo* CDG-stimulated splenocyte supernatant²¹⁵. To prove enhanced protective efficacy, Hu *et al.* demonstrated that mice immunized with ClfA adjuvanted with CDG elicited significantly higher levels of IgG1, IgG2a, IgG2b, and IgG3 than mice immunized with ClfA adjuvanted with alum, and these mice had a significantly higher protection following lethal challenge with methicillin-resistant *S. aureus* infection²¹⁶. Collectively, these results demonstrate that CDG is a potent adjuvant whose PRR activation capabilities can be exploited to enhance both humoral and cellular immune responses.

1.6.2 Polymeric Nanoparticles as Adjuvants

Polymers have been studied as biomaterials for tissue regeneration and drug delivery applications for decades, however their ability to adjuvant vaccines has recently become recognized (see Table 1.3 for a list of current polymeric adjuvants being studied). These materials show great promise when formulated as a nanoparticle-based vaccine delivery system^{14,15,17,205,217}. A nanoparticle is a very small particle whose size is on the order of $1-999 \times 10^{-9}$ meters. Polymeric nanoparticles of this small size scale offer many beneficial advantages from a vaccine delivery standpoint. They are generally considered to be biocompatible (i.e., – low level inflammation)¹³, stabilize subunit vaccines^{19,218–220}, have controlled release profiles that can enable single-dose vaccination^{14,221}, and can enhance vaccine shelf life storage over long time periods¹⁹. In addition, they have shown to exhibit immunomodulatory capabilities^{202–204} and can be functionalized for targeted delivery^{222,223}, therefore acting both as a vaccine delivery platform and immune potentiator. As APCs such as DCs and MØ are known to traffic to the draining lymph nodes and present antigen to T cells following internalization and activation of antigen, most current efforts are employed to try to enhance internalization of antigen and subsequent activation by APCs. This requires an understanding the physiochemical properties of the materials in order to best design formulations that are able to best adjuvant antigens.

Physical Properties of Polymeric Nanoparticles that Modulate Immune Responses

A strategy to increase antigen internalization by APCs is the physical internalization of nanoparticles encapsulating antigen. Factors that control cellular internalization of nanoparticles include size, charge, and geometry of the nanoparticles.

Size plays a vital role in targeting specific immune cells and generating appropriate responses. The first barrier that must be crossed in generating appropriate immune responses is the physical barrier, including the mucosa and epithelial barriers in the lungs. Controlling the size of the nanoparticles has been shown to control deposition, cellular uptake, and clearance rates in the lungs, thus allowing for targeting of specific alveolar compartments in the lungs that contain alveolar macrophages and lead to induction of adaptive immune responses²²⁴. Size is also a very important parameter as phagocytic cells, such as dendritic cells and macrophages, have size constraints in the particles that they phagocytize (Figure 1.8)²²⁵. Independent studies with polystyrene and PLGA particles have shown less effective particle uptake levels in microparticles than nanoparticles in DCs with *in vitro* assays, suggesting that DCs are more limited to internalizing particles below 1 μm in diameter^{226,227}. Champion *et al.* demonstrated that between 1-6 μm diameter, microparticles in the 2-3 μm diameter range had the highest internalization in rat alveolar macrophages after one hour²²⁸. Silva *et al.* showed that PLGA nanoparticles encapsulating OVA and the TLR-3 ligand Poly(I:C) were more readily internalized than microparticles, which led to increased presentation to CD8⁺ T cells *in vitro*²²⁷. In addition, they observed greater activation of CD8⁺ T cells *in vivo*, suggesting that nanoparticles must be internalized in order to enhance immune responses to vaccines.

Surface charge plays a critical role in the uptake of nanoparticles. For example, it was observed that 1 μm -sized polystyrene particles modified with various positively charged ligands were more readily internalized by a larger percentage of dendritic cells *in vitro* than their negatively charged counterparts²²⁶. Although size was also shown to

be critical for enhancing the percentage of cells that internalized particles, increasing the positive charge of the particle increased the size of particles that these DCs were able to internalize.

One final physical property consideration is shape of the material. Champion *et al.* demonstrated that rod-shaped particles were less readily up taken by macrophages than spherical particles, and success of the macrophage to initiate phagocytosis depended on the side of the rod initially contacted by the cell²²⁹. In total, consideration of these physical properties of the nanoparticles is important in the effective delivery of antigen into APCs by nanoparticle-based vaccine formulations.

Chemical Properties of Polymeric Nanoparticles that Modulate Immune Responses

In addition to the physical properties of the nanoparticle, the chemistry of the material chosen is an important consideration for nanoparticle design. The chemical properties of the polymer and the payload dictates how the payload will associate, and subsequently distribute, within the particle²³⁰. In addition, the molecular structure and type of bond linkages in the polymer dictate the degradation kinetics of the polymer and also whether the polymer matrix is surface vs. bulk eroding (Table 1.4)²³¹.

Copolymerization of monomers is a powerful strategy that allows for the tuning of the erosion kinetics of the nanoparticles, as increasing the copolymer composition of amphiphilic monomers can increase the ability of water to penetrate the polymer matrix, and therefore the degradation rate and subsequent rate of release of the payload^{231,232}.

Beyond controlling the release kinetics, tuning copolymer composition plays a role in cellular uptake by APCs, and ultimately the immune response to a given antigen.

Petersen *et al.* demonstrated that polyanhydride nanoparticle internalization by bone marrow-derived DCs (BMDCs) *in vitro* correlated with increased sebacic acid composition, which corresponded with elevated expression of CD40L on their surface¹⁶. Ulery *et al.* demonstrated that altering copolymer composition of polyanhydride nanoparticles dictated the number and size of nanoparticles that were internalized by BMDCs¹⁵. Interestingly, copolymer chemistry also controlled the persistence of the nanoparticles within the cells, with the most persistent chemistry displaying 'pathogen mimicking' properties that mimicked those of *Yersinia pestis*, as evidenced by intracellular persistence and cell surface marker expression of MHC II and costimulatory molecules¹⁵.

1.6.3 Polyester Nanoparticle Adjuvants

Polyesters are a class of biodegradable polymers that consist of repeating units of either monomer, dimer, or block chains bound by ester linkages in the polymer backbone²³¹. Generally, ester linkages in these polymers with long aliphatic backbones are considered fairly stable bonds, however polyesters with short monomer backbones, such as those with the hydroxyl group bound to the α -carbon (termed poly(α -hydroxy acids) are less stable and degrade over much shorter time spans via hydrolysis of the ester, making them attractive for use as both a drug delivery and vaccine delivery vehicle^{197,233}.

PLGA

Poly(lactic-co-glycolic acid) (PLGA) is a poly(α -hydroxy acid) that has changed the landscape of the medical industry, whose applications as biodegradable sutures, tissue scaffolds, as well as drug and vaccine delivery devices is one of the greatest contributions of biomedical engineering. This material is biocompatible, biodegradable, and is currently licensed for use by the US Food and Drug Administration (FDA) and the European Medicines Agency. It is currently licensed for use as sutures (Vicryl[®], Vicryl Rapide[®], Polysorb[®], and Purasorb[®]), and has been widely studied as a nanoparticle-based drug and vaccine delivery device, as well as a tissue scaffold for regenerative medicine^{234–236}.

PLGA is a copolymer consisting of monomeric carboxylic acids polylactic acid (PLA) and polyglycolic acid (PGA) (Table 1.5). The polymer degrades via hydrolysis of the ester linkage, whose monomeric degradation products are safe and enter the citric acid cycle, excreting as carbon dioxide and water^{236–238}. Both of these monomers have unique properties that enable fine tuning of the copolymer characteristics when varying the monomeric ratio. For example, PLA contains a methyl group bound to its α -carbon, which endows it an increased hydrophobicity compared to PGA²³⁶. Therefore, PLGA copolymers with a higher molar ratio of PLA are more hydrophobic and result in a slower degradation rate²³⁷. It has been reported that 50:50, 75:25, and 85:15 PLGA copolymers have degradation times of 1-2 months, 4-5 months, and 5-6 months, respectively²³⁹.

PLGA can be fabricated into nanoparticles typically via an oil-in-water single emulsion, in which polymer is dissolved into an organic solvent, the payload is then

added and the suspension is emulsified in larger volume of water, with the resultant precipitate dried to reduce cleavage of the ester bonds²³⁶. For hydrophilic proteins, a water-oil-water double emulsion technique can be employed, where the protein is first dissolved into water, emulsified with the polymer/solvent solution, and finally emulsified in a larger volume of water²³⁶. One detriment to using the double emulsion technique for PLGA nanoparticle synthesis is that low encapsulation efficiencies have been reported, making this synthesis route unattractive from a feasibility standpoint.

PLGA has been studied as a nanoparticle-based vaccine delivery platform^{235,240}. It is believed that nanoparticles are internalized by phagocytic cells, where they then escape the phagolysosome and enter the cytosol, continuing to release antigen and enhance cross presentation to CD8⁺ T cells²³⁵. Silva *et al.* observed enhanced activation of CD8⁺ T cells, as well as a balanced Th₁/Th₂ antibody response, following immunization with 50:50 PLGA nanoparticles encapsulating ovalbumin and poly(I:C)²⁴¹.

The mechanism behind how PLGA both degrades and releases its payload is complex. Depending on the hydrophilicity of the payload, its affinity to PLGA, and copolymer chemistry, the release rate from PLGA nanoparticles can involve desorption of surface-bound protein, diffusion from the polymer matrix following water penetration, and erosion of the nanoparticle matrix²³⁷. The combined effect of the latter two phenomena is a process called bulk erosion. During bulk erosion, water is able to penetrate into the bed of the polymer faster than the surface erosion rate, resulting in swelling of the polymer, uniform degradation of the polymer matrix, and release of the payload (Figure 1.9)²³¹. The uniform swelling of the polymer matrix can result in the rapid release of encapsulated payloads, which makes sustained release difficult to

achieve. Additionally, the degradation rate of PLGA is acid-catalyzed, hence the carboxylic acid degradation products can undergo autocatalysis, where the carboxylic acid products further enhance the degradation rate of the surrounding polymer and enhances bulk erosion²³¹. This can be detrimental to protein stability as prolonged exposure to water and the low pH environment can denature proteins. In fact, the pKa of lactic acid and glycolic acid is 3.08 and 3.83, respectively, making PLGA one of the more acidic biomaterials being investigated (Table 1.6). The prolonged exposure of water in the polymer matrix can also cause denaturing of labile proteins. Therefore, although PLGA has shown much promise as a vaccine delivery device, the issues of bulk erosion, acidic degradation products, and low encapsulation efficiencies further the motivation to design new materials that can overcome such deficiencies.

1.6.4 Polyanhydride Nanovaccines

Polyanhydrides are a novel class of polymers that, like PLGA, have proven effective as a nanoparticle-based vaccine delivery formulation. These materials have proven biocompatible, biodegradable, and are also approved by the FDA. These materials have shown much promise as both drug and vaccine delivery vehicles for a wide variety of applications^{242–244}.

This class of polymers consists of repeating dicarboxylic acid monomers linked via anhydride bonds. Their degradation products are biocompatible and readily enter the citric acid cycle and are excreted as carbon dioxide or harmless dicarboxylic acid monomers²⁴⁵. Polyanhydrides are polymerized via an anhydride exchange mechanism. The synthesis of polyanhydrides was originally reported in 1909 by Bucher *et al.* for isophthalic and terephthalic acids, in which the diacids were dissolved in acetic

anhydride, the solvent distilled off at 200°C, and finally the viscous product maintained at temperature for approximately an hour to yield the final product²⁴⁶. As aliphatic polyanhydrides were known to be highly hydrolytically labile, Conix *et al.* adapted this method for the synthesis of aromatic dicarboxylic acids in 1958, demonstrating high glass transition temperatures and slower degradation kinetics via resistance to hydrolysis due to enhanced hydrophobicity²⁴⁷.

Their first use as a biodegradable device was demonstrated by Robert Langer in 1980, who demonstrated that the degradation of aromatic polyanhydrides could be utilized for the sustained, near zero-order release of cholic acid²⁴⁸. In fact, aided by their safety and biodegradability, the Gliadel[®] wafer, an aromatic polyanhydride copolymer wafer comprising of a 20:80 molar ratio of 1,3-bis-(*p*-carboxyphenoxy)propane and sebacic acid, was approved by the FDA for the sustained release of BCNU, a chemotherapeutic agent used to treat malignant gliomas. These wafers are inserted into the resected areas of the brain, where it releases the active compound over prolonged periods of time. It wasn't until 1993 that Robert Langer's laboratory demonstrated the use of polyanhydrides as a protein delivery device, showing high encapsulation efficiency, structural stability, and zero-order release of multiple model and therapeutic proteins²⁴⁴.

Since then, polyanhydrides have demonstrated efficacy as a vaccine delivery vehicle for numerous antigens. Work out of our laboratory has thoroughly investigated polyanhydride nanoparticle-based vaccines (i.e., nanovaccines) against multiple bacterial and viral pathogens^{14,15,17,205,217}. The polyanhydrides studied consist of random copolymers comprising the aliphatic dicarboxylic acid sebacic acid (SA) and aromatic

dicarboxylic acids 1,6-bis(*p*-carboxyphenoxy)hexane (CPH) and 1,8-bis(*p*-carboxyphenoxy)-3,6-dioxaoctane (CPTEG) (Table 1.5). CPTEG has shown to have the highest rate of erosion, on the order of days, owed to its amphiphilic properties via incorporation of triethylene glycol into the backbone of the monomer²³². Sebacic acid is an aliphatic monomer, and thus has the next highest rate of erosion, which has been reported to be on the order of days to weeks²⁴⁵. Lastly, CPH is a highly hydrophobic monomer, whose erosion rate has been reported to be months to years²³². However, by synthesizing random copolymers and varying the copolymer composition, it is possible to control the rate of degradation of the polymer and subsequent release of encapsulated proteins^{232,249}.

One beneficial characteristic of polyanhydrides that is advantageous over PLGA is that polyanhydrides are hydrophobic and thus exhibit surface erosion, where the rate of water penetration into the polymer matrix is slower than the rate of erosion at the water/polymer interface. This results in the polymer solely degrading inward from the surface of the material, allowing for predictable and sustained release of encapsulated proteins (Figure 1.9). The surface erosion characteristics of polyanhydrides preserves encapsulated proteins, preventing protein aggregation and denaturation by precluding water penetration into the polymer bed; in addition, the dicarboxylic acid degradation products are less acidic than PGA and PLA, and are less detrimental to protein stability.

Polyanhydride nanovaccines provide vaccine delivery benefits and adjuvant properties that make them well suited as a vaccine delivery platform and have been extensively studied as a nanovaccine platform against infectious pathogens such as influenza, BRSV, *Streptococcus pneumoniae*, *Yersinia pestis*, and *Bacillus*

anthracis^{14,15,19,217,219}. These materials exhibit high biocompatibility with minimal injection site reactivity^{13,250,251} (i.e., tenderness, swelling, and pain) in comparison to traditional adjuvants, such as alum, which has been associated with immunization site tenderness and pain. The sustained release of antigen from polyanhydride nanovaccines allows for enhanced bioavailability of antigen to drive adaptive immune responses and enables single-dose administration and dose-sparing capabilities^{14,18,204,252}. In addition, varying polyanhydride copolymer composition has shown to modulate internalization and persistence within APCs *in vitro*, as well as induction of both cellular and humoral immune responses *in vivo*, indicating the ability to tailor polymer chemistry in order to rationally design nanovaccines that optimally inducing antigen-specific protective immunity^{15,16,204,222,223,253–259}.

1.7 Conclusions

Despite the significant advancements in the understanding of pathogenesis of deadly pathogens such as *Y. pestis* and *B. anthracis*, and the ability to work with excellent animal models for respiratory infections such as BRSV, there is a dearth of FDA-approved vaccines that are highly protective against these pathogens. In addition, in the event of potential weaponization of pathogens such as *Y. pestis* and *B. anthracis*, there is a need for vaccines that can provide both rapid and long-lived protective immunity, while also being capable of dose sparing and enhancing shelf stability for rapid response mass immunization strategies. Current vaccine approaches utilize subunit vaccines due to concerns of undesirable side effects with whole cell or attenuated viral vaccines, however these subunit proteins are generally weakly

immunogenic when administered alone and require the addition of an adjuvant to enhance immune responses. The current pool of FDA-approved adjuvants is fairly limited and it would be highly desirable to expand this list of available adjuvants to provide the ability to tailor immune responses through a combinatorial adjuvant approach. In addition, these next-generation adjuvants should provide the ability to enable single dose vaccination, dose sparing, and enhanced shelf stability. Adjuvants such as CDNs and polyanhydride nanovaccines are attractive next-generation adjuvants which, through a combinatorial approach, are capable of providing robust immunity while also enhancing the long-term shelf stability of labile proteins.

1.8 Tables

Table 1.1. Examples of 1st generation adjuvants.

Delivery Systems	Immune Potentiators
Alum	MPL and synthetic derivatives
Calcium phosphate	MDP and derivatives
Tyrosine	CpG oligonucleotides
Liposomes	Alternative bacterial or viral components (i.e., flagellin)
Virosomes	Lipopeptides
Emulsions	Saponins
Microparticles/nanoparticles	dsRNA
Iscoms	Small molecule immune potentiators (resiquimod)
Virus-like particles	CDNs (i.e., CDG, CDA)
Hydrogels/Micelles	Cytokines/Chemokines

Table 1.2. List of Current FDA-approved adjuvants.

Adjuvant	Constituents	Commercial Vaccine Formulation(s)	Manufacturer
Aluminum salts	Aluminum hydroxide	Aluminum salts have been used in a wide variety of vaccines	N/A
	Aluminum phosphate		
	Potassium aluminum sulfate (alum)		
	Mixed aluminum salts		
MPL	Synthetic derivative of LPS	Cervarix (see AS04)	Invivogen
MF59	Squalene oil in water emulsion	Fluad	Novartis
SD-101	Proprietary TLR-9 agonist	HEPLISAV-B	Dynavax
AS01b	Liposomal-based adjuvant containing MPL and the saponin QS-21	Shingrix	GlaxoSmithKline
AS03	Alpha tocopherol emulsified with MF59	Influenza A (H5N1) Virus Monovalent Vaccine	GlaxoSmithKline
AS04	MPL adsorbed to alum	Cervarix	GlaxoSmithKline

Table 1.3 Examples of polymeric adjuvants currently studied.

Polymer Class	Examples	Vaccines studied with	References
Polyanhydrides	CPTEG:CPH, CPH:SA	F1-V, rPA, Influenza NP & HA, PspA, BRSV F & G	14,15,19,205,217,219
Polyesters	PLA, PGA, PLGA	TT, MP rgp120, BSA, HbsAg	260–262
Polymethacrylates	Ethylene Glycol Methyl Ether MA, Hydroxypropyl MA, Isobornyl MA, HEMA	N.A.	203,263,264
Pentablock copolymer gels	PDEAEM based gels, PEG-PCL- PLA-PCL-PEG based gels	Ovalbumin, QA	217,265–267
Poly(N-iso- propylacrylamide- co-acrylic acid)	(Chemical modifications)	N.A.	202
Polyphosphazene polyacids	PCPP, PCEP	Hepatitis B surface antigen, X-31 influenza	268,269

Table 1.4. List of various classes of polymers and their respective polymer erosion front width $(D/k)^{1/2}$ and erosion velocity $(Dk)^{1/2}$ (adapted from ²⁷⁰).

Polymers	k_r (1/s)	D (cm ² /s)	$(D/k)^{1/2}$	$(Dk)^{1/2}$
poly(anhydride)	2E-03	1E-08	20 μ m	2 mm/day
poly(ortho ester)	5E-05	1E-08	140 μ m	1 mm/day
poly(α -hydroxyl ester)	7E-09	1E-07	40 mm	7 μ m/day
poly(amide)	3E-13	1E-08	2 m	50 nm/day

Table 1.5. Chemical structure of polyester and polyanhydride adjuvants.

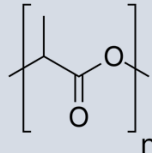
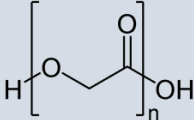
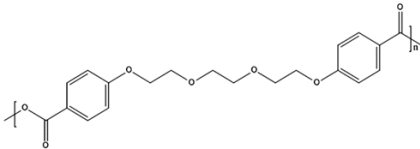
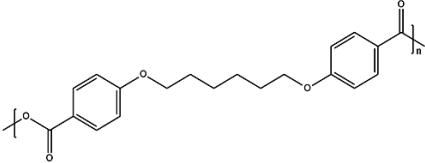
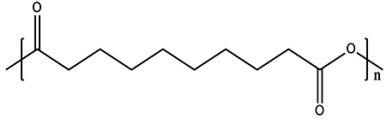
Polymer Class	Examples	Polymer Structure
Polyesters	Lactic acid	
	Glycolic acid	
Polyanhydrides	1,8-bis (<i>p</i> -carboxyphenoxy)-3,6-dioxaoctane (CPTEG)	
	1,6-bis(<i>p</i> -carboxyphenoxy) hexane (CPH)	
	Sebacic acid (SA)	

Table 1.6. pKa values of various polyester and polyanhydride monomers.

Polymer	pKa
Glycolic acid	3.83 ²⁷¹
Lactic acid	3.08 ²⁷²
1,6-bis(<i>p</i> -carboxyphenoxy)hexane	3.7 & 6.7 ²⁷³
1,8-bis(<i>p</i> -carboxyphenoxy)-3,6-dioxaoctane	5.8 & 8.4 ²³²
Sebacic acid	4.8 & 5.6 ²⁷³

1.9 Figures

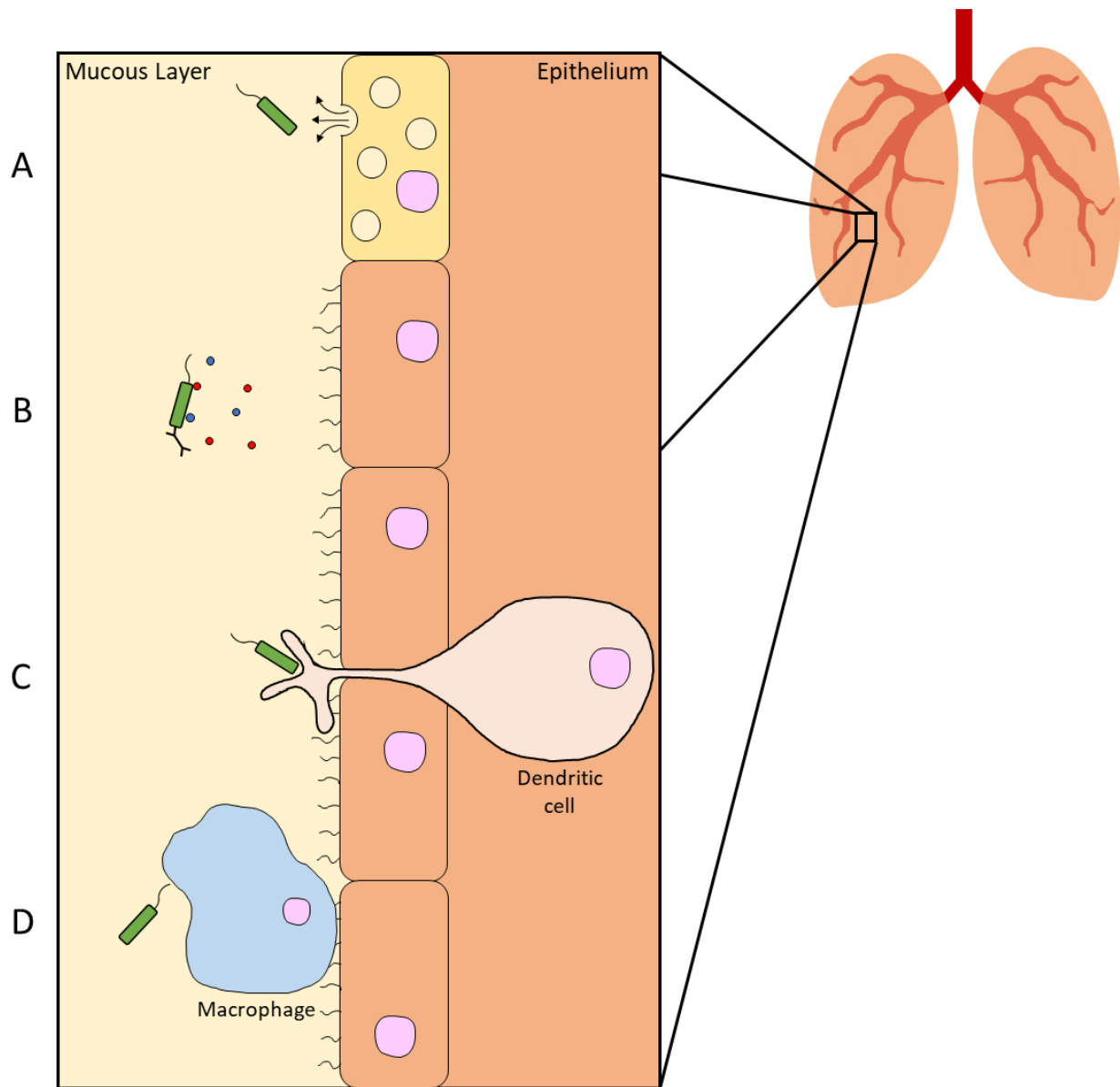


Figure 1.1. Host defense against foreign pathogens in the lungs. The lungs contain multiple fronts against foreign pathogens, including (A) a secreted mucus layer from goblet cells (depicted yellow cell) that prevents bacterial adhesion and (B) secreted antibodies, β -defensins, lysozyme, lactoferrin, and other proteins responsible for either killing the pathogen or blocking adhesion. In addition (C) CD103⁺ dendritic cells and (D) alveolar macrophages act as sentinels, ready to phagocytose and initiate robust innate and adaptive immune responses against detected foreign pathogens.

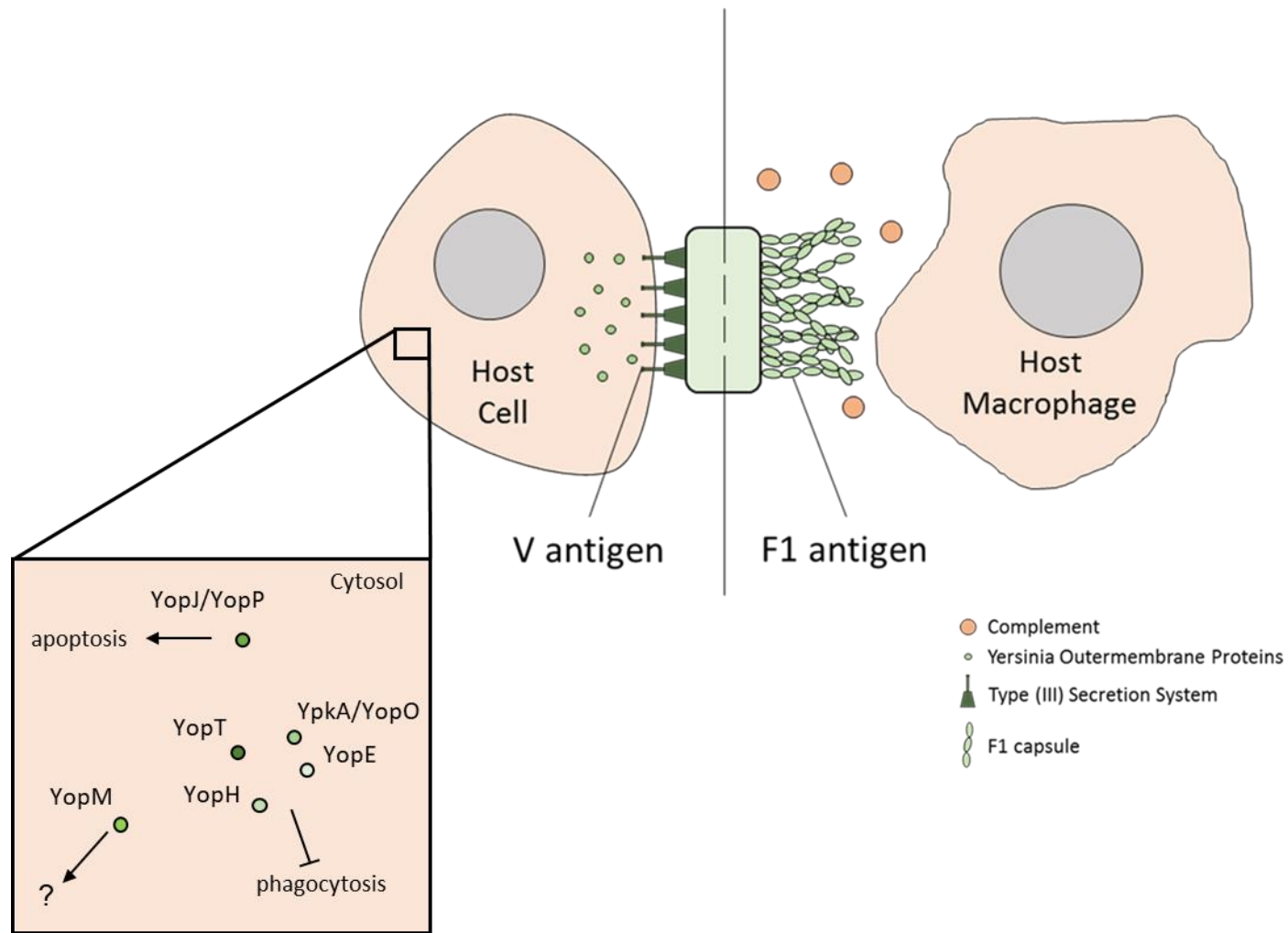


Figure 1.2. *Yersinia pestis* virulence factors. *Y. pestis* is capable of expressing the fraction 1 (F1) protein capsule on its surface, which prevents opsonization of the bacteria. In addition, this pathogen can express the type (III) secretion system, in which yersinia outer membrane proteins are inserted into the host cell cytosol and disrupt cell signalling pathways that disable phagocytosis of the pathogen and induce apoptotic pathways.

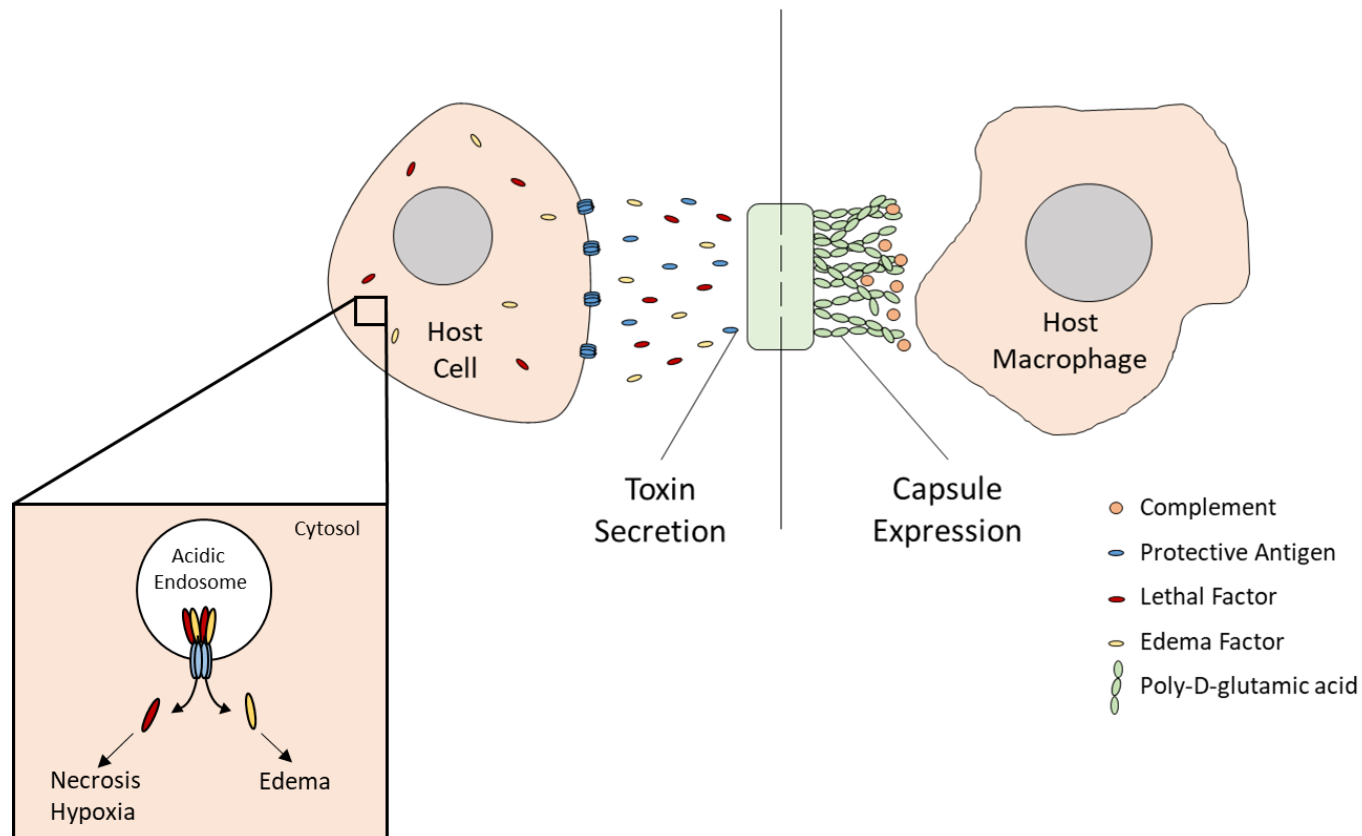


Figure 1.3. B anthracis virulence factors. *B. anthracis* is capable of expressing the polyglutamic acid capsule on its surface, which prevents opsonization of the bacteria. In addition, this pathogen can secrete a tripartite toxin, consisting of protective antigen, lethal factor, and edema factor. Protective antigen binds to the host cell membrane and enables transport of lethal factor and edema factor into the host cytosol, which play a role in inducing necrosis and edema, respectively.

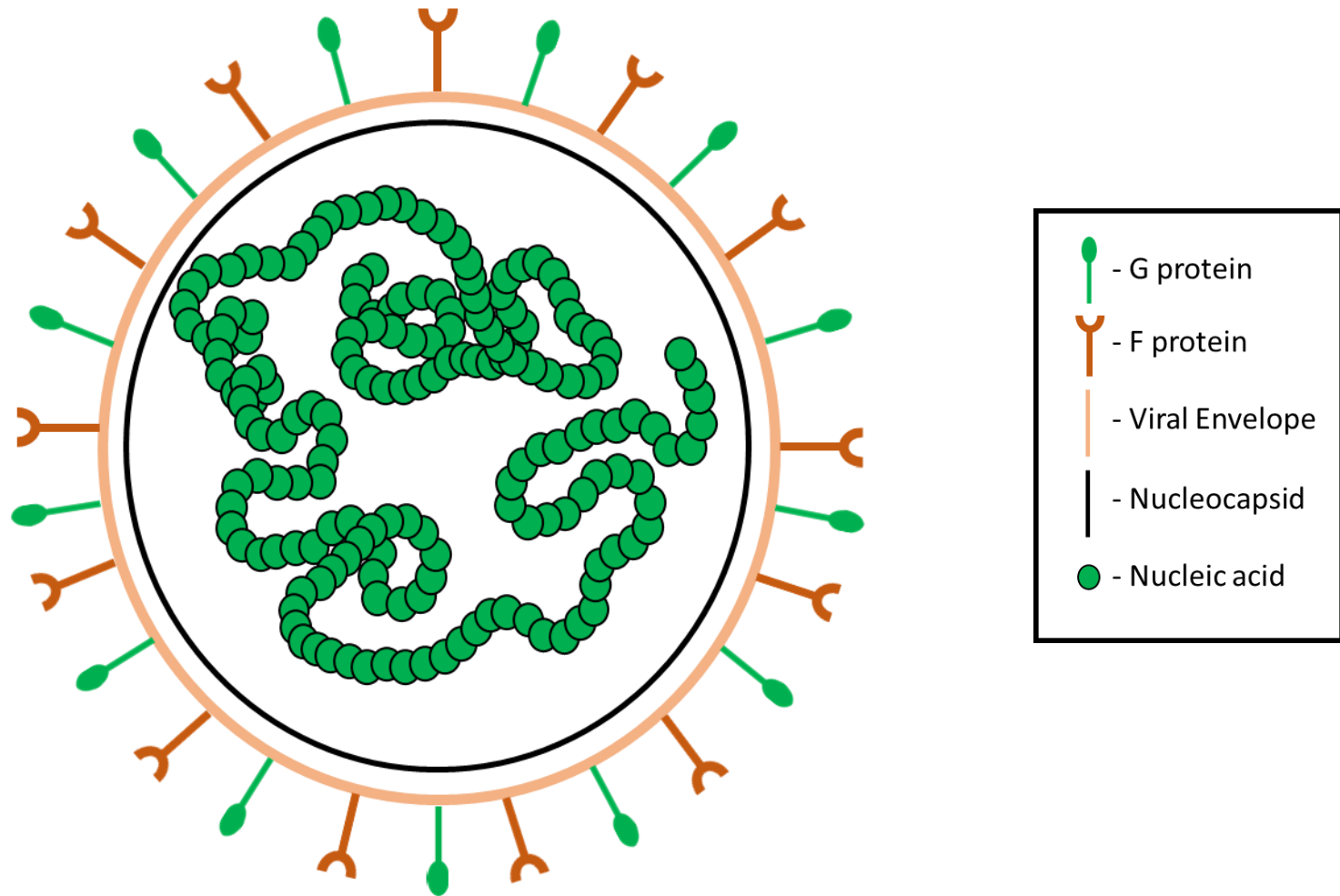


Figure 1.4. BRSV structure and virulence factors. BRSV is an enveloped, negative-stranded RNA virus which expresses the glycoproteins G and F on its surface. G is responsible for binding to host cells, while F initiates fusion of the viral envelope to the plasma membrane, which releases the nucleocapsid into the host cytosol and allows the virus to transcribe viral proteins and further replication.

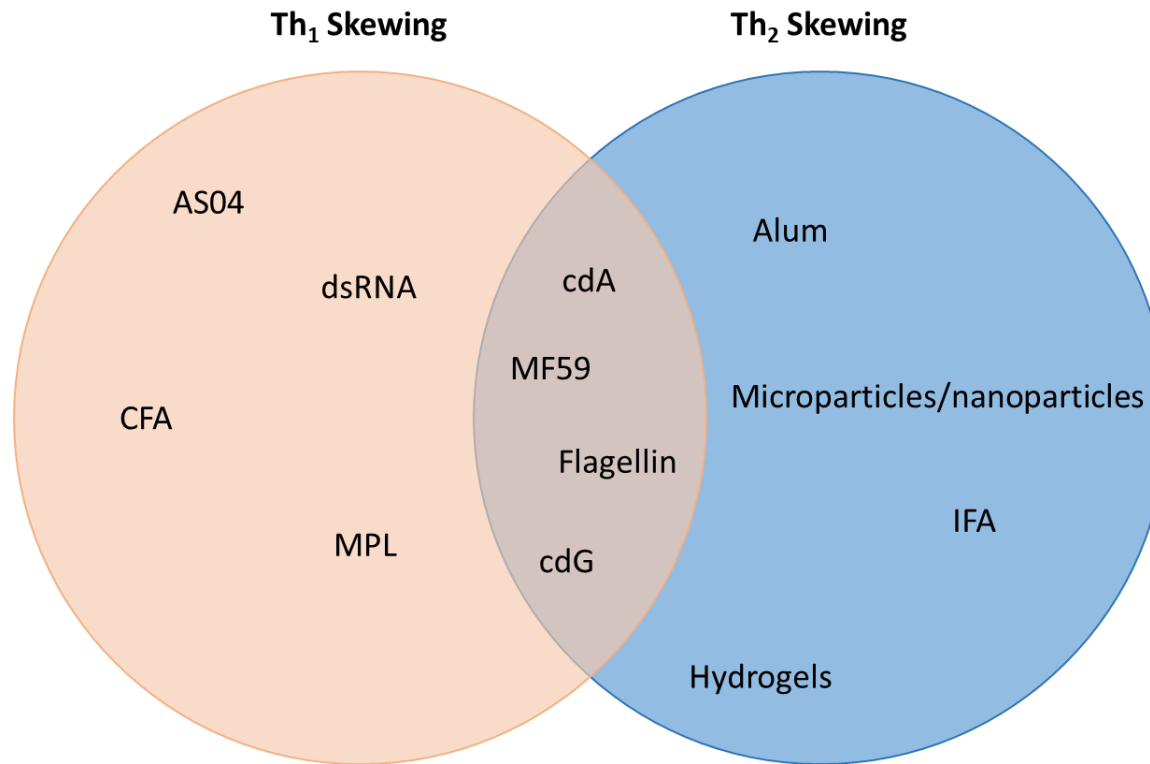


Figure 1.5. Immune skewing of adjuvants. Adjuvants that have traditionally been defined as delivery vehicles, such as alum, microparticles/nanoparticles, incomplete Freund's adjuvant, and hydrogels, tend to skew immune responses toward a Th₂ phenotype, while immune potentiators, such as double-stranded RNA and monophosphoryl lipid A, tend to skew immune responses toward a Th₁ phenotype. Some second generation adjuvants are capable of balancing the Th phenotype, or help skew the immune response of traditional delivery vehicle systems toward a Th₁ phenotype. Next-generation adjuvants, such as cyclic dinucleotides (i.e., CDG and CDA) and rationally-designed polymeric nanoparticles, can provide a balanced Th phenotype.

Cyclic di-GMP

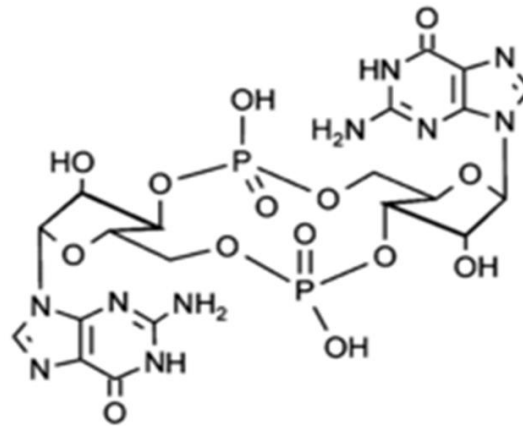


Figure 1.6. Chemical structure of cyclic-diGMP (CDG). Cyclic dinucleotides small molecules composed of two purine molecules linked together, with CDG being composed of two GMP molecules linked by two 3'-5' phosphodiester bonds. This molecule has recently been recognized as a universal secondary messenger molecule in Gram-negative bacteria, playing a variety of roles in bacterial development, motility, biofilm formation, and virulence.

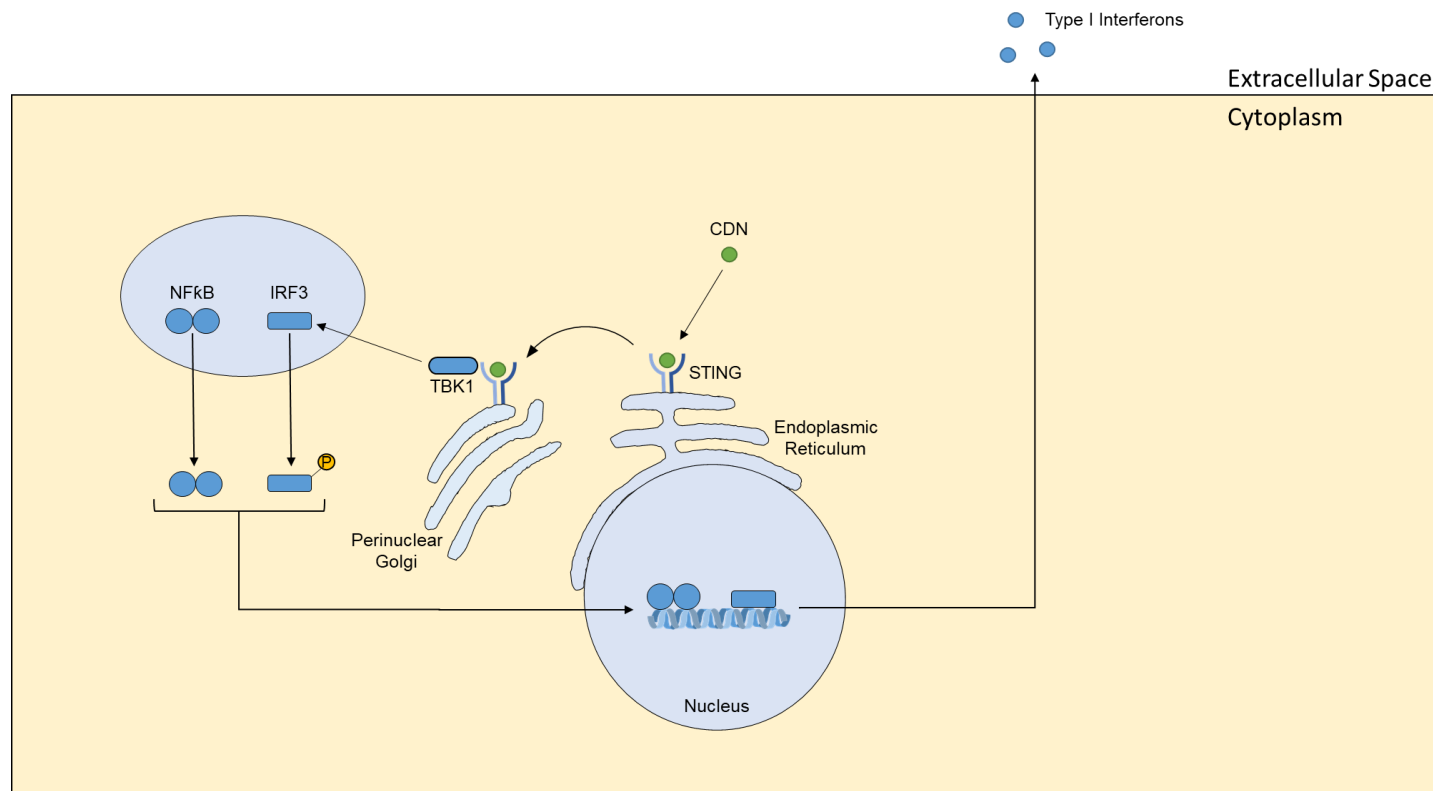


Figure 1.7. Stimulator of Interferon Genes (STING) pathway. Cyclic dinucleotides activate cells through binding to STING, an endoplasmic reticulum membrane protein. Following binding, STING forms a complex with TANK-binding kinase I (TBK1), which then traffics to perinuclear Golgi structures. TBK1 is then shuttled to endolysosomal vesicles, where it phosphorylates the transcription factors interferon regulatory factor 3 (IRF3) and nuclear factor- κ B (NF κ B). These activated transcription factors then migrate to the nucleus, where they initiate the production of cytokines, such as the type I interferons, that exhibit anti-pathogen activity.

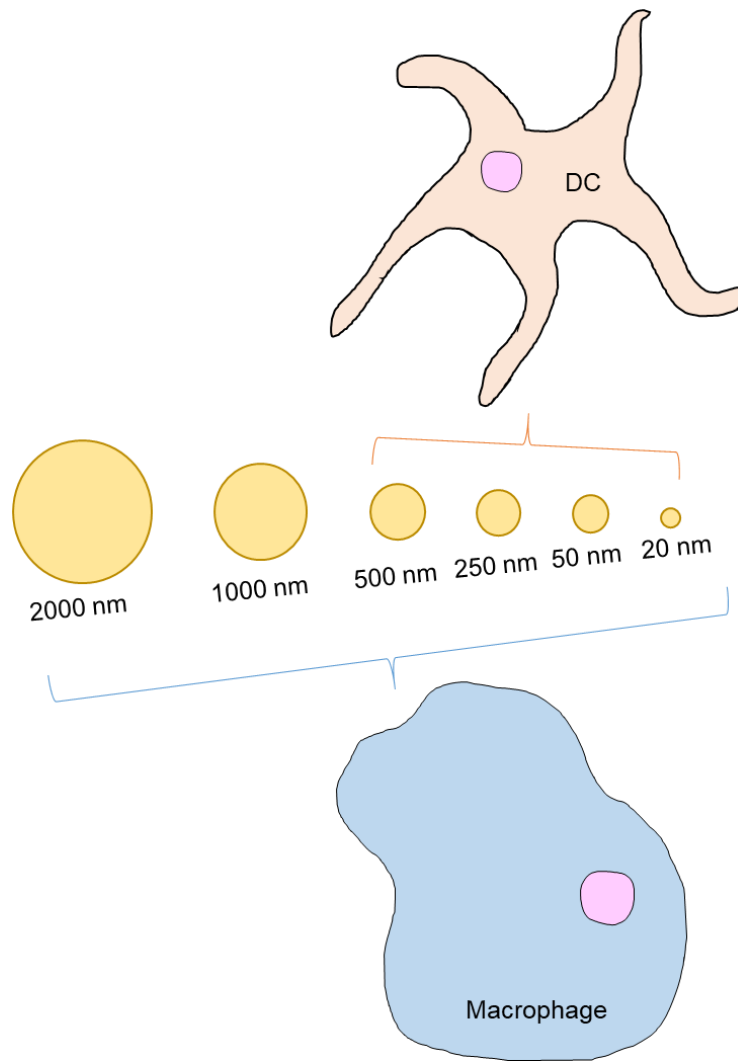


Figure 1.8. Sizes of particles/pathogens internalized by antigen presenting cells.

Dendritic cells are typically limited to internalizing particles below 1 μm in diameter, while macrophages can internalize particle greater than 1 μm , with highest efficiency of internalizing microparticles of 2-3 μm in diameter.

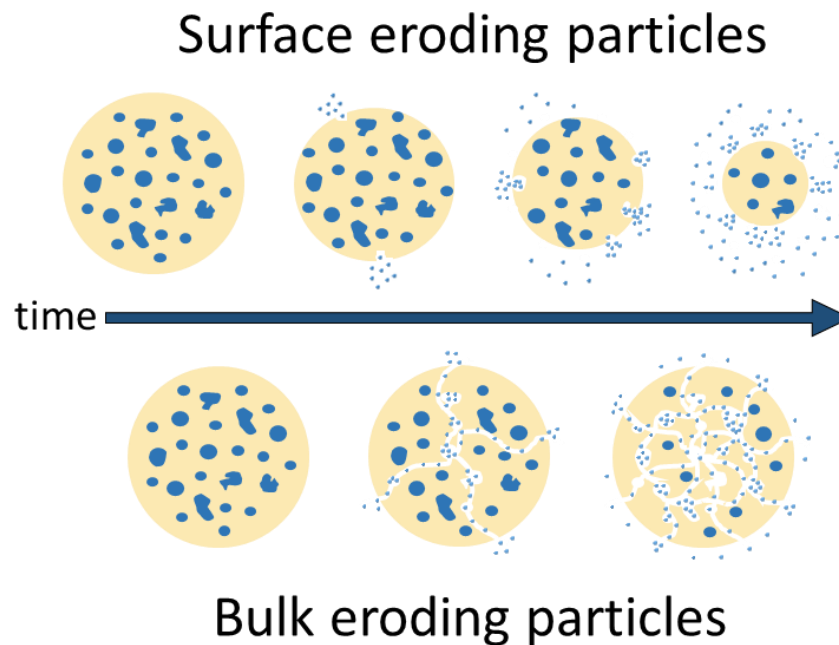


Figure 1.9. Bulk erosion vs. surface erosion. During bulk erosion, water is able to penetrate into the bulk of the polymer faster than the surface of the polymer erodes, resulting in swelling of the polymer, uniform degradation of the polymer matrix, and release of the payload. The uniform swelling of the polymer matrix can result in the rapid release of encapsulated payloads, which makes sustained release difficult to achieve. During surface erosion, the rate of water penetration into the polymer matrix is slower than the rate of erosion at the polymer surface. This results in the polymer solely degrading inward from the surface of the material, allowing for predictable and sustained release of encapsulated proteins. Surface erosion characteristics preserve encapsulated proteins, preventing protein aggregation and denaturation by precluding water penetration into the polymer bulk.

CHAPTER 2. RESEARCH OBJECTIVES AND THESIS ORGANIZATION

The overall goal of this thesis is to design a single dose polyanhydride nanoparticle-based vaccine platform that is capable of providing rapid and long-lived protective immunity against multiple respiratory pathogens, including pneumonic plague, inhalation anthrax, and RSV. In order to achieve this, the *Y. pestis* fusion protein F1-V and *B. anthracis* protein PA were encapsulated into polyanhydride nanoparticles formulated with a noncanonical CDG adjuvant, dithio-R_P,R_P-[cyclic diguanosine monophosphate (R,R-CDG), which has shown to enhance CD8⁺ T cell responses and promotes Th₁ responses over canonical CDG, and these formulations were administered to mice. Additionally, the BRSV F and G glycoproteins were encapsulated into polyanhydride nanoparticles and administered to neonatal calves. The stability of F1-V and PA upon release from polyanhydride particles has been established previously^{19,220}. As for *Y. pestis*, the protective efficacy of a single dose polyanhydride nanovaccine encapsulating F1-V has been demonstrated in mice 280 days PI, however the induction of rapid protective immunity has not been shown (after 14 days PI)¹⁵. In addition, the protective efficacy of a PA-based polyanhydride nanovaccine has not been evaluated *in vivo*. Similarly, the efficacy of a polyanhydride nanovaccine against BRSV has not been evaluated *in vivo*. Lastly, despite the previous successes of traditional polyanhydride nanovaccines, there is still room for improved design of polyanhydride copolymers with improved thermal properties, payload stability, and internalization by APCs for applications in drug and vaccine delivery.

The specific goals of this thesis are to:

- 1) Demonstrate the rapid and long-lived protective efficacy of a combination F1-V-based nanovaccine in female C57BL/6 mice against *Y. pestis* CO92 lethal challenge.
- 2) Demonstrate the rapid and long-lived anti-PA antibody responses to a combination PA-based nanovaccine in female A/J mice through *in vitro* toxin neutralization assays.
- 3) Demonstrate the protective efficacy of a combination BRSV F/G protein-based nanovaccine in cattle.
- 4) Describe the synthesis and design of CPTEG:SA nanoparticles with improved thermal properties, payload stability, and internalization by APCs for applications in drug and vaccine delivery.

The thesis is organized as follows. Chapter III will describe work showing protective efficacy of an F1-V-based polyanhydride combination nanovaccine against pneumonic plague. Chapter IV will describe work showing the anti-PA antibody responses of a PA-based polyanhydride combination nanovaccine against anthrax toxin. Chapter V will describe work showing protective efficacy of a polyanhydride nanovaccine against BRSV. Chapter VI will describe work showing the synthesis and design of CPTEG:SA nanoparticles. Finally, Chapter VII will summarize the results of these thesis chapters and highlight future work that can continue to increase our understanding of nanoparticle-based vaccine design and protective efficacy against respiratory pathogens.

CHAPTER 3. SINGLE-DOSE COMBINATION NANOVACCINE INDUCES BOTH RAPID AND LONG-LIVED PROTECTION AGAINST PNEUMONIC PLAGUE

Modified from a manuscript under review in the journal *Acta Biomaterialia*

Danielle A Wagner-Muñiz^{1,#}, Sean M Kelly^{2,#}, Andrew C Petersen¹, Nathan Peroutka-Bigus^{1,3}, Ross J Darling¹, Bryan H Bellaire^{1,3,4}, Michael J Wannemuehler^{1,4*}, and Balaji Narasimhan^{2,4,*}

¹Department of Veterinary Microbiology and Preventive Medicine, Iowa State University, Ames, IA, USA

²Department of Chemical and Biological Engineering, Iowa State University, Ames, IA, USA

³Interdepartmental Microbiology Program, Iowa State University, Ames, IA, USA

⁴Nanovaccine Institute, Iowa State University, Ames, IA, USA

indicates these authors contributed equally to this manuscript

***Correspondence:**

Balaji Narasimhan
nbalaji@iastate.edu

Michael J. Wannemuehler
mjwannem@iastate.edu

Keywords: pneumonic plague; polyanhydride; nanovaccine; cyclic dinucleotide; combination

Abstract

Yersinia pestis, the causative agent of pneumonic plague, induces a highly lethal infection if left untreated. Currently, there is no FDA-approved vaccine against this pathogen; however, USAMRIID has developed a recombinant fusion protein, F1-V that has shown to induce protection against pneumonic plague. Many F1-V-based vaccine formulations require prime-boost immunization to achieve protective immunity, and there are limited reports of rapid induction of protective immunity (≤ 14 days post-immunization (DPI)). The STimulator of INterferon Genes agonists cyclic dinucleotides (CDNs) have been shown to be promising vaccine adjuvants. Polyanhydride nanoparticle-based vaccines (i.e., nanovaccines) have also shown to enhance immune responses due to their dual functionality as adjuvants and delivery vehicles. In this work, a combination nanovaccine was designed that comprised F1-V-loaded nanoparticles combined with the CDN, dithio-R_P,R_P-cyclic di-guanosine monophosphate, to induce rapid and long-lived protective immunity against pneumonic plague. All mice immunized with a single dose combination nanovaccine were protected from *Y. pestis* lethal challenge within 14 DPI and demonstrated enhanced protection over F1-V adjuvanted with CDNs alone. In addition, 75 percent of mice receiving the single dose of the combination nanovaccine were protected from challenge at 182 DPI, while maintaining high levels of antigen-specific serum IgG. ELISPOT analysis of vaccinated animals at 218 DPI revealed F1-V-specific long-lived plasma cells in bone marrow. Microarray analysis of revealed the presence of serum antibody with high affinity for a broad range of F1 and V linear epitopes. These results demonstrate that combining the adjuvanticity

of CDNs with a nanovaccine delivery system enables induction of both rapid and long-lived protective immunity against *Y. pestis*.

3.1 Introduction

Plague has relentlessly affected humans throughout history, accounting for an estimated 200 million deaths ^{1,52} and continues to persist worldwide, with the latest outbreak occurring in Madagascar in 2017. Plague is caused by the non-motile, facultative intracellular, Gram-negative bacterium *Yersinia pestis* ²⁷⁴. Pneumonic plague, the respiratory manifestation of *Y. pestis* infection, is transmitted through aerosolized droplets ⁵⁵. In the case of pneumonic plague, treatment with intravenous or oral ciprofloxacin and doxycycline over 48 hours is successful, though mortality rates quickly approach 90-100% if left untreated for 24-36 hours post-infection ¹.

The threat of weaponization of *Y. pestis* is high, largely evidenced by its history of such use ⁵². Though the United States and 103 other countries co-signed an agreement to terminate biological weapons programs in 1972, *Y. pestis* remains listed as a Tier 1 Select Agent. Currently, there is no FDA-approved vaccine against *Y. pestis*, making it critical to develop a protective vaccine with the capability to provide both rapid and long-lived immunity in the event of mass exposure of aerosolized *Y. pestis* to civilian or military populations. As *Y. pestis* is predominantly an extracellular pathogen, many vaccination strategies have focused on developing strong humoral immunity, characterized by neutralizing antibodies against the V antigen and opsonizing antibodies against the F1 capsule ^{83,88,275,276}. In mice, anti-F1 IgG antibody titers have been shown to correlate with protection ⁸³. Additionally, mAb 7.3, which binds to the V

antigen, has been shown to neutralize *Y. pestis in vitro* and provides passive protection against lethal challenge ^{88,93}.

The United States Army Medical Research Institute of Infectious Diseases (USAMRIID) developed a recombinant fusion protein, F1-V, containing both full length of both F1 and V proteins, and shows promise as a target antigen for *Y. pestis* ^{92,95,277,278}. This vaccine has long shown promise as a vaccine candidate against both pneumonic and bubonic plague in rodents ^{95,277,278}. In fact, it was recently shown that F1-V adjuvanted with aluminum hydroxide (alum) using an IM/SC prime-boost regimen provided complete protection against intranasal challenge with virulent *Y. pestis* CO92 in mice, guinea pigs, and macaques ⁹². Additionally, serum collected from immunized macaques conferred passive protection to mice. Despite such success, this vaccine formulation is most often administered as a prime-boost regimen; in the event of mass exposure, it would be ideal to use single dose formulations that can provide rapid immunity in as short a time frame as possible and that can maintain long-lived protective immunity.

Cyclic dinucleotides (CDNs), a class of small molecule adjuvants, are recognized as microbial-associated molecular patterns (MAMPs) by the pattern recognition receptor (PRR) STING (STimulator of INterferon Genes) ²⁷⁹, resulting in the phosphorylation of transcription factors NFkB and IRF3 and the induction of type I interferon (IFN), which is associated with anti-pathogenic activity ^{211,212}. Cyclic di-guanosine monophosphate (3), the most well-studied CDN to date, has been recognized as a universal secondary messenger molecule in Gram-negative bacteria, playing a role in bacterial development, motility, and virulence ²¹⁰. Vaccines adjuvanted with CDG induce a balanced immune

response, characterized by equal presence of IgG subclasses in serum ²¹⁵, and have been shown to elicit significantly higher antibody titers than alum-adjuvanted formulations ²¹⁶.

Biodegradable polyanhydride particles, a novel class of adjuvants and delivery vehicles, possess a multitude of beneficial characteristics to address challenges faced by many current vaccines ²⁸⁰. Comprised of 1,6-bis(*p*-carboxyphenoxy)hexane (CPH) and 1,8-bis(*p*-carboxyphenoxy)-3,6-dioxaoctane (CPTEG), these materials are highly biocompatible demonstrating minimal injection-site reactivity when administered as particles ^{13,250} and whose non-toxic dicarboxylic acid degradation products are safely excreted from the body ²⁴³. Their amphiphilic properties allow for stabilization of labile proteins ^{19,220,281}, provide sustained release of encapsulated proteins via surface erosion kinetics ^{14,18,19,232}, and allow for enhanced shelf stability of encapsulated proteins, even at elevated temperatures (e.g., 40 °C) ¹⁹. Additionally, polyanhydride particles display inherent adjuvanticity demonstrating chemistry-dependent internalization, persistence, and activation of antigen presenting cells *in vitro*, as well as the ability to prime humoral and cell-mediated immune responses *in vivo* ^{15,16,204,206,222,223,253–259}. These properties have enabled the study of polyanhydride nanoparticle-based vaccines (i.e., nanovaccines) against multiple bacterial and viral pathogens ^{14,15,17,19,217}.

Previous work from our laboratories demonstrated that encapsulation of F1-V into polyanhydride particles maintained F1-V structure and prolonged antigen bioavailability ²²⁰, and a single, intranasal dose of F1-V nanovaccine provided complete protection against lethal challenge of *Y. pestis* for at least 280 days post-immunization (DPI) ¹⁵. In addition to long-lived protective immunity, it is also important that vaccines

induce rapid (i.e., ≤ 14 days) protective immunity to counter acute outbreaks of disease. Designing next-generation vaccine platforms that provide *both* rapid and long-lived immunity against highly lethal pathogens will likely require novel approaches including developing new adjuvants or vaccine regimen with combination adjuvants to enhance both rapid and long-lived protective immunity. Herein, the design and evaluation of a combination nanovaccine, comprising of F1-V-containing polyanhydride nanoparticles and a non-canonical CDG CDN adjuvant (containing 2',5'-3'-5' phosphate linkages) is described. This nanovaccine formulation synergistically combines the adjuvant properties of polyanhydride nanoparticles and CDNs to induce rapid immune responses and facilitate the induction of long-lived protective immunity against pneumonic plague.

3.2 Material and Methods

3.2.1 Materials

Chemicals used for CPTEG and CPH diacid and polymer synthesis included 1,6-dibromohexane, triethylene 4-*p*-hydroxybenzoic acid, and 1-methyl-2-pyrrolidinone, purchased from Sigma-Aldrich (St. Louis, MO). Chloroform, petroleum ether, ethyl ether, hexanes, sodium hydroxide, toluene, sulfuric acid, acetonitrile, dimethyl formamide, acetic anhydride, methylene chloride, pentane, and potassium carbonate were purchased from Fisher Scientific (Fairlawn, NJ). 4-*p*-fluorobenzonitrile was purchased from Apollo Scientific (Cheshire, UK). Deuterated chloroform used for ^1H NMR analysis was purchased from Cambridge Isotope Laboratories (Andover, MA). Dithio- R_P , R_P -cyclic di-guanosine monophosphate (R,R-Cyclic di-GMP (CDG)) was provided by Aduro Biotech (Berkeley, CA). Complete cell culture medium reagents

RPML 1640 and penicillin-streptomycin were purchased from Mediatech (Herndon, VA); heat inactivated fetal calf serum was purchased from Atlanta Biologicals (Atlanta, GA). *Y. pestis*, strain CO92 (NR-641) and the *Y. pestis* fusion protein F1-V (NR-4526) were obtained from the Biodefense and Emerging Infections Repository (Manassas, VA).

3.2.2 Polyanhydride Synthesis

CPTEG and CPH diacids were synthesized as previously described^{232,255}. 20:80 CPTEG:CPH copolymer synthesis was performed using melt polycondensation²³². Copolymer composition and molecular weight were estimated using end group analysis of ¹H NMR (DXR 500) spectra.

3.2.3 Nanoparticle Synthesis

10 % (w/w) F1-V-loaded 20:80 CPTEG:CPH nanoparticles were synthesized using flash nanoprecipitation, as described previously²⁰⁴. Briefly, F1-V and 20:80 CPTEG:CPH copolymer was dissolved in methylene chloride at 2 mg/mL and 20 mg/mL, respectively, sonicated at 30 Hz for approximately 30 seconds, and poured into pentane chilled to -20 °C at a methylene chloride:pentane ratio of 1:250. Nanoparticles were imaged using scanning electron microscopy (SEM; JEOL 840 A, JEOL Ltd., Tokyo, Japan), and nanoparticle mean size and size distribution were determined using ImageJ (National Institutes of Health, Bethesda, MD). Nanoparticle zeta potential was measured using Zetasizer Nano (Malvern Instruments, Worcestershire, UK).

3.2.4 Protein Release and Encapsulation Efficiency

To quantify released protein, approximately 2 mg of nanoparticles were suspended in 500 μ L of PBS, sonicated for 15 seconds, and placed on a shaker plate at 37 °C. Periodically, 400 μ L aliquots of sample supernatant were withdrawn and sample volumes were reconstituted with 400 μ L of fresh PBS. After 32 days, 40 mM sodium hydroxide was used in place of PBS to catalyze the release of any remaining protein. Protein released from F1-V-loaded 20:80 CPTEG:CPH nanoparticles was quantified using a microbichoninic acid (microBCA) assay (Thermo Fisher Scientific, Waltham, MA), and percent by mass of protein released over time was calculated as the cumulative protein released from nanoparticles at each time point divided by total mass of protein released. To quantify protein encapsulation efficiency, approximately 1 mg of nanoparticles was suspended in 500 μ L of 40 mM sodium hydroxide solution, sonicated for 15 seconds, and placed on a shaker plate at 37 °C. Frequently, 400 μ L samples of supernatant were withdrawn and sample volumes were reconstituted with 400 μ L of 40 mM sodium hydroxide. Protein released from F1-V-loaded 20:80 CPTEG:CPH nanoparticles was quantified using a microBCA assay, and the encapsulation efficiency was calculated as the sum of the protein released from the nanoparticles divided by the initial mass of protein.

3.2.5 Animals

Seven to eight-week old female C57BL/6NCrl mice were purchased from Charles River (Wilmington, MA). Mice were housed under specific pathogen-free conditions where all bedding, caging, water, and feed were sterilized prior to use. All studies were

conducted with the approval of the Iowa State University Institutional Animal Care and Use Committee (IACUC).

3.2.6 Immunization and Serum Collection

Groups comprised of C57BL/6NCrI mice (n = 8-16/group) were immunized once subcutaneously at the nape of the neck with either of the following formulations: 50 µg F1-V + 35 µg CDNs (R,R-CDG, Aduro Biotech), 36-50 µg F1-V encapsulated into 500 µg of 20:80 CPTEG:CPH nanoparticles, 36-50 µg F1-V encapsulated into 500 µg of 20:80 CPTEG:CPH nanoparticles + 35 µg CDNs, or saline in a total volume of 200 µL. Blood was collected from mice via saphenous vein and serum was separated following centrifugation (10,000 rcf for 10 min) at 13, 14, 36, 49, 79, 101, 121, 150, and 178 DPI. An additional serum sample was obtained from mice sacrificed for ELISPOT analysis at 218 DPI via cardiac exsanguination. Serum was stored at -20°C until analysis. Bronchoalveolar lavage (BAL) fluid was collected post-euthanization by introducing a catheter needle through a small incision made in the trachea and injecting/aspirating 700 µL of PBS thrice.

3.2.7 ELISA

Anti-F1-V antibody titers were determined via ELISA, as previously described ¹⁴. Briefly, high-binding Costar 590 EIA/RIA microtiter plates (Corning) were coated overnight with 100 µL of a 0.5 µg/mL solution of F1-V at 4 °C. After washing the wells, microtiter plates were blocked for two hours with a solution of 2.5% (w/v) powdered skim milk dissolved in PBS-Tween with 0.05% Tween 20, pH 7.4, that had been

incubated for two hours at 56 °C to inactivate any endogenous phosphatase activity. Following block, microtiter plates were washed thrice with PBS-T. Serum obtained from immunized mice was added at a dilution of 1:200 and serially diluted in PBS-T containing 1% (v/v) goat serum. Each sample was tested in duplicate. Following incubation overnight at 4°C, plates were washed thrice with PBS-T, after which secondary antibody was added at a dilution of 1 µg/mL. Secondary antibodies used in these studies were: alkaline phosphatase-conjugated goat anti-mouse IgG heavy and light chain, IgG1 and IgG2c (Jackson ImmunoResearch). Plates were incubated for two hours at room temperature and then washed three times with PBS-T. To each well, 100 µL of alkaline phosphatase substrate (Fisher Scientific, Pittsburgh, PA) was added at a concentration of 1 mg/mL dissolved in 50 mM sodium carbonate, 2 mM magnesium chloride buffer at pH 9.3 for colorimetric development. Plates were analyzed after 30 min using a SpectraMax M3 microplate reader at a wavelength of 405 nm. Titer is reported as the reciprocal of serum dilution at which the optical density (OD) value was at most 0.2, a conservative endpoint greater than the average OD of saline-mouse serum, at a 1:200 dilution, plus two standard deviations.

3.2.8 ELISPOT

MultiScreen 96-well plates (Millipore Sigma, Billerica, MA) were pretreated with 35 % ethanol for one minute, washed three times with PBS, and coated overnight at 4 °C with 0.5 µg/mL F1-V in PBS. The following day, plates were dumped and blocked with complete tissue culture medium consisting of RPMI 1640 (Gibco, Grand Island, NY), 10% (v/v) fetal calf serum, 1% (v/v) penicillin-streptomycin, and 1% (v/v) L-

glutamine for at least two hours at 37 °C. Plates were dumped and single cell suspensions of bone marrow or splenic lymphocytes harvested from mice between 214-218 days post-immunization were added to the plates at 500,000 cells per well and placed in a 37 °C incubator for two hours. Plates were then washed three times with PBS, another three times with PBS-T, and alkaline phosphatase-conjugated goat anti-mouse IgG (H+L) secondary antibody (Jackson ImmunoResearch) was added to the wells at a 1:500 dilution in 1% (v/v) goat serum PBS-T for two hours at room temperature. Plates were washed six times with PBS-T and 25 µL per well of BCIP/NBT liquid substrate (Millipore Sigma) was added to the wells and developed for 15 min at room temperature. Plates were emptied, the bottoms removed, and gently washed with nanopure water, after which they were left to dry completely. Spots were counted using an AID Multispot Reader (AID, Strassberg, Germany). AID EliSpot software (Version 6.0) was used for data analysis.

3.2.9 Peptide Microarray Printing and Analysis

Twenty seven 14- to 17-mer linear peptides (11 amino acid overlaps) spanning the full length of F1 antigen and fifty three 15- to 17-mer linear peptides (11 or 12 amino acid overlaps) spanning the full length of V antigen, as well as full length proteins F1-V, *Bacillus anthracis* protective antigen (PA), and chicken egg ovalbumin (OVA) were printed onto Nexterion Slide AL (Schott, Louisville, KY) using a BioRobotics MicroGRID II microarray printer (Genomic Solutions, Inc. Ann Arbor, MI). Peptides and proteins were dissolved into DMSO at 10 mg/mL to ensure dissolution, then diluted 10-fold in water to 1 mg/mL. The solution was diluted to bring the final concentration to 0.5 mg/mL

in 1x print buffer (5% (v/v) DMSO, 137 mM NaCl, 9 mM KOH, 11.3 mM NaH₂PO₄). The full length F1-V fusion protein was used as a positive control, while PA and OVA were used as negative controls. Slides were printed with 16 arrays per slide, each array containing 16x16 spots per array, with peptides printed in a serpentine pattern in triplicate. Following printing, slides were vacuum sealed and stored at -80 °C until further use.

Microarray slides were warmed to room temperature and then placed on a hot plate at 37 °C for 30 min to dry; the slides were then placed immediately in a blocking solution consisting of 1 % BSA (w/v) in PBS-T for one hour. Slides were subsequently blocked for one hour in 1 % (v/v) goat serum PBS-T, then thrice washed with PBS-T and placed into a 16-well incubation chamber (Nexterion IC-16) to separate individual arrays. Serum was added at a 1:20 dilution for one hour at room temperature with gentle agitation. Slides were washed thrice with PBS-T and biotinylated goat anti-mouse IgG (H+L) secondary antibody (Jackson ImmunoResearch) was added to wells at 1:1000 dilution for one hour at room temperature with gentle agitation. Slides were washed thrice with PBS-T. Streptavidin Alexa Fluor 555 conjugate was added to wells at a 1:1000 dilution for 30 min at room temperature with gentle agitation. Slides were removed from incubation chambers, washed thrice with PBS-T, followed by another three washes with PBS. Slides were spun dry by centrifugation and read on the Scanarray 5000 laser scanner (GSI Lumonics, Bedford, MA).

The scanned images of the microarray slides were analyzed using SoftWorRx Tracker v2.8 software (Applied Precision, Inc., Issaquah, WA) to detect and quantify the fluorescence of each spot. R (v3.4.1) software was used to calculate the background-

corrected fluorescence of each spot as the mean fluorescence intensity of each spot minus the median background fluorescence intensity surrounding the spot. The mean fluorescence intensity for each peptide or protein was calculated as the average of the corresponding triplicate background-corrected fluorescence spot values, and a heat map was generated based upon the magnitude of individual mouse serum responses to each peptide. Saline-treated mouse serum was used as a negative control.

3.2.10 Lethal Challenge

Y. pestis CO92 (NR-641) was obtained from BEI Resources. Frozen stocks were prepared in advance of challenges. *Y. pestis* was initially grown on brain heart infusion (BHI) agar at 28 °C for 72 h; a single colony was isolated and inoculated in BHI broth and cultivated for 24 h at 28 °C while shaking at 120 rpm. Glycerol solution was added to the broth to bring final glycerol concentration to 5% (v/v). Aliquots were snap frozen and stored at -72 °C. Prior to challenge experiments, aliquots of the frozen stock were thawed and cultured on tryptic soy agar (TSA) with 1% bovine hemoglobin at 37°C and 5% CO₂ to check viability and CFU enumeration. For challenge experiments, frozen *Y. pestis* stocks were thawed and diluted in room temperature PBS. Groups of C57BL/6NCrl mice immunized as described previously were anesthetized with an intraperitoneal injection of ketamine/xylazine cocktail and infected intranasally with 5,700, 7,000, or 10,700 CFU (14 DPI) or 6,500 CFU (218 DPI) of *Y. pestis* CO92 in a 50 µL volume. *Y. pestis* bacterial suspension was administered intranasally to nares of mice by a micropipette. CFU enumeration was performed on infectious inoculum preceding to and following infection of the animals to determine infectious dose

administered. Animals were checked daily for morbidity and mortality over the course of two weeks. All activities were performed in an animal biosafety level 3 (ABSL-3) laboratory at Iowa State University with protocols approved by the Iowa State University Institutional Animal Care and Use Committee and Institutional Biosafety Committee.

3.2.11 Statistical Analyses

Statistical analyses on ELISA and survival were performed using the Mantel-Cox log rank test and the one-way analysis of variance (ANOVA) using Tukey's multiple comparisons test. Statistical significance in microarray serum responses to each peptide between vaccinated groups of animals was evaluated using Student's t test. A p-value ≤ 0.05 was considered to be statistically significant. All analyses were performed using GraphPad Prism v. 7.0 (GraphPad, La Jolla, CA).

3.3 Results

3.3.1 F1-V Nanovaccine Characterization

Following synthesis, the F1-V nanovaccine was characterized for size distribution, surface charge, release kinetics, and encapsulation efficiency of encapsulated F1-V. The size of the F1-V nanovaccine was consistent with previous work¹⁵, with a mean diameter of 228 ± 78 nm and a polydispersity index of 0.12, indicating a narrow size distribution (Figure 3.1A and 3.1B). Zeta potential measurements of the F1-V nanovaccine demonstrated a negative surface charge, -34.8 ± 1.4 mV. In order to provide sufficient antigen to induce a robust immune response for rapid protection, while also sustaining the release of antigen to induce long-lived

protective immunity, this nanoparticle formulation was designed with a high (10% w/w) loading of F1-V providing a biphasic release profile that was characterized by an initial burst of approximately 75% of the protein released within the first 24 h, followed by slow zero order release over time (Figure 3.1C). The encapsulation efficiency of the F1-V within the various nanoparticle batches was 51-72%.

3.3.2 Combination Nanovaccine Induces Rapid Protective Immunity

In order to assess the potential of CDNs and nanovaccines to rapidly stimulate protective immunity, C57BL/6NCrl mice (n=12-16 per group) were immunized subcutaneously with a single dose of one of the following vaccine formulations: i) soluble F1-V adjuvanted with CDNs (CDN Vaccine), ii) F1-V encapsulated into 20:80 CPTEG:CPH nanoparticles (Nanovaccine), iii) F1-V encapsulated into 20:80 CPTEG:CPH nanoparticles co-adjuvanted with CDNs (Combination Nanovaccine), or iv) saline alone. Blood samples were collected from immunized animals at 13 DPI (Figure 3.2A, C, E). Anti-F1-V total IgG antibody titers from CDN Vaccine- and Combination Nanovaccine-immunized animals evaluated at 13 DPI were similar in magnitude and showed significantly ($p \leq 0.0001$) higher titers than sera from animals immunized with the Nanovaccine alone.

Mice were challenged intranasally 14 DPI with escalating lethal doses of *Y. pestis* CO92 in separate studies and survival was assessed over a period of two weeks (Figure 3.2B, D, F). All naïve (i.e., saline-treated) mice succumbed to infection within four days of challenge, while all Nanovaccine-immunized mice succumbed over a period of eight days following challenge (Figure 3.2B). In contrast, immunization with

Combination Nanovaccine yielded 100 % protection against all challenge doses, while immunization with CDN Vaccine showed decreasing levels of efficacy with increasing challenge doses. Immunization with the Combination Nanovaccine provided significantly better protection ($p \leq 0.05$) compared to the CDN Vaccine when challenged at 7,000 and 10,700 CFU.

3.3.3 Combination Nanovaccine Enhances Long-lived Protective Immunity

Previous work from our laboratories has shown the potential for a single dose nanovaccine, consisting of a soluble bolus of F1-V and F1-V containing nanoparticles, to enhance long-lived antibody responses for at least 280 DPI and provide protective immunity^{14,15}. To evaluate the potential for a single dose of the CDN vaccine and the two nanovaccines (with no soluble F1-V bolus) to induce long-lived protective immunity, separate groups of C57BL/6NCrl mice (n=8-12 per group) were immunized subcutaneously with the same formulations as above and anti-F1-V total IgG titers were evaluated between 14 and 218 DPI (Figure 3.3A and Supplementary Figure 3.1). At all time points, sera from both Combination Nanovaccine-immunized and CDN Vaccine-immunized mice showed comparable and significantly ($p \leq 0.0001$) higher titers than sera from Nanovaccine-immunized mice. Serum was analyzed at 14, 79 and 178 DPI for presence of class-switched anti-F1-V IgG1, IgG2c and IgG3 antibodies (Supplementary Figure 3.2). All vaccination regimens produced detectable IgG1 at 14 and 79 DPI significant ($p \leq 0.0001$) over background, with Combination Nanovaccine and CDN Vaccine groups also showing significant ($p \leq 0.04$) responses at 178 DPI (Supplementary Figure 3.2A). Additionally, Combination Nanovaccine- and CDN

Vaccine-immunized animals showed significantly ($p \leq 0.05$) higher IgG1 titers compared to Nanovaccine-immunized mice at 79 DPI. Sera from animals immunized with both Combination Nanovaccine and CDN Vaccine exhibited significantly ($p \leq 0.0001$) higher IgG2c antibody titers at all time points, and IgG3 at 14 DPI, compared to sera from Nanovaccine-immunized and Saline-treated mice (Supplementary Figure 3.2B and C). Lastly, a subset of mice ($n=2-4$) were euthanized 214-218 DPI and BAL fluid was collected for evaluation of anti-F1-V lung IgG (Supplementary Figure 3.3) and IgA. The BAL fluid recovered from the animals immunized with Combination Nanovaccine and CDN Vaccine was found to have significantly ($p \leq 0.05$) higher total anti-F1-V IgG compared to that from animals immunized with Nanovaccine or treated with Saline. No IgA was detected in the BAL fluid (data not shown).

After the single sc immunization, mice were challenged intranasally at 182 DPI with a lethal dose of *Y. pestis* CO92 (6,500 CFU) and survival assessed over a two-week period (Figure 3.3B). All naïve mice succumbed to infection within three days of challenge. Both the Combination Nanovaccine and CDN Vaccine immunization regimens induced superior protection ($p \leq 0.01$) when compared to the Nanovaccine- or saline-immunized mice. Specifically, immunization with the Combination Nanovaccine provided 75% protection from lethal challenge and immunization with the CDN Vaccine provided 62% protection.

3.3.4 Combination Nanovaccine Provides Broad Antibody IgG Recognition to F1-V Linear Epitopes

A linearly overlapping peptide array was used to identify F1-V-specific IgG (H+L) antibodies in serum collected from mice immunized with either CDN Vaccine,

Nanovaccine, or Combination Serum from Nanovaccine and naïve control mice collected at 14, 79, and 178 DPI was reactive to 14- to 17-mer linear peptides spanning the full length of F1 antigen, 15- to 17-mer linear peptides spanning the full length of V antigen, and F1-V fusion protein (Figure 3.4). The antibody response to F1-V and all linear epitopes in mouse serum collected at 14 DPI was noticeably lower than at 79 and 178 DPI. In addition, naïve mouse serum did not bind appreciably to either F1-V, or any F1 or V peptides, at any time point evaluated.

Serum from CDN Vaccine- and Combination Nanovaccine-immunized animals elicited antibodies that bound multiple linear peptides from F1 and V antigens across all time points, with responses observed to peptides F1-3, F11, and V45-46 at all time points evaluated ($p < 0.05$ compared to non-vaccinated mice). At 178 DPI, serum antibody from both CDN Vaccine- and Combination Nanovaccine-immunized animals continued to react with peptides F9, V18, V32, and V44 (Fig. 4, blue arrows). Serum from mice immunized with Nanovaccine possessed fewer F1- and V-peptide specific antibodies compared to CDN Vaccine- and Combination Nanovaccine-immunized animals, however, responses to peptides F1-3 and V44-45 were observed at all time points evaluated.

3.3.5 Combination Nanovaccine Induces Long-lived Plasma Cells

As anti-F1-V-specific serum antibody was found to persist for at least 218 days, ELISPOT analysis was performed on cells harvested from spleen and bone marrow at 214-218 DPI to demonstrate the presence of the long-lived antibody secreting cells (ASCs). Analysis of bone marrow revealed a significantly ($p < 0.05$) higher number of

F1-V-specific ASCs in CDN Vaccine- and Combination Nanovaccine-immunized mice compared to non-vaccinated (dashed line) mice (Figure 3.5A). There was no difference in the number of ASCs in the bone marrow of Nanovaccine-immunized mice compared to non-vaccinated mice. Additionally, there was no difference in the number of ASCs detected in the spleens harvested from immunized mice versus naïve mice at 218 DPI (Figure 3.5B). Analysis of ASC-derived antibody IgG subclass expression revealed a trend of a greater number of F1-V-specific IgG2c ASCs present in the bone marrow of CDN Vaccine- and Combination Nanovaccine-immunized mice compared to non-vaccinated mice 218 DPI; however, this difference was not statistically significant (Supplementary Figure 3.4). There was no difference in the number of F1-V-specific IgG2c ASCs in the spleen 218 DPI, nor was there a difference in the number of F1-V-specific IgG1 ASCs between all vaccine groups in either spleen or bone marrow.

3.4 Discussion

With increasing concern of biological weaponization, it is of paramount importance to enhance preparedness with biodefense vaccines that can induce both rapid and long-lived protective immunity. To date, there is no FDA-approved vaccine against the weaponizable *Y. pestis*. An efficacious, single-dose vaccine would be vitally important to induce rapid and long-lived protective immunity both in the critical window of time immediately following an exposure event as well as for military personnel against potential exposure after deployment. Previous work on pneumonic plague vaccines from other laboratories has shown some immunization success using aluminum hydroxide-based and TLR-targeting adjuvants; however, many of these

studies required prime-boost vaccination^{92,95,99,277,278,282}. A few studies have demonstrated the ability to induce protective immunity within 14 DPI against pneumonic plague challenge with strains other than CO92^{283–285}.

The goal of this work was to incorporate the benefits of two novel adjuvants (i.e., CDNs and polyanhydride nanoparticles) in order to design a single-dose, combination vaccine that would provide both rapid and long-lived immunity. Previously, it was shown that a single dose of intranasally administered nanovaccine containing 40 µg soluble F1-V antigen and 10 µg F1-V encapsulated into polyanhydride nanoparticles provided 100 % protection for at least 280 DPI¹⁵. Additionally, it was previously demonstrated that intranasally administered 20:80 CPTEG:CPH nanoparticles elicited demonstrable F1-V-specific antibody titers as early as 14 DPI²⁰⁴. Motivated by these studies, a combination nanovaccine including R,R-CDG CDNs and F1-V-containing 20:80 CPTEG:CPH nanoparticles was designed with rapid release of ~ 70 % of the antigen (Figure 3.1) in order to initiate the adaptive immune response. This current work highlights the potent immunostimulatory properties of polyanhydride nanoparticle- and CDN-based combination adjuvants, which individually could not provide rapid protection (i.e., at 14 DPI) when the challenge inoculum contained $\geq 7,000$ CFU *Y. pestis*; however, when administered together, rapid and complete protection against all three lethal doses of *Y. pestis* was achieved (Figure 3.2). The results indicate that while the CDN vaccine induced a similar anti-F1-V antibody titer as did the Combination Nanovaccine formulation, only the latter formulation induced rapid protection (14 DPI) against all three challenge doses of *Y. pestis* CO92, suggesting a qualitative difference in the immune response induced by the Combination Nanovaccine formulation.

Therefore, it is possible that polyanhydride nanoparticles modulated immune responses beyond humoral immunity. Indeed, previous reports have demonstrated that vaccinated B cell-deficient μ MT mice were protected from lethal challenge with the KimD27 strain of *Y. pestis*²⁸⁶ and that blocking IFN- γ and TNF- α in F1-V-vaccinated C57BL/6NCrl mice resulted in loss of protection against *Y. pestis* CO92²⁸⁷. As previously mentioned, polyanhydride particles display inherent adjuvanticity demonstrating the ability to prime humoral and cell-mediated immune responses *in vivo*^{15,16,204,206,222,223,253–259,288}; therefore, the nanovaccine regimen may be activating cellular immune responses that contribute to the protection at higher challenge doses of *Y. pestis* CO92.

The focus on the importance of serum antibody to the immunity induced by plague vaccines is based largely on the following: 1) human patients infected with *Y. pestis* demonstrate long-lived antibody responses to F1 and V antigens with little to no demonstrable T cell responses²⁸⁹; 2) monoclonal antibodies passively transferred to mice have been shown to be protective against lethal challenge^{93,275,276}; 3) direct neutralization of LcrV has been shown to be necessary to prevent Yop translocation into macrophages *in vitro*⁸⁸; 4) murine challenge models have suggested that anti-F1 IgG1 antibody titer correlates with survival⁸³; and 5) mucosal and serum anti-V antigen antibodies are the best correlates for survival against pneumonic plague in mice²⁹⁰. Regardless of the route of immunization, the induction or presence of anti-V neutralizing antibodies in the lungs is likely critical for protection against pneumonic plague; and, it has been demonstrated that intratracheally administered monoclonal antibody (mAb) 7.3 protected mice against lethal intranasal challenge^{96,291,292}. The results herein support this notion, as high IgG levels in peripheral blood and BAL fluid were observed

218 DPI (Supplementary Figures 3.1 and 3.3) following a single, subcutaneous administration of the Combination Nanovaccine.

Elevated antibody responses observed in this work are in agreement with previously reported studies that demonstrated that the use of CDG as an adjuvant enhances antibody responses compared to traditional adjuvants^{213,215,216,293}. In this work, the resultant antibody responses induced by both the Combination Nanovaccine and CDN Vaccine were characterized by high affinity, class-switched F1-V-specific IgG1 and IgG2c by 14 DPI (Figure 3.2 and Supplementary Figure 3.2). Following a single SC immunization, the antibody response was also characterized by a stable F1-V-specific antibody response over 218 DPI that was accompanied by evidence of F1-V-specific long-lived plasma cells in the bone marrow, however these titers were not necessarily correlated with protection at 182 DPI (Supplementary Figure 3.1 & Figure 3.5).

Using microarray analysis, potential protective immunodominant peptides were identified that were consistent with previously published reports. Xiao *et al.* identified monoclonal antibodies (mAbs) that bound to peptides F1-2, V19-20, and V28 and together conferred protection against lethal challenge²⁷⁶. In the current study, responses to F1-3 were observed in sera from immunized mice at all time points. It has also been reported that a neutralizing mAb BA5 binds amino acids 196-225, corresponding to peptides V31-39, and protects mice against systemic challenge²⁹⁴. Consistent with this study, serum antibody recognized the V32 peptide suggesting that the CDN Vaccine and Combination Nanovaccine elicited antibodies with potentially similar neutralizing capacity as mAb BA5. Khan *et al.* previously characterized peptides 'b' (a.a. 46-60) and 'g' (a.a. 256-270) as B cell epitopes²⁹⁵. Similar antibody responses

were observed in this study to peptides F9 (a.a. 49-65) and V44-46 (a.a. 258-286). Interestingly, there are no previous reports of antibody recognition of peptide F11 (a.a. 61-77) or V18 (a.a. 102-118), and, therefore, these regions may be of interest for further research. Together, these results suggest that both CDN Vaccine and Combination Nanovaccine elicited polyclonal antibody responses that recognized multiple linear epitopes.

Encapsulation of antigen into polyanhydride nanoparticles can provide many benefits for labile proteins including maintenance of protein structure and adjuvant activity for multiple vaccine antigens ^{19,219,296,297}, including F1-V ²²⁰. The surface eroding characteristics of these particles enables chemistry-dependent release kinetics of antigen providing for single-dose (i.e., no booster) vaccination ^{14,15,17}. Previously, polyanhydride nanoparticles have shown the ability to adjuvant pneumococcal surface protein A (PspA) resulting in the induction of complete protection of mice from a lethal challenge of *S. pneumoniae* that was comparable to that induced by alum-adsorbed PspA with markedly less injection site reactogenicity ^{13,17}. In addition to the adjuvanticity of the polyanhydrides, previous reports have demonstrated that protein structure and functional activity of the labile recombinant protective antigen from *Bacillus anthracis* was maintained upon encapsulation and release from polyanhydride nanoparticles after storage for at least four months at temperatures up to 40 °C ¹⁹. Consequently, encapsulation of proteins into polyanhydride nanoparticles has the capability to both enhance protective immunity and provide extended shelf storage, both of which may be beneficial with respect to stockpiling biodefense vaccines such as plague vaccines.

In summary, these results indicate that the Combination Nanovaccine is a promising vaccine candidate against *Y. pestis* based on its ability to induce both rapid and long-lived protective immunity. Immune responses to F1-V were characterized by long-lived high antibody titers, increased breadth of antibody responses to a broader array of epitopes, and induction of long-lived plasma cells in the bone marrow for at least 218 DPI. With the ability to enhance immune responses to F1-V and potential for enhance shelf stability of labile proteins, the Combination Nanovaccine shows promise as a next-generation vaccine platform against weaponized *Y. pestis*.

3.5 Acknowledgements

The authors acknowledge financial support from NIH-NIAID (R01 AI111466) and the Nanovaccine Institute. The authors thank Drs. David Kanne, Chudi Ndubaku, and Thomas Dubensky Jr at Aduro Biotech for providing the CDG used in the immunization experiments, as well as Dr. Chris Minion at Iowa State University for providing the BioRobotics MicroGRID II microarray printer used for printing microarray slides. The authors also acknowledge Dr. Thomas Waldschmidt at the University of Iowa for his guidance in ELISPOT assay development. The authors would also like to thank Min Zhang at Iowa State University for assistance with the statistical analyses. B.N. acknowledges the support of the Vlasta Klima Balloun Faculty Chair.

3.6 Author Contributions

DW-M and SK performed the experiments and analyzed the data. ACP and RJD helped with the development of the microarray experiments and data analysis. NPB and

BHB performed the challenge studies and analyzed the data. MW, BN, DW-M, and SK designed the experimental plan. All authors participated in the writing of the manuscript.

3.7 Conflict of Interest Statement

The authors declare that the research was conducted in the absence of any commercial or financial relationships that could be construed as a potential conflict of interest.

3.8 Figures

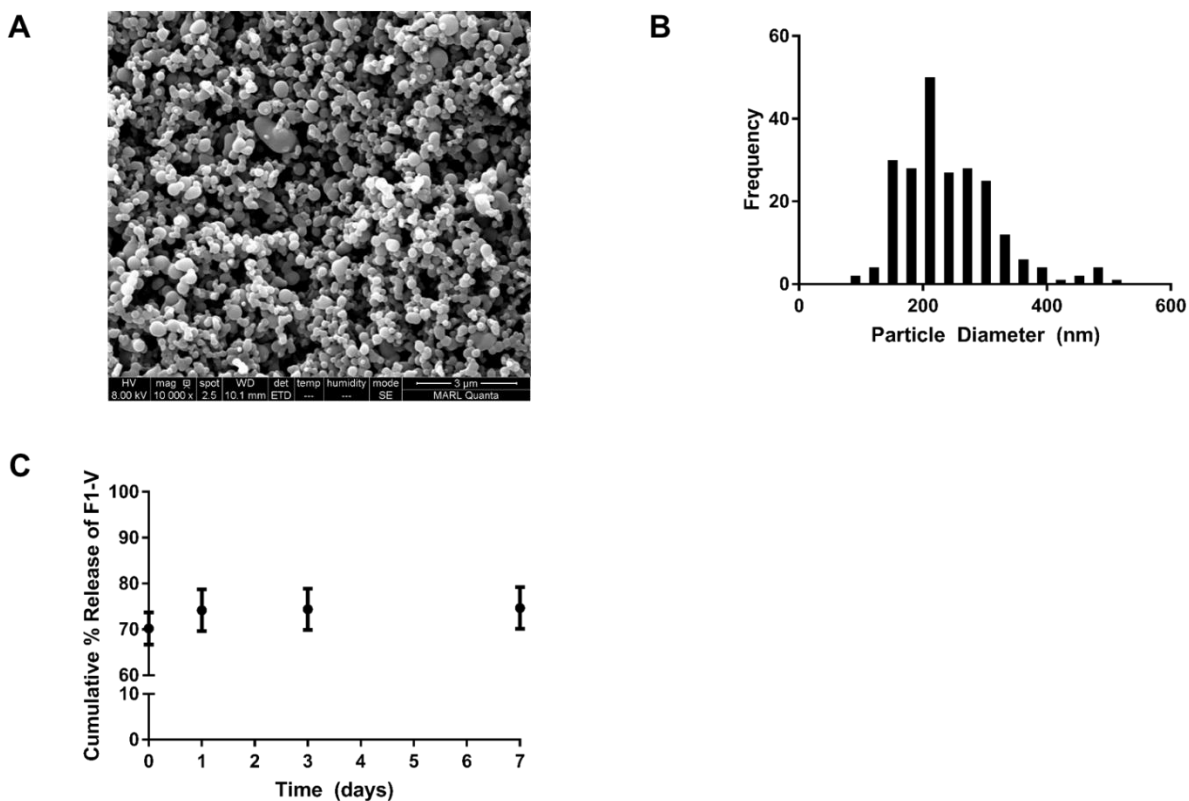


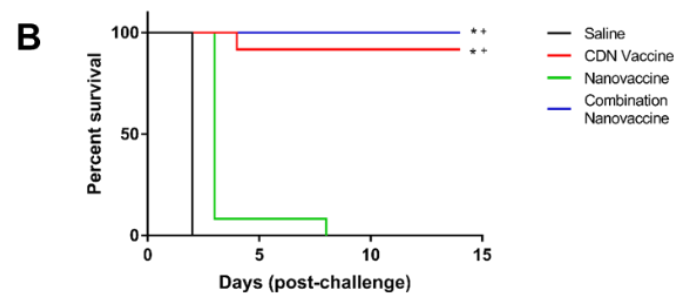
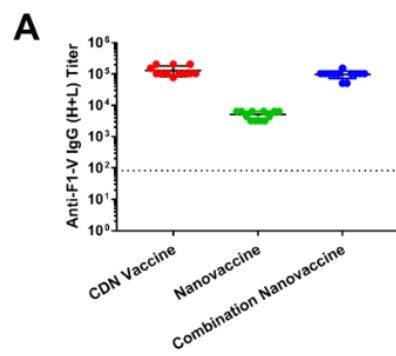
Figure 3.1. Characterization of F1-V Nanovaccine. A) Representative scanning electron photomicrograph of F1-V nanovaccine (scale bar = 3 μm). B) Nanoparticle size

distribution of the F1-V nanovaccine (228 ± 78 nm), determined via ImageJ analysis. C)

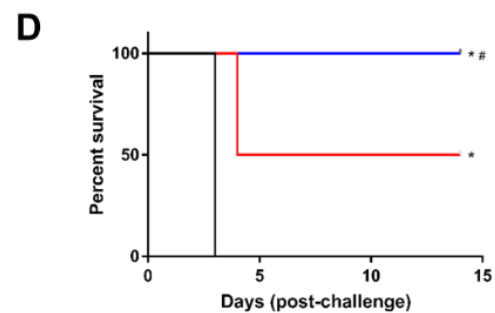
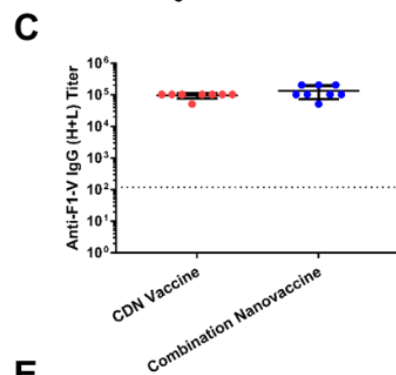
Cumulative in vitro F1-V release profile from the nanovaccine. Nanoparticles were

suspended in PBS (pH 7.4) and released protein was quantified via a microBCA assay.

5,700 CFU



7,000 CFU



10,000 CFU

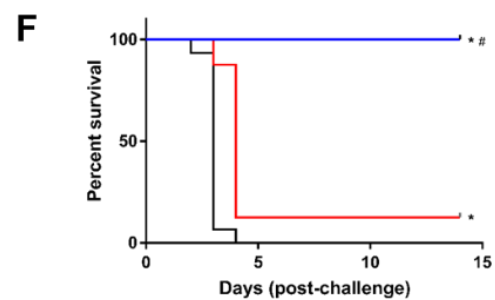
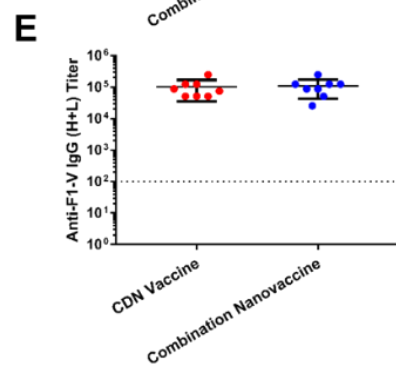


Figure 3.2. Combination Nanovaccine provides rapid protective immunity against lethal *Y. pestis* challenge.

Groups of C57BL/6NCrl mice (n=12-16 per group) were immunized subcutaneously with the following groups: F1-V + CDNs (CDN Vaccine), F1-V encapsulated into nanoparticles (Nanovaccine), F1-V encapsulated into nanoparticles + CDNs (Combination Nanovaccine) or saline. (A,C,E) Serum was collected at 13 DPI and evaluated via ELISA for total anti-F1-V IgG antibody titers. The dashed line represents anti-F1-V IgG (H+L) antibody titers from saline-treated mice as a negative control. * $p \leq 0.0001$ compared to Nanovaccine and saline. Mice were challenged at 14 DPI with (B) 5,700 CFU, (D) 7,000 CFU, or (F) 10,700 CFU *Y. pestis* CO92 and survival was monitored for two weeks post-challenge. * $p \leq 0.0001$ compared to saline-treated mice. + $p \leq 0.0001$ compared to Nanovaccine-immunized mice. # $p \leq 0.05$ compared to CDN Vaccine-immunized mice.

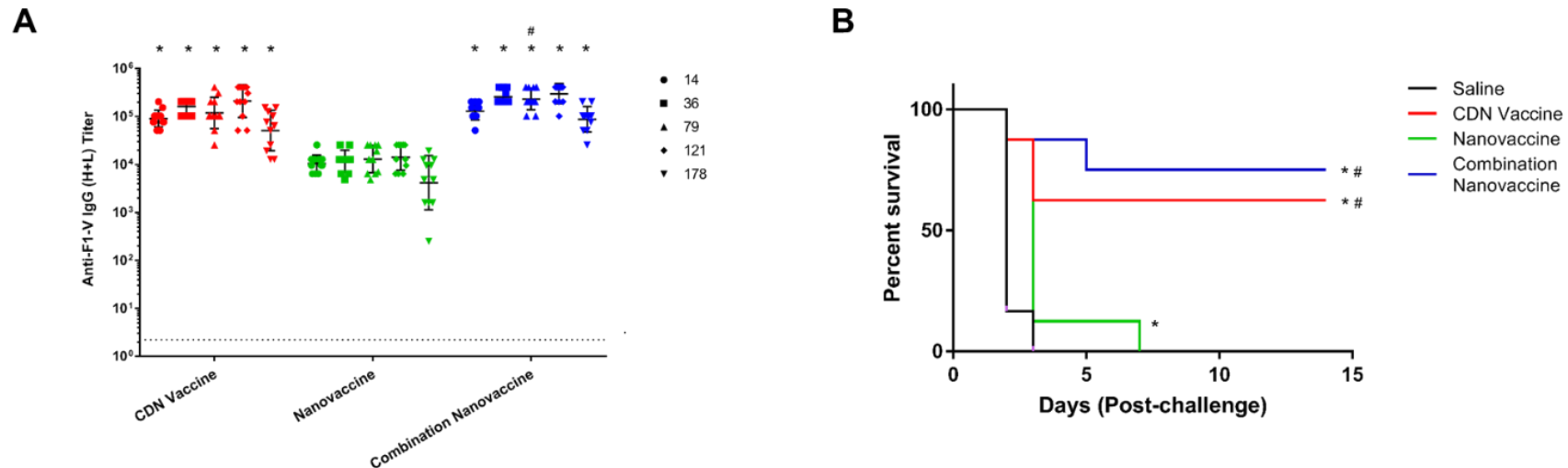


Figure 3.3. Combination Nanovaccine provides long-lived protective immunity against lethal *Y. pestis* challenge.

Groups of C57BL/6NCrl mice (n=12-16 per group) were immunized subcutaneously with the following treatments: F1-V + CDNs (CDN Vaccine), F1-V encapsulated into nanoparticles (Nanovaccine), F1-V encapsulated into nanoparticles + CDNs (Combination Nanovaccine) or saline. (A) Serum samples were collected at 14, 36, 79, 121, and 178 DPI and analyzed for total anti-F1-V IgG (H+L) antibodies via ELISA. The dashed line represents the background anti-F1-V IgG (H+L) antibody response from naive mice. # $p \leq 0.05$ compared to CDN Vaccine. * $p \leq 0.0001$ compared to Nanovaccine-immunized and saline-treated mice. (B) Mice were challenged at 182 DPI with 6500 CFU *Y. pestis* CO92 and survival was monitored for two weeks post-challenge. # $p \leq 0.01$ compared to Nanovaccine-immunized mice. * $p \leq 0.05$ compared to Saline-treated mice.

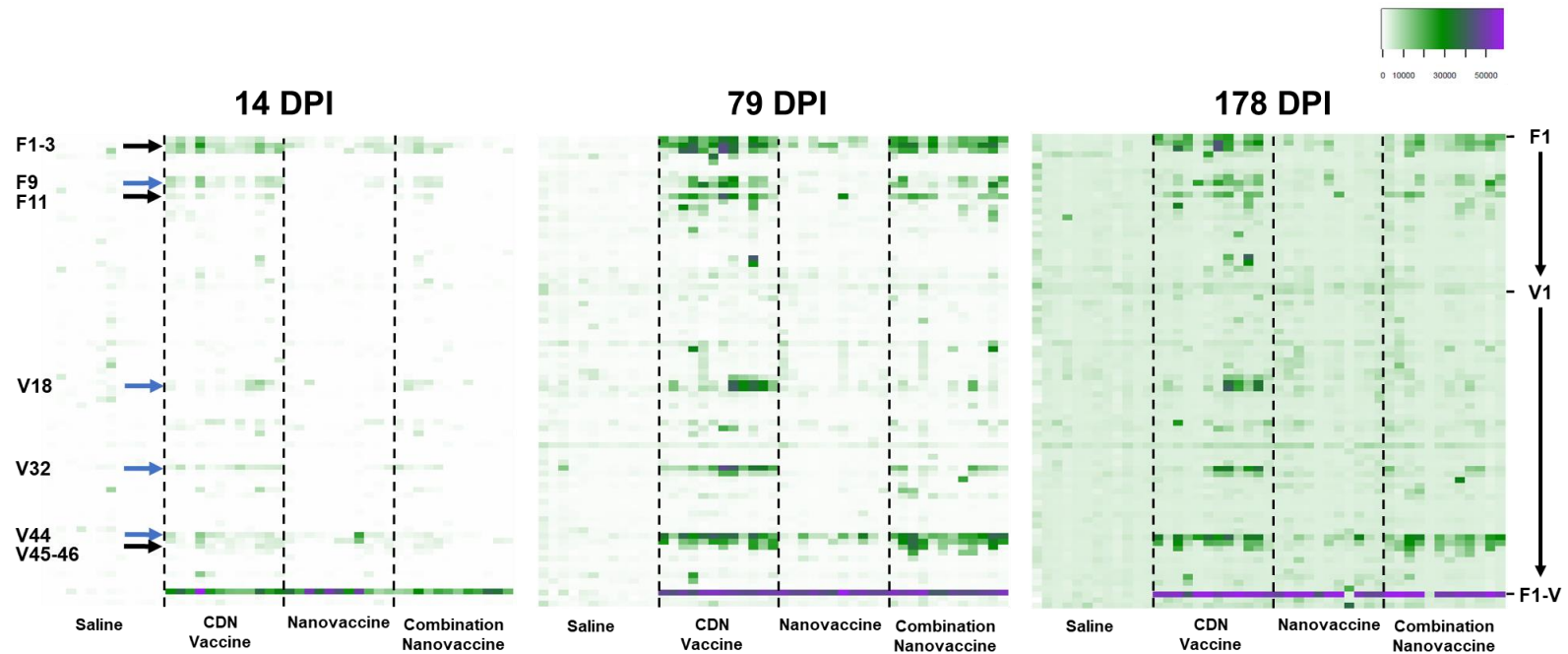


Figure 3.4. Combination Nanovaccine and CDN Vaccine provide broad antibody responses to potentially protective linear epitopes. Serum samples collected from C57BL/6NCrl mice (n=12-16 per group) immunized with either saline, CDN Nanovaccine, Nanovaccine, or Combination Nanovaccine at 14, 79, and 178 DPI was analyzed for total anti-F1-V IgG antibodies against twenty-seven 14- to 17-mer linear peptides (11 amino acid overlaps) from the F1 antigen and fifty-three 15- to 17-mer linear peptides (11 or 12 amino acid overlaps) from the V antigen. The peptides were covalently bound to microarray slides as described in Materials and Methods. Each row corresponds to a specific peptide, the top row representing peptide F1 and the proceeding downward rows corresponding to each following linear peptide incrementally through peptide V53. Each column represents responses from a single mouse. The mean fluorescence intensity of serum responses to each peptide is represented by a range of color from white (no response) to purple (maximum response). The full-length F1-V fusion protein was used as a positive control, and Bacillus anthracis protective antigen (PA) and chicken egg ovalbumin (OVA) were used as negative controls. Black arrows indicate significance ($p < 0.05$) of Combination Nanovaccine and CDN Vaccine serum compared to naïve serum at all time points evaluated. Blue arrows indicate significance ($p < 0.05$) of Combination Nanovaccine and CDN Vaccine serum compared to naïve serum at 179 DPI.

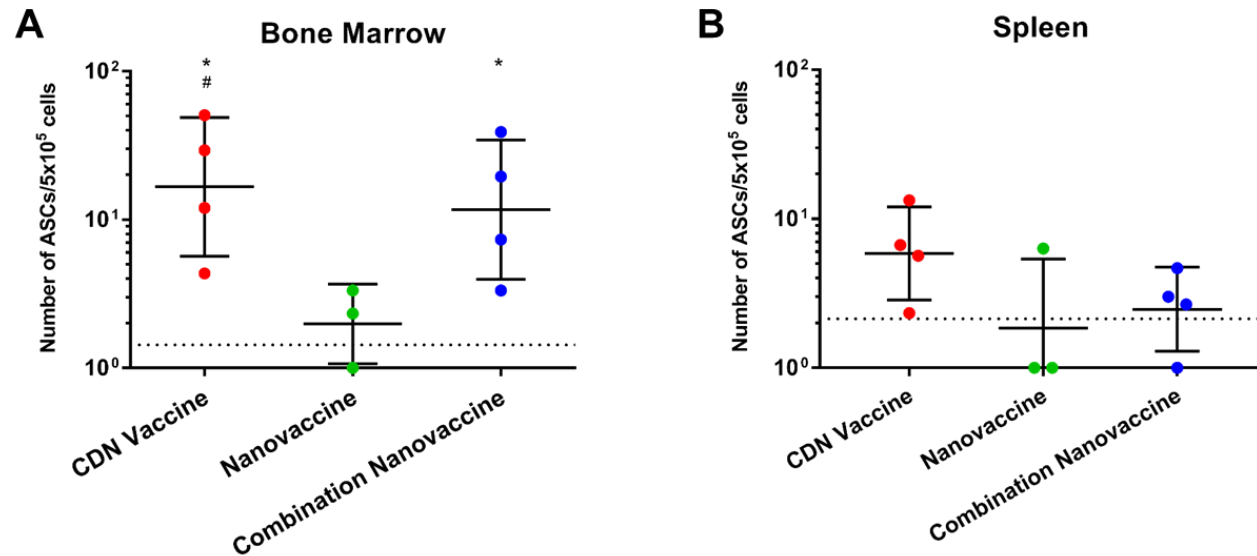
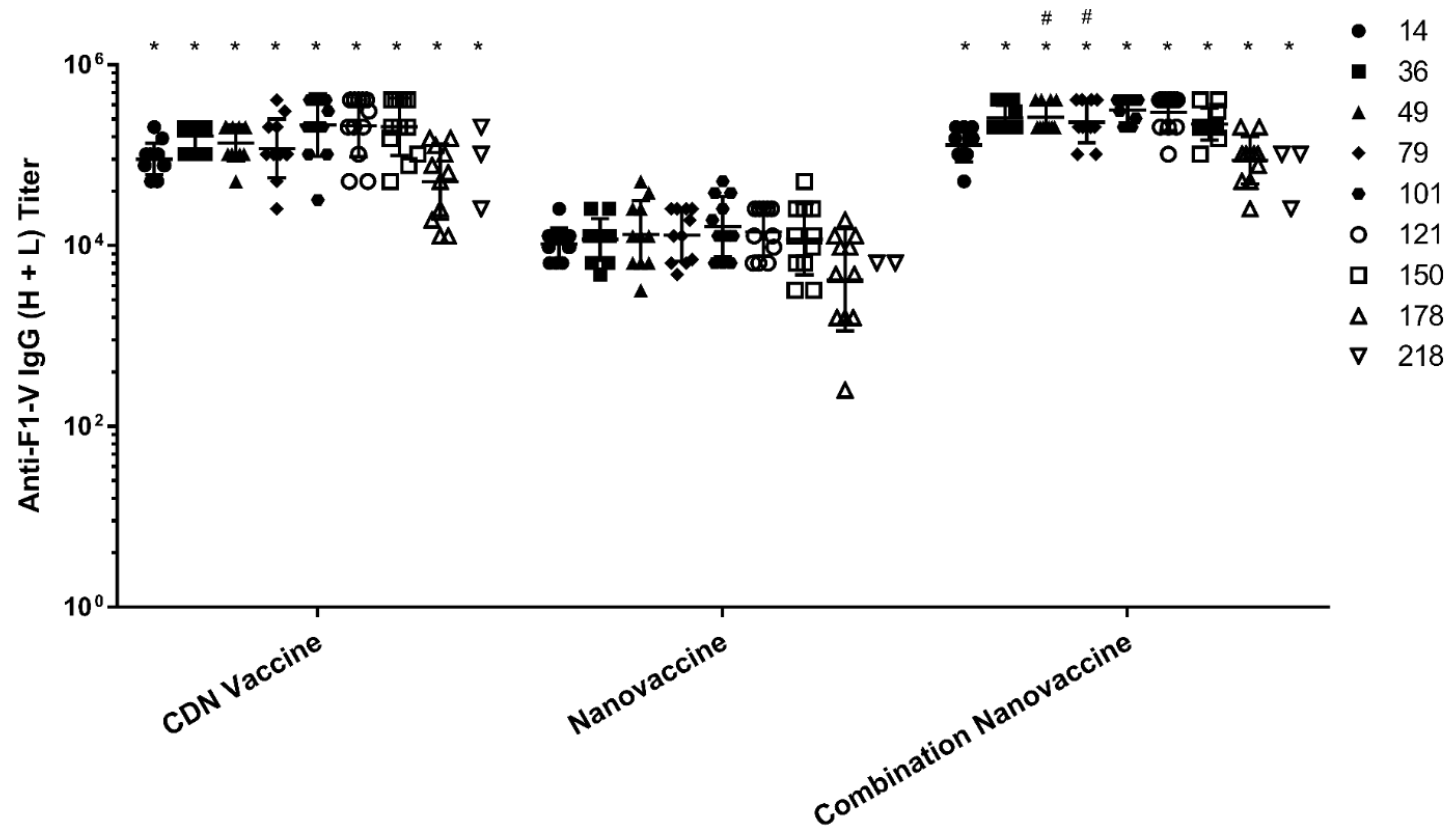
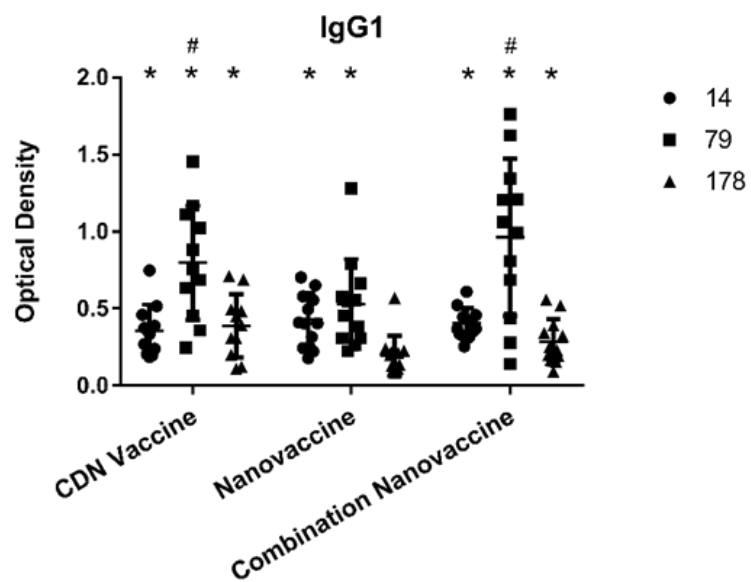
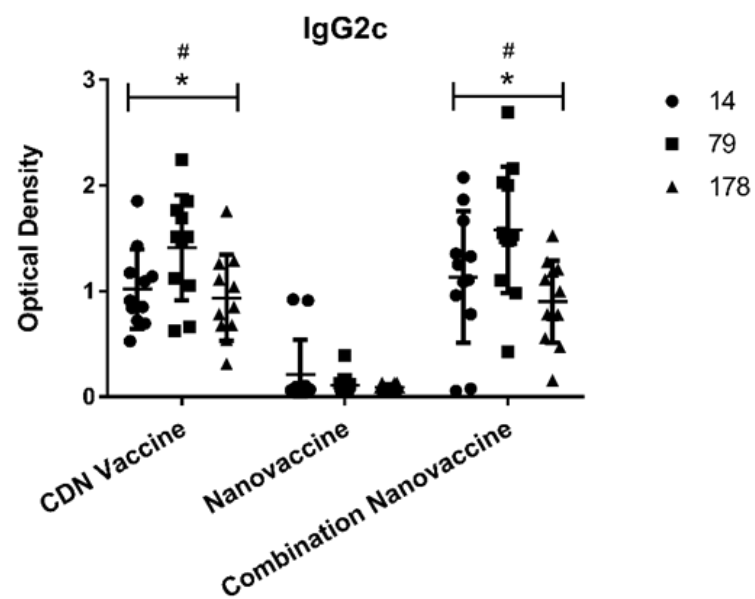
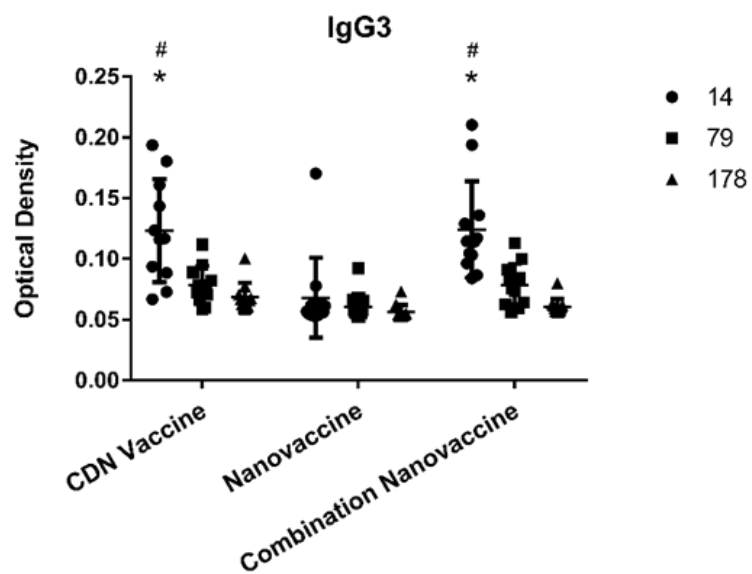
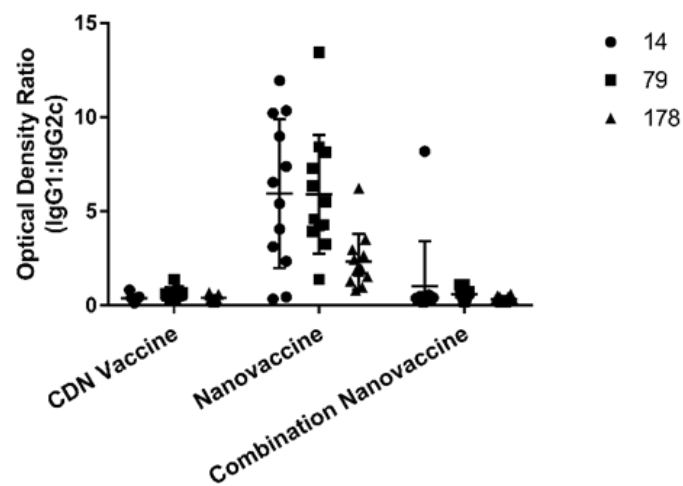


Figure 3.5. Long-lived antibody responses to F1-V originate from long-lived plasma cells in the bone marrow.

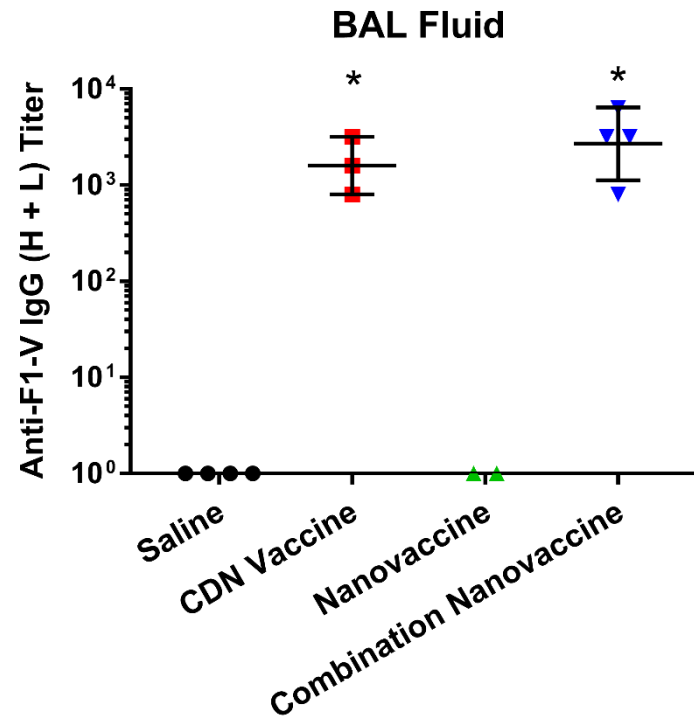
Bone marrow and splenic lymphocytes were harvested at 213-218 DPI from groups (n=3-4/group) of C57BL/6NCrl mice immunized with CDN Vaccine, Nanovaccine, Combination Nanovaccine regimens, or treated with saline, and were analyzed via ELISPOT for the number of F1-V-specific antibody secreting cells. Data represent the number of F1-V-specific antibody secreting cells per 500,000 cells in either A) bone marrow or B) spleen from individual mice from one experiment. The dashed line represents the number of F1-V-specific ASCs per 500,000 cells determined from saline-treated mice as a negative control * $p \leq 0.02$ compared to saline-treated mice. # $p \leq 0.03$ compared to Nanovaccine-immunized mice.



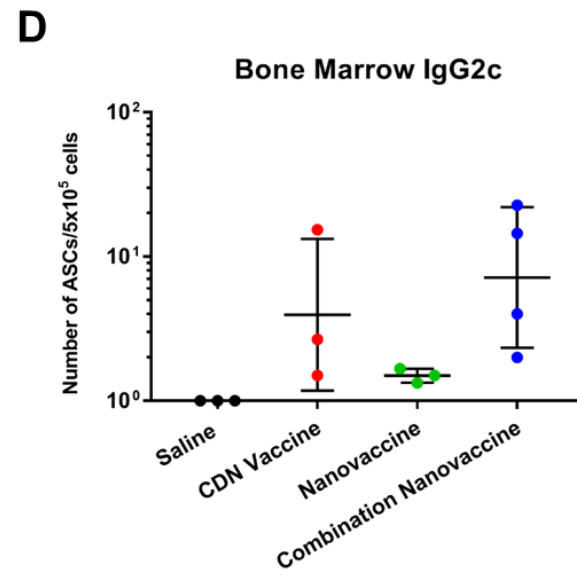
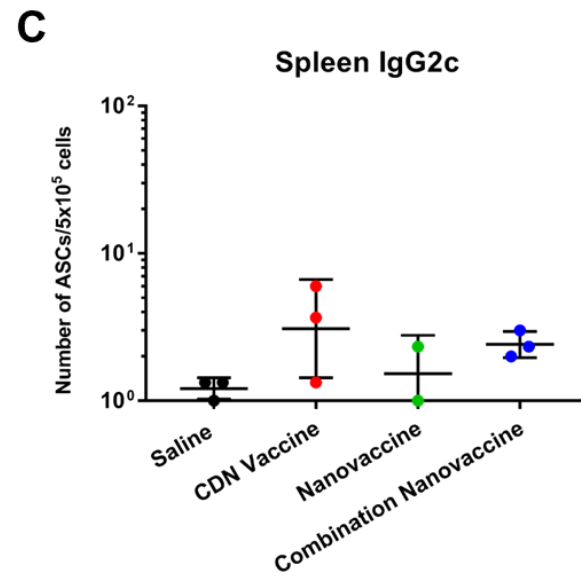
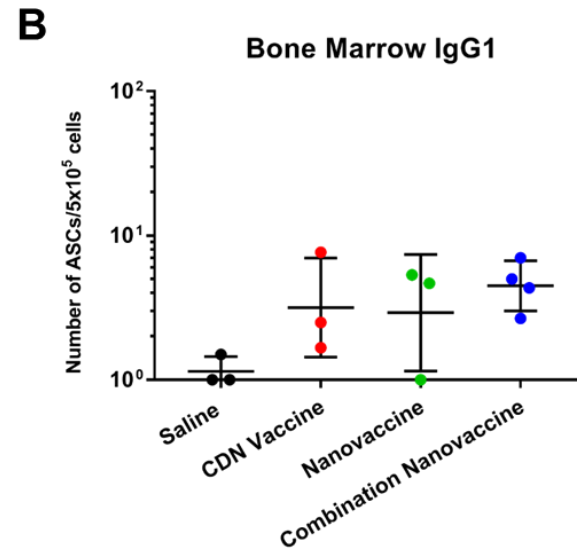
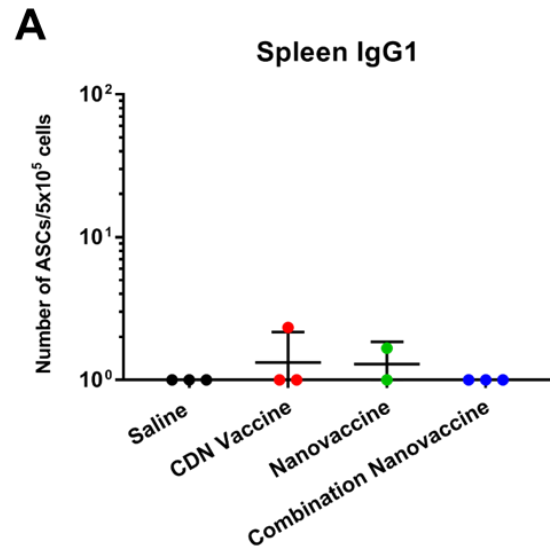
Supplemental Figure 3.1. Combination Nanovaccine provides long-lived antibody responses to F1-V. Groups of C57BL/6NCrl mice (n=12-16 per group) were immunized subcutaneously with the following treatments: F1-V + CDNs (CDN Vaccine), F1-V encapsulated into nanoparticles (Nanovaccine), F1-V encapsulated into nanoparticles + CDNs (Combination Nanovaccine) or saline. Serum samples were collected at 14, 36, 49, 79, 101, 121, 150, 178, and 218 DPI and analyzed for total anti-F1-V IgG (H+L) antibodies via ELISA. # $p \leq 0.05$ compared to CDN Vaccine. * $p \leq 0.0001$ compared to Nanovaccine-immunized and saline-treated mice.

A**B****C****D**

Supplemental Figure 3.2. Combination Nanovaccine induces class-switched antibody responses to F1-V. Groups of C57BL/6NCrl mice (n=12-16 per group) were immunized subcutaneously with the following treatments: F1-V + CDNs (CDN Vaccine), F1-V encapsulated into nanoparticles (Nanovaccine), F1-V encapsulated into nanoparticles + CDNs (Combination Nanovaccine) or saline. Serum samples were collected at 14, 79, and 178 DPI and analyzed for A) anti-F1-V IgG1, B) anti-F1-V IgG2c, and C) anti-F1-V IgG3 antibodies via ELISA. D) Ratio of anti-F1-V IgG1 to IgG2c responses in immunized mice. * $p \leq 0.0001$ compared to saline-treated mice. # $p \leq 0.05$ compared to Nanovaccine-immunized mice.



Supplemental Figure 3.3. Combination Nanovaccine induces long-lived antibody responses in BAL fluid against F1-V. Groups of C57BL/6NCrl mice (n=12-16 per group) were immunized subcutaneously with the following treatments: F1-V + CDNs (CDN Vaccine), F1-V encapsulated into nanoparticles (Nanovaccine), F1-V encapsulated into nanoparticles + CDNs (Combination Nanovaccine) or saline. BAL fluid was collected 213-218 DPI and assessed for total anti-F1-V IgG (H+L) antibodies via ELISA. * $p \leq 0.0001$ compared to Nanovaccine-immunized and saline-treated mice.



Supplemental Figure 3.4. Long-lived anti-F1-V IgG1 and IgG2c antibody secreting cell responses in bone marrow and spleen. Groups of C57BL/6NCrl mice (n=12-16 per group) were immunized subcutaneously with the following treatments: F1-V + CDNs (CDN Vaccine), F1-V encapsulated into nanoparticles (Nanovaccine), F1-V encapsulated into nanoparticles + CDNs (Combination Nanovaccine) or saline. Bone marrow and spleen lymphocytes were harvested at 213-218 DPI from groups (n=3-4/group) of mice and were analyzed via ELISPOT for the number of F1-V-specific IgG1 and IgG2c antibody secreting cells from spleen (panels A and C) or bone marrow (panels B and D). Data points represent the number of F1-V-specific antibody secreting cells per 500,000 bone marrow or spleen cells from individual mice from one experiment.

CHAPTER 4. SINGLE-DOSE COMBINATION NANOVACCINE INDUCES BOTH RAPID AND LONG-LIVED TOXIN NEUTRALIZING ANTIBODY RESPONSES AGAINST BACILLUS ANTHRACIS TOXIN

Part of this work is adapted from the thesis work of Ross Jeffrey Darling title “The STING of inflammatory adjuvants: Is the Toll too high?”

Modified from a manuscript to be submitted to *Int J Nanomedicine*

Sean M. Kelly¹, Kristina R. Larsen², Ross Darling², Michael J. Wannemuehler², Balaji Narasimhan^{1,3}

¹Department of Chemical and Biological Engineering, Iowa State University, Ames, IA

²Department of Veterinary Microbiology and Preventive Medicine, Iowa State University, Ames, IA

³Nanovaccine Institute, Ames, IA

Abstract

Bacillus anthracis, the causative agent of anthrax, continues to be one of the most prominent biological warfare and bioterrorism threats. Vaccination is likely to remain the most cost effective and patient friendly protective regimen to counter this threat in the foreseeable future. The commercially available AVA BioThrax, while currently the best option available, has a number of shortcomings where improvement would lead to a more practical and effective vaccine for use in the case of an exposure event. Identification of more effective adjuvants and novel delivery platforms is necessary in order to improve not only the effectiveness of the anthrax vaccine, but also enhance shelf stability and ease-of-use to improve patient compliance. In previous studies, cyclic dinucleotides have proven to be uniquely effective at inducing a

beneficial inflammatory environment that leads to high titer antibodies post-vaccination capable of providing rapid protection against *Yersinia pestis*. This makes them an ideal adjuvant candidate for an antitoxin vaccine where rapid generation of neutralizing titers is critical. Polyanhydride particles have proven to be effective at adjuvanting the vaccine associated adaptive immune response, as well as enhancing stability of encapsulated antigen. Here, we evaluate the individual contributions of cyclic dinucleotides, polyanhydride nanoparticles, and a combination thereof to elicit both rapid and long-lasting neutralizing antibody titers against the recombinant protective antigen (PA) from *B. anthracis*.

4.1 Introduction

Bacillus anthracis is a Gram-positive, spore-forming bacteria that is the causative agent of the disease anthrax, whose spores are capable of lasting decades to centuries in the environment¹⁰⁶. The natural course of infection for humans can occur via multiple routes, including through the skin via an open wound or flea bite (cutaneous anthrax), ingestion of infected meat (gastrointestinal anthrax), or direct inhalation of anthrax-containing spores (inhalation anthrax). This disease has devastated mankind throughout human history, proposed to have caused the plague of Athens (430–427 BCE)², and causing numerous infections throughout the 19th and 20th centuries in textile workers who came into contact with goat hair, sheep or alpacas wool². However, this pathogen has been used as a bioterror agent as well, with the Japanese experimenting on prisoners during World War II with various pathogens, including anthrax¹⁰³. Despite the agreement cosigned between the United States and 103 other countries to stop biological weapons

research in 1972, there still remains a concern of possible biological weaponization of lethal pathogens such as *B. anthracis*, especially due to the durability of the spores.

The main virulence factors associated with *B. anthracis* are displayed on two plasmids. The first plasmid, a 183-kb plasmid pXO1, allows *B. anthracis* to secrete the bipartite exotoxins, lethal toxin (LT) and edema toxin (ET), which have been shown to modulate innate cell signaling processes, including oxidative burst in macrophages, chemotaxis, cytokine secretion, and cellular activation¹⁰². There are three proteins that are secreted that make up the two bipartite toxins. They are protective antigen (PA), edema factor (EF), and lethal factor (LF). It has been revealed that transcription of the toxin genes is located on a pathogenicity island and is regulated by the anthrax toxin activator protein, a pleiotropic regulator protein, and also carbon dioxide and bicarbonate, thus inferring that recognition of the host tissue environment activates toxin secretion¹⁰². The second plasmid, pXO2, is a 96-kb plasmid that encodes for poly-γ-D glutamic acid (PGA), a polypeptide capsule that encapsulates the bacteria and blocks phagocytosis¹⁰². Interestingly, expression of PGA is also upregulated by the presence of carbon dioxide, further suggesting that bacterial virulence is increased following recognition of the host tissue environment¹⁰².

Most vaccine strategies center around inclusion of PA as it is believed that neutralizing its ability to heptamerize and translocate LF and EF into the host cell cytosol is critical to prevent dissemination of the bacteria and toxemia associated with mortality¹⁰². Indeed, a number of monoclonal antibodies have been generated that confer toxin neutralizing capacity *in vitro* and *in vivo*¹³⁵. A recent study demonstrated that anti-PA antibody titer and toxin neutralization titer following prime-boost vaccination did

correlate with protection in New Zealand white rabbits challenged intranasally with Ames strain spores¹³⁸. In a similar study with guinea pigs, it was shown that antibody titer did not correlate with protection, however toxin neutralization titer correlated with protection following prime-boost vaccination¹³⁹.

The currently FDA-approved vaccine Biothrax Anthrax Vaccine Adsorbed (AVA) consists of a cell-free supernatant adsorbed to aluminum hydroxide. It is believed that PA is the most immunogenic component of the AVA vaccine, and that anti-PA neutralizing antibodies are the correlate for protection. However, this vaccine currently requires five vaccinations in the first 18 months, followed by yearly boosters afterward in order to maintain protective immunity; thus there is still a need for a vaccine that can provide rapid and long-lasting protective immunity in the event of an exposure or outbreak event.

Cyclic dinucleotides (CDNs), a class of small molecule adjuvants, are recognized as microbial-associated molecular patterns (MAMPs) by the pattern recognition receptor (PRR) STING (STimulator of Interferon Genes)²⁷⁹, resulting in the phosphorylation of transcription factors NFκB and IRF3 and the induction of type I interferon (IFN), which is associated with anti-pathogenic activity^{211,212}. Cyclic di-guanosine monophosphate, the most well-studied CDN to date, has been recognized as a universal secondary messenger molecule in Gram-negative bacteria, playing a role in bacterial development, motility, and virulence²¹⁰. Vaccines adjuvanted with CDG induce a balanced immune response, characterized by equal presence of IgG subclasses in serum²¹⁵, and have been shown to elicit significantly higher antibody titers than alum-adjuvanted formulations²¹⁶.

Polyanhydride nanoparticle-based vaccines (i.e., nanovaccines) represent another vaccine adjuvant platform that has proven to enhance immune responses for a wide number of antigens, including recombinant PA (rPA). In previous studies, nanoparticles encapsulating rPA have shown the ability to maintain protein structure and functional activity following release²¹⁹. The ability to release functionally active protein was maintained for at least four months when stored on the shelf, even at elevated temperature up to 40 °C. Of note, polyanhydride chemistries that contained CPTEG and CPH best maintained the secondary and tertiary structures of rPA, as well as its functional activity. In addition, 20:80 CPTEG:CPH nanoparticles enhanced rPA shelf stability over 50:50 CPTEG:CPH nanoparticles. Previous work from our laboratories have shown that polyanhydride nano- and microparticle-based systems encapsulating antigen are capable of adjuvanting encapsulated antigen, allowing for dose sparing, and have shown to provide complete protection against multiple bacterial pathogens such as *Streptococcus pneumoniae* and *Yersinia pestis* intranasal challenge^{14,15,17,18,204,206}.

Previous studies from our laboratory have demonstrated that a combination of polyanhydride nanoparticles and CDNs were capable of providing complete protection against lethal pneumonic plague in only 14 DPI (see Chapter 3). Herein, we evaluated the efficacy of 20:80 CPTEG:CPH polyanhydride nanoparticles encapsulating rPA in combination with CDNs to elicit rapid and long-lasting anti-rPA antibody responses, characterized by anti-rPA antibody responses and *in vitro* toxin neutralization, with potential for long term shelf storage.

4.2 Methods and Materials

4.2.1 Materials

Chemicals used for the polymer and nanoparticles synthesis: 4-*p*-hydroxybenzoic acid, tri-ethylene-glycol, 1,6- dibromohexane were obtained from Sigma Aldrich (St. Louis, MO); dimethyl formamide, acetic acid, acetonitrile, acetic anhydride, toluene, methylene chloride, pentane were purchased from Fisher Scientific (Fairlawn, NJ) and 4-p-fluorobenzonitrile was purchased from Apollo Scientific (Cheshire, UK).

4.2.2 Polymer Synthesis

Monomers of 1,8-bis(*p*-carboxyphenoxy)-3,6-dioxaoctane (CPTEG) and 1,6-bis(*p*-carboxyphenoxy) hexane (CPH) was used to synthesize the copolymer 20:80 CPTEG:CPH via melt polycondensation reaction as previously described^{232,255}. The purity and molecular weight of the copolymer was characterized using ¹H nuclear magnetic resonance spectroscopy in deuterated chloroform. The molecular weight of the copolymer was near 5.3 kDa.

4.2.3 Particle Synthesis

Polyanhydride nanoparticles encapsulating 6.8% rPA (BEI resources, Cat# NR-3780, Manassas, VA), from *Bacillus anthracis*, by weight were synthesized using 20:80 CPTEG:CPH, via flash nanoprecipitation as essentially as previously described²⁰⁴. Briefly, 20:80 CPTEG:CPH polymer was dissolved in methylene chloride at a concentration of 20 mg/mL and rPA was suspended in this solution at a concentration of

2 mg/mL. This solution was poured into pentane at a solvent to anti-solvent ratio of 1:250. The nanoparticles were then collected using vacuum filtration.

4.2.4 Animals

Female A/J mice of six to eight weeks of age were obtained from Jackson Laboratory (Bar Harbor, ME). All studies involving the use of animals was carried out in accordance with and approval from the Iowa State University institutional animal care and use committee.

4.2.5 Vaccinations

Separate groups of 6-8 week old female A/J mice were immunized subcutaneously (sc) with one of the following vaccine formulations: 1) 5 µg rPA encapsulated in 73.5 µg of 20:80 CPTEG:CPH (6.8% wt/wt) nanoparticles (Nanovaccine), 2) 5 µg soluble rPA adjuvanted with 25 µg cyclic dinucleotide cdG (dithio-RP,RP-cyclic diguanosine monophosphate, CDN) (Aduro Biotech, Berkley, CA), 3) a combination of 5 µg rPA encapsulated in 73.5 µg of 20:80 CPTEG:CPH (6.8% wt/wt) nanoparticles adjuvanted with 25 µg CDN (Combination Nanovaccine), 4) 5 µg soluble rPA alone (PA), or 5) 5 µg soluble rPA adsorbed to a 1:9 dilution of Alhydrogel adjuvant 2% (Alhydrogel) (Invivogen, San Diego, CA).

4.2.6 Serum Antibody

Vaccinated mice were bled via saphenous vein at the indicated time points post vaccination and serum was collected and stored at -20°C until used for analysis. Anti-rPA serum antibody titers were measured via indirect ELISA. Costar 3590 96-well EIA/RIA high binding plates (Corning, Corning NY) were coated with 100 μL of PA (0.5 $\mu\text{g}/\text{mL}$ in PBS) and incubated overnight at 4°C . Plates were blocked using either 2% (w/v) Difco gelatin in PBS (0.05 M, PH 7.2) containing 0.05% Tween-20 (PBS-T) for 2 h at room temperature (Figure 4.2) or 2.5% (w/v) powdered skim milk dissolved in PBS-Tween with 0.05% Tween 20, pH 7.4, that had been incubated for 2 h at 56°C to inactivate any endogenous phosphatase activity (Figures 4.3 and 4.4). After three washes using PBS-T, serum samples were titrated across the plate using two-fold serial dilutions, starting at 1:200 (Figure 4.2) or 1:100 (Figures 4.3 and 4.4), in PBS-T containing 1% (v/v) normal goat serum. Samples were incubated overnight at 4°C . After three washes in PBS-T, an alkaline phosphatase conjugated goat anti-mouse IgG (H+L) secondary detection antibody (Cat# 115-005-003, Jackson ImmunoResearch, West Grove, PA) was diluted 1:1000, and 100 μL was added to the wells and allowed to incubate at room temperature for 2 h. Plates were washed three times with PBS-T and alkaline phosphatase substrate (Cat# BP2534, Fischer Scientific, Hampton, NH) was added at 1 mg/mL in buffer containing 50 mM sodium carbonate, 2 mM magnesium chloride, and sodium bicarbonate added to achieve a pH of 9.3. Color was allowed to develop for 30 min (Figures 4.3 and 4.4) or 2 h (Figure 4.2) and analyzed using the SpectraMAX 190 (Molecular Devices, San Jose, CA) at a wavelength of 405 nm.

4.2.7 Cell Culture

J774 cells were cultured and maintained in DMEM (Cat #15-013-CV, Corning) medium supplemented with 100 U/mL penicillin and 100 µg/mL streptomycin, 2 mM glutamine, and 10% FBS.

4.2.8 Toxin Neutralization Assay

In order to assess neutralizing activity of serum from vaccinated mice, a J774 cell based killing assay was used essentially as previously described^{298,299}. Briefly, J774 cells were seeded into 96-well flat bottom plates (Costar, Cat #3595) at a concentration of 4×10^4 cells/well and allowed to adhere for 18 hours. Serum samples were prepared in separate 96-well plates by adding 100 µL of serum at a 1:50 dilution and serially diluting them across the plate with two-fold dilutions. The serum samples were then incubated for 30 min with rPA and LF (BEI resources, Cat# NR-28544), at constant concentrations of 50 ng/mL and 40 ng/mL respectively, and then added to the prepared J774s. The cell-serum-toxin mixture was allowed to incubate for 4 hours after which 25 µL of a 5 mg/mL solution of 3-[4,5-dimethylthiazol-2-yl]-2,5-diphenyltetrazolium bromide (MTT) reagent (Invitrogen, Cat# M6494, Carlsbad, CA) was added. After two hours of incubation, supernatants were removed and 100 µL of dimethyl sulfoxide (Fisher Scientific, Cat# D128-500, Hampton, NH) was added to lyse and solubilize formazan crystals. The OD at 555 nm was measured on a SpectraMAX 190 and recorded for each sample.

4.2.9 Statistical Analysis

Data generated during anti-rPA serum IgG ELISAs were log2 transformed and analyzed within each time point via one-way ANOVA with a Tukey post-test for multiple comparisons. Cell based toxin neutralization experiments were analyzed by calculating an area under the curve for each treatment group with the baseline set at the negative control. Difference between treatments were determined via one-way ANOVA with a Tukey post-test for multiple comparison. All analyses were performed using GraphPad Prism 8.0 (GraphPad Software, La Jolla, CA).

4.3 Results

4.3.1 Polyanhydride Nanoparticle Characterization

Following synthesis, the 10%-loaded rPA (w/w) 20:80 CPTEG:CPH nanoparticles were characterized for size distribution and encapsulation efficiency of encapsulated F1-V. The size of the nanoparticles was consistent with previous work ¹⁵, with a mean diameter of 255 ± 98 nm and a polydispersity index of 0.15, indicating a narrow size distribution (Figure 4.1). The encapsulation efficiency of the rPA within the nanoparticles was 68%.

4.3.2 Polyanhydride Nanovaccine Elicits High and Long Lasting Anti-PA Antibody Responses

In order to assess the ability of the CDNs and polyanhydride nanoparticles to elicit anti-rPA responses, female A/J mice (n = 4 per group) were immunized subcutaneously with a single dose of one of the following vaccine formulations: i) 5 µg soluble rPA (sPA), ii) 5 µg soluble rPA adjuvanted with 25 µg CDNs (CDN Vaccine), iii)

5 µg rPA encapsulated into polyanhydride nanoparticles (6.8% w/w) (Nanovaccine), or iv) 5 µg rPA encapsulated into polyanhydride nanoparticles (6.8% w/w) co-adjuvanted with 25 µg CDNs (Combination Nanovaccine). Serum samples were collected at 2-, 4-, 8-, and 15-weeks post-vaccination and anti-rPA total IgG antibody titers were evaluated at each time point.

The vaccinated A/J mice rapidly attained high anti-rPA titers and maintained them over time (Figure 4.2). The only formulations able to significantly improve the A/J antibody titers over that induced by sPA alone were the CDN Vaccine and the Combination Nanovaccine. The 15-week time point indicated the serum of animals immunized with the Combination Nanovaccine had the highest titers and this elevated titer was maintained compared to rPA alone. Analysis of the serum of animals immunized with the Nanovaccine alone indicated that this formulations was insufficient in terms of rapidly enhancing the magnitude of the anti-rPA antibody response. These results suggest that the CDNs are able to induce rapid and long-lived antibody response to rPA in A/J mice, which may be improved when combine with polyanhydride nanoparticles.

4.3.3 Polyanhydride Nanovaccine Elicits Rapid Toxin Neutralization Antibodies against the Anthrax Toxin

Next, the ability of the Combination Nanovaccine to induce anti-rPA antibody responses was compared to an alhydrogel-adjuvanted vaccine formulation in female A/J mice. In order to normalize by the dose of antigen for comparison between the Combination Nanovaccine and alhydrogel-adjuvanted vaccine, rPA was adjuvanted with a 1:9 dilution of alhydrogel (~0.9-1.1 mg/mL aluminum content). Female A/J mice (n = 8

per group) were immunized subcutaneously with a single dose of one of the following vaccine formulations: i) 5 µg soluble rPA (sPA), ii) 5 µg soluble rPA adjuvanted with alhydrogel (Alhydrogel), or iii) 5 µg rPA encapsulated into polyanhydride nanoparticles co-adjuvanted with 25 µg CDNs (Combination Nanovaccine).

Blood samples were collected from immunized animals 15 days post-immunization (DPI). Anti-rPA total IgG antibody titers in sera of mice immunized with either the Alhydrogel formulation or Combination Nanovaccine were similar and had significantly ($p \leq 0.0001$) higher total IgG anti-rPA antibody titers compared to titers in sera of mice immunized with soluble rPA alone (Figure 4.3A). Interestingly, despite having similar magnitude of total IgG, the Combination Nanovaccine induced significantly ($p = 0.008$) higher toxin neutralizing antibody responses compared to the Alhydrogel formulation at 15 DPI, determined via integrating the area under the curve of the Log_2 transformed serum dilution curves (Figure 4.3B and Table 4.1). Therefore, these results indicate a qualitative difference in the anti-rPA response induced by the Combination Nanovaccine and Alhydrogel formulations, with the combination of polyanhydride nanoparticles and CDNs improving the anthrax toxin neutralizing response over that of alhydrogel, despite having similar magnitude anti-rPA IgG antibody titers.

4.3.4 Combination Nanovaccine and Alhydrogel formulation Elicit Similar Long Term Anti-PA Responses

Serum samples were additionally collected 30- and 46-days post-vaccination from female A/J mice immunized with the above vaccine formulations in order to compare the long term anti-rPA antibody response elicited by the Combination

Nanovaccine and Alhydrogel formulation. The magnitude of anti-rPA response between mice vaccinated with either formulations was similar across all time points evaluated, with significantly ($p \leq 0.0001$) higher anti-rPA total IgG antibody titers compared to animals vaccinated with soluble rPA (Figure 4.4A). The ability of serum from Combination Nanovaccine-immunized mice to neutralize lethal toxin was similar to that of the Alhydrogel formulation by 46 DPI (Figure 4.4B). Thus, the total anti-rPA IgG response and PA neutralizing serum responses in mice immunized with either the Combination Nanovaccine and Alhydrogel formulations was similar after 15 DPI, despite the higher earlier responses elicited by the Combination Nanovaccine by 15 DPI. Additionally, the Combination Nanovaccine formulation successfully induced high titer anti-rPA IgG responses rapidly, which was maintained over time.

4.4 Discussion

In this work, the ability of a combination polyanhydride nanoparticle-based vaccine platform co-adjuvanted with CDNs to induce neutralizing antibodies against the protective antigen of *B. anthracis* was evaluated. The results of this work illustrated the induction of high titer neutralizing antibodies with a single-dose formulation of rPA-containing polyanhydride nanoparticles co-adjuvanted with CDNs, which were able to elicit significantly higher anti-rPA toxin neutralizing antibodies compared to PA adjuvanted with alhydrogel by 15 DPI, despite having similar overall anti-rPA total IgG titers.

While natural inhalation infection of humans with *B. anthracis* spores is rare, its durable spores and high lethality capable of infecting hundreds of thousands of

individuals with a single aerosol dispersion, places *B. anthracis* in a position of prominence as a major biological warfare agent^{300–302}. The difficulty in diagnosing anthrax, with its early onset of cold-like symptoms, is one of the major hurdles in managing the response to a widespread release event of *B. anthracis* spores^{102,301}. If anthrax infection is identified early after exposure, intervention or prophylaxis with antibiotics is critical to prevent serious illness and death. This antibiotic regimen must be adhered to for an extended period of time as spores can persist in a dormant state and cause disease well after the initial exposure^{302–304}. In order to respond to a large-scale release, a therapeutic intervention would require a largescale stockpile of antibiotics to be readily available at all times and would require that health care workers follow up with individuals to improve upon historically poor patient compliance³⁰⁵. Another class of therapeutic interventions in development are toxin neutralizing monoclonal antibodies (mAb). Neutralizing mAbs would provide benefits over antibiotic usage as the two to four-week half-life of the mAbs after infusion could prove effective at preventing severe disease with limited treatments^{306,307}.

While these effective treatment options are available, deploying them on any large scale remains a public health obstacle. Treatments including vaccination for higher risk populations or those who have been exposed or were potentially exposed remains the most cost effective and most patient friendly option available^{308,309}. Even as one of the ideal approaches to dealing with *B. anthracis* as a biological agent, current vaccines targeting PA have room for improvement. The major issues that need to be resolved in next generation anti-PA vaccines are: i) reducing the number of doses required to effectively induce high neutralizing titer; ii) identification of adjuvants that

skew responses to neutralizing epitopes rather than towards non-neutralizing epitopes; and iii) improving the shelf-life stability of the PA protein and formulated vaccines^{310–315}.

Encapsulation of protein payloads, including PA, into polyanhydride particle formulations has demonstrated the stability enhancing properties that encapsulation can provide during storage and upon protein release^{19,218}. This enhanced stability provided by polyanhydride nanoparticles would be particularly advantageous in the stockpiling and storage of vaccine doses to be readily distributed should the need arise.

In immunization studies evaluating the immune response of female A/J mice, the NP formulation with 100% of the rPA encapsulated did not result in a measurable increase in anti-PA antibody titers compared to that induced by rPA alone (Figure 4.2). The inclusion of CDNs as a co-adjuvant, either alone or combined with the NP formulation, led to increases in anti-rPA titers across all time points evaluated. At 108 days after the single dose immunization of A/J mice, the total anti-rPA IgG response induced by the Combination Nanovaccine exhibited the greatest titer suggesting there is a potential immunological benefit when antigen is encapsulated within and released from nanoparticles over time (Figure 4.2).

This propensity of CDNs to induce rapid toxin neutralizing titers could lead to rapid immunity for individuals in an effected area and limit the danger of the resulting exclusion zone created by *B. anthracis* spores. Rapid generation of neutralizing antibodies would also have the potential of reducing the extended (60+ days) of prophylactic antibiotic treatments used when potential exposure has occurred. In cell-based toxin neutralization assays, all tested vaccine formulations induced detectible neutralization of the holotoxin as evidenced by the inhibition of cell death (Figures 4.3

and 4.4 and Table 4.1), however at 15 DPI the Combination Nanovaccine was able to elicit significantly higher neutralizing antibodies in A/J mice compared to that of rPA adjuvanted with alhydrogel, which closely resembles the response induced by the commercially available AVA vaccine (Figure 4.3). This early high titer responses observed illustrate a potential strength for vaccination after a large-scale dispersal event.

In conclusion, a Combination Nanovaccine comprising polyanhydride nanoparticles co-adjuvanted with CDNs was able to elicit both rapid and durable anti-rPA antibody responses.

4.5 Tables

Table 4.1. Summary of toxin neutralization assays.

Days Post-Immunization	Vaccine Formulation	Area Under Curve
15	sPA	1.03 ± 0.50
	Alhydrogel	$5.90 \pm 0.65^*$
	Combination Nanovaccine	$10.36 \pm 0.95^{*\$}$
46	sPA	8.51 ± 1.08
	Alhydrogel	$19.85 \pm 0.72^*$
	Combination Nanovaccine	$21.33 \pm 0.74^*$

*indicates significant differences ($p \leq 0.05$) from sPA

$\$$ indicates significant differences ($p \leq 0.05$) from Alhydrogel

4.6 Figures

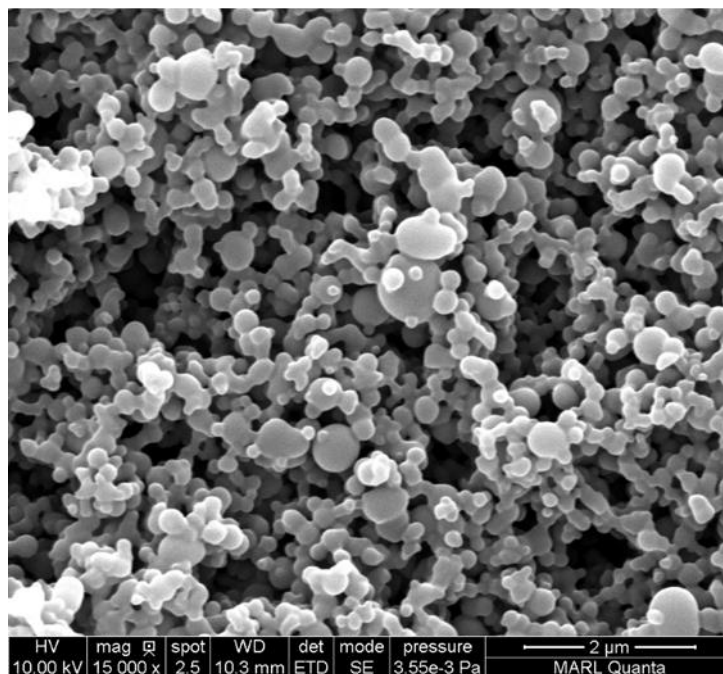


Figure 4.1. Characterization of PA Nanovaccine. A) Representative scanning electron micrograph image of PA nanovaccine (scale bar = 2 μm). Nanoparticle mean diameter was 255 ± 98 nm, determined via ImageJ analysis.

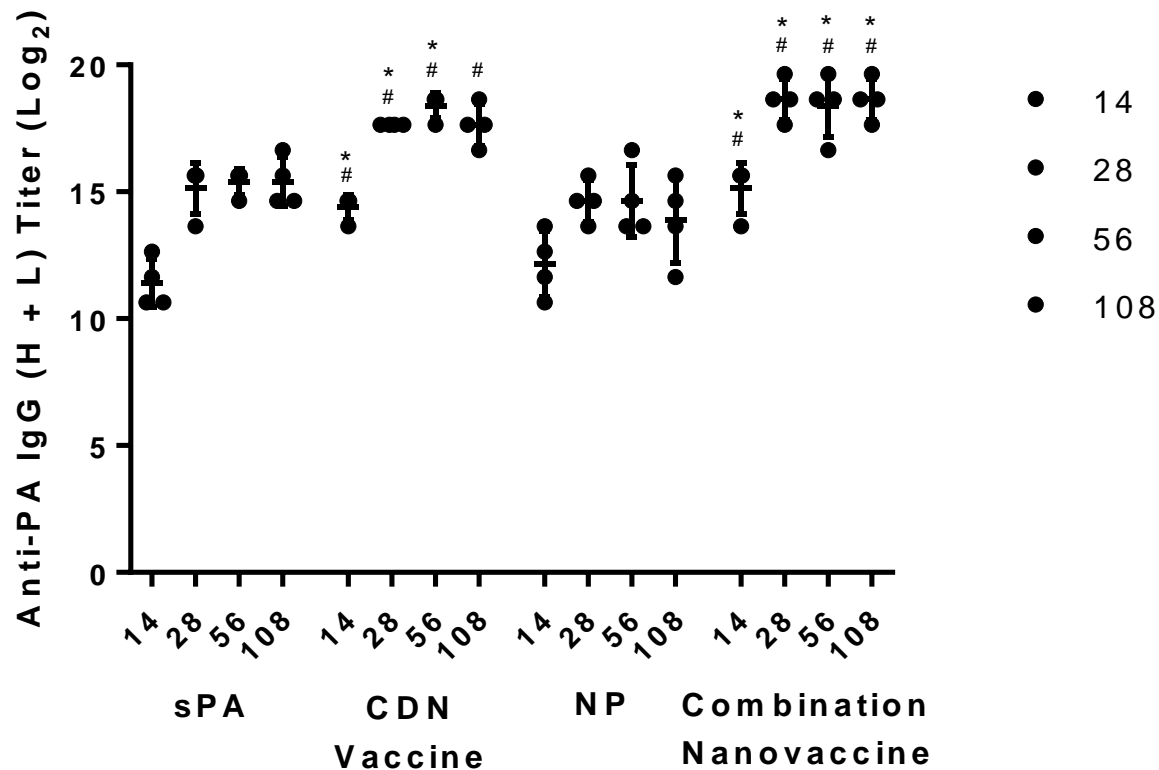


Figure 4.2. Combination Nanovaccine induces antibodies against protective antigen. A/J (n=4) mice were vaccinated subcutaneously against the PA protein from *B. anthracis*. The formulations consisted of 5 µg rPA encapsulated in 20:80 CPTEG:CPH nanoparticles (NP), 5 µg soluble rPA adjuvanted with 25 µg CDNs (CDN Vaccine), a combination of 5 µg rPA encapsulated in 20:80 CPTEG:CPH nanoparticles adjuvanted with 25 µg CDN (Combination Nanovaccine), or 5 µg soluble rPA alone (sPA). Total serum IgG antibody titer to rPA was quantified via ELISA at 2-weeks, 4- weeks, and 8-weeks post-immunization. Titer values were Log₂ transformed and compared at each time point for statistical significance between treatment groups via an ordinary one-way ANOVA with a Tukey's multiple comparison test. P value is indicated as follows for each comparison indicated (*#@\$=p<0.05) (#=NP, \$=CDN Vaccine, @=Combination Nanovaccine, *=sPA). Individual animals are shown with bars indicating mean ± SEM.

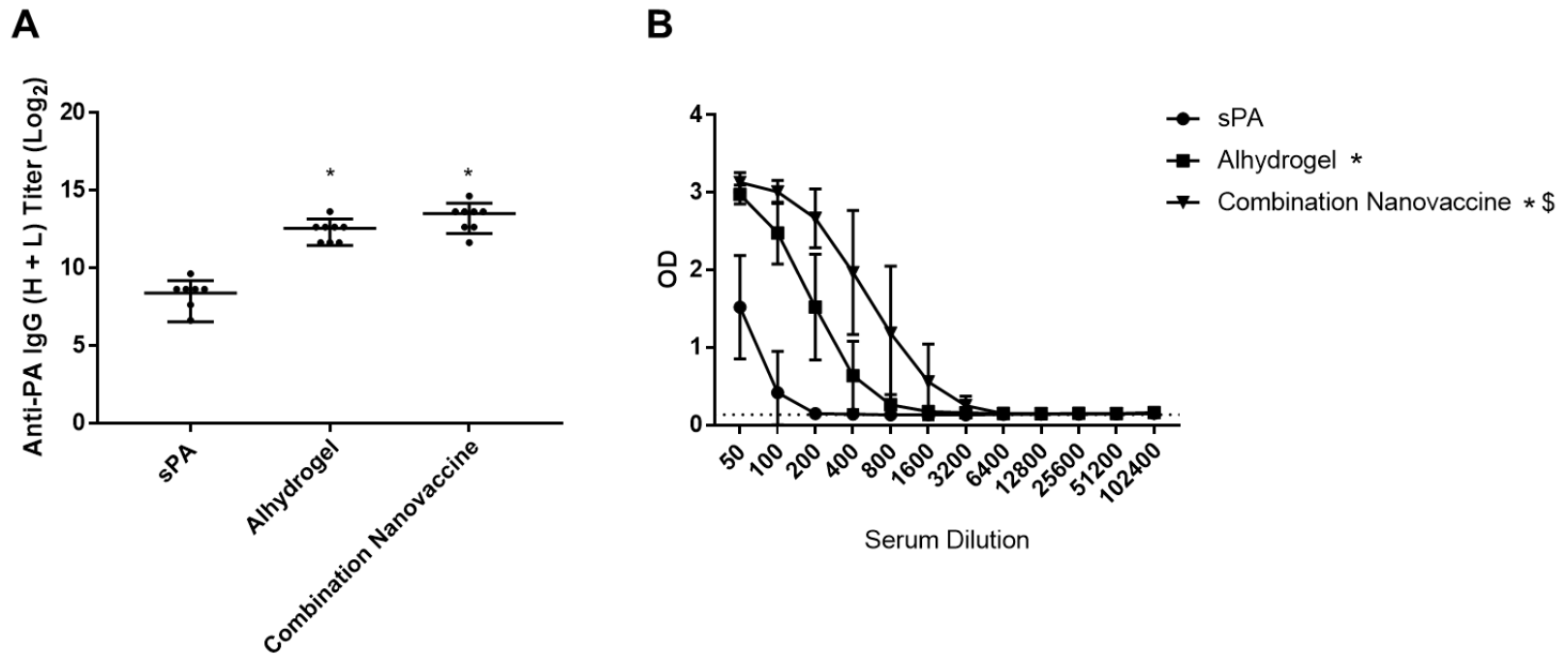


Figure 4.3. Combination Nanovaccine elicits rapid toxin neutralizing antibodies against protective antigen. A/J (n=8) mice were vaccinated subcutaneously against the PA protein from *B. anthracis*. The formulations consisted of 5 µg soluble rPA adsorbed to a 1:9 dilution of alhydrogel (Alhydrogel), a combination of 5 µg rPA encapsulated in 20:80 CPTEG:CPH nanoparticles adjuvanted with 25 µg CDN (Combination Nanovaccine), or 5 µg soluble rPA alone (sPA). (A) Total serum IgG antibody titer to rPA was quantified via ELISA at 15 days post-immunization. Titer values were Log₂ transformed and compared at each time point for statistical significance between treatment groups via an ordinary one-way ANOVA with a Tukey's multiple comparison test. *P* value is indicated as follows for each comparison indicated (*#@\$=p<0.05) (\$=Alhydrogel, @=Combination Nanovaccine, *=sPA). Individual animals are shown with bars indicating mean ± SD. (B) Neutralizing antibody titers were determined in serum collected 15 days post-immunization via an MTT assay. Dilution values were Log₂ transformed and the mean area under the curve (AUC) was calculated for each treatment group. The AUC was compared between treatment groups via one-way ANOVA with a Tukey's multiple comparison test. *P* value is indicated as follows (*@\$=p<0.05) (@=Combo, \$=Alhydrogel *=sPA) as compared to all other groups in the figure legend. The lower dotted line indicates the no sample control average OD (0.136). Group averages are shown with error bars indicating mean ± SD.

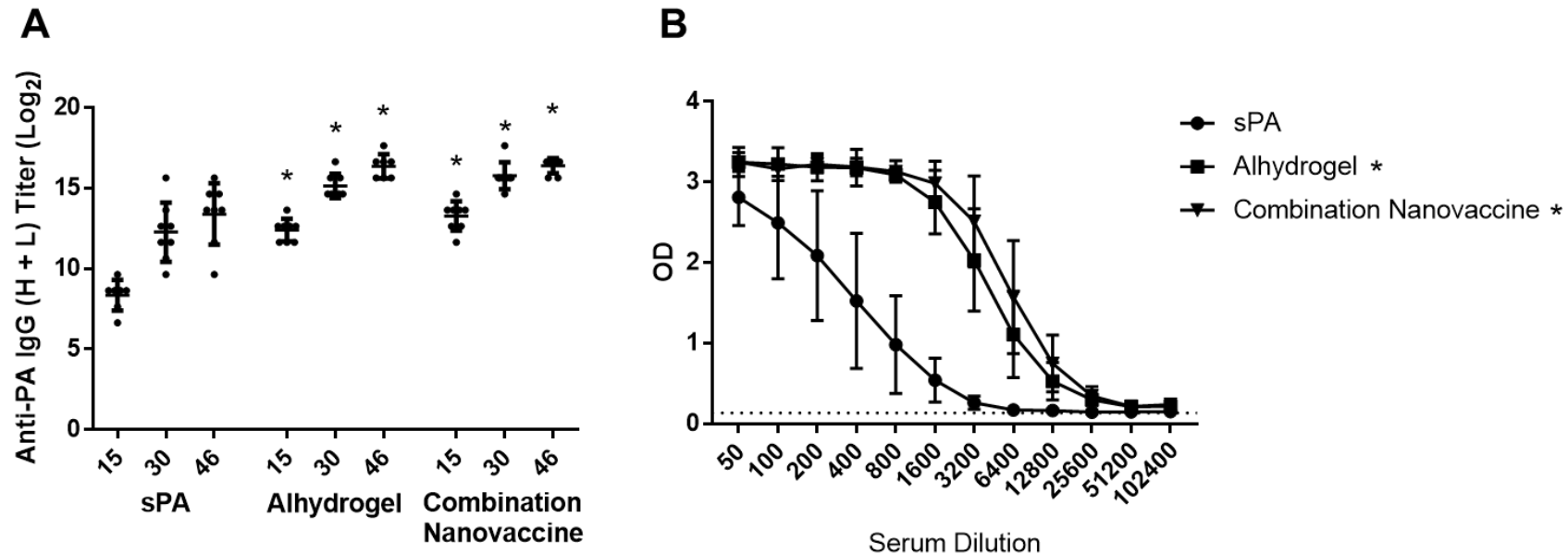


Figure 4.4. Combination Nanovaccine elicits similar long term toxin neutralizing antibodies against protective antigen compared to alhydrogel. A/J (n=8) mice were vaccinated subcutaneously against the PA protein from B. anthracis. The formulations consisted of 5 µg soluble rPA adsorbed to a 1:9 dilution of alhydrogel (Alhydrogel), a combination of 5 µg rPA encapsulated in 20:80 CPTEG:CPH nanoparticles adjuvanted with 25 µg CDN (Combination Nanovaccine), or 5 µg soluble rPA alone (sPA). (A) Total serum IgG antibody titer to rPA was quantified via ELISA at 15, 30, and 46 days post-immunization. Titer values were Log₂ transformed and compared at each time point for statistical significance between treatment groups via an ordinary one-way ANOVA with a Tukey's multiple comparison test. P value is indicated as follows for each comparison indicated (*\$@=p<0.05) (\$=Alhydrogel, @=Combo, *=sPA). Individual animals are shown with bars indicating mean ± SD. (B) Neutralizing antibody titers were determined in serum collected 46 days post-immunization via an MTT assay. Dilution values were Log₂ transformed and the mean area under the curve (AUC) was calculated for each treatment group. The AUC was compared between treatment groups via one-way ANOVA with a Tukey's multiple comparison test. P value is indicated as follows (*@\$=p<0.05) (\$=Alhydrogel, @=Combo, *=sPA) as compared to all other groups in the figure legend. The lower dotted line indicates the no sample control average OD (0.136). Group averages are shown with error bars indicating mean ± SD.

CHAPTER 5. EFFICACY OF MUCOSAL POLYANHYDRIDE NANOVACCINE AGAINST RESPIRATORY SYNCYTIAL VIRUS INFECTION IN THE NEONATAL CALF

Published in *Scientific Reports* 2018:8:1-15

Jodi L. McGill^{1,4}, Sean M. Kelly², Pankaj Kumar^{1,5}, Savannah Speckhart^{1,6}, Shannon L. Haughney², Jamie Henningson¹, Balaji Narasimhan^{2,4}, Randy E. Sacco^{3,4}

¹Department of Diagnostic Medicine and Pathobiology, Kansas State University, Manhattan, KS

²Department of Chemical and Biological Engineering, Iowa State University, Ames, IA

³Ruminant Diseases and Immunology Research Unit, National Animal Disease Center, Agricultural Research Service, USDA, Ames, IA

⁴Nanovaccine Institute, Ames, IA

⁵Current address: Charles River Laboratories, Spencerville, OH

⁶Current address: Department of Animal Science, University of Tennessee, Knoxville, TN

Abstract

Human respiratory syncytial virus (HRSV) is a leading cause of severe acute lower respiratory tract infection in infants and children worldwide. Bovine RSV (BRSV) is closely related to HRSV and a significant cause of morbidity in young cattle. BRSV infection in calves displays many similarities to RSV infection in humans, including similar age dependency and disease pathogenesis. Polyanhydride nanoparticle-based vaccines (i.e., nanovaccines) have shown promise as adjuvants and vaccine delivery vehicles due to their ability to promote enhanced immunogenicity through the route of administration, provide sustained antigen exposure, and induce both antibody- and cell-mediated immunity. Here, we developed a novel, mucosal nanovaccine that

encapsulates the post-fusion F and G glycoproteins from BRSV into polyanhydride nanoparticles and determined the efficacy of the vaccine against RSV infection using a neonatal calf model. Calves receiving the BRSV-F/G nanovaccine exhibited reduced pathology in the lungs, reduced viral burden, and decreased virus shedding compared to unvaccinated control calves, which correlated with BRSV-specific immune responses in the respiratory tract and peripheral blood. Our results indicate that the BRSV-F/G nanovaccine is highly immunogenic and, with optimization, has the potential to significantly reduce the disease burden associated with RSV infection in both humans and animals.

5.1 Introduction

Human respiratory syncytial virus (HRSV) is a leading cause of severe acute lower respiratory tract disease in infants and young children worldwide⁷ and accounts for up to 70% of hospitalized bronchiolitis cases in industrialized countries⁸. Globally, there are an estimated 33 million new episodes of HRSV-associated disease in children under five years of age with more than 100,000 resultant deaths³¹⁶. Severe RSV infection has been linked with the development and exacerbation of recurrent wheezing and asthma¹⁰, and is a predisposing factor to the development of otitis media¹¹. To date, there are no safe and effective vaccines available for HRSV.

RSV-specific immune responses are directed against a number of viral proteins; however, the fusion (F) and attachment (G) proteins appear to be the most important targets¹⁶⁷; and thus represent attractive options for the development of subunit vaccines. The F protein exists in two forms on the virion surface: a metastable pre-

fusion form and a stable post-fusion trimer. Post-fusion F contains two major neutralizing epitopes, antigenic sites II and IV¹⁸⁴. Vaccines utilizing post-fusion F elicit high-affinity, site-II directed neutralizing antibodies and have been shown to be highly efficacious in mice and cotton rats^{185,186}. Post-fusion F is also highly stable, making it an appealing candidate for incorporation into a subunit vaccine. Reports in mice have shown that vaccines that elicit G-protein specific antibody and T cell responses are protective against RSV infection^{187,188}. Bastien *et al.* also demonstrated that immunization with a conserved peptide from the BRSV G protein afforded partial protection against BRSV infection in cattle¹⁸⁸. The F and G protein have also been shown suitable vaccine targets in cattle, as recombinant vector-vaccines targeting the BRSV F^{190,317} and G^{190,192,318} proteins, and recombinant plasmid-based strategies targeting the G protein^{192,193}, have both been shown to reduce virus shedding and BRSV-associated lung pathology in challenged calves.

A significant barrier to the development of a safe and efficacious vaccine for use against HRSV has been the lack of a suitable animal model. Although mice and cotton rats are commonly used to test candidate vaccines, they are only semi-permissive for HRSV replication, and the pathogenesis of disease significantly differs from that observed in human infants (recently reviewed in ¹⁶¹). Bovine respiratory syncytial virus (BRSV) is genetically and antigenically closely related to HRSV and is a primary cause of severe acute lower respiratory tract disease in young cattle. Although host specific, BRSV and HRSV display similar epidemiology, pathogenesis and clinical expression in their respective hosts. Development of an efficacious vaccine for BRSV poses similar challenges to that faced for HRSV, particularly the need to immunize the very young,

the presence of maternally-derived antibodies and the possibility for the development of vaccine-enhanced disease. Thus, the calf is an ideal model for testing novel vaccine candidates and determining appropriate correlates of vaccine-induced protection from infection.

Polyanhydride nanoparticle-based vaccines (i.e., nanovaccines) have been studied extensively as a vaccine adjuvant and/or delivery platform and provide a safe, efficacious alternative to traditional vaccines²⁸⁰. These biodegradable polymers are based on 1,6-bis(*p*-carboxyphenoxy)hexane (CPH), 1,8-bis(*p*-carboxyphenoxy)-3,6-dioxaoctane (CPTEG), and sebacic anhydride (SA). They are biocompatible^{13,250}, have shown to stabilize labile proteins^{19,220,281}, and demonstrate sustained release of encapsulated proteins due to their surface-erodible properties^{14,18,19,232}, allowing for the possibility of single-dose administration. In addition, polyanhydride nanovaccines display chemistry-dependent cellular uptake and intracellular persistence by antigen presenting cells (APC)^{15,16,223}, which can aid in adjuvanting poorly immunogenic proteins. These nanovaccines can be delivered using multiple routes of administration, including intranasally (i.n.)^{14,15,204,319}. Finally, these nanoadjuvants have been shown to induce sustained humoral³²⁰ and cellular immunity^{297,321}. These properties have been exploited to design nanovaccine formulations against multiple pathogens, including *Yersinia pestis*, *Bacillus anthracis*, *Streptococcus pneumoniae*, and influenza A virus²⁸⁰. The nanovaccine chosen for the current studies is based on the amphiphilic 50:50 CPTEG:CPH due to its enhanced pathogen-mimicking characteristics¹⁵, improved stability of encapsulated antigen^{19,220}, and suitability as an effective formulation for i.n. delivery^{14,15,204,319}.

Here, we report the development of a polyanhydride-based nanovaccine that contains the recombinant post-fusion F and G proteins from BRSV and demonstrate for the first time, that a single, i.n. immunization of the BRSV-F/G nanovaccine induces robust local cellular and humoral immunity in the respiratory tract, reduced virus-associated pathology, reduced viral burden, and decreased incidence of virus shedding in neonatal calves.

5.2 Materials and Methods

5.2.1 Protein Production and Purification

Recombinant F protein

The recombinant fusion (F) protein was produced by Genscript (Piscataway, NJ) using a recombinant baculovirus expression system. The expression scheme was selected based upon previous publications^{322–324}. The F protein from BRSV strain 375 (L158-T529, GenBank FJ543092.1) was expressed with a truncation at the COOH terminus, as described by Wathen *et al.*³²³. The construct was then modified at the 3' end with the addition of a linker sequence, a GCN4 trimerization domain and a HIS-tag. Sf9 cells were grown in Sf-900 II SFM Expression Medium (Life Technologies) and maintained in Erlenmeyer Flasks at 27° C in an orbital shaker. One day before transfection, the cells were seeded in 6 wells. On the day of transfection, DNA and Cellfectin II (Life Technologies) were added into the plate with cells ready for transfection. Cells were incubated in Sf-900 II SFM for 5-7 days at 27° C before harvest. The supernatant was collected after centrifugation and designated as P1 viral stock. P2 was amplified for later infection. For preparation of the recombinant protein, Sf9 cells

were infected with the recombinant P2 virus and incubated for 5-7 days at 27° C before harvest. Cell pellets were harvested and lysed using Triton-X 100 lysis buffer and the precipitation of cell lysate was dissolved using urea. The target protein was obtained by one-step purification using a Ni column and 8 M urea-based wash buffer. Fractions were pooled and refolded followed by 0.22 µm filter sterilization. The proteins were analyzed by SDS-PAGE and Western blot by using standard protocols for molecular weight and purity measurements. The primary antibody for Western blot was Mouse-anti-his mAb (GenScript,). The protein concentration was determined by Bradford protein assay with BSA as a standard. The protein was confirmed to contain <0.1 EU/µg (LAL Endotoxin Assay Kit, Genscript).

Recombinant G protein

Recombinant G protein was expressed with the assistance of the Protein Production Group, COBRE Center for Protein Structure and Function, University of Kansas. The ectodomain of the attachment (G) protein from BRSV strain 375 (S67-I257, GenBank L10925.1) was modified at the 3' end by a HIS-tag and expressed in *E.coli* using the pTBSG vector as previously described³²⁵. For production of the recombinant protein, recombinant *E. coli* was grown overnight in LB media containing ampicillin and chloramphenicol. The cells were induced with IPTG for 3 hours, then cells were pelleted. The cell pellets were lysed in 20 mM Tris buffer (pH 8.0) containing 1% Triton-X 100 and frozen. The cell lysate was sonicated until the suspension was no longer viscous and then the soluble fraction removed by centrifugation. The insoluble fraction (inclusion bodies) was solubilized in urea buffer (6 M urea, 50 mM Tris-HCl (pH

8.0), and 500 mM NaCl). The solubilized fraction was purified by Ni-NTA Affinity Chromatography. The endotoxin levels on the resulting purified fractions were confirmed to be less than 1 EU/ μ g.

5.2.2 Polymer Synthesis and Characterization

CPTEG and CPH monomer synthesis and 50:50 CPTEG:CPH copolymer synthesis using melt polycondensation were performed as described previously^{206,232}. Copolymer composition and molecular weight were determined using ¹H NMR (DXR 400), specifically by end group analysis of NMR spectra. The copolymer molecular weight was determined to be 5,003 g/mol with a molar composition of 48% CPTEG and 52% CPH.

5.2.3 Nanoparticle Synthesis

50:50 CPTEG:CPH nanoparticles encapsulating 2.4% w/w protein, consisting of 1.9% w/w G protein and 0.5% w/w F protein, were synthesized using water/oil/oil nanoprecipitation²⁵⁶. Briefly, F and G proteins were dissolved into nanopure water at 178 μ g/ML. 50:50 CPTEG:CPH copolymer was dissolved in methylene chloride at 20 mg/ML, and the protein solution was pipetted into the solvent. The mixture was sonicated (30 Hz for 30 s), and poured into a non-solvent (pentane chilled to -10 °C) at a solvent to non-solvent ratio of 1 to 250. The suspension was immediately vacuum filtered to recover nanoparticles encapsulating the proteins, with a yield of ca. 62%. Nanoparticles not encapsulating protein (i.e., “empty” nanoparticles) were synthesized as a control using the same procedure as described above. For preliminary *in vitro*

studies, CPTEG:CPH nanoparticles were also generated using a cocktail of overlapping, 20-mer peptides from the BRSV G protein. The peptides were encapsulated at 2% w/w protein using the protocol described above. The G-protein peptide nanoparticles were used for the alveolar macrophage studies in Figure 5.2C and the moDC data in Supplementary Figure 5.1.

5.2.4 Protein Release Assay

BRSV-G nanoparticles were incubated in microcentrifuge tubes at a concentration of 20 mg/ml in 0.5 ml of 0.1 M PBS buffer (pH 7.4). Samples were sonicated (30 Hz for 30 s) and placed in a shaker incubator at 37 °C. Samples were centrifuged at 10,000 rcf for 10 min and 0.4 ml of supernatant was removed and replaced with fresh buffer at indicated time points. Aliquots were stored at 4 °C and protein mass released was measured via micro bicinchoninic acid (microBCA) analysis at an absorbance of 562 nm. After 35 days, unreleased protein was extracted by 40 mM NaOH using 0.2 ml per microcentrifuge tube, as described³²⁶. The mass of protein released was determined via microBCA analysis and the encapsulation efficiency, which was defined as the total amount of protein released divided by the initial mass of protein, was calculated.

5.2.5 Animals

BRSV-F/G protein immunogenicity studies

Peripheral blood and sera were collected from eight female adult Holstein cows housed at the Kansas State University Dairy in Manhattan, KS. Animals from this herd have BRSV-specific antibodies and BRSV-specific CD4 T cells³²⁷.

5.2.6 Vaccine Studies

Twenty-four, colostrum replete, mixed-gender Holstein calves were enrolled at 2-3 weeks of age and were randomly assigned to four treatment groups (n=6 animals/group): unvaccinated, uninfected controls; unvaccinated and challenged with BRSV strain 375; i.n. vaccination with 190 mg total 'empty' CPTEG:CPH nanoparticles, followed by BRSV challenge; i.n. vaccination with 190 mg total BRSV-F/G-loaded CPTEG:CPH nanoparticles, followed by BRSV challenge. Each calf received ~0.9 mg total of the recombinant BRSV-F/G proteins. I.n. vaccines were administered in a volume of 5 mL sterile saline, with 2.5 mL injected into each nostril.

Nasal fluid samples were collected at weekly intervals following vaccination, and on days 2, 4 and 6 post BRSV challenge. Commercial, polyurethane sponges were cut into 1-2 inch squares and autoclaved. Sponges were dampened with 1 mL of sterile saline and then a single square was inserted into the calf's nostril for 5-10 minutes. The sponges were then removed, placed in a tube and an additional 1 mL of sterile saline was added. Liquid was recovered from each sponge by squeezing in the barrel of a 5 mL syringe. The resulting nasal fluid was then aliquoted and frozen at -80° C for later use.

All animal procedures were conducted in strict accordance with federal and institutional guidelines and were approved by the Kansas State University Institutional Animal Care and Use Committee.

5.2.7 BRSV Inoculum and Aerosol Challenge Model

BRSV strain 375 was prepared from virus stock re-isolated from the lung of an infected animal and passaged less than 4 times on bovine turbinate (BT) cells. The

viral inoculum was determined free of contaminating BVDV by PCR. Calves were inoculated via aerosol challenge with $\sim 10^4$ TCID₅₀/mL of BRSV strain 375 as previously described³²⁸.

5.2.8 Antigen Recall Assays

Peripheral blood mononuclear cells (PBMCs) were prepared as previously described³²⁷. Cells were labeled with Cell Trace Violet per manufacturer's instructions (Life Technologies) and 5×10^6 cells/mL were plated in round-bottom 96-well plates with 5 μ g/mL recombinant BRSV F or G protein or 0.01 MOI of BRSV. For immunogenicity studies, BRSV-F/G was encapsulated into the CPTEG:CPH particles, then released as described, and used to stimulate PBMCs. Plates were incubated for 6 days at 37° C in a 5% CO₂ incubator. Cell culture supernatants were stored at -80° C. PBMC were resuspended in FACS buffer and stained with antibodies specific to bovine CD3, CD4 and CD8 as previously described³²⁷. Cells were analyzed using a BD LSR Fortessa X20 and FlowJo Software (Treestar).

5.2.9 Necropsy and Pathological Evaluation

Calves were euthanized on day 7 post-infection (p.i.) by barbiturate overdose. Pathological evaluation was performed similar to previous descriptions^{328,329}. The extent of gross pneumonic consolidation was evaluated using the scoring system similar to that outlined in³²⁹, and is shown in Supplementary Table 5.1.

Bronchoalveolar lavage fluid (BAL) was collected by introducing 500 mL of sterile, ice-cold PBS through the trachea. Samples of affected and unaffected lungs

were collected from multiple sites for histopathological evaluation. Tissues were fixed by immersion in 10% neutral buffered formalin and processed by routine paraffin-embedment and sectioning. Five μm sections were stained for hematoxylin and eosin. Microscopic lesions were evaluated by a pathologist (Dr. Kumar) in a blinded manner. The severity of the lung lesions was scored based upon the criteria outlined in Supplementary Table 5.2.

5.2.10 *In vitro* Analysis of Nanoparticle Immunogenicity in Bovine APC

Monocyte-derived dendritic cells (moDC) were prepared from adult cows housed at the KSU dairy. The moDC were generated using a protocol previously described by Werling *et al.*³³⁰. Recombinant bovine IL-4 and recombinant bovine GM-CSF were purchased from Kingfisher Biotech, Inc. After 6 days, moDC were seeded at 5×10^5 cells per well in 24-well plates and incubated with 10 $\mu\text{g/mL}$ 'empty' or BRSV-F/G loaded CPTEG:CPH particles. Alveolar macrophages were isolated from the BAL fluid of normal calves at the National Animal Disease Center in Ames, IA. Macrophages were seeded at 5×10^5 cells per well in 24-well plates and stimulated as above, using the CPTEG:CPH G-peptide loaded nanoparticles. In both sets of experiments, mock cultures were treated with media only. After 18 hours, the cells were preserved for qPCR analysis. After 48 hours, cell culture supernatants were harvested and stored at -80°C until later analysis.

5.2.11 Real-time PCR

RNA isolation, cDNA preparation and qPCR were performed as described³²⁷. The primers for bovine IL-8 and IL-12p40 have been published³²⁸. Relative gene

expression was determined using the $2^{-\Delta\Delta C_t}$ method³³¹, with RPS9 as the reference housekeeping gene.

For quantitation of NS2 copy number, lung samples from a representative gross lesion and non-lesioned tissue from each calf were collected and stored in RNAlater. RNA was isolated from lung tissue samples using Trizol Reagen (Life Technologies). Total RNA was quantified by Nanodrop and 500 ng of total RNA were used in each reaction. cDNA synthesis and quantitative rtPCR reactions were carried out using the Taqman RNA-to-CT 1-step kit (Applied Biosystems) per manufacturer's instructions using the following primers and probes: NS2 forward, 5'-GAACGACAGGCCACATTTA-3'; NS2 reverse, 5'-AGGCATTGGAAATGTACCATA-3'; NS2 probe, 5'-/56-FAM/TGAAGCTAT/ZEN/TGCATAAAGTGGGTAGCACA/3IABkFQ/-3'; S9 forward, 5'-GTGAACATCCCGTCCTTCAT-3'; S9 reverse, 5'-TCTTGGCGTTCTTCCTCTTC-3'; S9 probe, 5'-/56-FAM/AAGTCGATG/ZEN/TGCTTCTGCGAGTCC/3IABkFQ/-3'. The reactions were performed on an Agilent MX3000P Real-Time PCR machine with the following cycling conditions: 48° C hold for 15 minutes; 95° C hold for 10 minutes; 40 cycles of 95° C for 15 s, then 60°C for 1 minute. Standard curves for NS2 and S9 genes were run in parallel with test samples, and all standards and test samples were run in triplicate. Viral NS2 copy numbers were calculated using standard curves and normalized to S9 to correct for differences in input material.

5.2.12 Virus Isolation

Nasal swabs were collected from each calf on days 0, 3 and 6 p.i. and placed in sterile PBS. Virus isolations were performed as previously described³²⁸.

5.2.13 ELISAs and Multiplex Cytokine Immunoassay

A multiplex immunoassay (Aushon Biosystems) was used to quantify cytokine secretion in supernatants from bovine alveolar macrophages as previously described³²⁷.

Bovine IL-17A, IFN γ , IL-6, IL-1 β and TNF α VetSet ELISA Development kits were purchased from Kingfisher Biotech, Inc. The bovine IL-4 ELISA kit was purchased from Thermo Fisher Scientific. ELISAs were performed according to kit manufacturer's instructions.

Indirect ELISAs were used to quantify IgA in the nasal and BAL fluid. Indirect ELISAs were also used to determine the immunogenicity of the BRSV F and G proteins prior to encapsulation, and following release from the CPTEG:CPH nanoparticles. For the IgA quantification, ELISA plates were coated overnight at 4° C with 3 μ g/mL F or G protein, or with 100 μ L/well of BRSV stock ($\sim 10^4$ TCID₅₀). For the immunogenicity studies, the ELISA plates were coated overnight at 4° C with 5 μ g/mL total of the F and G protein (2.5 μ g/mL or each), with ~ 5 μ g/mL of the BRSV F and G proteins that had been encapsulated and released from the CPTEG:CPH nanoparticles, or with 100 μ L/well of BRSV stock ($\sim 10^4$ TCID₅₀). Negative control wells were coated with 100 μ L/well cell culture media prepared from uninfected BT. Nasal fluid samples were diluted 1:2 and treated with 10 mM dithiothreitol (DTT) for 1 hour at 37° C prior to performing the ELISAs. BAL samples were diluted 1:2 but were not treated with DTT. Serum samples were diluted 1:1000. All samples were plated in duplicates, incubated for 2 hours at room temperature and then washed. Mouse anti-bovine IgA-HRP (Bethyl Laboratories) was used at 0.5 μ g/mL. Mouse anti-bovine IgG-HRP (Bethyl Laboratories) was used at 0.5 μ g/mL for the immunogenicity experiments. Plates were developed using Pierce 1-Step Ultra TMP Substrate (ThermoScientific Pierce). The

reaction was stopped with the addition of 0.2 M H₂SO₄ and plates were read at an optical density of 450 nm and 540 nm using an automated plate reader.

5.2.14 Virus Neutralization Assay

BT cells were seeded into 96-well flat-bottomed plates. Nasal fluid samples were serially diluted two-fold in serum-free tissue culture medium. BRSV (100 TCID₅₀ units) was added to the diluted samples and incubated for 30 minutes at 37° C. The tissue culture media was removed from the cell monolayers and replaced with the nasal fluid/virus samples. Each sample was assayed in triplicate. The virus was allowed to infect for 90 minutes at 37° C with occasional rocking, and then the cell monolayers were washed and returned to complete cell culture medium. The plates were observed for cytopathic effect daily for 10 days. The virus neutralizing antibody titer was recorded as the reciprocal of the last dilution of the fluid that was able to prevent infection in 100% of the triplicate wells.

5.2.15 Statistics

Statistical analysis was performed using Prism v6.0f software (GraphPad Software, Inc.). The data were analyzed using a Kruskal-Wallis test followed by Dunn's Multiple Comparisons posttest.

5.2.16 Data Availability

The datasets generated during and/or analyzed during the current study are available from the corresponding author on reasonable request.

5.3 Results

5.3.1 *In vitro* Release Kinetics of BRSV-F/G Nanoparticles

We produced a recombinant form of the post-fusion F protein from BRSV strain 375 using a baculovirus expression system; and a recombinant form of the G protein from BRSV strain 375 using an *E. coli* expression system as described in Materials and Methods. The recombinant BRSV F and G proteins were then co-encapsulated at 2.4% by weight into 50:50 CPTEG:CPH nanoparticles.

The release kinetics of the BRSV-F/G nanovaccine was simulated by using 2% G protein-loaded 50:50 CPTEG:CPH nanoparticles (Figure 5.1A). The data show that approximately 40% of G protein encapsulated within the nanoparticles was released within 35 days. This amphiphilic formulation provided zero-order sustained release of the immunogen over the first seven days, followed by a slower rate of release beyond day seven. The encapsulation efficiency of G protein in the nanovaccine was ca. 20%. The G protein release kinetics are consistent with previous observations of protein release kinetics from polyanhydride nanoparticles^{14,19,219,220,232,332}.

5.3.2 Immunogenicity of Recombinant BRSV-F/G is Preserved Following Release from CPTEG:CPH Nanoparticles

We next confirmed that the recombinant BRSV F and G proteins were immunogenic and stable following encapsulation and release from the 50:50 CPTEG:CPH nanovaccine. As shown in Figure 5.1B, serum IgG from BRSV-vaccinated cows recognized both BRSV and the recombinant F and G proteins, with no difference in the response to the encapsulated and released F and G proteins. Serum from the colostrum-deprived animals did not react with BRSV or the recombinant

proteins. As shown in Figure 5.1C, CD4 T cells from BRSV-immune cows underwent clonal expansion in recall response to BRSV, recombinant BRSV-F/G and the released BRSV-F/G proteins. We observed no significant differences in the response to the encapsulated and released proteins compared to the unencapsulated recombinant proteins.

5.3.3 Amphiphilic CPTEG:CPH Particles Activate Bovine Monocyte-derived Dendritic Cells (moDC)

Previous reports have shown that CPTEG:CPH nanoparticles have the capacity to activate murine antigen presenting cells^{16,253}. Therefore, we determined if the 50:50 CPTEG:CPH nanovaccine was similarly immunogenic in the bovine system. MoDC were generated from adult, BRSV-immune cows. The cells were stimulated with 10 µg/mL of ‘empty’ or BRSV-F/G-loaded CPTEG:CPH nanoparticles and expression of IL-8 and IL-12p40 was assessed by qPCR, and inflammatory cytokine production was assessed by ELISA. Consistent with reports from mice, the nanovaccine induced moDC activation, as measured by increased expression of IL-8 and IL-12p40 (Figure 5.2A) and increased production of IFN γ , IL-6, IL-1 β and TNF α (Figure 5.2B). In Figure 5.2C, alveolar macrophages were stimulated with 10 µg/mL CPTEG:CPH nanoparticles that were ‘empty’, as in Figure 5.2A and 5.2B, or were stimulated with CPTEG:CPH nanoparticles that were loaded with overlapping 20-mer peptides from the BRSV G protein. Inflammatory cytokine production was measured by multiplex immunoassay. Consistent with our results in Figure 5.2A and 5.2B, we observed increased inflammatory cytokine expression by nanovaccine-stimulated alveolar macrophages compared to untreated controls, and observed no difference in the response to ‘empty’

or peptide-loaded nanoparticles (Figure 5.2C). In separate experiments, we also determined the capacity of the G-peptide loaded nanoparticles to activate moDC. Consistent with our results in Figure 5.2, moDC increased inflammatory cytokine production (data not shown) and upregulated surface expression of costimulatory molecules (Supplementary Figure 5.1) in response to CPTEG:CPH nanoparticle treatment, and we observed no differences between the ‘empty’ and G-peptide loaded nanoparticles. Together our results confirm that the CPTEG:CPH nanoparticles are immunogenic for bovine antigen presenting cells and demonstrate that this response is largely independent of the antigen payload, as ‘empty’ particles, peptide-loaded particles, and particles loaded with recombinant F and G proteins elicit similar inflammatory responses.

5.3.4 In vivo Immunogenicity and Efficacy of the BRSV-F/G Nanovaccine

To determine the efficacy of the BRSV-F/G CPTEG:CPH nanovaccine in neonatal calves, animals were vaccinated i.n. with 190 mg ‘empty’ CPTEG:CPH nanoparticles or 190 mg BRSV-F/G-loaded nanoparticles. Four weeks later, calves were challenged via aerosol inoculation with $\sim 10^4$ BRSV strain 375.

Calves were monitored daily for clinical signs and rectal temperatures. Several animals in the unvaccinated group demonstrated elevated temperatures (40-41° C) for 1-2 days during infection; however, the fevers were not prolonged and no significant differences in body temperature were observed between vaccinated and unvaccinated groups. Mild clinical signs were observed in the BRSV challenged animals, including coughing, increased respiration rates and increased expiratory effort. Clinical signs of

experimental BRSV infection were apparent starting on days 4-6 after infection and were recorded in at least some animals from each group. Mild clinical signs were observed in 4/6 calves in the unvaccinated control group, 3/6 calves in the 'empty' nanovaccine-administered groups and 2/6 of the BRSV-F/G nanovaccine administered group. However, due to variability between animals and disease kinetics, the clinical scores did not differ significantly between vaccinated and unvaccinated groups. No clinical signs were observed in the uninfected control animals at any time during the study.

5.3.5 Reduced Gross and Microscopic Pathology in BRSV-F/G Nanovaccine-Administered calves

Animals were euthanized on day 7 p.i. We observed gross lesions in these animals that were consistent with our previous reports³²⁸. The lesions were bilateral and most frequently observed in the cranioventral lung lobes, consisting of multifocal to coalescing areas of firm, pneumonic consolidation (Figure 5.3A). The extent of gross pathology in the lungs was evaluated using the criteria outlined in Supplementary Table 5.1. Unvaccinated control animals developed large, diffuse gross lesions, affecting as much as 40-50% of the lung, while calves receiving the BRSV nanovaccine demonstrated fewer lesions and a significant reduction in the area of lung affected (Figure 5.3B).

Representative micrographs from an uninfected control calf (i), an unvaccinated positive control calf (ii), an 'empty' nanovaccine-administered calf (iii) and a BRSV-F/G vaccinated calf (iv) are shown in Figure 5.3C. Cumulative histopathology scores are depicted in Figure 5.3D. The scores for the individual histopathological categories are

presented in Supplementary Figure 5.2. Pulmonary lesions were most pronounced in the unvaccinated control animals and included thickened alveolar septa with infiltrates of macrophages, lymphocytes and occasional neutrophils; and bronchioles filled with neutrophils, sloughed epithelial cells and necrotic cell debris. Five of the six BRSV-F/G nanovaccine-administered calves exhibited reduced histological lesions compared to the unvaccinated calves, with only mild peribronchiolar lymphocytic infiltration and minor accumulation of alveolar exudates. We observed no evidence that the BRSV-F/G nanovaccine promoted the development of enhanced or exacerbated disease.

5.3.6 Reduced Viral Burden and Reduced Virus Shedding in BRSV-F/G Nanovaccine-administered Calves

Nasal swabs and lung tissues were assessed for virus isolation. BRSV was isolated from 5/6 unvaccinated calves on day 3 p.i., and 6/6 animals on day 6 p.i.. Virus was isolated from the lungs of all 6 unvaccinated controls at necropsy. In contrast, BRSV was isolated from only 2/6 BRSV-F/G nanovaccine-administered calves on day 3, and 1/6 on day 6 p.i. Virus was isolated from the lungs of this same animal on day 7 p.i. BRSV was isolated from the nasal swabs of 4/6 calves in the 'empty' nanovaccine-administered group on days 3 and 6 after infection, and from the lung tissues of 3/6 calves on day 7 p.i. We did not isolate virus from the nasal swabs collected from any of the animals on day 0 (prior to BRSV challenge), nor did we isolate BRSV from the nasal swabs or lung tissues of the uninfected control calves.

We performed qPCR for the BRSV NS2 gene on lung tissues collected on day 7 p.i. Consistent with our virus isolation results, BRSV-F/G nanovaccine-administered

calves demonstrated significantly reduced quantities of viral RNA compared to their unvaccinated cohorts (Figure 5.4).

5.3.7 BRSV-specific IgA in the Nasal and BAL Fluid of BRSV-F/G Nanovaccine-administered Calves

Nasal fluid samples were assessed for BRSV-, F- and G-specific IgA following vaccination and challenge. We observed no significant changes in BRSV-specific IgA on day 28 after vaccination. By day 6 after infection, BRSV-F/G nanovaccine-administered calves demonstrated a significant increase in virus-specific IgA compared to the unvaccinated calves or animals receiving the ‘empty’ nanovaccine (Figure 5.5A). We also observed increased BRSV-, F- and G-specific IgA in the BAL fluid from BRSV-F/G nanovaccine-administered calves by day 7 after infection (Figure 5.5B).

We performed virus-neutralization assays using nasal fluid to determine if neutralizing antibody responses were generated in the respiratory tract. On day 28-post vaccination (day 0 prior to challenge), we measured low titers of neutralizing antibody in the nasal fluid of all animals, with no significant differences observed between treatment groups (Table 5.1). By day 6 after infection, we observed an increase in neutralizing antibody titers in the nasal fluid of all BRSV-challenged groups, and noted significantly higher titers ($p \leq 0.01$) in the nasal fluid of BRSV-F/G nanovaccine-administered animals compared with the unvaccinated control animals. Importantly, these results indicate that a single dose of the BRSV-F/G nanovaccine promotes significant production of neutralizing, BRSV-specific antibodies in the respiratory tract of neonatal calves.

Given the importance of developing an RSV vaccine that is efficacious in the face of maternal antibody, we selected colostrum-replete animals for these studies. Calves

in all groups demonstrated pre-existing BRSV-specific IgG in the serum, with neutralizing antibody titers ranging from 16-256 on the day of vaccination; 16-128 on day 28 post-vaccination (day 0, prior to challenge); and 8-128 on day 6 after challenge. We observed no significant differences between treatment groups, nor did we observe any consistent changes in serum neutralizing titers related to BRSV-F/G nanovaccine-administration or BRSV challenge.

5.3.8 BRSV-specific Cellular Responses in the Lungs and Peripheral Blood of BRSV-F/G Nanovaccine-administered Calves

Prior to challenge, we detected no significant BRSV-, F- and G-protein specific CD4 or CD8 T cell proliferation in PBMCs from any groups. By day 6 p.i., we measured significant antigen-specific proliferation by CD4 T cells from BRSV-F/G nanovaccine-administered calves in response to both live virus and the recombinant proteins (Figure 5.6A). PBMCs from the BRSV-F/G nanovaccine-administrated animals also secreted IFN γ and IL-17A in response to whole virus and the recombinant proteins (Figure 5.6B). Levels of IL-4 were below the limit of detection for all groups (data not shown).

Mononuclear cells were isolated from the BAL on day 7 p.i. and stimulated with whole virus, F or G protein as in Figure 5.6A. We measured a significant increase in the concentration of IFN γ and IL-17 in the BAL cell culture supernatants from the BRSV-F/G nanovaccine-administered calves, but not control calves, in response to protein or whole virus stimulation (Figure 5.6C).

5.4 Discussion

RSV infection has a devastating, worldwide impact on human health and despite significant efforts, no approved vaccine currently exists for use against the disease in humans. Similarly, although vaccines have been widely available for BRSV for decades, their efficacy in the field is problematic, and BRSV infection in calves continues to have significant impacts on animal health and the agricultural economy^{162,163}. The two diseases, HRSV infection in humans and BRSV infection in calves, present with striking similarities in pathogenesis and host immunity (recently reviewed in¹⁶¹). Thus, the calf model represents authentic host-pathogen interaction that faithfully replicates many aspects of human RSV infection, and is therefore an ideal model for testing novel vaccine candidates and determining appropriate correlates of vaccine-induced protection. Here, we vaccinated animals that were less than one month of age and had BRSV-specific maternally-derived antibodies. A single, i.n. administration of the BRSV-F/G nanovaccine induced mucosal, anti-viral immunity and protected most animals from virulent BRSV challenge. Calves receiving the BRSV-F/G nanovaccine mounted cellular and humoral immune responses in the upper and lower respiratory tract (Figures 5.5 and 5.6, and Table 5.1); exhibited a reduced viral burden in the lungs on day 7 post challenge (Figure 5.4); and developed significantly fewer gross and microscopic lesions in the lungs compared to unvaccinated control animals (Figure 5.3).

Our amphiphilic, polyanhydride nanovaccine platform, which is based upon CPTEG:CPH copolymers, offers a number of advantages over other polymeric nanoparticle systems, including: inherent adjuvant properties^{15,16,253,333}; the tendency of

the particles to surface erode³³⁴, thus stabilizing the encapsulated proteins and maintaining the structural and biological features of the antigens for longer periods of time^{19,219,220,332}; the ability to provide sustained and tunable antigen release kinetics²³²; and the ability to degrade at a neutral pH, into non-toxic and non-mutagenic carboxylic acids³³⁵. Consistent with previous reports showing that polyanhydride nanoparticles can protect labile proteins from degradation^{19,219,220,281,332,335}, we demonstrated here that the *in vitro* antigenicity of the BRSV F and G proteins was preserved following encapsulation and release from the 50:50 CPTEG:CPH particles (Figure 5.1). We observed no significant changes in the capacity of BRSV-specific polyclonal antibodies or BRSV-specific CD4 T cells to recognize the recombinant proteins following their release from the nanoparticles, which is critical for vaccine efficacy. The length of antigen exposure is a vital factor dictating the establishment of long-term immunity, and consistent with prior reports, the CPTEG:CPH nanoparticles used here provided sustained antigen release of the BRSV G protein, with only ~40% of the recombinant protein released by 30 days *in vitro*. In agreement with our *in vitro* findings suggesting that the BRSV-F/G nanovaccine should be stable and immunogenic, our *in vivo* vaccine experiments demonstrated that a single i.n. vaccination, containing a suboptimal dose of antigen, was sufficient to protect a majority of calves from severe BRSV infection.

As previously mentioned, neutralizing IgG and IgA are believed to have a role in protection from RSV. However, we still have a poor understanding of the immune responses that are most important for protection from RSV disease in the neonate, and even less appreciation for the role of maternal antibody in protection from infection. Some studies suggest that maternal antibody can prevent RSV infection^{173,174}; and

systemic, prophylactic administration of Palivizumab, a monoclonal antibody that is specific to the RSV F protein, is effective at reducing RSV-related hospitalization in high-risk infants³³⁶. However, both human infants^{175–177} and calves¹⁷⁸ with maternal antibodies still develop severe RSV disease; and in infants, there is no correlation between titers of virus-specific maternal IgG and prevention of hospitalization with RSV^{176,179}. In agreement, despite significant titers of maternally-derived serum antibodies, our unvaccinated control animals developed BRSV disease, including transient fevers, clinical signs, severe pathology in the lungs and significant viral shedding.

Adults repeatedly infected with RSV demonstrate robust levels of IgA in nasal secretions, which has shown to prevent virus replication in the upper airways, regardless of serum Ig levels^{170,171}. Mucosal IgA also plays an important role in reducing the occurrence and severity of RSV infection in infants and children¹⁷⁷. Our results reinforce this conclusion, demonstrating that BRSV-F/G vaccinated calves mounted a significant IgA response in the nasal cavity and BAL that increased rapidly in the days following virulent BRSV challenge. However, in adults, IgA responses can wane¹⁷¹ and the IgG response may be more important in long-term protection. We chose to use calves with BRSV-specific maternal antibodies, as it is the most stringent and physiologic model in which to test our novel vaccine platform. We were unable to measure any changes in BRSV serum neutralizing titers following administration of the BRSV-F/G nanovaccine, or following virulent BRSV challenge. Thus, it is currently unknown if a single administration of the BRSV-F/G nanovaccine induces systemic antibody responses. In the future, it may be necessary to dissect the contributions of

systemic vs. mucosal vaccine-induced immunity in calves with low or no BRSV-specific maternal antibodies.

We observed a significant rise in neutralizing antibody titers in the nasal secretions of the BRSV-F/G nanovaccine administered calves (Table 5.1). Based upon the results of our ELISA analysis, this response is presumably mediated by neutralizing IgA. Interestingly, however, we also observed a rapid increase (nearly 4-fold) in neutralizing titer in the nasal fluid of the unvaccinated control calves by six days post infection. It is possible that the early neutralizing response we observed in the unvaccinated and 'empty' nanovaccine administered calves was mediated by BRSV-specific IgM, which has been previously observed in nasal secretions from children hospitalized with human RSV infection³³⁷, and was shown to appear more rapidly than RSV-specific IgA.

The RSV F protein is a type I viral fusion protein that is synthesized as a precursor that is proteolytically cleaved by furin into disulfide-linked fragments¹⁸⁴. It is highly conserved between virus strains, as well as between HRSV and BRSV, demonstrating approximately 80% homology³³⁸. The F protein exists in two forms on the virion surface: a metastable pre-fusion form and a stable post-fusion trimer. The post-fusion form of the F protein contains two major neutralizing epitopes, antigenic sites II and IV¹⁸⁴. High-affinity, site-II directed neutralizing antibodies are protective in mice and cotton rats^{185,186}. When considering the design of an F protein based subunit vaccine, protein stability is of paramount concern, and the post-fusion F is advantageous due to its highly stable nature. The prefusion F protein contains antigenic site Ø, and recent evidence suggests that this epitope is the primary target for

neutralizing antibodies in humans³³⁹. Vaccine formulations incorporating the pre-fusion form of the F protein are highly efficacious in rodent models^{169,181,183,340}; and a highly efficacious prefusion F vaccine was also recently reported for BRSV³³⁸, suggesting that the antigenic σ site is conserved and of immunologic relevance to the calf model as well. Stable expression of the prefusion F protein is not trivial and hurdles exist with respect to affordable, consistent production of sufficient quantities of stable, prefusion F for use in subunit vaccines. However, the availability of the crystal structure^{338,341}, and improved strategies to express and stabilize the prefusion F^{168,169,183}, significantly enhance the feasibility of a subunit based prefusion F vaccine. In the future, we plan to examine the stability and efficacy of a mucosal, prefusion F-based nanovaccine in neonates.

In summary, we have shown here that a single, intranasal administration of the BRSV-F/G nanovaccine elicits mucosal and systemic antiviral immunity, resulting in reduced virus-associated pathology and reduced viral burdens in animals vaccinated at \leq one month of age. The results of our *in vivo* efficacy studies warrant further evaluation of the BRSV-F/G nanovaccine for protection against RSV infection in both humans and cattle, and have encouraged us to continue to refine the polyanhydride chemistries and vaccine formulations to optimize their efficacy against RSV infection in neonates.

5.5 Tables

Table 5.1. Virus neutralization titers measured in the nasal fluid on day 28 (day 0 before challenge) and day 6 post-challenge. Data are presented as the mean (range) titer per group. **p < 0.01 compared to unvaccinated control animals.

Group	Day 28 (challenge day) mean neutralization titer (range)	Day 6 mean neutralization titer (range)
Negative controls	5 (2–8)	4 (2–8)
Unvaccinated	4.6 (2–8)	20 (8–32)
Empty nanovax	5.3 (4–8)	34.6 (16–64)
BRSV-F/G nanovax	20 (8–32)	108 (64–256)**

5.6 Figures

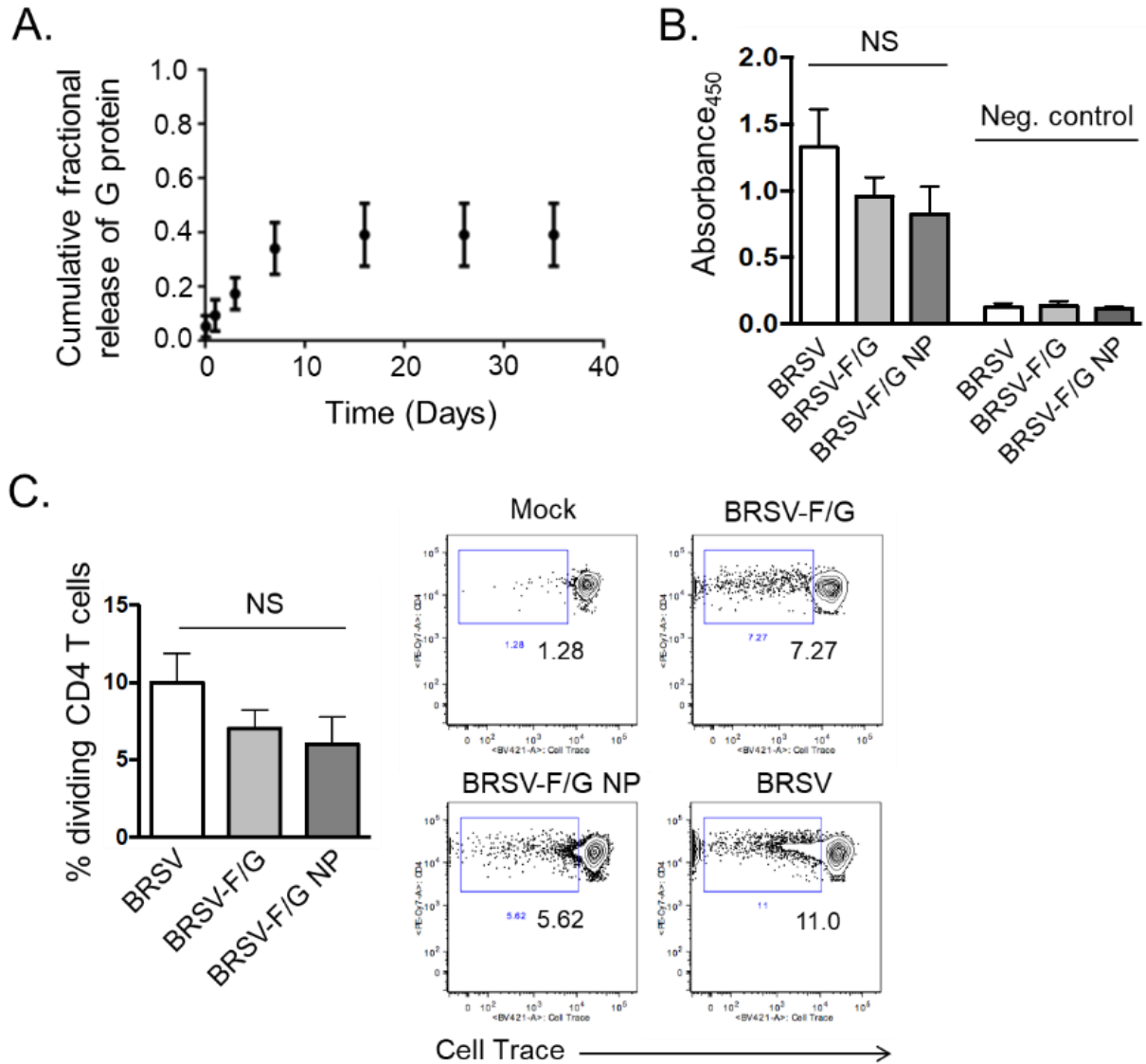


Figure 5.1. Recombinant BRSV F and G proteins are stable and immunogenic following encapsulation and release from polyanhydride nanoparticles. (A) G protein release kinetics from polyanhydride nanoparticles. Data shown is the cumulative mass fraction of G protein released from 50:50 CPTEG:CPH nanoparticles. Data represent means \pm SEM. Results are representative of three independent experiments with duplicate samples used in each experiment. (B) ELISA plates were

coated with 5 $\mu\text{g/mL}$ (2.5 $\mu\text{g/mL}$ each) of the recombinant F and G proteins (BRSV-F/G), or with 100 μL /well of BRSV virus stock ($\sim 10^4$ TCID₅₀) grown in BT cells.

Recombinant BRSV F and G proteins were encapsulated in 50:50 CPTEG:CPH particles and released as described. The released proteins were also coated onto ELISA plates at ~ 5 $\mu\text{g/mL}$ (BRSV-F/G NP). Sera from BRSV-immune cows were diluted 1:1000 and added to the plates. The binding of bovine IgG to the virus or recombinant proteins was measured by absorbance. Sera were also collected from 2 colostrum-deprived calves, diluted 1:1000, and included as negative control samples.

(C) PBMC were labeled with Cell Trace Violet and stimulated for 6 days with 5 $\mu\text{g/mL}$ of the recombinant BRSV F and G proteins; 5 $\mu\text{g/mL}$ recombinant BRSV F and G proteins that were encapsulated and released from the CPTEG:CPH particles; or 0.01 MOI of BRSV strain 375. Pokeweed Mitogen was used at a concentration of 1 $\mu\text{g/mL}$ as a positive control. Mock stimulated samples (negative control wells) were cultured with cRPMI and were used to correct for background proliferation. After 6 days, antigen-specific CD4 T cell proliferation was assessed by flow cytometry. Representative flow plots and aggregate results are shown in C. Background levels of proliferation were subtracted and results are presented as change over mock. (B and C) Results are pooled from 2-3 independent experiments for a total of $n=8-10$ animals. Data represent means \pm SEM. * $p<0.05$ ** $p<0.01$ NS: not significant compared to BRSV.

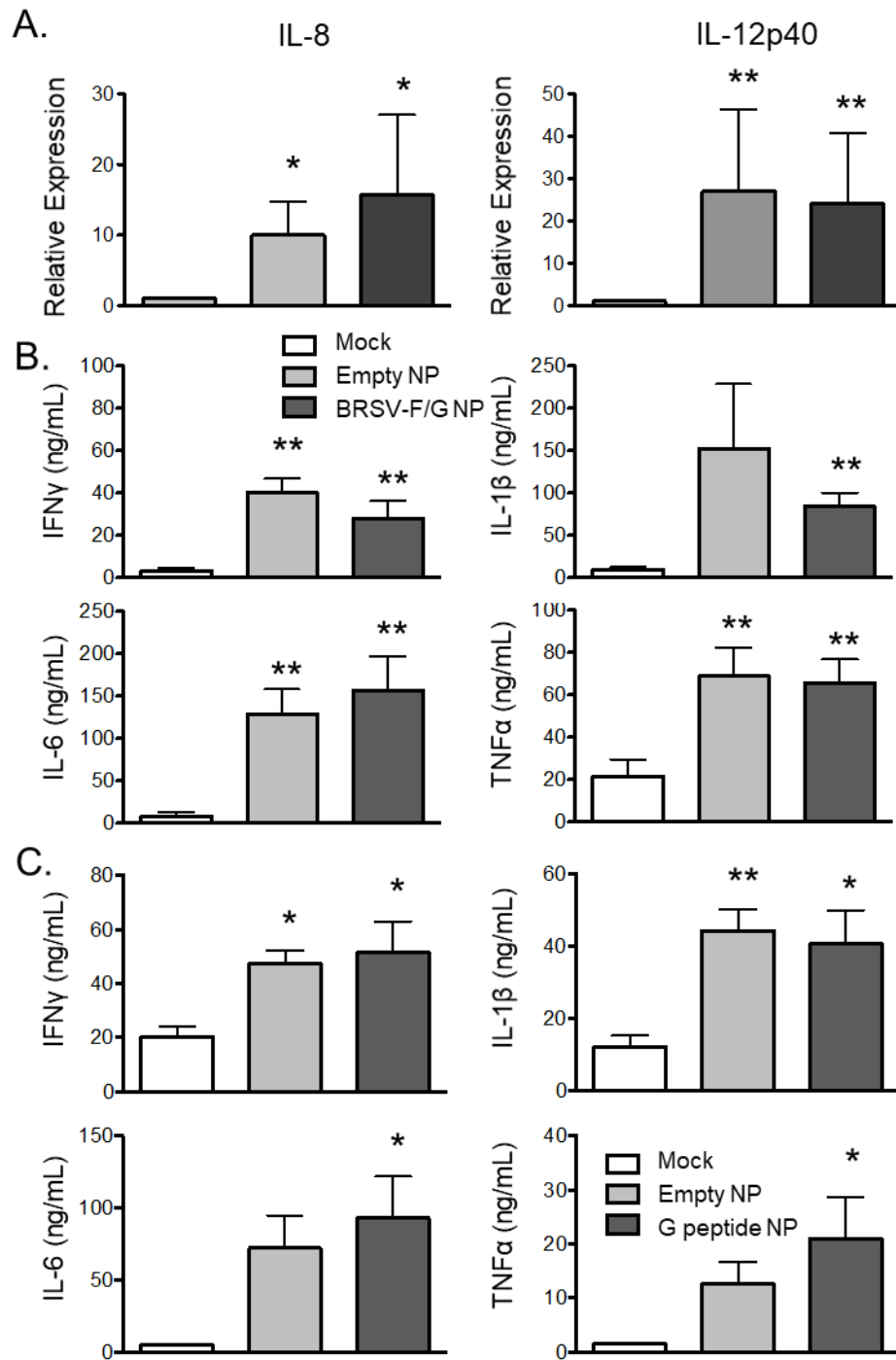


Figure 5.2. Polyanhydride nanoparticles activate bovine APC. Bovine moDC were seeded at 5×10^5 cells per well in a 24-well plate and stimulated with 10 $\mu\text{g/mL}$ 'empty' or BRSV-F/G-loaded 50:50 CPTEG:CPH particles. Mock cultures were treated with media

only. (A) After 18 hours, RNA was isolated from the cells and analyzed by qPCR for expression of IL-8 and IL-12p40. For qPCR analysis, results were normalized to the housekeeping gene RPS-9, and expressed relative to unstimulated control samples. (B) After 48 hours, cell culture supernatants were collected and analyzed by ELISAs for concentrations of IFN γ , IL-6, IL-1 β and TNF α . (C) Alveolar macrophages were isolated from the BAL fluid of healthy calves and were seeded at a concentration of 5×10^5 cells per well in 24-well plates. The macrophages were stimulated with empty CPTEG:CPH particles or with CPTEG:CPH nanoparticles that were loaded with peptides from the BRSV G protein. Mock cultures were treated with media only. After 48 hours, cell culture supernatants were analyzed by multiplex immunoassay. A-C: Results were pooled from two independent experiments for a total of n=8-10 animals. Data represent means \pm SEM. *p<0.05 **p<0.01 compared to mock stimulated cultures.

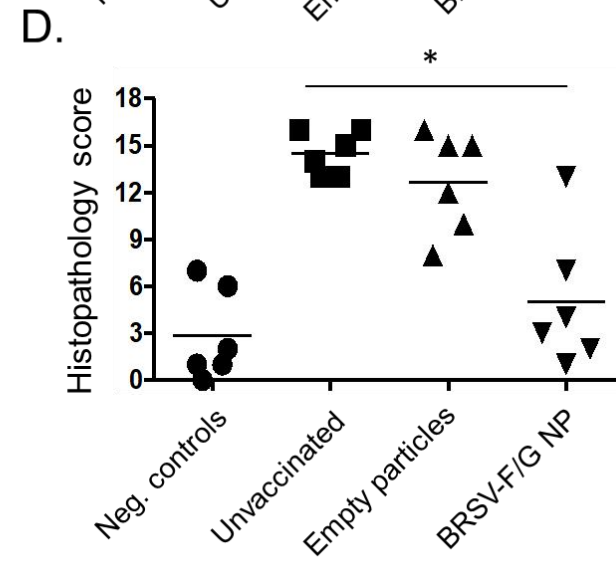
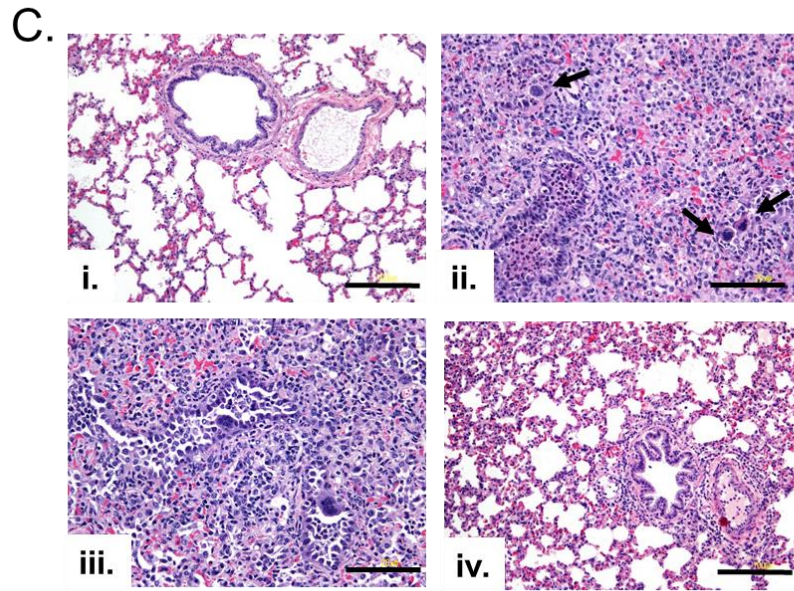
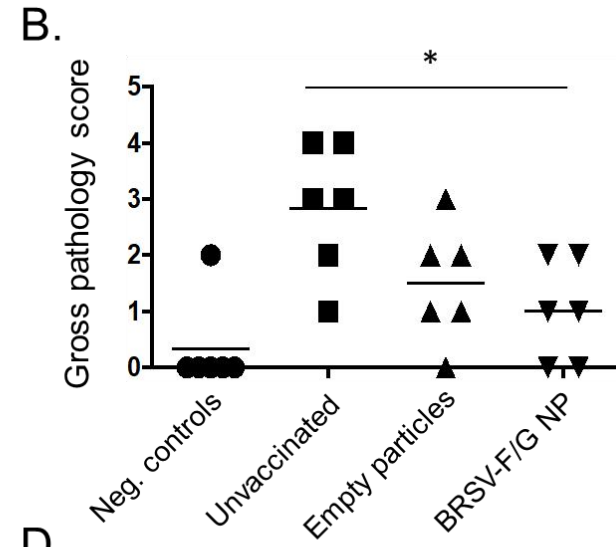
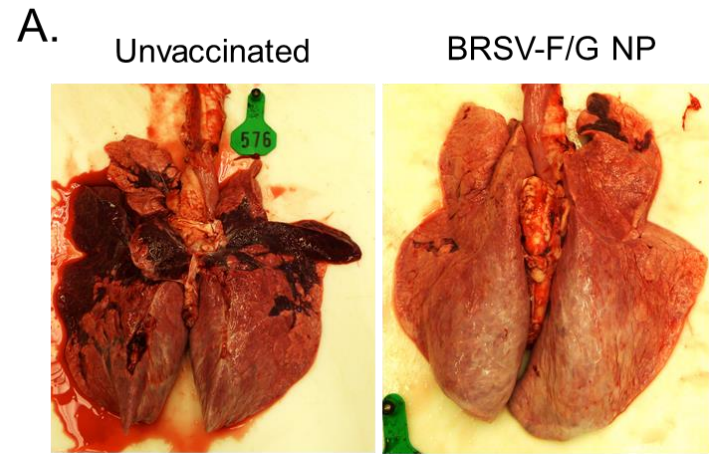


Figure 5.3. Reduced BRSV-associated gross and microscopic pathology in BRSV-F/G nanovaccine-administered calves. Treatment groups included unvaccinated, uninfected negative control calves; unvaccinated calves challenged with BRSV strain 375; calves vaccinated with ‘empty’ nanoparticles and challenged with BRSV strain 375; and calves vaccinated with the BRSV-F/G nanovaccine and challenged with BRSV strain 375. Animals were euthanized and necropsied on day 7 after challenge. The extent of gross pneumonic consolidation was evaluated based upon the percent of lung affected: a score of 0 was given to lungs free of lesions; 1 was given to lungs with 1-5% affected; 2 was given for 5-15% affected; 3 with 15-30% affected; 4 to lungs with 30-50% of consolidated tissue; and 5 for lungs <50% affected. Representative images from an unvaccinated, infected calf and a calf which received the BRSV-F/G nanovaccine are depicted in (A). Aggregate gross pathology results from all groups and all animals are presented in (B). (C) Sections of lung were collected from multiple locations and microscopic lesions were evaluated by a pathologist in a blinded manner. The severity of the lung lesions was scored based upon six criteria as outlined in Supplementary Table 5.2. Representative histological images from each of the four groups of calves: uninfected control calf (i), unvaccinated calf (ii), an empty nanovaccinated control calf (iii) and a BRSV nanovaccine-administered calf (iv). Hematoxylin and eosin stain. (i) and (iv)- Normal lung architecture. Note bronchioles are lined by normal tall columnar epithelium and there is no inflammation in the airways. (ii) and (iii)- Severe bronchointerstitial pneumonia with necrotizing bronchiolitis. Bronchioles are filled with degenerate neutrophils, sloughed epithelial cells and necrotic cell debris. (ii) The bronchiolar epithelial cells occasionally form multinucleated syncytia cells (arrows). Alveoli contain variable combinations of macrophages, syncytial

cells with foamy vacuolated cytoplasm, lymphocytes and lesser numbers of neutrophils. (iii) The affected bronchioles show syncytia within the lining epithelium and some inflammatory cells mixed with desquamated cells within the lumen. (i and iv) Black scale bars represent 100 μm . (ii and iii) Black scale bars represent 20 μm . Aggregate microscopic pathology results are presented in (D). Results represent n=6 animals/group. The lines indicate the means of each group *p<0.05 compared to unvaccinated control calves.

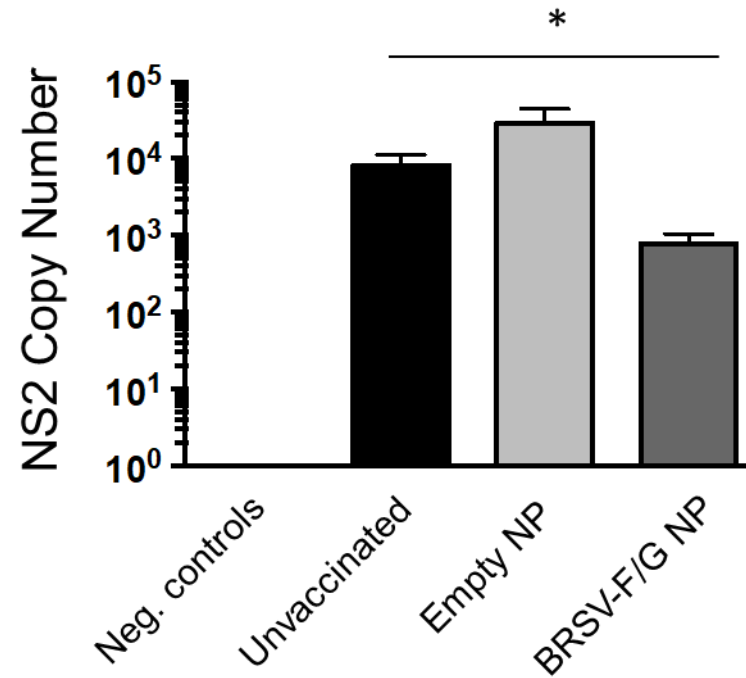


Figure 5.4. Reduced viral burden in the lungs of BRSV-F/G nanovaccine-administered calves. Treatment groups are outlined in Figure 5.3. Samples were collected from lesion and non-lesion sites of the lungs were collected on day 7 post-challenged and preserved in RNALater. Tissues were then analyzed by qPCR for the BRSV NS2 gene. Viral NS2 copy numbers were calculated using standard curves and normalized to the housekeeping gene, S9, to correct for differences in input material. Results represent n=6 animals/group. Data represent means \pm SEM. *p<0.05 compared to unvaccinated control calves.

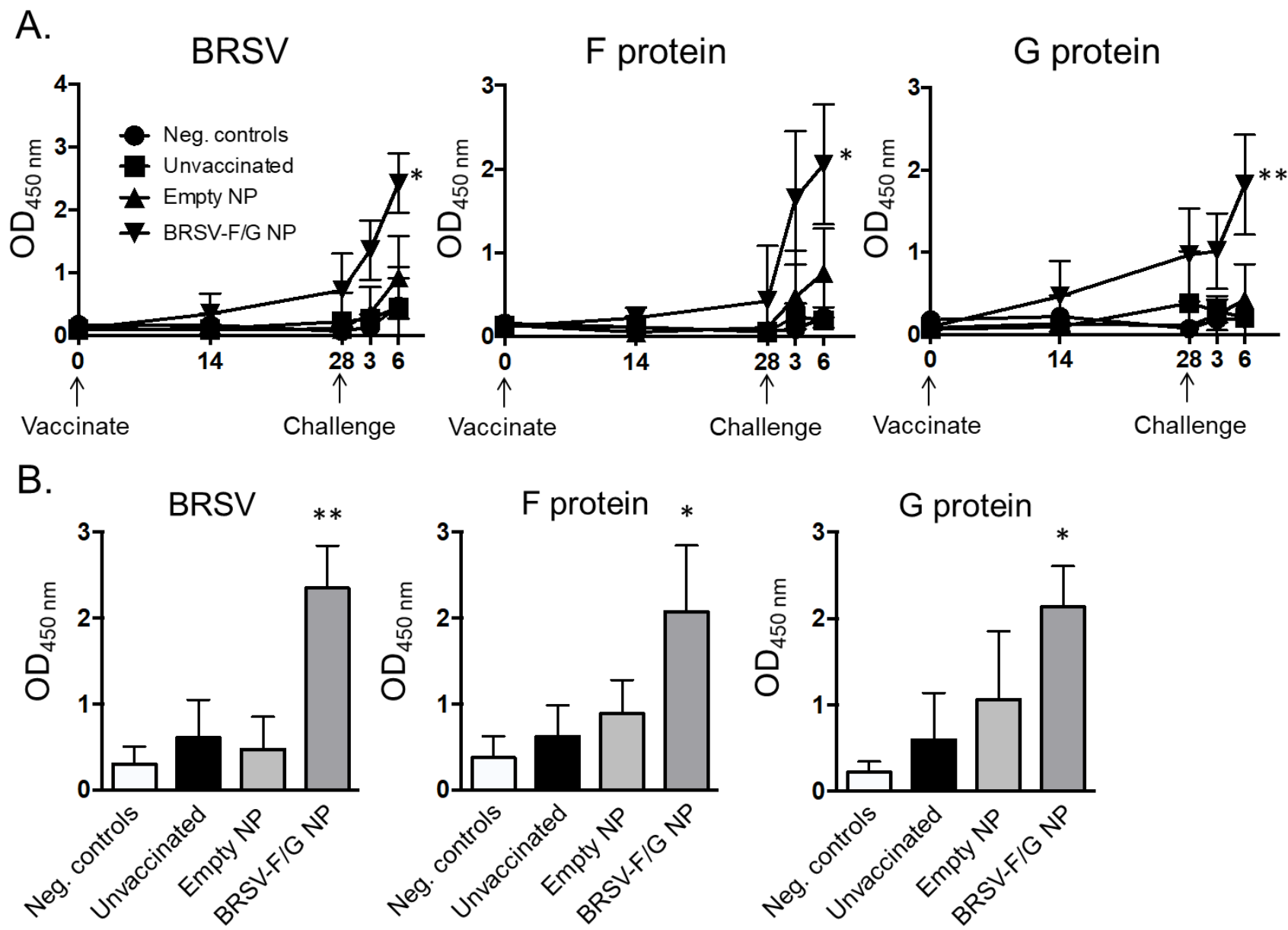


Figure 5.5. Increased BRSV-specific IgA in the nasal fluid and BAL fluid of BRSV-F/G nanovaccine-administered calves. Treatment groups are outlined in Figure 5.3. Nasal fluid was collected on days 0, 14 and 28 post-vaccination, and on days 3 and 6 post-challenge. BAL fluid was collected during necropsy on day 7 post-challenge. The samples were diluted 1:2. Indirect ELISAs were used to quantify BRSV-, F-protein or G-protein specific IgA in (A) nasal fluid and (B) BAL fluid. Results represent n=6 animals/group. Data represent means \pm SEM. * $p < 0.05$ ** $p < 0.01$ compared to unvaccinated control calves.

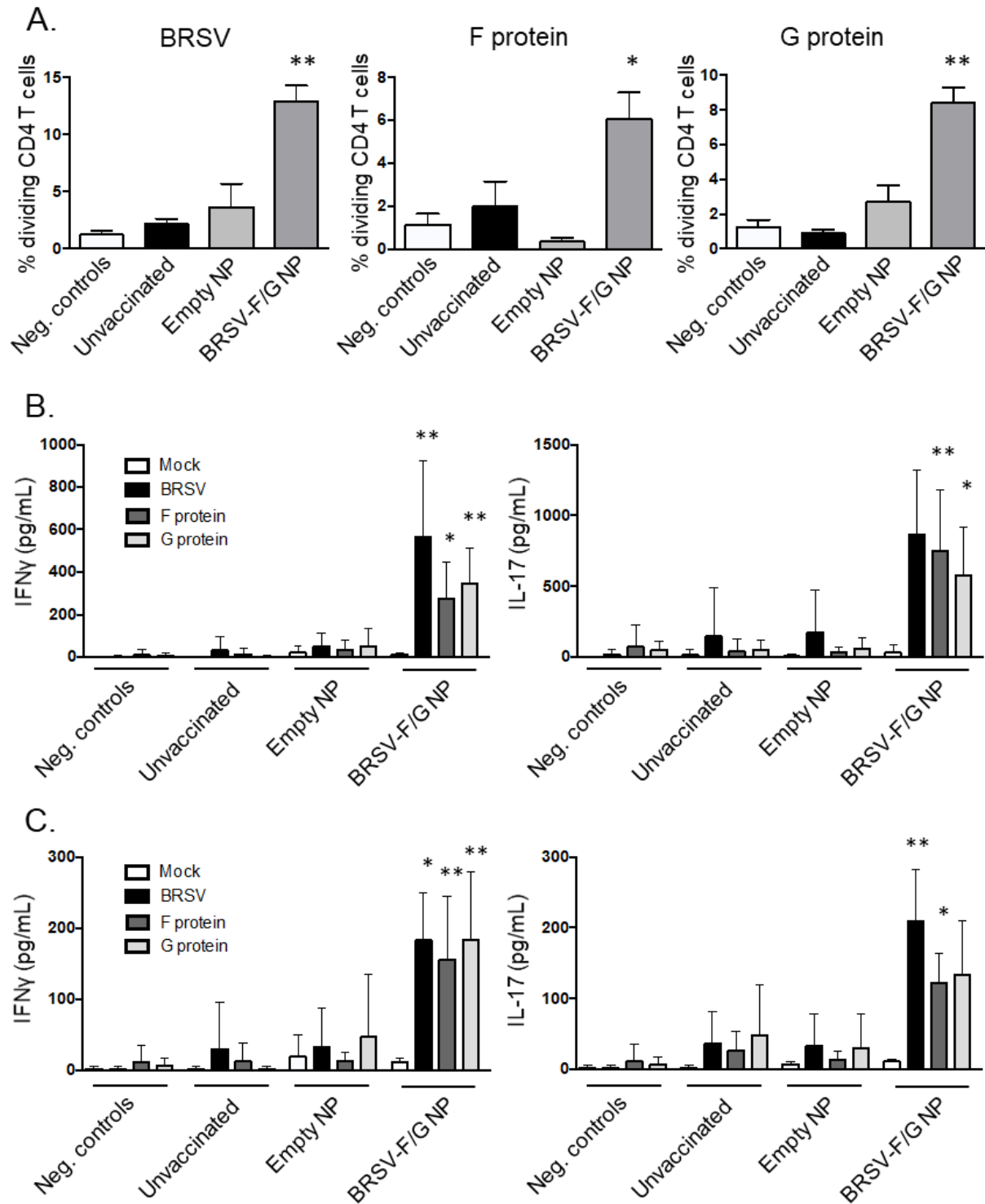


Figure 5.6. Enhanced BRSV-specific T cell responses in the peripheral blood and BAL of BRSV-F/G nanovaccine administered calves. PBMC were collected on day 6

post-challenge, labeled with Cell Trace Violet and stimulated for 6 days with 5 µg/mL of the recombinant BRSV F and G proteins, or 0.01 MOI of BRSV strain 375. Pokeweed Mitogen was used at a concentration of 1 µg/mL as a positive control. Mock stimulated samples (negative control wells) were cultured with cRPMI and were used to correct for background proliferation. (A) After 6 days, antigen-specific CD4 T cell proliferation was assessed by flow cytometry, as measured by dilution of the Cell Trace Violet dye. Background levels of proliferation were subtracted and results are presented as change over mock. (B) Stimulated cell culture supernatants were collected after 6 days and concentrations of IFN γ (left panel) and IL-17A (right panel) were measured by commercial sandwich ELISAs. (C) BALs were performed on day 7 post-challenge. Cells were enumerated and stimulated for 6 days with recombinant BRSV F protein, G protein or BRSV as in A. After 6 days, cell culture supernatants were collected and concentrations of IFN γ (left panel) and IL-17A (right panel) were measured by commercial sandwich ELISAs. Results represent n=6 animals/group. Data represent means \pm SEM. *p<0.05 **p<0.01 compared to unvaccinated controls.

CHAPTER 6. SYNTHESIS AND CHARACTERIZATION OF NOVEL RAPIDLY-DEGRADING POLYANHYDRIDES AS VACCINE ADJUVANTS

Manuscript to be submitted to *ACS Biomaterials Science and Engineering* on September 7, 2019

Sean M Kelly¹, Akash Mitra¹, Srishti Mathur¹, Adam Mullis¹, Balaji Narasimhan^{1,2,*}

¹Department of Chemical and Biological Engineering, Iowa State University, Ames, IA, USA

²Nanovaccine Institute, Iowa State University, Ames, IA, USA

***Correspondence:**

Balaji Narasimhan
nbalaji@iastate.edu

Keywords: polyanhydride; nanovaccine; rational design;

Abstract

There is a currently a need to develop adjuvants that are best suited to simultaneously enhance immune responses, induce immunologic memory, improve patient compliance (i.e., reduce doses and inflammation), and provide vaccine shelf stability for stockpiling and deployment to harsh environments in developing countries. Biodegradable polyanhydrides have been investigated extensively to overcome such challenges. It has been shown that controlling copolymer composition can result in chemistry-dependent immunomodulatory capabilities. These studies have revealed that copolymers rich in sebacic acid (SA) are highly internalized by antigen presenting cells

and confer improved shelf stability of encapsulated proteins, while copolymers rich in 1,8-bis(*p*-carboxyphenoxy)-3,6-dioxaoctane (CPTEG) also exhibit enhanced internalization by and activation of APCs, in addition to providing superior retention of protein stability following encapsulation and release. However, to date CPTEG:SA copolymers have not been synthesized and described. In this work, we hypothesized that new copolymers composed of CPTEG and SA would combine the advantages of both monomers in terms of enhanced thermal properties, maintaining antigenicity of encapsulated proteins following nanoparticle synthesis, and superior cellular internalization by APCs. Here, we describe the synthesis and design of novel CPTEG:SA nanoparticles with improved thermal properties, payload stability, and internalization by antigen presenting cells for applications in vaccine delivery. The performance of these new CPTEG:SA formulations was compared to that of the more commonly used polyanhydride copolymers.

6.1 Introduction

There are many challenges associated with developing vaccination strategies to prevent pathogens from establishing infection in the host. With the advent of recombinant subunit protein-based vaccines, the need has increased to develop adjuvants that are best suited to enhance immune responses, induce immunologic memory, improve patient compliance (i.e., reduce doses and inflammation), and provide vaccine shelf stability for stockpiling and deployment to harsh environments. While traditional adjuvants enhance immune responses, some of them (e.g., MPLA, aluminum-based salts) induce inflammation and adverse reactions at the injection

site³⁴² and must be refrigerated for extended storage, limiting their use for long term storage or in harsh environments⁶.

Nanoparticle-based technologies have long been investigated as a delivery vehicle/adjuvant system for vaccines³⁴³. It has been shown that nanoparticle characteristics, such as size²²⁸, shape^{229,344}, charge²²⁶, and chemistry¹⁵ can be used to control cellular uptake, and ligation of the polymer can aid in targeting draining lymph nodes³⁴⁵, thus enabling targeted delivery of the payload. Biodegradable polymer-based nanoparticle systems are promising for vaccine delivery due to their facile synthesis, ability to protect encapsulated proteins from enzymatic degradation, and degradation-controlled sustained release²⁴⁹ or pulsatile release mechanisms³⁴⁶. Poly(lactic-co-glycolic acid) is the most widely investigated polymer in this category and is FDA-approved for use in sutures, showing promise for vaccine delivery³⁴⁷. However, PLGA exhibits bulk erosion which, along with the relatively high acidity of its degradation products (pKa glycolic acid: 3.83²⁷¹; lactic acid: 3.08²⁷²), can cause denaturation of encapsulated proteins³⁴⁸.

Biodegradable polyanhydrides have also been investigated extensively to overcome such challenges and meet the abovementioned vaccine requirements²⁸⁰. Comprised of 1,6-bis(*p*-carboxyphenoxy) hexane (CPH), 1,8-bis(*p*-carboxyphenoxy)-3,6-dioxaoctane (CPTEG), and sebacic acid (SA), these materials are safe, biodegradable, exhibit mild inflammation, and are currently FDA-approved for use to treat malignant glioblastomas. Controlling copolymer composition has been shown to enhance cellular uptake^{16,349}, ultimately resulting in chemistry-dependent immunomodulatory capabilities^{13,255}. These materials have proven an efficacious

vaccine adjuvant platform, evidenced by sustained antibody responses to numerous antigens^{14,17,204,297,350}, enhanced germinal center formation²⁵², increased cytotoxic T cell responses²⁸⁸, and protection against multiple bacterial and viral infections^{14,205,217}.

Previous work has shown that SA-rich chemistries are highly internalized by antigen presenting cells¹⁶ (APCs) and confer improved shelf stability of encapsulated proteins¹⁹. CPTEG-rich chemistries also exhibit enhanced internalization by and activation of APCs¹⁶, in addition to providing superior retention of protein stability following encapsulation and release¹⁹. In this work, we hypothesized that new copolymers composed of CPTEG and SA would combine the advantages of both monomers in terms of enhanced thermal properties, maintaining antigenicity of encapsulated proteins following nanoparticle synthesis, and superior cellular internalization by APCs. Here, we describe the synthesis and design of novel CPTEG:SA nanoparticles with improved thermal properties, payload stability, and internalization by APCs for applications in vaccine delivery. The performance of these new CPTEG:SA formulations was compared to that of the more commonly used 20:80 CPTEG:CPH, 50:50 CPTEG:CPH, and 20:80 CPH:SA copolymers.

6.2 Materials and Methods

6.2.1 Materials

Sebacic acid (99%), bovine serum albumin, and chemicals used for CPTEG and CPH diacid and polymer synthesis, including 1,6-dibromohexane, triethylene 4-*p*-hydroxybenzoic acid, and 1-methyl-2-pyrrolidinone were purchased from Sigma-Aldrich (St. Louis, MO). Chloroform, petroleum ether, ethyl ether, hexanes, sodium hydroxide,

toluene, sulfuric acid, acetonitrile, dimethyl formamide, acetic anhydride, methylene chloride, pentane, and potassium carbonate were purchased from Fisher Scientific (Fairlawn, NJ). 4-*p*-fluorobenzonitrile was purchased from Apollo Scientific (Cheshire, UK). Deuterated chloroform used for ^1H NMR analysis was purchased from Cambridge Isotope Laboratories (Andover, MA). RAW 264.7 and J774 cells were purchased from American Type Culture Collection (ATCC; Manassas, VA) and were used for assays.

6.2.2 Animals

Female BALB/c mice (6–7-week-old) were purchased from Charles River Laboratories (Wilmington, MA). The Institutional Animal Care and Use Committee (IACUC) at Iowa State University approved all protocols involving animals.

6.2.3 Copolymer Synthesis and Characterization

CPTEG and CPH diacids were synthesized as previously described^{232,255}. CPTEG:CPH and CPH:SA copolymer synthesis was performed using melt polycondensation²³². For synthesis of the novel CPTEG:SA copolymer, 2 g of total monomer (the mass of each monomer varied depending on copolymer composition) and 90 mL of acetic anhydride were added to a 100 mL round bottom flask and reacted for 30 min at 125 °C in an oil bath. The acetic anhydride was removed using a rotary evaporator, and the dried product was then reacted for 1 hr at 140 °C in an oil bath under vacuum (0.2 torr). The solid product was dissolved in approximately 20 mL of methylene chloride overnight and precipitated in 1 L hexanes to isolate the copolymer. Copolymer composition and molecular weight were estimated using end group analysis

of ^1H NMR (DXR 500, Bruker) spectra. Copolymer thermal properties (glass transition temperature and melting point) were determined using differential scanning calorimetry (Q2000, TA Instruments). The relative crystallinity of CPTEG:SA copolymers was determined using wide angle X-ray diffraction (Siemens D500, Siemens/Bruker).

The number average sequence length, degree of randomness, and reactivity ratios of CPTEG:SA copolymers was determined from ^1H NMR spectra, using methods described previously³⁵¹. Films were made for contact angle measurements by dissolving copolymer in methylene chloride at 50 mg/mL, 300 μL was pipetted on a 6 cm glass slide, heated to 80 $^\circ\text{C}$ for 10 s and spin coated (WS-650Mz-23NPPB, Laurell Technologies, North Wales, UK) for 30 s at 2000 rpm with a 1500 rpm/s acceleration rate. An average of eight contact angle measurements of each chemistry of CPTEG:SA films was performed using a goniometer (NRL 100, ramé-hart, Succasunna, NJ) with 2 μL droplets of nanopure water.

6.2.4 Erosion Kinetics

Films were prepared by dissolving copolymers in methylene chloride at a concentration of 150 mg/mL and allowed to dry overnight. The scintillation vials containing dried copolymer were then heated to their respective melting points for one minute and then allowed to cool to room temperature. 15 mL of nanopure water was pipetted into each vial and 15 mL was removed and replaced daily over 45 days of study. Samples were lyophilized, the dry mass was weighed, and the cumulative mass was determined over the course of the study. In separate vials, samples of the film were collected on days 15, 30, and 45, the film samples lyophilized, dissolved in deuterated DMSO, and characterized for copolymer composition by ^1H NMR.

6.2.5 Nanoparticle Synthesis and Characterization

For protein stability characterization, CPTEG:SA nanoparticles, either empty or encapsulating OVA (5% w/w), were synthesized via flash nanoprecipitation, as previously described²⁰⁴. For release experiments, CPTEG:SA nanoparticles encapsulating bovine serum albumin (BSA; 2% w/w) were spray dried using a Buchi B90 HP spray dryer (Büchi, Flawil, Switzerland). Briefly, for spray dried nanoparticle synthesis, polymer was dissolved in chloroform at 10 mg/mL with 5 mM sodium dioctyl sulfosuccinate as an emulsifier. Then model protein, BSA was dissolved in nanopure water at 4 mg/mL, pipetted at a 1:20 (water:solvent) ratio into the solvent, and emulsified with the polymer via sonication for 30 s. The emulsion was spray dried at room temperature (pump rate 10%, spray rate 100%, gas flow rate 100 L/min, inlet temperature ~30 °C). CPTEG:SA nanoparticles were imaged using scanning electron microscopy (SEM; JEOL 840 A, JEOL Ltd., Tokyo, Japan), and nanoparticle mean size and size distribution were determined using ImageJ (National Institutes of Health, Bethesda, MD). Nanoparticle zeta potential was measured using Zetasizer Nano (Malvern Instruments, Worcester, UK).

6.2.6 Protein Release Kinetics

For protein release characterization, approximately 5 mg of nanoparticles was suspended in 250 μ L of PBS, sonicated for 30 s, and placed on a shaker incubator at 37 °C. 200 μ L were removed and replaced with fresh PBS at indicated time points, and released protein was measured via micro bicinchoninic assay (Thermo Fisher Scientific, Waltham, MA). Following 30 days of release, the buffer was changed to 40 mM sodium hydroxide to catalyze the release of any remaining protein and this information was

utilized to determine the encapsulation efficiency, which was calculated as the total amount of protein released divided by the theoretical amount of protein used for nanoparticle synthesis.

6.2.7 Protein Release Characterization

For protein characterization studies of OVA released from 5% (w/w) CPTEG:SA nanoparticles, 5 mg of each nanoparticle formulation was suspended in 250 μ L nanopure water, sonicated for approximately 15 seconds, and the samples were allowed to release overnight (~18 h), after which the samples were centrifuged at 15,000 rcf for 5 mins and 200 μ L supernatant was removed. The protein released was quantified via micro bicinchoninic acid assay, and the samples were diluted to 40 μ g/mL for Native PAGE gel analysis (see below). To determine changes in the tertiary structure of the protein, the samples (40 μ g/mL) were excited at a wavelength of 280 nm and the emission was measured over the range of 300 – 450 nm using a SpectraMax M3 fluorescent spectrometer (Molecular Devices, Sunnyvale, CA). To determine changes in the secondary structure of the protein, circular dichroism spectra were acquired using a Jasco J-715 spectrophotometer (Jasco Analytical Instruments, Easton, MD) of the samples (20 μ g/mL) over a range of 195 – 260 nm.

6.2.8 Native PAGE Gel Analysis

Native PAGE gel analysis was performed using release supernatants from flash nanoprecipitated 5%-loaded (w/w) OVA CPTEG:SA nanoparticles. Samples concentrations were adjusted to 20 μ g/mL, then diluted with an equal volume of native

sample buffer (Bio-Rad, catalog # 161-0738), and 25 μ L of each diluted sample was added to the respective wells of a polyacrylamide gel (4-20% MP TGX Gel 10W 30 μ L, Bio-Rad, catalog #4561093). The gel was subjected to 150 V for 60 min using 25 mM Tris, 192 mM glycine running buffer, placed in fixative solution (40% (v/v) ethanol, 10% (v/v) acetic acid) for three hours, and then stained overnight using flamingo fluorescent gel stain (Bio-Rad, catalog # 161-0491). The stained gel was imaged using a Typhoon 9400 flatbed scanner (GE Healthcare, Pittsburgh, PA).

6.2.9 ELISA

ELISA analysis of OVA released from CPTEG:SA nanoparticles was performed as previously described¹⁴. Briefly, high-binding Costar 590 EIA/RIA microtiter plates (Corning) were coated overnight with 100 μ L of a 0.5 μ g/mL solution of OVA released from the nanoparticles at 4 °C. After washing the wells, microtiter plates were blocked for two hours with a solution of 2.5% (w/v) powdered skim milk dissolved in PBS-Tween with 0.05% Tween 20, pH 7.4, that had been incubated for two hours at 56 °C to inactivate any endogenous phosphatase activity. Following block, microtiter plates were washed thrice with PBS-T. Pooled serum obtained from OVA-immunized mice was added at a dilution of 1:200 and serially diluted in PBS-T containing 1% (v/v) goat serum. Each sample was tested in duplicate. Following incubation overnight at 4°C, plates were washed thrice with PBS-T, after which the secondary antibody alkaline phosphatase-conjugated goat anti-mouse IgG heavy and light chain (Jackson ImmunoResearch) was added at a dilution of 1 μ g/mL. Plates were incubated for two hours at room temperature and then washed three times with PBS-T. To each well, 100

μ L of alkaline phosphatase substrate (Fisher Scientific, Pittsburgh, PA) was added at a concentration of 1 mg/mL dissolved in 50 mM sodium carbonate, 2 mM magnesium chloride buffer at pH 9.3 for colorimetric development. Plates were analyzed after 30 min using a SpectraMax M3 microplate reader at a wavelength of 405 nm. Titer is reported as the reciprocal of serum dilution at which the optical density (OD) value was at most 0.2, a conservative endpoint greater than the average OD of saline-mouse serum, at a 1:200 dilution, plus two standard deviations.

6.2.10 Differentiation of Bone Marrow-derived Dendritic Cells (BMDCs)

Bone marrow was harvested from femurs and tibia of BALB/c mice and differentiated into dendritic cells using a protocol previously described³⁵². Briefly, bone marrow isolates were harvested by flushing the tibia or femur with 10% FBS RPMI. Cells were counted and subsequently plated on petri dishes at 4×10^6 cells/plate in 10 mL media. 10 ng/mL of granulocyte macrophage colony stimulating factor (GM-CSF) was added to the plates on day 0 and fresh GM-CSF and media was added on day 3. On days 6 and 8 of culture, 10 mL of media was replaced with fresh GM-CSF and media, and the cells harvested on day 10 for nanoparticle stimulation assays.

6.2.11 Biocompatibility and Cellular Internalization of CPTEG:SA Nanoparticles

For biocompatibility assays, the murine RAW 264.7 monocyte/macrophage cell line was seeded in flat bottom 96 well tissue culture plates at a density of 100,000 cells/well (100 μ L) and allowed to adhere overnight. The following morning, 100 μ L was added to the wells containing empty CPTEG:SA nanoparticles at concentrations ranging

from 500 $\mu\text{g/mL}$ serially diluted two-fold down to 7.8 $\mu\text{g/mL}$ for 24 hours, after which 25 μL of MTT reagent (2.5 mg/mL) was added to the wells and allowed to react for two hours. The entire volume was carefully pipetted off and 300 μL DMSO was added to the wells and absorbance measurements were made at 540 nm, using 690 nm as a background subtraction. The cell viability was calculated as the background corrected absorbance of the samples divided by the background corrected absorbance of unstimulated cells.

For cell internalization, the murine J774 monocyte/macrophage cell line, human THP-1 cell line, and murine BMDCs were seeded in flat bottom 24 well tissue culture plates at cell density of 500,000 cells/well (500 μL cell culture media) and allowed to adhere overnight. The following morning, 500 μL culture media was added to the wells containing CPTEG:SA nanoparticles encapsulating $\text{Cd}_x\text{Se}_{1-x}/\text{ZnS}_{\text{core/shell}}$ fluorescent nanocrystals (1% w/w; excitation 405 nm; emission 450 nm; Cytodiagnostics, Burlington, Ontario, Canada) at a concentration of 125 $\mu\text{g/mL}$ for 2.5 h, after which the cells were scraped, fixed, and the samples assessed for nanoparticle-positive cells via flow cytometry. In order to properly differentiate nanoparticles and nanocrystals from cells, control tubes were also analyzed containing solely the nanocrystal-loaded nanoparticles in addition to a tube containing nanocrystals alone suspended in buffer.

6.3 Results

CPTEG:SA copolymers were synthesized with the following criteria in mind: 1) the thermal properties of the copolymers must be above body temperature (37 $^{\circ}\text{C}$) to maintain discreteness of the nanoparticles and encapsulated protein stability at *in vivo*

temperatures, 2) the synthesized nanoparticles must be discrete to maintain suspension quality for ease of administration, and 3) the nanoparticles must maintain antigenicity of protein during encapsulation and release. Once these criteria were met, the nanoparticles were evaluated for their biocompatibility and APC internalization.

6.3.1 CPTEG:SA Copolymer Structural Characterization

CPTEG:SA copolymers were synthesized by varying CPTEG molar composition from 0 – 25 mol%. Unfortunately, copolymers in molecular weight ranges of 10,000-20,000 Da resulted in an oily substance (data not shown) that was unsuitable for further processing; however, increasing the reaction time to maintain the molecular weight between 20,000-30,000 Da resulted in a solid mass for all copolymers synthesized (Table 6.1). It should be noted that CPTEG:SA copolymers with >25 mol% CPTEG were not studied further because the copolymers were less solid, sticky, and failed to result in discrete nanoparticles (data not shown).

^1H NMR spectra of these copolymers revealed characteristic peaks associated with CPTEG²³² and SA³⁵¹, with aromatic CPTEG proton peaks located in the $\delta = 6.8$ -8.1 ppm range, and inner chain proton peaks located between 3.6-4.4 ppm (Figure 6.1A). Characteristic SA proton peaks were located at between 1.35-2.65 ppm. As expected, increasing the molar ratio of CPTEG in the copolymer backbone resulted in an increase in the proton peaks associated with CPTEG and the copolymer composition matched that of the feed composition, consistent with previous studies with CPH:SA and CPTEG:CPH copolymers^{232,351,353}. Further analysis of ^1H NMR spectra of CPTEG:SA copolymers revealed a decrease in average sequence length with increasing CPTEG

content, in line with previous reports for other polyanhydride copolymers (Figure 6.1B)^{351,354}. All copolymers studied exhibited alternating or random copolymer formation, evidenced by degree of randomness values of approximately 2.0 (Table 6.1). This was further confirmed by calculating the reactivity ratios r_1 and r_2 , which were determined to be $r_1 = 1.0 - 1.8$ and $r_2 = 1.0 - 1.8$ using the Mayo-Lewis method, or $r_1 = 1.46$ and $r_2 = 1.01$ using the Fineman-Ross method, indicating that either monomer can be added to the copolymer backbone at comparable rates, as is the case for random copolymers.

Thermal analysis of the copolymers demonstrated increased melting temperatures with increasing SA molar composition, ranging from 52 °C for 25:75 CPTEG:SA to 78 °C for poly(SA) (Figure 6.2A and Table 6.1). Wide angle X ray diffraction analysis of powders of the copolymers revealed semi-crystalline properties of all copolymers analyzed, with an increase in relative crystallinity with increasing SA molar composition, ranging from 26% for 25:75 CPTEG:SA to 59% for poly(SA) (Figure 6.2B and Table 6.1). Therefore, CPTEG:SA copolymers demonstrate characteristic properties consistent with those previously observed in other polyanhydride copolymers and the investigated copolymer chemistries exhibited desirable thermal properties for vaccine stability *in vivo* and long-term shelf storage.

6.3.2 Erosion Kinetics of Polyanhydride Films

To assess the relative erosion kinetics of CPTEG:SA copolymers compared to traditional polyanhydride copolymers, copolymer films were prepared for contact angle measurements to determine their hydrophobicity, followed by characterization of their

erosion kinetics. Interestingly, contact angle measurements of CPTEG:SA copolymer films of various copolymer composition revealed that hydrophobicities were relatively similar with varying copolymer composition, with 10:90 CPTEG:SA having the highest contact angle (76°) and 80:20 CPTEG:SA having the lowest (57°) (Figure 6.3A). The erosion kinetics data demonstrated a more rapid erosion profile for all CPTEG:SA copolymers studied compared to that of 20:80 CPTEG:CPH and 20:80 CPH:SA films (Figure 6.3B). The erosion rate of CPTEG:SA films increased with increasing SA molar composition (approximately 150-200 mg eroded over 45 days), compared to 20:80 CPTEG:CPH and 20:80 CPH:SA films, which had approximately 100 and 50 mg eroded over 45 days, respectively. This trend was also observed with the release of BSA from spray dried 2% (w/w) CPTEG:SA nanoparticles, in which increasing SA content resulted in a more rapid release of encapsulated protein over the course of 30 days (Figure 6.3C). ¹H NMR analysis of copolymer film samples performed at 15, 30, and 45 days revealed a decrease in SA composition in the films over time, indicating that SA-SA bonds are more water labile than CPTEG-CPTEG or CPTEG-SA bonds (Table 6.2). Therefore, CPTEG:SA copolymers exhibit rapid erosion rates compared to conventional 20:80 CPTEG:CPH and 20:80 CPH:SA copolymers and the rate of erosion can be tuned by modulating copolymer composition.

6.3.3 CPTEG:SA Nanoparticles Stabilize Protein Payloads and Provide Sustained Release

Nanoparticles based on CPTEG:SA copolymers were synthesized in order to assess the size, discreteness, and ability to encapsulate and release antigenically stable protein (hen egg ovalbumin was used as a model antigen in these studies).

Empty particles synthesized using flash nanoprecipitation method were discrete, with sizes ranging from 575 – 1054 nm, and with narrow size distributions (Figure 6.4 and Table 6.3). These diameters are slightly larger than those typically reported for CPTEG:CPH¹⁷ and CPH:SA³⁵⁵ nanoparticles. Zeta potential measurements of the nanoparticles showed zeta potentials ranging from -28.7 to -35.3 mV, consistent with previous reports for other polyanhydride nanoparticles (Table 6.3)¹⁷.

CPTEG:SA nanoparticles were investigated for their ability to encapsulate and release stable antigen. Native PAGE gel analysis of hen egg ovalbumin (OVA) released from 5% (w/w) OVA-loaded CPTEG:SA nanoparticles demonstrated that all CPTEG:SA chemistries maintained the native conformational stability of the encapsulated antigen upon release (Figure 6.5A). Further analysis of OVA using circular dichroism revealed that the secondary structure of the released antigen was preserved (Figure 6.5B). In addition, fluorescence spectroscopy analysis of OVA revealed that the tertiary structure of released antigen was maintained (Figure 6.5C). Interestingly, there was a trend in increasing fluorescence signal from samples with higher CPTEG molar composition, matching that of the OVA standard. These studies indicated that CPTEG:SA nanoparticles can be synthesized into discrete nanoparticles that maintain protein stability following encapsulation and release.

6.3.4 CPTEG:SA Nanoparticles Are Biocompatible and Enhance Cellular Internalization

CPTEG:SA nanoparticles were evaluated for their biocompatibility as well as degree of internalization by APCs. An MTT assay performed on CPTEG:SA nanoparticles incubated with RAW 264.7 cells demonstrated that these nanoparticles

maintained cell viability at >75% for nanoparticle concentrations of up to 62.5 µg/mL (Figure 6.6A). Interestingly, there was a trend in increasing cell viability with increasing CPTEG molar composition for concentrations >62.5 µg/mL. In comparison, 20:80 CPTEG:CPH nanoparticles demonstrated similar biocompatibility, however these particles maintained higher cell viability at concentrations >62.5 µg/mL.

When CPTEG:SA nanoparticles were incubated with three different APC types, murine J774 monocyte/macrophage cell line, human THP-1 monocyte/macrophage cell line, and murine BMDCs, the data showed a high degree of internalization of these particles by all three cell types. Formulations rich in SA displayed the highest degree of uptake across all three cell types (Figure 6.6B). Interestingly, depending on the cell type, 5:95 CPTEG:SA, 10:90 CPTEG:SA, and 15:85 CPTEG:SA copolymers had rates of internalization greater than or equal to poly(SA), while 20:80 CPTEG:SA nanoparticles providing the same degree of internalization as poly(SA) in J774 and THP-1 cells, but not in BMDCs. The 25:75 CPTEG:SA nanoparticles had the lowest degree of internalization, with significantly lower rates of cell internalization than all other formulations. These results demonstrate the biocompatibility of CPTEG:SA nanoparticles and show that copolymer chemistries with molar composition ≤ 20 mol% are highly internalized by APCs, with certain chemistries having enhanced internalization rates compared to poly(SA) nanoparticles.

6.4 Discussion

There is a growing body of literature on the efficacy of nanoparticles for protein therapeutics as well as novel adjuvant technologies that enhance immune responses to

vaccines, in particular subunit vaccines^{208,356–358}. Polymeric nanoparticles are a promising class of carriers/adjuvants due to their facile synthesis and their ability to stabilize encapsulated payloads, ligate the polymer with various targeting ligands for targeted delivery, and tune release kinetics through copolymerization. Polyanhydrides have been investigated as a protein and vaccine delivery platform due to their surface erosion characteristics, which enhances stability of encapsulated payloads^{19,219,220,332}. In addition, their degradation products are less acidic than that of PLGA, with pKas of 5.8 & 8.4 (CPTEG)²³², 3.7 & 6.7 (CPH)²⁷³, and 4.8 & 5.6 (SA)²⁷³. In this work, a new class of polyanhydride copolymers comprising of CPTEG and SA were synthesized in order to confer enhanced thermal properties for long term storage, ease of administration (discrete particles that suspend well), retention of protein stability following encapsulation and release, and improved uptake by APCs.

In addition to chemical properties of polymers being critical for maintaining protein conformational stability, maintaining thermal stability of both the antigen and the nanoparticle formulation is critical in the design of future vaccines for long term storage^{19,359}. Maintaining protein conformational stability of antigen is critical for developing robust immune responses to vaccines because linked recognition plays a role in the affinity maturation process of B cells in germinal centers³⁶⁰. Having the protein sequestered within a rigid polymer matrix with high thermal properties will allow for maintenance of protein stability during encapsulation and antigenicity of the payload upon release. In addition, the desirable thermal properties can also help retain particle discreteness and morphology for long term storage, which would enable stockpiling vaccines for mass vaccination against highly lethal bioterrorism pathogens, or for

deployment to harsh environments. We have previously shown that CPH:SA copolymers rich in SA were best able to maintain the antigenicity of *Bacillus anthracis* protective antigen (PA) for at least four months, and this was attributed to the high thermal properties of SA, despite the inability of the copolymer to release antigenic protein compared to CPTEG:CPH copolymers¹⁹. Hence, it was hypothesized that copolymers of CPTEG and SA would have high thermal properties due to the high melting point (78 °C) of poly(SA), and copolymerization with CPTEG would improve antigenicity of the released protein. In our studies, CPTEG molar compositions upwards of 25% yielded melting points of at least 52 °C. These melting points are similar to those observed with CPH:SA copolymers (melting points of 20:80 CPH:SA and 50:50 CPH:SA are 66 °C and 50 °C, respectively³⁶¹).

Copolymers based on CPTEG:CPH or CPH:SA have demonstrated sustained release of encapsulated protein payloads over extended time periods, on the order of months³²⁶. In this work, it was observed that CPTEG:SA copolymers had faster erosion kinetics (on the order of weeks) than the traditionally used 20:80 CPTEG:CPH and 20:80 CPH:SA copolymers. The ability to tune the film erosion rate was dictated by the copolymer composition, consistent with previous reports for CPTEG:CPH copolymers²³². Despite having similar contact angles, chemistries rich in SA had the fastest rates of erosion and this was corroborated by ¹H NMR spectroscopy measurements of the films over time, which showed that SA molar composition of the films decreased over time. These rapid erosion characteristics may be desirable for both drug and vaccine delivery, in order to have finer control over protein release

kinetics, or by cocktailing these nanoparticle chemistries with slower releasing copolymer formulations such as 20:80 CPTEG:CPH.

The hydrophobicity of polyanhydrides results in surface erosion characteristics, which in addition to higher pKa values, allows for protection of the structural stability of encapsulated proteins^{19,220,281}. Copolymers containing CPTEG have previously demonstrated to maintain the stability of encapsulated proteins, with 50:50 CPTEG:CPH copolymers typically best at maintaining protein structure and antigenicity following release^{19,219,220,332}. Despite the enhanced thermal properties of SA-rich chemistries (poly(SA) and 20:80 CPH:SA), it was previously shown that copolymers rich in SA resulted in loss of stability of *Bacillus anthracis* protective antigen, and subsequently its antigenicity, which was attributed to the greater acidity of SA degradation products compared to CPTEG and CPH diacids¹⁹. Therefore, it was hypothesized that copolymerizing the more protein-favorable CPTEG with SA might be able to maintain protein structure and antigenicity following encapsulation. CPTEG:SA nanoparticles encapsulating OVA maintained protein stability via native PAGE gel analysis and circular dichroism, however it was observed that copolymers richer in CPTEG tended to best maintain the tertiary structure of the OVA, thus making them an attractive candidate for protein encapsulation.

Polyanhydride nanovaccines display chemistry-dependent cellular internalization and intracellular persistence by APCs which can aid in adjuvanting poorly immunogenic proteins. This has been observed to be enhanced in polymer chemistries rich in CPTEG molar composition¹⁶, which had the highest degree of internalization and persistence in RAW264.7 macrophages¹⁵. In BMDCs, copolymer chemistries rich in SA had the

highest percentage of cellular internalization, even greater than CPTEG-rich chemistries¹⁶. In this work, CPTEG:SA nanoparticles exhibited high rates of internalization by APCs. Interestingly, although previously poly(SA) nanoparticles had been shown to be the most highly internalized formulation (ref), multiple CPTEG:SA compositions (5:95 CPTEG:SA, 10:90 CPTEG:SA, and 15:85 CPTEG:SA) showed rates of internalization greater than or equal to that of poly(SA), depending on the cell type. This observation is hypothesized to occur due to synergy between the cellular internalization and activation mechanism(s) of CPTEG and SA-rich copolymers^{16,256}. These properties, along with observations that CPTEG-rich chemistries best retain the secondary and tertiary structures of encapsulated proteins^{19,219,220}, make CPTEG:SA copolymers particularly promising in the design of new carriers and adjuvants.

In summary, this work described the synthesis and characterization of novel copolymers based on CPTEG and SA with favorable thermal properties for *in vivo* protein/vaccine delivery and long-term shelf storage. The CPTEG:SA nanoparticles maintain protein stability and antigenicity upon release, are biocompatible, and are highly internalized by APCs, making them an attractive candidate for further study as a vaccine adjuvant/delivery system.

6.5 Tables

Table 6.1. CPTEG:SA copolymer characterization

Chemistry	Molecular Weight (Daltons)	Melting Point (°C)	Relative Crystallinity (%)	Degree of Randomness
poly(SA)	10466 – 18727	76.7 ± 2.0	58.7	1
5:95 CPTEG:SA	20119 – 24062	74.6 ± 1.8	55.7	2.6
10:90 CPTEG:SA	20601 – 29083	70.0 ± 1.9	48	2.2
15:85 CPTEG:SA	20571 – 24944	64.5 ± 2.4	40.6	2.1
20:80 CPTEG:SA	19978 – 30828	58.9 ± 3.2	35	2.1
25:75 CPTEG:SA	25578 – 31455	52.3 ± 3.5	26	2.1

Table 6.2. CPTEG:SA copolymer film composition over time

Chemistry	Time point	Mole Fraction CPTEG	Mole Fraction SA
5:95 CPTEG:SA	Day 15	0.05	0.95
	Day 30	0.06	0.94
	Day 45	0.06	0.94
15:85 CPTEG:SA	Day 15	0.28	0.72
	Day 30	0.28	0.72
	Day 45	0.38	0.62
25:75 CPTEG:SA	Day 15	0.39	0.61
	Day 30	0.38	0.62
	Day 45	0.48	0.52

Table 6.3. Characterization of CPTEG:SA nanoparticles

Chemistry	Diameter (nm)	Polydispersity Index	Zeta Potential (mV)
poly(SA)	655.6 ± 197.3	0.091	-31.7 ± 6.7
5:95 CPTEG:SA	605.7 ± 284.2	0.220	-33 ± 9.3
10:90 CPTEG:SA	575.3 ± 252.0	0.192	-33.7 ± 8.9
15:85 CPTEG:SA	619.6 ± 279.5	0.203	-35.3 ± 9.0
20:80 CPTEG:SA	1054.3 ± 477.2	0.205	-29.6 ± 12.7
25:75 CPTEG:SA	798.5 ± 292.7	0.134	-28.7 ± 8.8

6.6 Figures

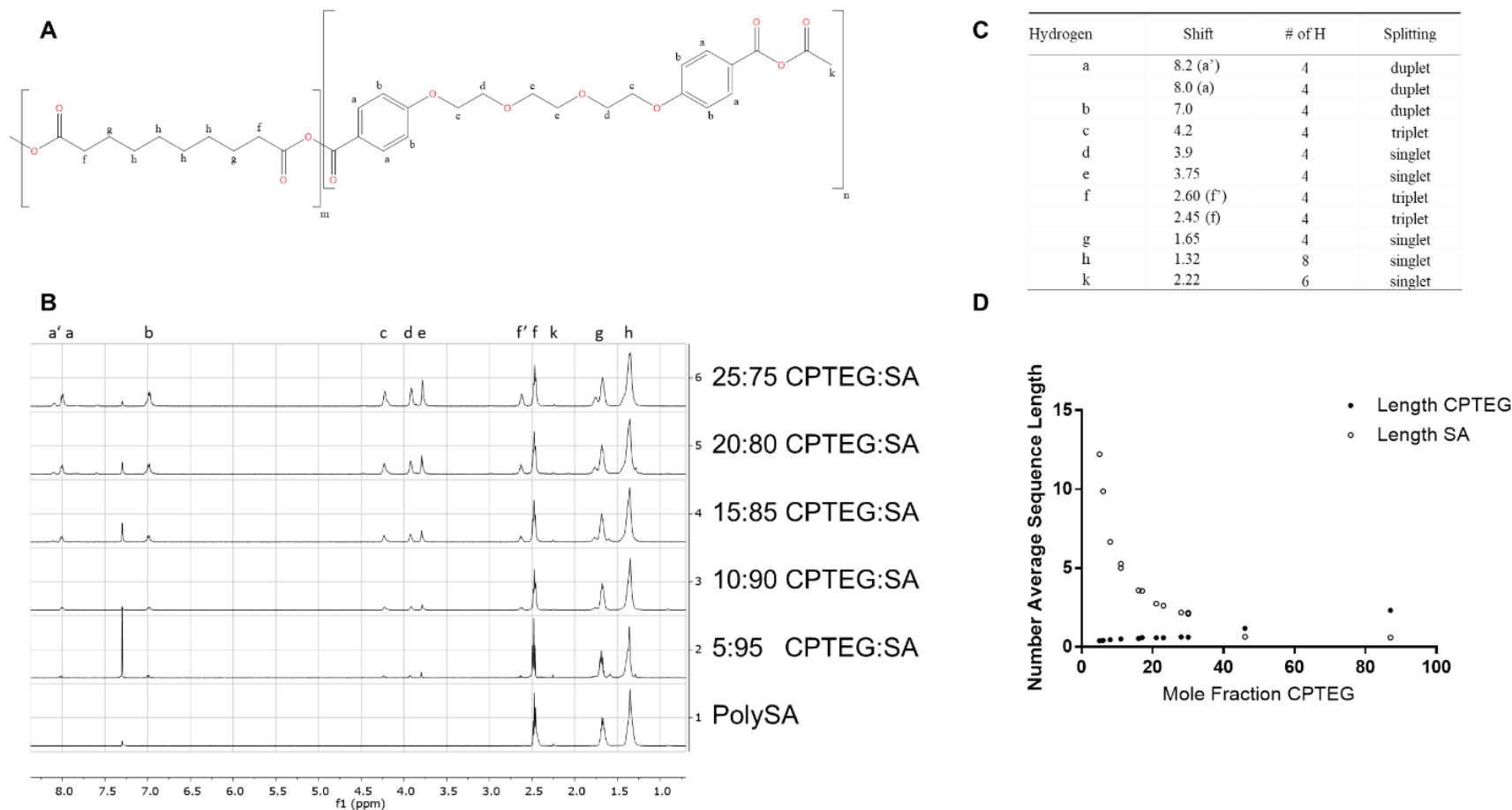


Figure 6.1. CPTEG:SA copolymers demonstrate characteristic polyanhydride physical properties via NMR spectroscopy. (A) Molecular structure of CPTEG:SA copolymer. (B) NMR spectra of CPTEG:SA copolymers. (C) Description of hydrogens in copolymer backbone for ^1H NMR spectra. (D) Number average sequence lengths of repeating CPTEG or SA units determined from ^1H NMR spectra.

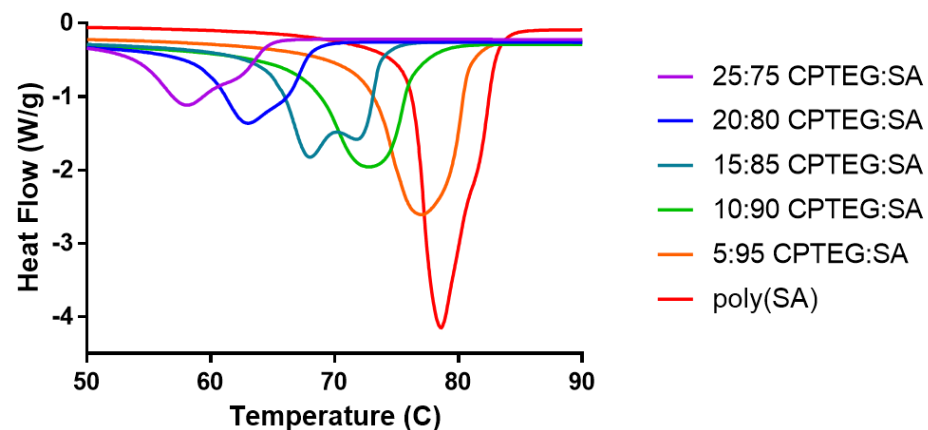
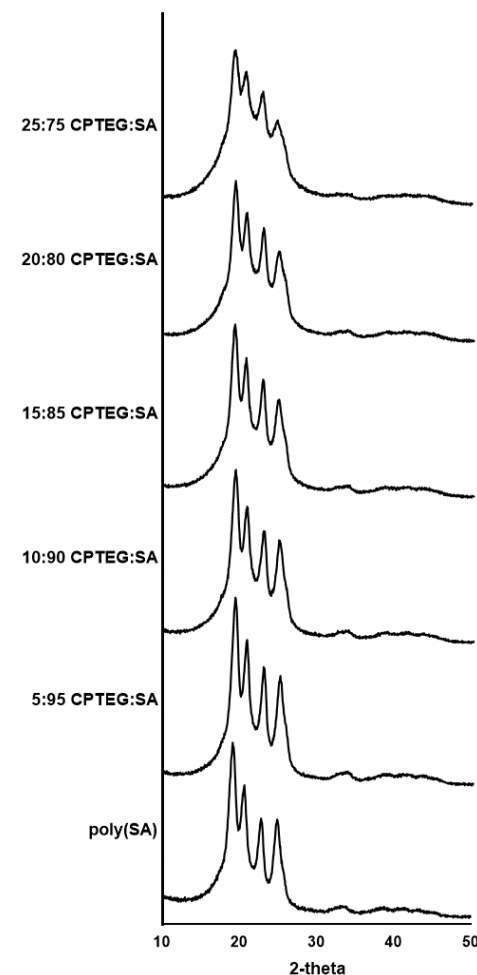
A**B**

Figure 6.2. CPTEG:SA copolymers demonstrate characteristic polyanhydride physical properties via DSC and WAXD. (A) Heat flow vs. temperature plot of CPTEG:SA copolymer powders measured via differential scanning calorimetry (DSC). The melting point of the polymer was determined as the minima of the endotherm of each chemistry. (B) Wide angle X ray diffraction (WAXD) spectrogram of CPTEG:SA copolymer powders.

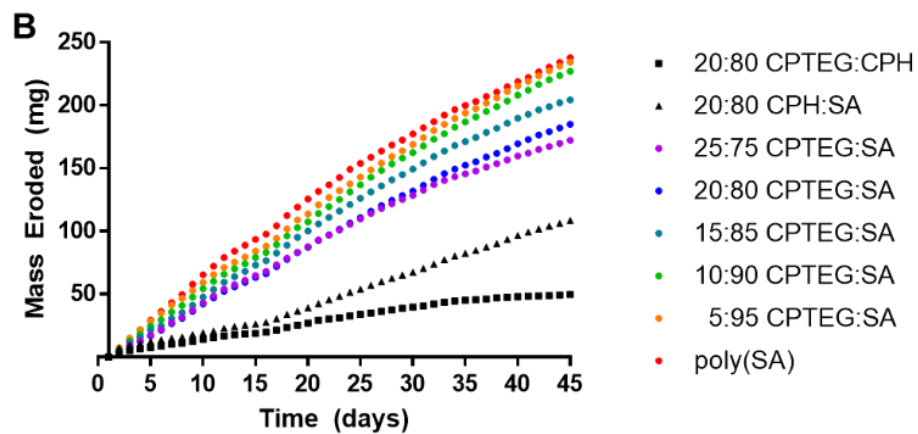
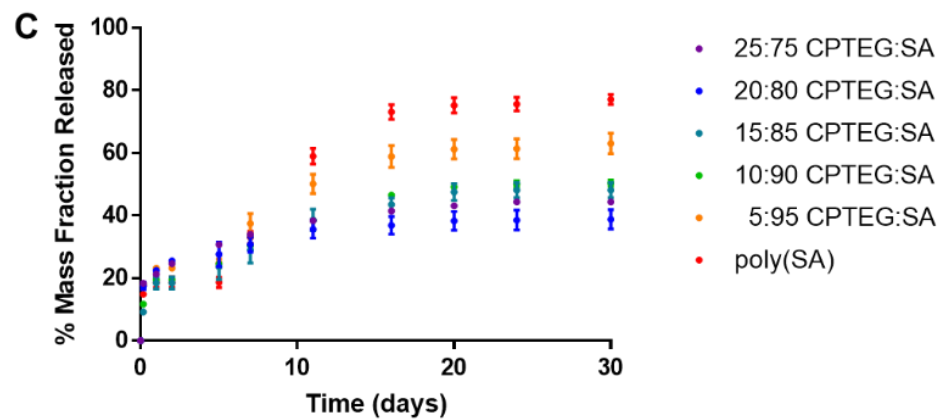
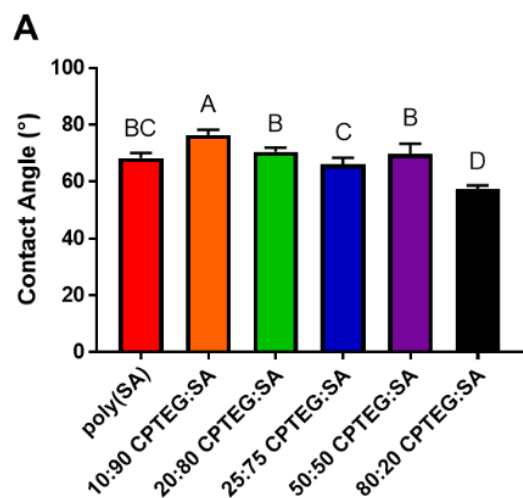
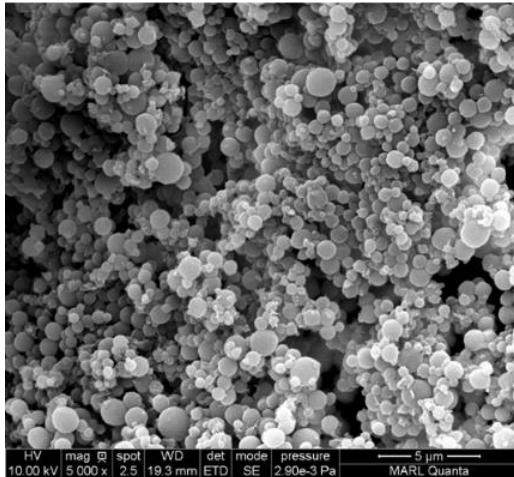
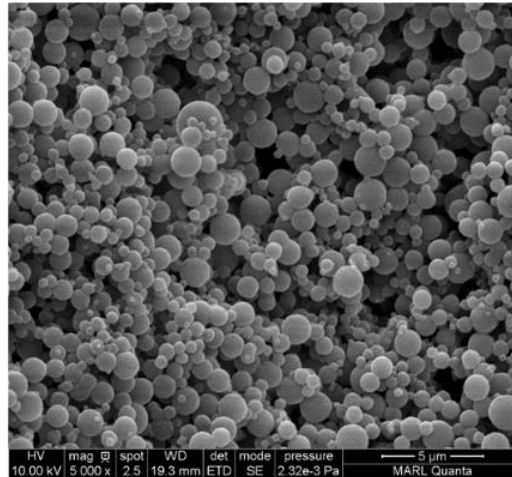


Figure 6.3. CPTEG:SA copolymers demonstrate chemistry-dependent erosion kinetics. (A) Contact angle measurements of CPTEG:SA copolymer films fabricated via spin coating on glass slides. (B) Mass of CPTEG:SA copolymer films eroded as a function of time. 15 mL supernatants were collected daily and the entire volume was replaced with fresh nanopure water. (C) Cumulative % mass fraction released from spray dried 2% (w/w) BSA-loaded CPTEG:SA nanoparticles. Statistical significance for contact angle measurements was determined via an ordinary one-way ANOVA with a Tukey's multiple comparison test. Differences in letters above each copolymer chemistry indicate significant differences ($p \leq 0.05$) in contact angle measurements between the various copolymers.

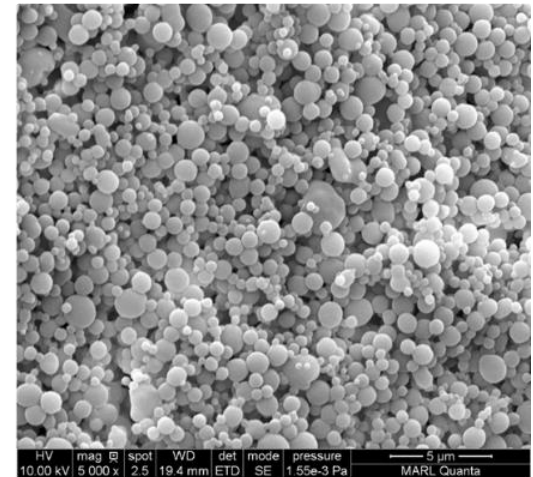
poly(SA)



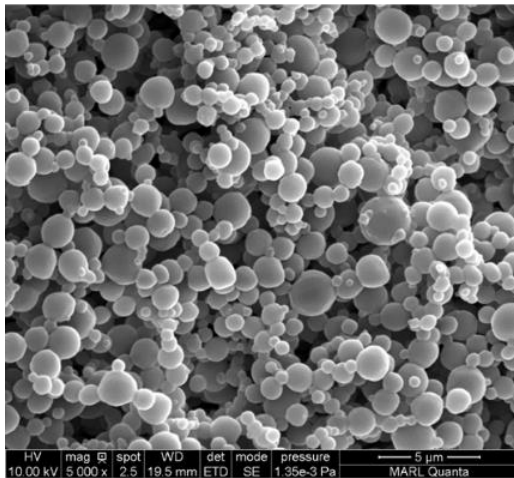
5:95 CPTEG:SA



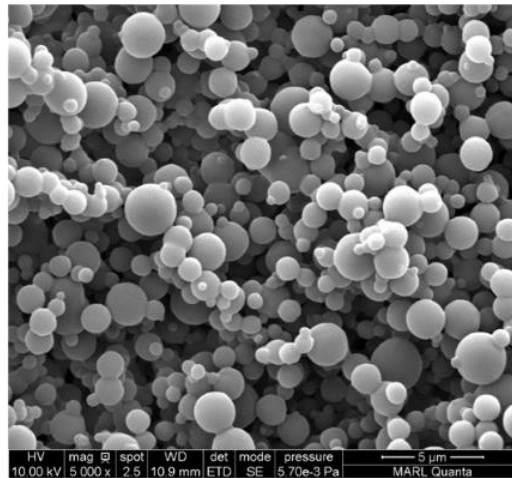
10:90 CPTEG:SA



15:85 CPTEG:SA



20:80 CPTEG:SA



25:75 CPTEG:SA

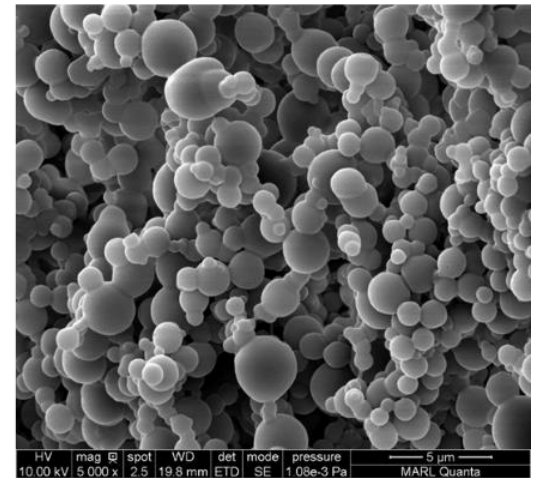


Figure 6.4. CPTEG:SA nanoparticles can be fabricated into discrete nanoparticles with narrow size distribution.

SEM images of empty CPTEG:SA nanoparticles fabricated via flash nanoprecipitation. Briefly, copolymer was dissolved in methylene chloride at a concentration of 20 mg/mL. The solution was poured into a bath of pentane at a 1:250 volumetric ratio (methylene chloride: pentane), and the resulting suspension was vacuum filtered to collect the nanoparticles. The mean diameter of the nanoparticles were as follows: poly(SA) - 655.6 ± 197.3 nm, 5:95 CPTEG:SA - 605.7 ± 284.2 nm, 10:90 CPTEG:SA - 575.3 ± 252.0 nm, 15:85 CPTEG:SA - 619.6 ± 279.5 nm, 20:80 CPTEG:SA - 1054.3 ± 477.2 nm, 25:75 CPTEG:SA - 798.5 ± 292.7 nm.

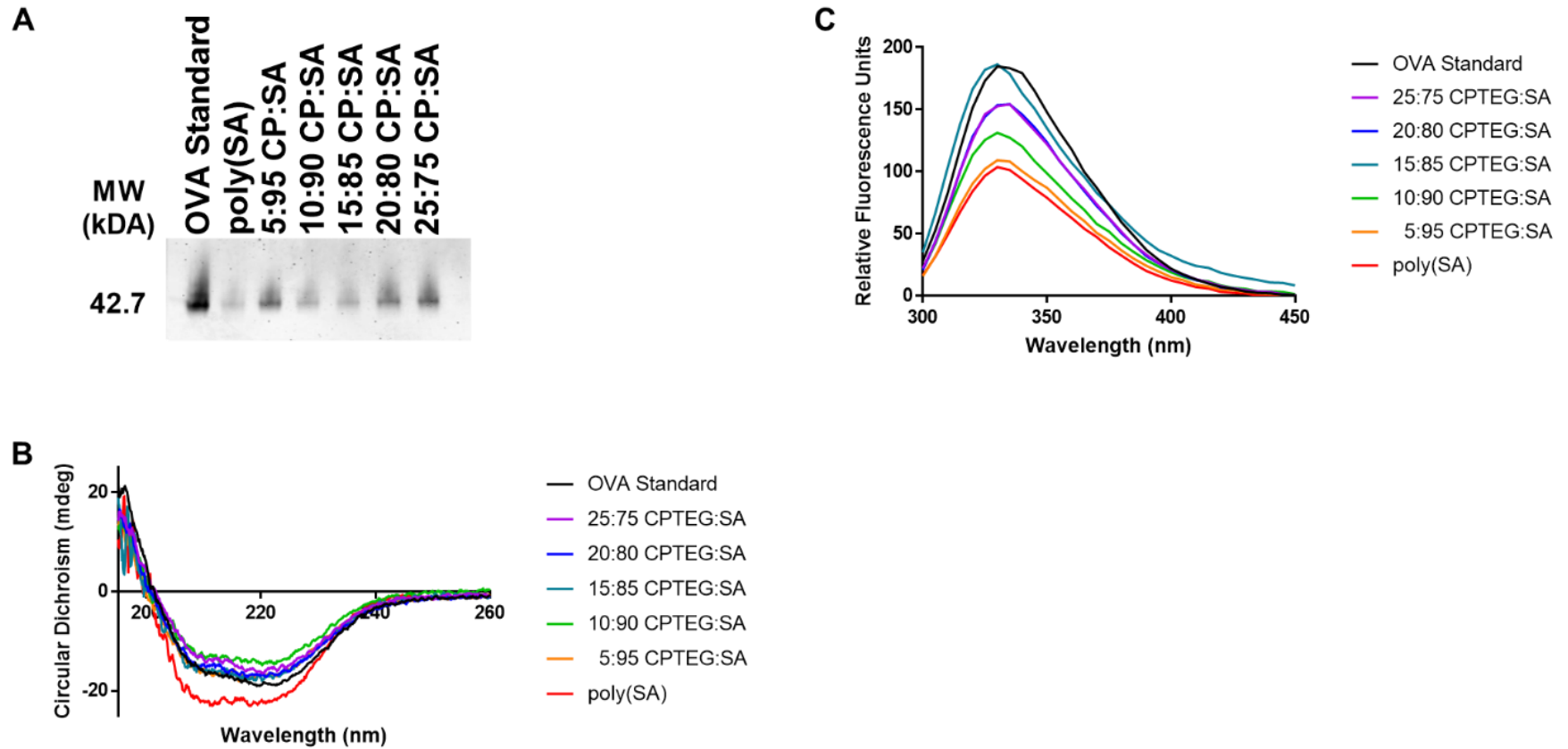


Figure 6.5. CPTEG:SA nanoparticles maintain protein conformational stability following encapsulation and release. (A) Native PAGE gel analysis of OVA released from 5% (w/w) OVA-loaded CPTEG:SA nanoparticles. Released OVA concentration was measured via microBCA and diluted to 40 $\mu\text{g/mL}$ for analysis. (B) Circular dichroism spectra of OVA released from 5% (w/w) OVA-loaded CPTEG:SA nanoparticles. Released OVA concentration was measured via microBCA and diluted to 20 $\mu\text{g/mL}$ for analysis. (C) Fluorescence spectra of OVA released from 5% (w/w) OVA-loaded CPTEG:SA nanoparticles. Released OVA concentration was measured via microBCA and diluted to 40 $\mu\text{g/mL}$ for analysis. Samples were excited at 280 nm and fluorescence was measured from 300-450 nm.

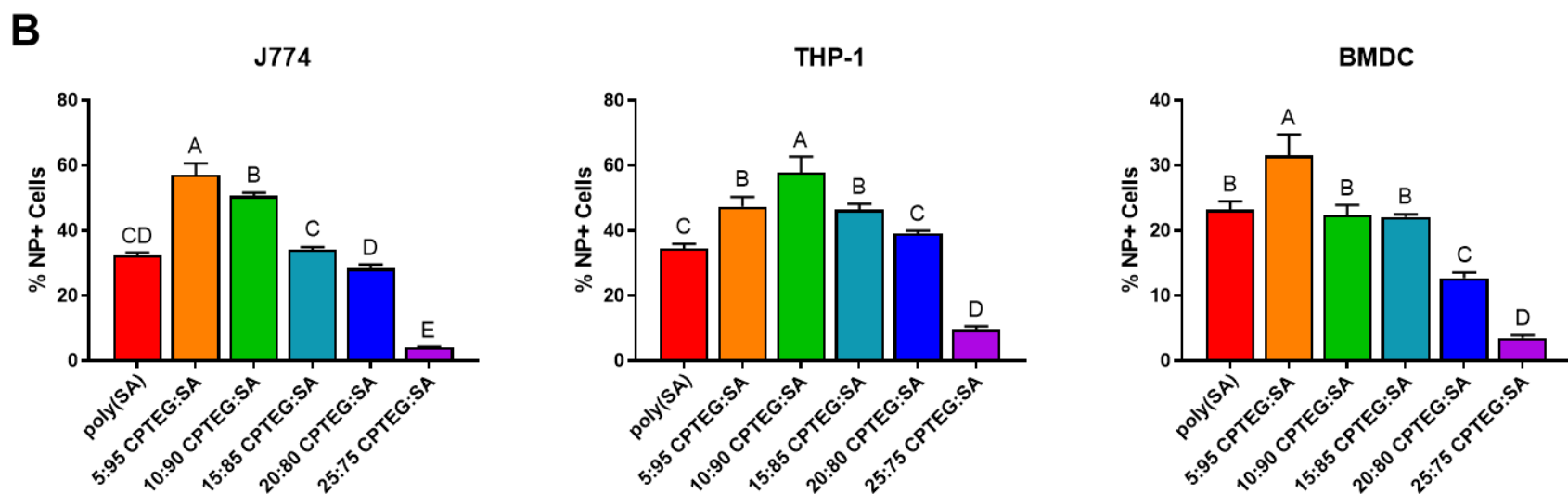
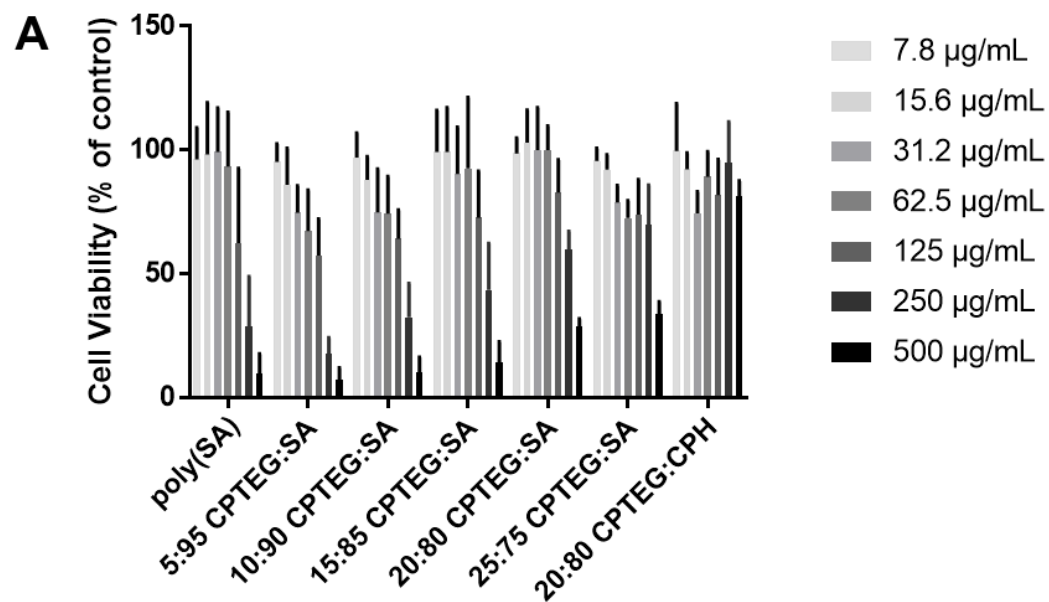


Figure 6.6. CPTEG:SA nanoparticles are biocompatible and exhibit high rates of internalization by antigen

presenting cells. (A) MTT assay of CPTEG:SA nanoparticles incubated with the murine RAW 264.7

monocyte/macrophage cell line. Cells were incubated with varying concentrations of the empty nanoparticles for 24 hours, after which MTT reagent was added to the wells to determine cell viability. (B) Cell internalization assay of CPTEG:SA nanoparticles incubated with the murine J774 monocyte/macrophage cell line, human THP-1 monocyte/macrophage cell line, and murine bone-marrow-derived dendritic cells. CPTEG:SA nanoparticles encapsulating fluorescent nanocrystals (1% w/w) were incubated with cells for 2.5 hours at 125 $\mu\text{g/mL}$ and flow cytometry analysis was performed to determine the percentage of nanoparticle-positive cells. Statistical significance for contact angle measurements was determined via an ordinary one-way ANOVA with a Tukey's multiple comparison test. Differences in letters above each copolymer chemistry indicate significant differences ($p \leq 0.05$) between the various treatment groups.

CHAPTER 7. CONCLUSIONS AND ONGOING/FUTURE RESEARCH

7.1 Conclusions

There is an urgent and unmet need for developing vaccines that can provide rapid and long-lived protective immunity against potential biological warfare agents such as *Y. pestis*³⁶² and *B. anthracis*¹⁰³, as well as vaccines that are capable of inducing robust mucosal immune responses in the lungs against pathogens such as RSV^{7,8}. Unfortunately, there are no FDA-approved vaccines available against *Y. pestis*³⁶³ and RSV³⁶⁴, and the FDA-approved AVA vaccine against anthrax requires multiple immunizations over an 18-month time period to achieve protective immunity, which is not effective in the event of an outbreak scenario. Current promising approaches against these pathogens are focused on using subunit vaccines due to the adverse effects of live-attenuated strains of the organisms^{82,84}; however, the inclusion of adjuvants in these vaccines to boost the immune response is necessary¹⁹⁴.

Polyanhydride nanovaccines are a promising next-generation vaccine adjuvant platform against lethal respiratory pathogens that allow for sustained release and dose sparing¹⁸, immunomodulation in a chemistry-dependent manner^{15,17,204,255}, and stabilization of protein antigens for extended periods at elevated temperatures¹⁹. Hence, this work sought to investigate the ability of polyanhydride-based vaccines, or nanovaccines, at inducing protective immune responses against multiple bacterial pathogens.

The work described in Chapter 3 investigated the efficacy of a combination of polyanhydride nanovaccines with the synthetic co-adjuvant cyclic dinucleotide (CDN) RR-CDG to provide both rapid and long term protective immunity against lethal

pneumonic plague challenge. Female C57BL/6 mice immunized with polyanhydride nanovaccine encapsulating F1-V co-administered with CDNs demonstrated rapid (14 DPI) and long-lived (182 DPI) protective immunity against lethal IN *Y. pestis* challenge, thus highlighting the benefits of using a combination-adjuvant approach that both enhance immune responses. The work described in Chapter 4 extended this idea by showing that a combination nanovaccine encapsulating rPA and RR-CDG induced rapid neutralizing antibody responses against the anthrax lethal toxin after 15 DPI, which were greater than those of rPA adsorbed to alhydrogel.

The results of these two studies highlight the potential for combination adjuvants, where each component of the vaccine formulation may contribute beneficial properties to enhance protection. In both studies, polyanhydride nanoparticles alone were unable to enhance the magnitude of the overall IgG response to the antigens, however they were necessary for providing complete protection against escalating challenge doses of pneumonic plague. The CDN co-adjuvant RR-CDG was necessary for eliciting rapid and durable antibody responses against both antigens, however failed to provide rapid protection against pneumonic plague at higher challenge doses.

Beyond eliciting rapid protective immunity against biodefense pathogens, polyanhydride nanovaccines are a proven vaccine adjuvant platform against a number of respiratory pathogens, including *Streptococcus pneumoniae*¹⁷, *influenza*^{204,217,350}, and *respiratory syncytial virus* (Chapter 5). The work described in Chapter 5 demonstrated that a polyanhydride nanovaccine encapsulating the BRSV F and G glycoproteins enhanced mucosal adaptive immune responses against BRSV, exhibited in its ability to

reduce pathology in the lungs, viral burden, and virus shedding, while also enhancing mucosal IgA production and CD4⁺ T cell proliferation and cytokine secretion.

In addition to their well-documented ability to adjuvant vaccines, polyanhydride nanovaccines provide thermal stability of encapsulated antigens¹⁹, thus highlighting their additional ability to eliminate the cold chain. Despite the superior ability of SA-rich copolymer chemistries to improve vaccine shelf stability, the acidity of SA degradation products may negatively impact protein stability^{19,219,220,332}. Hence, the work in Chapter 6 described the synthesis and characterization of novel polyanhydride copolymers based on CPTEG and SA with favorable thermal properties for *in vivo* protein/vaccine delivery and long-term shelf storage. The CPTEG:SA nanoparticles maintained protein stability and antigenicity upon release, are biocompatible, and are highly internalized by APCs, making them an attractive candidate for further study as a vaccine adjuvant/delivery system. These properties are all likely beneficial in the design of future vaccines, where maintaining vaccine stability outside of the cold chain will dramatically reduce cost of storage and improve delivery to remote areas where refrigeration may not be possible, or for military personnel deployed to harsh environments.

In summary, the work described in this thesis demonstrated how combination nanovaccines enhanced both rapid and long-lived protective immune responses against a wide variety of viral and bacterial respiratory pathogens, including RSV, *Y. pestis*, and *B. anthracis*, and have favorable thermal properties that may allow extended shelf storage and elimination of the cold chain.

7.2 Ongoing/Future Work

Due to the success of the combination nanovaccine in providing complete protection against pneumonic plague, providing a greater level of protection than either adjuvant platform alone (Chapter 3), understanding the mechanism of protection is of interest. Therefore, the following section will describe initial efforts to understand how the combination of polyanhydride nanovaccine and CDNs was able to protect against pneumonic plague challenge.

7.2.1 Neutralization of IFN γ /TNF α Impacts Pneumonic Plague Challenge Outcome

Previous studies have highlighted the role of IFN γ /TNF α in providing protection against pneumonic plague challenge, suggesting a role of cell-mediated immunity in protection against pneumonic plague^{98,365–367}. Previous studies have also demonstrated a role of T cells in protecting against fully virulent strains of *Y. pestis*^{97,366}. This appears to be in agreement with observations that despite generating high titer antibody responses against F1-V, African Green Monkeys are highly susceptible to pneumonic plague infection^{92,368,369}. Therefore, initial studies were conducted to evaluate the role of IFN γ /TNF α in the protective responses observed by the Combination Nanovaccine described in Chapter 3. In this work, female C57BL/6 mice (n=12 per group) were immunized subcutaneously with 50 μ g F1-V encapsulated into 20:80 CPTEG:CPH nanoparticles + 35 μ g CDNs (Combination Nanovaccine). Anti-F1-V total IgG antibody titers were evaluated at 13 DPI and a small cohort of mice (n=4 per group) were injected intraperitoneally with 1 mg each of anti-IFN γ and anti-TNF α monoclonal antibodies to neutralize these cytokines. The following day, the mice were challenged intranasally

with 7000 CFUs of *Y. pestis* CO92 and survival was monitored for 14 days post-challenge.

Serum responses analyzed 13 DPI showed similar high titer anti-F1-V IgG responses between control mice and those injected with the neutralizing antibodies (Figure 7.1A). In agreement with previous studies, it was observed that the protection afforded to mice injected with IFN γ /TNF α neutralizing antibodies was reduced compared to controls.

These results highlight the potential role of the combination of polyanhydride nanoparticles and CDNs at eliciting protective immune responses against pneumonic plague that extend beyond using antibody responses as the correlate of protection. Future work could expand upon this idea by investigating the role of each adjuvant in the formulation at inducing this response, as well as determining the source of each of these cytokines and their role in protection. In addition, due to the enhanced thermal properties and superior internalization of CPTEG:SA nanoparticles described in Chapter 6, it may be of interest to investigate F1-V-loaded CPTEG:SA nanovaccines against pneumonic plague, as well as perform long term shelf studies to compare F1-V stability in this novel polyanhydride chemistry compared to more traditional polyanhydrides. Understanding the underlying mechanism of action of the combination nanovaccine, as well as improving vaccine shelf stability, will enable improved rational design of future vaccines and build upon the successes described in this work.

7.3 Figures

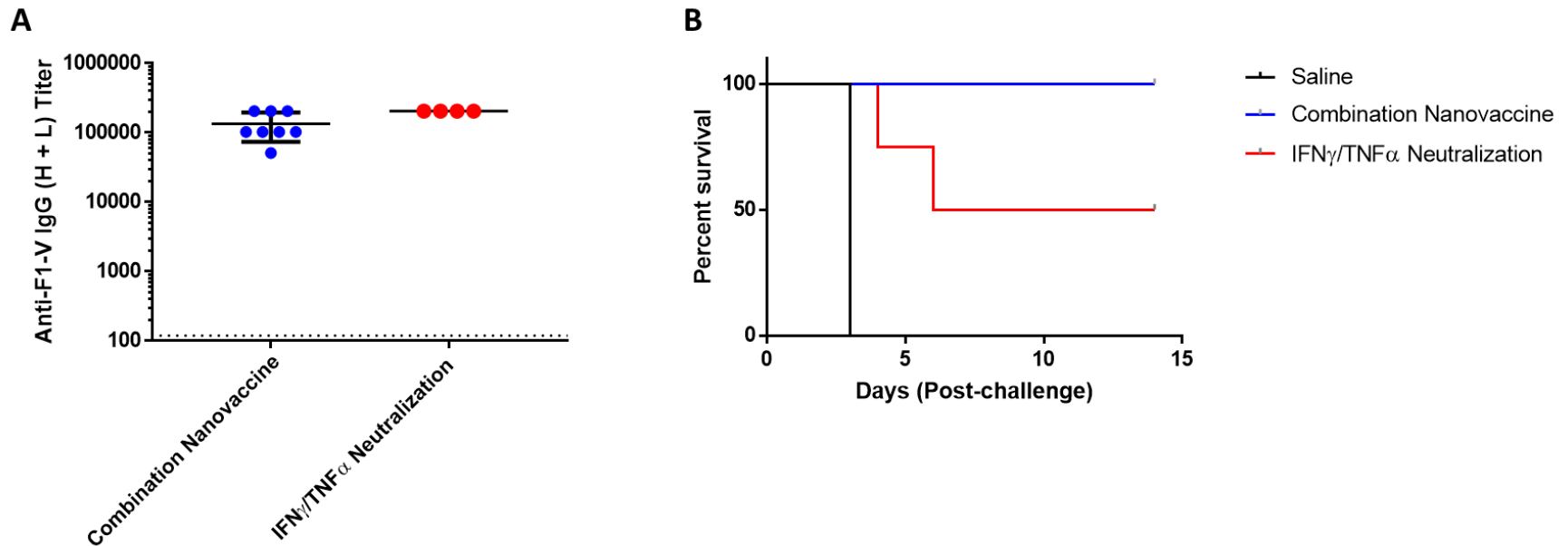


Figure 7.1. Neutralization of IFN γ /TNF α decreases the protective efficacy of the Combination Nanovaccine 14 days post-immunization. Female C57BL/6 mice (n=12 per group) were immunized subcutaneously with 50 μ g F1-V encapsulated into 20:80 CPTEG:CPH nanoparticles + 35 μ g CDNs (Combination Nanovaccine). Anti-F1-V total IgG antibody titers were evaluated at 13 DPI and a small cohort of mice (n=4 per group) were injected intraperitoneally with 1 mg each of anti-IFN γ and anti-TNF α monoclonal antibodies to deplete these cytokines. The following day, the mice were challenged intranasally with 7000 CFUs of *Y. pestis* CO92 and survival was monitored for 14 days post-challenge. (A) Anti-F1-V (H+L) IgG serum responses measured 13 DPI. (B) Survival of mice challenged with 7000 CFU *Y. pestis* CO92 14 DPI, with a small cohort (n=4 per group) injected intraperitoneally with IFN γ /TNF α neutralizing antibodies 24 hours prior to challenge.

BIBLIOGRAPHY

1. Pechous, R. D., Sivaraman, V., Stasulli, N. M. & Goldman, W. E. Pneumonic Plague: The Darker Side of *Yersinia pestis*. *Trends Microbiol.* **24**, 190–197 (2016).
2. Sternbach, G. The history of anthrax. *Journal of Emergency Medicine* **24**, 463–467 (2003).
3. Littman, R. J. The plague of Athens: Epidemiology and paleopathology. *Mount Sinai Journal of Medicine* **76**, 456–467 (2009).
4. Vaccine, I. of M. (US) C. to A. the S. and E. of the A. *et al.* *The Anthrax Vaccine: Is It Safe? Does It Work?* (National Academy Press, 2002). doi:10.17226/10310
5. Jones, L. S. *et al.* Effects of Adsorption to Aluminum Salt Adjuvants on the Structure and Stability of Model Protein Antigens. *J. Biol. Chem.* **280**, 13406–13414 (2005).
6. Clapp, T., Siebert, P., Chen, D. & Jones Braun, L. T. Vaccines with aluminum-containing adjuvants: Optimizing vaccine efficacy and thermal stability. *J. Pharm. Sci.* **100**, 388–401 (2011).
7. Collins, P. L. & Melero, J. A. Progress in understanding and controlling respiratory syncytial virus: Still crazy after all these years. *Virus Research* **162**, 80–99 (2011).
8. Henrickson, K. J., Hoover, S., Kehl, K. S. & Hua, W. National disease burden of respiratory viruses detected in children by polymerase chain reaction. *Pediatr. Infect. Dis. J.* **23**, S11–S18 (2004).
9. Nair, H. *et al.* Global burden of acute lower respiratory infections due to respiratory syncytial virus in young children: a systematic review and meta-analysis. *Lancet* **375**, 1545–1555 (2010).
10. Silvestri, M., Sabatini, F., Defilippi, A.-C. & Rossi, G. A. The wheezy infant - immunological and molecular considerations. *Paediatr. Respir. Rev.* **5**, 81–87 (2004).
11. Uhari, M., Hietala, J. & Tuokko, H. Risk of acute otitis media in relation to the viral etiology of infections in children. *Clin. Infect. Dis.* **20**, 521–524 (1995).
12. Lee, B. Y. *et al.* Economic impact of thermostable vaccines. *Vaccine* **35**, 3135–3142 (2017).
13. Huntimer, L. *et al.* Evaluation of Biocompatibility and Administration Site Reactogenicity of Polyanhydride-Particle-Based Platform for Vaccine Delivery. *Adv. Healthc. Mater.* **2**, 369–378 (2013).
14. Ulery, B. D. *et al.* Design of a protective single-dose intranasal nanoparticle-based vaccine platform for respiratory infectious diseases. *PLoS One* **6**, 1–8 (2011).

15. Ulery, B. D. *et al.* Rational design of pathogen-mimicking amphiphilic materials as nanoadjuvants. *Sci. Rep.* **1**, 198 (2011).
16. Petersen, L. K. *et al.* Activation of innate immune responses in a pathogen-mimicking manner by amphiphilic polyanhydride nanoparticle adjuvants. *Biomaterials* **32**, 6815–6822 (2011).
17. Wagner-Muñiz, D. A., Haughney, S. L., Kelly, S. M., Wannemuehler, M. J. & Narasimhan, B. Room Temperature Stable PspA-Based Nanovaccine Induces Protective Immunity. *Front. Immunol.* **9**, (2018).
18. Huntimer, L. *et al.* Single immunization with a suboptimal antigen dose encapsulated into polyanhydride microparticles promotes high titer and avid antibody responses. *J Biomed Mater Res B Appl Biomater* **101**, 91–98 (2013).
19. Petersen, L. K., Phanse, Y., Ramer-Tait, a. E., Wannemuehler, M. J. & Narasimhan, B. Amphiphilic polyanhydride nanoparticles stabilize bacillus anthracis protective antigen. *Mol. Pharm.* **9**, 874–882 (2012).
20. Kopf, M., Schneider, C. & Nobs, S. P. The development and function of lung-resident macrophages and dendritic cells. *Nat Immunol* **16**, 36–44 (2015).
21. Chiu, C. & Openshaw, P. J. Antiviral B cell and T cell immunity in the lungs. *Nat. Immunol.* **16**, 18–26 (2015).
22. Whitsett, J. A. & Alenghat, T. Respiratory epithelial cells orchestrate pulmonary innate immunity. *Nat. Immunol.* **16**, 27–35 (2015).
23. Burnett, D. Immunoglobulins in the lung. *Thorax* **41**, 337–344 (1986).
24. Hallstrand, T. S. *et al.* Airway epithelial regulation of pulmonary immune homeostasis and inflammation. *Clin. Immunol.* **151**, 1–15 (2014).
25. Moldoveanu, B. *et al.* Inflammatory mechanisms in the lung. *J. Inflamm. Res.* **2**, 1–11 (2009).
26. Riches, D. W. H., Sawyer, R. T., Fenton, M. J. & Martin, T. R. Innate Immunity in the Lungs. *Murray Nadel's Textb. Respir. Med.* **2**, 403–411 (2005).
27. Mildner, A. & Jung, S. Development and function of dendritic cell subsets. *Immunity* **40**, 642–656 (2014).
28. Swiecki, M. & Colonna, M. The multifaceted biology of plasmacytoid dendritic cells. *Nat. Rev. Immunol.* **15**, 471–485 (2015).
29. Stackaruk, M. L., Lee, A. J. & Ashkar, A. A. Type I interferon regulation of natural killer cell function in primary and secondary infections. *Expert Rev. Vaccines* **12**, 875–884 (2013).
30. Epelman, S., Lavine, K. J. & Randolph, G. J. Origin and Functions of Tissue Macrophages. *Immunity* **41**, 21–35 (2014).

31. Jenkins, S. J. & Hume, D. A. Homeostasis in the mononuclear phagocyte system. *Trends Immunol.* **35**, 358–367 (2014).
32. Duque, G. A. & Descoteaux, A. Macrophage cytokines: Involvement in immunity and infectious diseases. *Front. Immunol.* **5**, 1–12 (2014).
33. Ginhoux, F. & Jung, S. Monocytes and macrophages: developmental pathways and tissue homeostasis. *Nat. Rev. Immunol.* **14**, 392–404 (2014).
34. Hussell, T. & Bell, T. J. Alveolar macrophages: Plasticity in a tissue-specific context. *Nat. Rev. Immunol.* **14**, 81–93 (2014).
35. Chen, K. & Kolls, J. K. T Cell–Mediated Host Immune Defenses in the Lung. *Annu. Rev. Immunol.* **31**, 605–633 (2013).
36. Zhang, N. & Bevan, M. J. CD8+ T Cells: Foot Soldiers of the Immune System. *Immunity* **35**, 161–168 (2011).
37. Pennock, N. D. *et al.* T cell responses: naive to memory and everything in between. *AJP Adv. Physiol. Educ.* **37**, 273–283 (2013).
38. Sharpe, A. H. Mechanisms of costimulation. *Immunol. Rev.* **229**, 5–11 (2009).
39. Annunziato, F., Romagnani, C. & Romagnani, S. The 3 major types of innate and adaptive cell-mediated effector immunity. *J. Allergy Clin. Immunol.* **135**, 626–635 (2015).
40. Crotty, S. T Follicular Helper Cell Differentiation, Function, and Roles in Disease. *Immunity* **41**, 529–542 (2014).
41. De Silva, N. S. & Klein, U. Dynamics of B cells in germinal centres. *Nat. Rev. Immunol.* **15**, 137–148 (2015).
42. Nutt, S. L., Hodgkin, P. D., Tarlinton, D. M. & Corcoran, L. M. The generation of antibody-secreting plasma cells. *Nat. Rev. Immunol.* **15**, 160–171 (2015).
43. Heesters, B. A., van der Poel, C. E., Das, A. & Carroll, M. C. Antigen Presentation to B Cells. *Trends Immunol.* **37**, 844–854 (2016).
44. Treanor, B. B-cell receptor: From resting state to activate. *Immunology* **136**, 21–27 (2012).
45. Maul, R. W. & Gearhart, P. J. AID and somatic hypermutation. *Adv. Immunol.* **105**, 159–191 (2010).
46. Kometani, K. & Kurosaki, T. Differentiation and maintenance of long-lived plasma cells. *Curr. Opin. Immunol.* **33**, 64–69 (2015).
47. Stavnezer, J. Antibody Class Switching. *Adv. Immunol.* **61**, 79–146 (1996).
48. McComb, R. C. & Martchenko, M. Neutralizing antibody and functional mapping of *Bacillus anthracis* protective antigen—The first step toward a rationally designed anthrax vaccine. *Vaccine* **34**, 13–19 (2016).

49. Wen, Y., Mu, L. & Shi, Y. Immunoregulatory functions of immune complexes in vaccine and therapy. *EMBO Mol. Med.* **8**, 1120–1133 (2016).
50. Klasse, P. J. Neutralization of Virus Infectivity by Antibodies: Old Problems in New Perspectives. *Adv. Biol.* **2014**, 1–24 (2014).
51. Sarma, J. V. & Ward, P. A. The complement system. *Cell Tissue Res.* **343**, 227–235 (2011).
52. Riedel, S. Plague: From Natural Disease to Bioterrorism. *Baylor Univ. Med. Cent. Proc.* **18**, 116–124 (2005).
53. Plague. (2015). Available at: <https://www.cdc.gov/plague/faq/index.html>. (Accessed: 24th April 2018)
54. Ke, Y., Chen, Z. & Yang, R. Yersinia pestis: mechanisms of entry into and resistance to the host cell. *Front. Cell. Infect. Microbiol.* **3**, (2013).
55. Inglesby, T. V *et al.* Plague as a Biological Weapon. *JAMA* **283**, 2281 (2000).
56. Riedel, S. Biological warfare and bioterrorism: a historical review. *BUMC Proc.* **17**, 400–406 (2004).
57. Li, B. & Yang, R. Interaction between Yersinia pestis and the host immune system. *Infect. Immun.* **76**, 1804–1811 (2008).
58. Heine, H. S. *et al.* Natural history of Yersinia pestis pneumonia in aerosol-challenged BALB/c mice. *Antimicrob. Agents Chemother.* **57**, 2010–2015 (2013).
59. Gonzalez, R. J., Lane, M. C., Wagner, N. J., Weening, E. H. & Miller, V. L. Dissemination of a Highly Virulent Pathogen: Tracking The Early Events That Define Infection. *PLoS Pathog.* **11**, 1–18 (2015).
60. Trosky, J. E., Liverman, A. D. B. & Orth, K. Yersinia outer proteins: Yops. *Cell. Microbiol.* **10**, 557–565 (2008).
61. Journet, L., Agrain, C., Broz, P. & Cornelis, G. R. The Needle Length of Bacterial Injectisomes Is Determined by a Molecular Ruler. *Science (80-.)*. **302**, 1757–1760 (2003).
62. Chatterjee, S., Chaudhury, S., McShan, A. C., Kaur, K. & De Guzman, R. N. Structure and biophysics of type III secretion in bacteria. *Biochemistry* **52**, 2508–2517 (2013).
63. Michiels, T., Wattiau, P., Brasseur, R., Ruyschaert, J. M. & Cornelis, G. Secretion of Yop proteins by Yersiniae. *Infect. Immun.* **58**, 2840–2849 (1990).
64. Debord, K. L. *et al.* Immunogenicity and Protective Immunity against Bubonic Plague and Pneumonic Plague by Immunization of Mice with the Recombinant V10 Antigen, a Variant of LcrV. *Infect. Immun.* **74**, 4910–4914 (2006).
65. Fields, K. A., Nilles, M. L., Cowan, C. & Straley, S. C. Virulence role of V antigen of Yersinia pestis at the bacterial surface. *Infect. Immun.* **67**, 5395–5408 (1999).

66. Torruellas, J., Jackson, M. W., Pennock, J. W. & Plano, G. V. The *Yersinia pestis* type III secretion needle plays a role in the regulation of Yop secretion. *Mol. Microbiol.* **57**, 1719–1733 (2005).
67. LaRock, C. N. & Cookson, B. T. The *Yersinia* Virulence Effector YopM Binds Caspase-1 to Arrest Inflammasome Assembly and Processing. *Cell Host Microbe* **12**, 799–805 (2012).
68. Chung, L. K. *et al.* The *Yersinia* Virulence Factor YopM Hijacks Host Kinases to Inhibit Type III Effector-Triggered Activation of the Pyrin Inflammasome. *Cell Host Microbe* **20**, 296–306 (2016).
69. Spinner, J. L., Hasenkrug, A. M., Shannon, J. G., Kobayashi, S. D. & Hinnebusch, B. J. Role of the *Yersinia* YopJ protein in suppressing interleukin-8 secretion by human polymorphonuclear leukocytes. *Microbes Infect.* **18**, 21–29 (2016).
70. Pechous, R. D., Sivaraman, V., Price, P. A., Stasulli, N. M. & Goldman, W. E. Early Host Cell Targets of *Yersinia pestis* during Primary Pneumonic Plague. *PLoS Pathog.* **9**, (2013).
71. Du, Y. Role of Fraction 1 Antigen of *Yersinia pestis* in Inhibition of Phagocytosis. *Infect. Immun.* **70**, 1453–1460 (2002).
72. Felek, S. & Krukonis, E. S. The *Yersinia pestis* Ail Protein Mediates Binding and Yop Delivery to Host Cells Required for Plague Virulence. *Infect. Immun.* **77**, 825–836 (2009).
73. Sha, J. *et al.* Braun Lipoprotein (Lpp) Contributes to Virulence of *Yersiniae*: Potential Role of Lpp in Inducing Bubonic and Pneumonic Plague. *Infect. Immun.* **76**, 1390–1409 (2008).
74. Zhang, H. *et al.* Bacterial lipoprotein and lipopolysaccharide act synergistically to induce lethal shock and proinflammatory cytokine production. *J Immunol* **159**, 4868–4878 (1997).
75. Park, B. S. & Lee, J. O. Recognition of lipopolysaccharide pattern by TLR4 complexes. *Experimental and Molecular Medicine* **45**, (2013).
76. Miller, S. I., Ernst, R. K. & Bader, M. W. LPS, TLR4 and infectious disease diversity. *Nat. Rev. Microbiol.* **3**, 36–46 (2005).
77. Lathem, W. W., Price, P. A., Miller, V. L. & Goldman, W. E. A plasminogen-activating protease specifically controls the development of primary pneumonic plague. *Science (80-.).* **315**, 509–513 (2007).
78. Zhang, S. *et al.* Plasminogen Activator Pla of *Yersinia pestis* Utilizes Murine DEC-205 (CD205) as a Receptor to Promote Dissemination. *J. Biol. Chem.* **283**, 31511–31521 (2008).
79. Chung, L. K. & Bliska, J. B. *Yersinia* versus host immunity: How a pathogen evades or triggers a protective response. *Curr. Opin. Microbiol.* **29**, 56–62 (2016).

80. McIlwain, D. R., Berger, T. & Mak, T. W. Caspase Functions in Cell Death and Disease. *Cold Spring Harb. Perspect. Biol.* **5**, 1–28 (2013).
81. Eddy, J. L., Gielda, L. M., Caulfield, A. J., Rangel, S. M. & Lathem, W. W. Production of outer membrane vesicles by the plague pathogen *Yersinia pestis*. *PLoS One* **9**, (2014).
82. Feodorova, V. A. & Motin, V. L. Plague vaccines: Current developments and future perspectives. *Emerg. Microbes Infect.* **1**, e36–e36 (2012).
83. Williamson, E. D. *et al.* An IgG1 titre to the F1 and V antigens correlates with protection against plague in the mouse model. *Clin. Exp. Immunol.* **116**, 107–114 (1999).
84. Russell, P. *et al.* A comparison of Plague vaccine, USP and EV76 vaccine induced protection against *Yersinia pestis* in a murine model. **13**, 1551–1556 (1995).
85. Wid, B., Org, H. & Meyer, K. F. Effectiveness of Live or Killed Plague Vaccines in Man. *Bull. Org. mond. Sante* **42**, 653–666 (1970).
86. T.W. Burrows. Virulence of *Pasteurella pestis*. *Nature* **179**, 1246–1247 (1957).
87. T. W. Burrows. An Antigen determining Virulence in *Pasteurella pestis*. *Nature* **177**, 426–427 (1956).
88. Ivanov, M. I., Hill, J. & Bliska, J. B. Direct neutralization of type III effector translocation by the variable region of a monoclonal antibody to *Yersinia pestis* LcrV. *Clin. Vaccine Immunol.* **21**, 667–673 (2014).
89. Noel, B. L., Lilo, S., Capurso, D., Hill, J. & Bliska, J. B. *Yersinia pestis* can bypass protective antibodies to LcrV and activation with gamma interferon to survive and induce apoptosis in murine macrophages. *Clin. Vaccine Immunol.* **16**, 1457–1466 (2009).
90. Overheim, K. A. *et al.* LcrV Plague Vaccine with Altered Immunomodulatory Properties. *Infect. Immun.* **73**, 5152–5159 (2005).
91. Cornelius, C. A. *et al.* Immunization with Recombinant V10 Protects Cynomolgus Macaques from Lethal Pneumonic Plague. *Infect. Immun.* **76**, 5588–5597 (2008).
92. Quenee, L. E., Ciletti, N. A., Elli, D., Hermanas, T. M. & Schneewind, O. Prevention of pneumonic plague in mice, rats, guinea pigs and non-human primates with clinical grade rV10, rV10-2 or F1-V vaccines. *Vaccine* **29**, 6572–6583 (2011).
93. Hill, J. *et al.* Synergistic protection of mice against plague with monoclonal antibodies specific for the F1 and V antigens of *Yersinia pestis*. *Infect. Immun.* **71**, 2234–2238 (2003).
94. Williamson, E. D. *et al.* Recombinant (F1 + V) vaccine protects cynomolgus macaques against pneumonic plague. *Vaccine* **29**, 4771–4777 (2011).

95. Heath, D. G. *et al.* Protection against experimental bubonic and pneumonic plague by a recombinant capsular F1-V antigen fusion protein vaccine. *Vaccine* **16**, 1131–7 (1998).
96. Uddowla, S., Freytag, L. C. & Clements, J. D. Effect of adjuvants and route of immunizations on the immune response to recombinant plague antigens. *Vaccine* **25**, 7984–7993 (2007).
97. Szaba, F. M. *et al.* D27-pLpxL, an Avirulent Strain of *Yersinia pestis*, Primes T Cells That Protect against Pneumonic Plague. *Infect. Immun.* **77**, 4295–4304 (2009).
98. Szaba, F. M. *et al.* TNF α and IFN γ but Not Perforin Are Critical for CD8 T Cell-Mediated Protection against Pulmonary *Yersinia pestis* Infection. *PLoS Pathog.* **10**, 1–12 (2014).
99. Mizel, S. B. *et al.* Flagellin-F1-V fusion protein is an effective plague vaccine in mice and two species of nonhuman primates. *Clin. Vaccine Immunol.* **16**, 21–28 (2009).
100. Honko, A. N. & Mizel, S. B. Effects of Flagellin on Innate and Adaptive Immunity. *Immunol. Res.* **33**, 083–102 (2005).
101. Frey, S. E. *et al.* A phase I safety and immunogenicity dose escalation trial of plague vaccine, Flagellin/F1/V, in healthy adult volunteers (DMID 08-0066). *Vaccine* **35**, 6759–6765 (2017).
102. Moayeri, M., Leppla, S. H., Vrentas, C., Pomerantsev, A. P. & Liu, S. Anthrax Pathogenesis. *Annu. Rev. Microbiol.* **69**, 185–208 (2015).
103. Riedel, S. Anthrax: A Continuing Concern in the Era of Bioterrorism. *Baylor Univ. Med. Cent. Proc.* **18**, 234–243 (2005).
104. Meselson, M. *et al.* The Sverdlovsk Anthrax Outbreak of 1979. *Source Sci. New Ser.* **266**, 1202–1208 (1994).
105. Tasota, F., Henker, R. & Hoffman, L. Anthrax as a Biological Weapon: An Old Disease That Poses a New Threat. *Crit. Care Nurse* **22**, 21–36 (2002).
106. Dragon, D. C. & Rennie, R. P. The ecology of anthrax spores: tough but not invincible. *Canadian Veterinary Journal* **36**, 295–301 (1995).
107. Shafazand, S., Doyle, R., Ruoss, S., Weinacker, A. & Raffin, T. A. Inhalational anthrax: Epidemiology, diagnosis, and management. *Chest* **116**, 1369–1376 (1999).
108. Kamal, S. M., Rashid, A. M., Bakar, M. A. & Ahad, M. A. Anthrax: An update. *Asian Pac. J. Trop. Biomed.* **1**, 496–501 (2011).
109. Abramova, F. a, Grinberg, L. M., Yampolskaya, O. V & Walker, D. H. Pathology of inhalational anthrax in 42 cases from the Sverdlovsk outbreak of 1979. *Proc. Natl. Acad. Sci. U. S. A.* **90**, 2291–2294 (1993).

110. Ross, J. M. The pathogenesis of anthrax following the administration of spores by the respiratory route. *J. Pathol.* **73**, 485–494 (1957).
111. Guidi-Rontani, C. The alveolar macrophage: the Trojan horse of *Bacillus anthracis*. *Trends Microbiol.* **10**, 405–409 (2002).
112. Weiner, Z. P. & Glomski, I. J. Updating perspectives on the initiation of *Bacillus anthracis* growth and dissemination through its host. *Infect. Immun.* **80**, 1626–1633 (2012).
113. Cleret, A. *et al.* Lung Dendritic Cells Rapidly Mediate Anthrax Spore Entry through the Pulmonary Route. *J. Immunol.* **178**, 7994–8001 (2007).
114. Russell, B. H., Vasan, R., Keene, D. R. & Xu, Y. *Bacillus anthracis* internalization by human fibroblasts and epithelial cells. *Cell. Microbiol.* **9**, 1262–1274 (2007).
115. Scobie, H. M., Rainey, G. J. A., Bradley, K. A. & Young, J. A. T. Human capillary morphogenesis protein 2 functions as an anthrax toxin receptor. *Proc. Natl. Acad. Sci.* **100**, 5170–5174 (2003).
116. Bradley, K. A., Mogridge, J., Mourez, M., Collier, R. J. & Young, J. A. T. Identification of the cellular receptor for anthrax toxin. *Nature* **414**, 225–229 (2001).
117. Molloy, S. S., Bresnahan, P. A., Leppla, S. H., Klimpel, K. R. & Thomas, G. Human furin is a calcium-dependent serine endoprotease that recognizes the sequence Arg-X-X-Arg and efficiently cleaves anthrax toxin protective antigen. *J. Biol. Chem.* **267**, 16396–16402 (1992).
118. Arthur, J. S. C. & Ley, S. C. Mitogen-activated protein kinases in innate immunity. *Nat. Rev. Immunol.* **13**, 679–692 (2013).
119. Serezani, C. H., Ballinger, M. N., Aronoff, D. M. & Peters-Golden, M. Cyclic AMP: Master regulator of innate immune cell function. *Am. J. Respir. Cell Mol. Biol.* **39**, 127–132 (2008).
120. Scorpio, A. *et al.* Poly- γ -glutamate capsule-degrading enzyme treatment enhances phagocytosis and killing of encapsulated *Bacillus anthracis*. *Antimicrob. Agents Chemother.* **51**, 215–222 (2007).
121. Gu, C., Jenkins, S. A., Xue, Q. & Xu, Y. Activation of the Classical Complement Pathway by *Bacillus anthracis* Is the Primary Mechanism for Spore Phagocytosis and Involves the Spore Surface Protein BclA. *J. Immunol.* **188**, 4421–4431 (2012).
122. Jang, J. *et al.* Monoclonal antibody against the poly- γ -d-glutamic acid capsule of *Bacillus anthracis* protects mice from enhanced lethal toxin activity due to capsule and anthrax spore challenge. *Biochim. Biophys. Acta - Gen. Subj.* **1830**, 2804–2812 (2013).

123. Chen, Z. *et al.* Pre- and postexposure protection against virulent anthrax infection in mice by humanized monoclonal antibodies to *Bacillus anthracis* capsule. *Proc. Nat. Acad. Sci. USA* **108**, 739–44 (2011).
124. Chen, Z. *et al.* *Bacillus anthracis* capsular conjugates elicit chimpanzee polyclonal antibodies that protect mice from pulmonary anthrax. *Clin. Vaccine Immunol.* **22**, 902–908 (2015).
125. Ahn, H. *et al.* Poly-gamma-glutamic acid from *Bacillus subtilis* upregulates pro-inflammatory cytokines while inhibiting NLRP3, NLRC4 and AIM2 inflammasome activation. *Cell. Mol. Immunol.* **13**, 1–9 (2016).
126. Uchida, I. *et al.* Identification of a novel gene, *dep*, associated with depolymerization of the capsular polymer in *Bacillus anthracis*. *Mol. Microbiol.* **9**, 487–96 (1993).
127. Kozel, T. R. *et al.* mAbs to *Bacillus anthracis* capsular antigen for immunoprotection in anthrax and detection of antigenemia. *Proc. Natl. Acad. Sci.* **101**, 5042–5047 (2004).
128. Gates-Hollingsworth, M. A. *et al.* Immunoassay for capsular antigen of *Bacillus anthracis* enables rapid diagnosis in a rabbit model of inhalational anthrax. *PLoS One* **10**, 1–9 (2015).
129. Sutherland, M. D., Thorkildson, P., Parks, S. D. & Kozel, T. R. In vivo fate and distribution of poly- γ -D-glutamic acid, the capsular antigen from *Bacillus anthracis*. *Infect. Immun.* **76**, 899–906 (2008).
130. Boyer, A. E. *et al.* Kinetics of Lethal Factor and Poly-D-Glutamic Acid Antigenemia during Inhalation Anthrax in Rhesus Macaques. *Infect. Immun.* **77**, 3432–3441 (2009).
131. Jang, J. *et al.* The poly- γ -d-glutamic acid capsule of *Bacillus anthracis* enhances lethal toxin activity. *Infect. Immun.* **79**, 3846–3854 (2011).
132. Cho, M. H. *et al.* *Bacillus anthracis* capsule activates caspase-1 and induces interleukin-1 β release from differentiated THP-1 and human monocyte-derived dendritic cells. *Infect. Immun.* **78**, 387–392 (2010).
133. Weiss, S., Levy, H., Fisher, M., Kober, D. & Altboum, Z. Involvement of TLR2 in innate response to *Bacillus anthracis* infection. *Innate Immun.* **15**, 43–51 (2009).
134. Jeon, J. H. *et al.* The Poly- γ -D-Glutamic acid capsule surrogate of the *Bacillus anthracis* capsule is a novel Toll-Like receptor 2 Agonist. *Infect. Immun.* **83**, 3847–3856 (2015).
135. Lee, K. *et al.* *Bacillus*-derived poly- γ -glutamic acid reciprocally regulates the differentiation of T helper 17 and regulatory T cells and attenuates experimental autoimmune encephalomyelitis. *Clin. Exp. Immunol.* **170**, 66–76 (2012).
136. Jelacic, T. M. *et al.* Exposure to *Bacillus anthracis* capsule results in suppression of human monocyte-derived dendritic cells. *Infect. Immun.* **82**, 3405–3416 (2014).

137. Kim, S. *et al.* Bacillus subtilis-specific poly-gamma-glutamic acid regulates development pathways of naive CD4(+) T cells through antigen-presenting cell-dependent and -independent mechanisms. *Int. Immunol.* **21**, 977–90 (2009).
138. Little, S. F. *et al.* Defining a serological correlate of protection in rabbits for a recombinant anthrax vaccine. *Vaccine* **22**, 422–430 (2004).
139. Chun, J.-H. *et al.* Serological Correlate of Protection in Guinea Pigs for a Recombinant Protective Antigen Anthrax Vaccine Produced from Bacillus brevis. *Osong Public Heal. Res. Perspect.* **3**, 170–176 (2012).
140. Welkos, S. L. & Friedlander, A. M. Comparative safety and efficacy against Bacillus anthracis of protective antigen and live vaccines in mice. *Microb. Pathog.* **5**, 127–139 (1988).
141. Beedham, R. J., Turnbull, P. C. B. & Williamson, E. D. Passive transfer of protection against Bacillus anthracis infection in a murine model. *Vaccine* **19**, 4409–4416 (2001).
142. Rynkiewicz, D. *et al.* Marked enhancement of the immune response to BioThrax® (Anthrax Vaccine Adsorbed) by the TLR9 agonist CPG 7909 in healthy volunteers. *Vaccine* **29**, 6313–6320 (2011).
143. PUZISS, M. & Wright, G. G. STUDIES ON IMMUNITY IN ANTHRAX X. GEL-ADSORBED PROTECTIVE ANTIGEN FOR IMMUNIZATION OF MAN. *J. Bacteriol.* **85**, 230–236 (1962).
144. McBride, B. W. *et al.* Protective efficacy of a recombinant protective antigen against Bacillus anthracis challenge and assessment of immunological markers. *Vaccine* **16**, 810–817 (1998).
145. Ivins, B. E. E. *et al.* Comparative efficacy of experimental anthrax vaccine candidates against inhalation anthrax in rhesus macaques. *Vaccine* **16**, 1141–1148 (1998).
146. Cybulski, R. J., Sanz, P. & O'Brien, A. D. Anthrax vaccination strategies. *Mol. Aspects Med.* **30**, 490–502 (2009).
147. Vergis, J. M. *et al.* Immunization of mice with formalin-inactivated spores from avirulent Bacillus cereus strains provides significant protection from challenge with Bacillus anthracis Ames. *Clin. Vaccine Immunol.* **20**, 56–65 (2013).
148. Welkos, S. L. Plasmid-associated virulence factors of non-toxigenic (pX01-) Bacillus anthracis. *Microb. Pathog.* **10**, 183–198 (1991).
149. Glinert, I. *et al.* Revisiting the concept of targeting only Bacillus anthracis toxins as a treatment for anthrax. *Antimicrob. Agents Chemother.* **60**, 4878–4885 (2016).
150. Rhie, G. E. *et al.* A dually active anthrax vaccine that confers protection against both bacilli and toxins. *Proc. Natl. Acad. Sci. U. S. A.* **100**, 10925–10930 (2003).

151. Chabot, D. J. *et al.* Anthrax capsule vaccine protects against experimental infection. *Vaccine* **23**, 43–47 (2004).
152. Chabot, D. J. *et al.* Protection of rhesus macaques against inhalational anthrax with a *Bacillus anthracis* capsule conjugate vaccine. *Vaccine* **34**, 4012–4016 (2016).
153. Candela, T. *et al.* Cell-wall preparation containing poly- γ -D-glutamate covalently linked to peptidoglycan, a straightforward extractable molecule, protects mice against experimental anthrax infection. *Vaccine* **31**, 171–175 (2012).
154. Crowe, S. R. *et al.* Anthrax vaccination induced anti-lethal factor IgG: Fine specificity and neutralizing capacity. *Vaccine* **29**, 3670–3678 (2011).
155. Dumas, E. K. *et al.* Lethal factor antibodies contribute to lethal toxin neutralization in recipients of anthrax vaccine precipitated. *Vaccine* **35**, 3416–3422 (2017).
156. Ingram, R. J. *et al.* Natural Exposure to Cutaneous Anthrax Gives Long-Lasting T Cell Immunity Encompassing Infection-Specific Epitopes. *J. Immunol.* **184**, 3814–3821 (2010).
157. Baillie, L. W. *et al.* An anthrax subunit vaccine candidate based on protective regions of *Bacillus anthracis* protective antigen and lethal factor. *Vaccine* **28**, 6740–6748 (2010).
158. Castelán-Vega, J., Corvette, L., Sirota, L. & Arciniega, J. Reduction of Immunogenicity of Anthrax Vaccines Subjected to Thermal Stress, as Measured by a Toxin Neutralization Assay. *Clin. Vaccine Immunol.* **18**, 349–351 (2011).
159. Glomski, I. J., Corre, J.-P., Mock, M. & Goossens, P. L. Cutting Edge: IFN- γ -Producing CD4 T Lymphocytes Mediate Spore-Induced Immunity to Capsulated *Bacillus anthracis*. *J. Immunol.* **178**, 2646–2650 (2007).
160. Ingram, R. J. *et al.* Natural cutaneous anthrax infection, but not vaccination, induces a CD4⁺ T cell response involving diverse cytokines. *Cell Biosci.* **5**, 1–6 (2015).
161. Sacco, R. E., Durbin, R. K. & Durbin, J. E. Animal models of respiratory syncytial virus infection and disease. *Curr. Opin. Virol.* **13**, 117–122 (2015).
162. Theurer, M. E., Larson, R. L. & White, B. J. Systematic review and meta-analysis of the effectiveness of commercially available vaccines against bovine herpesvirus, bovine viral diarrhea virus, bovine respiratory syncytial virus, and parainfluenza type 3 virus for mitigation of bovine respiratory di. *J. Am. Vet. Med. Assoc.* **246**, 126–142 (2015).
163. Ellis, J. A. How efficacious are vaccines against bovine respiratory syncytial virus in cattle? *Vet. Microbiol.* **206**, 59–68 (2017).
164. Valarcher, J.-F. & Taylor, G. Bovine respiratory syncytial virus infection. *Vet. Res.* **38**, 153–180 (2007).

165. Wegzyn, C. *et al.* Safety and Effectiveness of Palivizumab in Children at High Risk of Serious Disease Due to Respiratory Syncytial Virus Infection: A Systematic Review. *Infect. Dis. Ther.* **3**, 133–158 (2014).
166. Zhang, L., Peeples, M. E., Boucher, R. C., Collins, P. L. & Pickles, R. J. Respiratory Syncytial Virus Infection of Human Airway Epithelial Cells Is Polarized, Specific to Ciliated Cells, and without Obvious Cytopathology. *J. Virol.* **76**, 5654–5666 (2002).
167. Meyer, G., Deplanche, M. & Schelcher, F. Human and bovine respiratory syncytial virus vaccine research and development. *Comp. Immunol. Microbiol. Infect. Dis.* **31**, 191–225 (2008).
168. Zhang, B. *et al.* Protection of calves by a prefusion-stabilized bovine RSV F vaccine. *npj Vaccines* **2**, 7 (2017).
169. Krarup, A. *et al.* A highly stable prefusion RSV F vaccine derived from structural analysis of the fusion mechanism. *Nat. Commun.* **6**, 8143 (2015).
170. Fishburne Wright, E., Chanock, R. M., John Mills, I. V & Van Kirk, J. E. Experimental Respiratory Syncytial Virus Infection of Adults. *J. Immunol.* **107**, 123–130 (1971).
171. Habibi, M. S. *et al.* Impaired antibody-mediated protection and defective iga b-cell memory in experimental infection of adults with respiratory syncytial virus. *Am. J. Respir. Crit. Care Med.* **191**, 1040–1049 (2015).
172. Tsutsumi, H., Matsuda, K., Yamazaki, H., Ogra, P. L. & Chiba, S. Different kinetics of antibody responses between IgA and IgG classes in nasopharyngeal secretion in infants and children during primary respiratory syncytial virus infection. *Pediatr. Int.* **37**, 464–468 (1995).
173. Chu, H. Y. *et al.* Respiratory Syncytial Virus Transplacental Antibody Transfer and Kinetics in Mother-Infant Pairs in Bangladesh. *J. Infect. Dis.* **210**, 1582–1589 (2014).
174. Glezen, W. P., Paredes, A., Allison, J. E., Taber, L. H. & Frank, A. L. Risk of respiratory syncytial virus infection for infants from low-income families in relationship to age, sex, ethnic group, and maternal antibody level. *J. Pediatr.* **98**, 708–715 (1981).
175. Stensballe, L. G. *et al.* Respiratory syncytial virus neutralizing antibodies in cord blood, respiratory syncytial virus hospitalization, and recurrent wheeze. *J. Allergy Clin. Immunol.* **123**, 398–403 (2009).
176. Jans, J. *et al.* Characteristics of RSV-Specific Maternal Antibodies in Plasma of Hospitalized, Acute RSV Patients under Three Months of Age. *PLoS One* **12**, 1–16 (2017).
177. Yamazaki, H. *et al.* Effect of maternal antibody on IgA antibody response in nasopharyngeal secretion in infants and children during primary respiratory syncytial virus infection. *J. Gen. Virol.* **75**, 2115–2119 (1994).

178. Kimman, T. G., Zimmer, G. M., Westenbrink, F., Mars, J. & van Leeuwen, E. Epidemiological study of bovine respiratory syncytial virus infections in calves: influence of maternal antibodies on the outcome of disease. *Vet. Rec.* **123**, 104–109 (1988).
179. Freitas, G. R. O. R. O. *et al.* Antibody response and avidity of respiratory syncytial virus-specific total IgG, IgG1, and IgG3 in young children. *J. Med. Virol.* **83**, 1826–1833 (2011).
180. Ngwuta, J. O. *et al.* Prefusion F-specific antibodies determine the magnitude of RSV neutralizing activity in human sera HHS Public Access. *Sci Transl Med* **7**, 309–162 (2015).
181. Liang, B. *et al.* Enhanced Neutralizing Antibody Response Induced by Respiratory Syncytial Virus Prefusion F Protein Expressed by a Vaccine Candidate. *J. Virol.* **89**, 9499–9510 (2015).
182. McLellan, J. S. *et al.* Structure-Based Design of a Fusion Glycoprotein Vaccine for Respiratory Syncytial Virus. *Science* (80-.). **342**, 592–598 (2013).
183. Stewart-Jones, G. B. E. *et al.* A Cysteine Zipper Stabilizes a Pre-Fusion F Glycoprotein Vaccine for Respiratory Syncytial Virus. *PLoS One* **10**, e0128779 (2015).
184. McLellan, J. S., Yang, Y., Graham, B. S. & Kwong, P. D. Structure of Respiratory Syncytial Virus Fusion Glycoprotein in the Postfusion Conformation Reveals Preservation of Neutralizing Epitopes. *J. Virol.* **85**, 7788–7796 (2011).
185. Raghunandan, R. *et al.* An insect cell derived respiratory syncytial virus (RSV) F nanoparticle vaccine induces antigenic site II antibodies and protects against RSV challenge in cotton rats by active and passive immunization. *Vaccine* **32**, 6485–6492 (2014).
186. Swanson, K. A. *et al.* Structural basis for immunization with postfusion respiratory syncytial virus fusion F glycoprotein (RSV F) to elicit high neutralizing antibody titers. *Proc. Natl. Acad. Sci.* **108**, 9619–9624 (2011).
187. Jorquera, P. A. *et al.* Nanoparticle Vaccines Encompassing the Respiratory Syncytial Virus (RSV) G Protein CX3C Chemokine Motif Induce Robust Immunity Protecting from Challenge and Disease. *PLoS One* **8**, e74905 (2013).
188. Bastien, N. *et al.* Immunization with a peptide derived from the G glycoprotein of bovine respiratory syncytial virus (BRSV) reduces the incidence of BRSV-associated pneumonia in the natural host. *Vaccine* **15**, 1385–1390 (1997).
189. Taylor, G. *et al.* Efficacy of a virus-vectored vaccine against human and bovine respiratory syncytial virus infections. *Sci. Transl. Med.* **7**, 300ra127 (2015).
190. Taylor, G. *et al.* Recombinant vaccinia viruses expressing the F, G or N, but not the M2, protein of bovine respiratory syncytial virus (BRSV) induce resistance to BRSV challenge in the calf and protect against the development of pneumonic lesions. *J. Gen. Virol.* **78**, 3195–3206 (1997).

191. Wyld, S. G. *et al.* Resistance to bovine respiratory syncytial virus (BRSV) induced in calves by a recombinant bovine herpesvirus-1 expressing the attachment glycoprotein of BRSV. *J. Gen. Virol.* **79**, 1759–1767 (1998).
192. Schrijver, R. S. *et al.* Immunization of cattle with a BHV1 vector vaccine or a DNA vaccine both coding for the G protein of BRSV. *Vaccine* **15**, 1908–1916 (1997).
193. Schrijver, R. S. *et al.* Comparison of DNA application methods to reduce BRSV shedding in cattle. *Vaccine* **16**, 130–134 (1998).
194. Brito, L. A. & O'Hagan, D. T. Designing and building the next generation of improved vaccine adjuvants. *J. Control. Release* **190**, 563–579 (2014).
195. Glenny ATCGP, Waddington H, W. U. Immunological notes. XVII–XXIV. *J Pathol Bacteriol* **29**, 31–40 (1926).
196. Theresa M. Allena, P. R. C. Liposomal drug delivery systems: From concept to clinical applications. *Adv. Drug Deliv. Rev.* **65**, 36–48 (2013).
197. Danhier, F. *et al.* PLGA-based nanoparticles: an overview of biomedical applications. *J. Control. Release* **161**, 505–22 (2012).
198. Casella, C. R. & Mitchell, T. C. Putting endotoxin to work for us: Monophosphoryl lipid A as a safe and effective vaccine adjuvant. *Cell. Mol. Life Sci.* **65**, 3231–3240 (2008).
199. Hutchison, S., Benson, R. A. & Brewer, J. M. Antigen depot is not required for alum adjuvant activity. 22–29 (2016).
200. HogenEsch, H. Mechanisms of stimulation of the immune response by aluminum adjuvants. *Vaccine* **20**, 34–39 (2002).
201. Wen, Y. & Shi, Y. Alum: an old dog with new tricks. *Emerg. Microbes Infect.* **5**, e25 (2016).
202. Bygd, H. C., Forsmark, K. D. & Bratlie, K. M. Altering in vivo macrophage responses with modified polymer properties. *Biomaterials* **56**, 187–197 (2015).
203. Kou, P. M. *et al.* Predicting biomaterial property-dendritic cell phenotype relationships from the multivariate analysis of responses to polymethacrylates. *Biomaterials* **33**, 1699–1713 (2012).
204. Haughney, S. L., Ross, K. A., Boggiatto, P. M., Wannemuehler, M. J. & Narasimhan, B. Effect of nanovaccine chemistry on humoral immune response kinetics and maturation. *Nanoscale* **6**, 13770–13778 (2014).
205. McGill, J. L. *et al.* Efficacy of mucosal polyanhydride nanovaccine against respiratory syncytial virus infection in the neonatal calf. *Sci. Rep.* **8**, 1–15 (2018).
206. Kipper, M. J., Shen, E., Determan, A. & Narasimhan, B. Design of an injectable system based on bioerodible polyanhydride microspheres for sustained drug delivery. *Biomaterials* **23**, 4405–4412 (2002).

207. Grun, J. L. & Maurer, P. H. Different T Helper Cell Subsets Elicited in Mice Utilizing Two Different Adjuvant Vehicles: The Role of Endogenous Interleukin 1 in Proliferative Responses. *Cell. Immunol.* **121**, 134–145 (1989).
208. Griesenauer, R. H. & Kinch, M. S. An overview of FDA-approved vaccines & their innovators. *Expert Rev. Vaccines* **16**, 1253–1266 (2017).
209. Didierlaurent, A. M. *et al.* Adjuvant system AS01: helping to overcome the challenges of modern vaccines. *Expert Rev. Vaccines* **16**, 55–63 (2017).
210. Jenal, U., Reinders, A. & Lori, C. Cyclic di-GMP: Second messenger extraordinaire. *Nat. Rev. Microbiol.* **15**, 271–284 (2017).
211. Danilchanka, O. & Mekalanos, J. J. Cyclic dinucleotides and the innate immune response. *Cell* **154**, 962–70 (2013).
212. Ishikawa, H. & Barber, G. N. STING is an endoplasmic reticulum adaptor that facilitates innate immune signalling. *Nature* **455**, 674–678 (2008).
213. Karaolis, D. K. R. *et al.* Bacterial c-di-GMP is an immunostimulatory molecule. *J. Immunol.* **178**, 2171–2181 (2007).
214. Karaolis, D. K. R. *et al.* Cyclic Di-GMP Stimulates Protective Innate Immunity in Bacterial Pneumonia. *Infect. Immun.* **75**, 4942–4950 (2007).
215. Ebensen, T. *et al.* The bacterial second messenger cyclic diGMP exhibits potent adjuvant properties. *Vaccine* **25**, 1464–1469 (2007).
216. Hu, D.-L. *et al.* c-di-GMP as a vaccine adjuvant enhances protection against systemic methicillin-resistant *Staphylococcus aureus* (MRSA) infection. *Vaccine* **27**, 4867–4873 (2009).
217. Ross, K. *et al.* Combination Nanovaccine Demonstrates Synergistic Enhancement in Efficacy against Influenza. *ACS Biomater. Sci. Eng.* **2**, 368–374 (2016).
218. Carrillo-Conde, B. R. *et al.* Sustained release and stabilization of therapeutic antibodies using amphiphilic polyanhydride nanoparticles. *Chem. Eng. Sci.* **125**, 98–107 (2015).
219. Haughney, S. L. *et al.* Retention of structure, antigenicity, and biological function of pneumococcal surface protein A (PspA) released from polyanhydride nanoparticles. *Acta Biomater.* **9**, 8262–8271 (2013).
220. Carrillo-Conde, B. *et al.* Encapsulation into amphiphilic polyanhydride microparticles stabilizes *Yersinia pestis* antigens. *Acta Biomater.* **6**, 3110–3119 (2010).
221. Lopac, S. K., Torres, M. P., Wilson-Welder, J. H., Wannemuehler, M. J. & Narasimhan, B. Effect of polymer chemistry and fabrication method on protein release and stability from polyanhydride microspheres. *J. Biomed. Mater. Res. B. Appl. Biomater.* **91**, 938–47 (2009).

222. Goodman, J. T. *et al.* Nanoparticle chemistry and functionalization differentially regulates dendritic cell-nanoparticle interactions and triggers dendritic cell maturation. *Part. Part. Syst. Charact.* **31**, 1269–1280 (2014).
223. Phanse, Y. *et al.* Functionalization of polyanhydride microparticles with di-mannose influences uptake by and intracellular fate within dendritic cells. *Acta Biomater.* **9**, 8902–8909 (2013).
224. Brenza, T. M. *et al.* Pulmonary Biodistribution and Cellular Uptake of Intranasally Administered Monodisperse Particles. *Pharm. Res.* **32**, 1368–1382 (2015).
225. Gamvrellis, A. *et al.* Vaccines that facilitate antigen entry into dendritic cells. *Immunol. Cell Biol.* **82**, 506–516 (2004).
226. Foged, C., Brodin, B., Frokjaer, S. & Sundblad, A. Particle size and surface charge affect particle uptake by human dendritic cells in an in vitro model. *Int. J. Pharm.* **298**, 315–322 (2005).
227. Silva, A. L. *et al.* Poly-(lactic-co-glycolic-acid)-based particulate vaccines: Particle uptake by dendritic cells is a key parameter for immune activation. *Vaccine* **33**, 847–854 (2015).
228. Champion, J. J. A., Walker, A. & Mitragotri, S. Role of particle size in phagocytosis of polymeric microspheres. *Pharm. Res.* **25**, 1815–1821 (2008).
229. Champion, J. a & Mitragotri, S. Role of target geometry in phagocytosis. *Proc. Natl. Acad. Sci. U. S. A.* **103**, 4930–4934 (2006).
230. Berkland, C., Kipper, M. J., Narasimhan, B., Kim, K. & Pack, D. W. Microsphere size, precipitation kinetics and drug distribution control drug release from biodegradable polyanhydride microspheres. *J. Control. Release* **94**, 129–141 (2004).
231. Kamaly, N., Yameen, B., Wu, J. & Farokhzad, O. C. Degradable Controlled-Release Polymers and Polymeric Nanoparticles: Mechanisms of Controlling Drug Release. *Chem. Rev.* **116**, 2602–2663 (2016).
232. Torres, M. P., Vogel, B. M., Narasimhan, B. & Mallapragada, S. K. Synthesis and characterization of novel polyanhydrides with tailored erosion mechanisms. *J. Biomed. Mater. Res. - Part A* **76**, 102–110 (2006).
233. Ulery, B. D., Nair, L. S. & Laurencin, C. T. Biomedical applications of biodegradable polymers. *J. Polym. Sci. Part B Polym. Phys.* **49**, 832–864 (2011).
234. Pan, Z. & Ding, J. Poly(lactide- co -glycolide) porous scaffolds for tissue engineering and regenerative medicine. *Interface Focus* **2**, 366–377 (2012).
235. Danhier, F. *et al.* PLGA-based nanoparticles: An overview of biomedical applications. *J. Control. Release* **161**, 505–522 (2012).
236. Sharma, S., Parmar, A., Kori, S. & Sandhir, R. PLGA-based nanoparticles: A new paradigm in biomedical applications. *Trends Anal. Chem.* **80**, 30–40 (2015).

237. Makadia, H. K. & Siegel, S. J. Poly Lactic-co-Glycolic Acid (PLGA) as Biodegradable Controlled Drug Delivery Carrier. *Polymers (Basel)*. **3**, 1377–1397 (2011).
238. Semete, B. *et al.* In vivo evaluation of the biodistribution and safety of PLGA nanoparticles as drug delivery systems. *Nanomedicine Nanotechnology, Biol. Med.* **6**, 662–671 (2010).
239. Middleton, J. C. & Tipton, A. J. Synthetic biodegradable polymers as orthopedic devices. *Biomaterials* **21**, 2335–2346 (2000).
240. Gregory, A. E., Titball, R. & Williamson, D. Vaccine delivery using nanoparticles. *Front. Cell. Infect. Microbiol.* **3**, (2013).
241. Silva, A. L. *et al.* Poly-(lactic-co-glycolic-acid)-based particulate vaccines: Particle uptake by dendritic cells is a key parameter for immune activation. *Vaccine* **33**, 847–854 (2015).
242. Chasin, M., Lewis, D. & Langer, R. Polyanhydrides for controlled drug delivery. *Biopharm Manufact* **1**, 33–46 (1983).
243. Kumar, N., Langer, R. S. & Domb, A. J. Polyanhydrides: an overview. *Adv. Drug Deliv. Rev.* **54**, 889–910 (2002).
244. Tabata, Y., Gutta, S. & Langer, R. Controlled Delivery Systems for Proteins Using Polyanhydride Microspheres. *Pharm. Res.* **10**, 487–496 (1993).
245. Katti, D. S., Lakshmi, S., Langer, R. & Laurencin, C. T. Toxicity, biodegradation and elimination of polyanhydrides. *Adv. Drug Deliv. Rev.* **54**, 933–961 (2002).
246. Bucher, J. & Slade, W. C. The Anhydrides of Isophthalic and Terephthalic acids. *J. Am. Chem. Soc.* **31**, 1319–1321 (1909).
247. Conix, A. Aromatic polyanhydrides, a new class of high melting fibre-forming polymers. *J. Polym. Sci.* **29**, 343–353 (1958).
248. Rosen, H. B., Chang, J., Wnek, G. E., Linhardt, R. J. & Langer, R. Bioerodible polyanhydrides for controlled drug delivery. *Biomaterials* **4**, 131–133 (1983).
249. Li, X., Petersen, L., Broderick, S., Narasimhan, B. & Rajan, K. Identifying Factors Controlling Protein Release from Combinatorial Biomaterial Libraries via Hybrid Data Mining Methods. *ACS Comb. Sci.* **13**, 50–58 (2011).
250. Vela-Ramirez, J. E. *et al.* Safety and Biocompatibility of Carbohydrate-Functionalized Polyanhydride Nanoparticles. *AAPS J.* **17**, 256–267 (2015).
251. Adler, A. F. *et al.* High throughput cell-based screening of biodegradable polyanhydride libraries. *Comb. Chem. High Throughput Screen.* **12**, 634–45 (2009).
252. Vela Ramirez, J. E. *et al.* Polyanhydride Nanovaccines Induce Germinal Center B Cell Formation and Sustained Serum Antibody Responses. *J. Biomed. Nanotechnol.* **12**, 1303–1311 (2016).

253. Torres, M. P. *et al.* Polyanhydride microparticles enhance dendritic cell antigen presentation and activation. *Acta Biomater.* **7**, 2857–2864 (2011).
254. Petersen, L. K., Xue, L., Wannemuehler, M. J., Rajan, K. & Narasimhan, B. The simultaneous effect of polymer chemistry and device geometry on the in vitro activation of murine dendritic cells. *Biomaterials* **30**, 5131–5142 (2009).
255. Kipper, M. J., Wilson, J. H., Wannemuehler, M. J. & Narasimhan, B. Single dose vaccine based on biodegradable polyanhydride microspheres can modulate immune response mechanism. *J. Biomed. Mater. Res. - Part A* **76**, 798–810 (2006).
256. Ulery, B. D. *et al.* Polymer chemistry influences monocytic uptake of polyanhydride nanospheres. *Pharm. Res.* **26**, 683–690 (2009).
257. Carrillo-Conde, B. R., Ramer-Tait, A. E., Wannemuehler, M. J. & Narasimhan, B. Chemistry-dependent adsorption of serum proteins onto polyanhydride microparticles differentially influences dendritic cell uptake and activation. *Acta Biomater.* **8**, 3618–28 (2012).
258. Chavez-Santoscoy, A. V. *et al.* Tailoring the immune response by targeting C-type lectin receptors on alveolar macrophages using “pathogen-like” amphiphilic polyanhydride nanoparticles. *Biomaterials* **33**, 4762–4772 (2012).
259. Carrillo-Conde, B. *et al.* Mannose-functionalized ‘pathogen-like’ polyanhydride nanoparticles target C-type lectin receptors on dendritic cells. *Mol. Pharm.* **8**, 1877–1886 (2011).
260. J. Raghuvanshi G. P. Talwar, R. J. Levy, V. Labhasetwar, R., A. M. Enhanced immune response with a combination of alum and biodegradable nanoparticles containing tetanus toxoid. *J. Microencapsul.* **18**, 723–732 (2001).
261. Jiang, W. & Schwendeman, S. P. Stabilization of Tetanus Toxoid Encapsulated in PLGA Microspheres. *Mol. Pharm.* **5**, 808–817 (2008).
262. Cleland, J. L. Single-administration vaccines: controlled-release technology to mimic repeated immunizations. *Trends Biotechnol.* **17**, 25–29 (1999).
263. Kholodovych, V. *et al.* Prediction of biological response for large combinatorial libraries of biodegradable polymers: Polymethacrylates as a test case. *Polymer (Guildf)*. **49**, 2435–2439 (2008).
264. Kohn, J., Welsh, W. J. & Knight, D. A new approach to the rationale discovery of polymeric biomaterials. *Biomaterials* **28**, 4171–4177 (2007).
265. Adams, J. R., Haughney, S. L. & Mallapragada, S. K. Acta Biomaterialia Effective polymer adjuvants for sustained delivery of protein subunit vaccines. *Acta Biomater.* **14**, 104–114 (2015).
266. Bobbala, S., Tamboli, V., McDowell, A., Mitra, A. K. & Hook, S. Novel Injectable Pentablock Copolymer Based Thermoresponsive Hydrogels for Sustained Release Vaccines. *AAPS J.* **18**, 261–9 (2016).

267. Adams, J. R., Goswami, M., Pohl, N. L. B. & Mallapragada, S. K. Synthesis and functionalization of virus-mimicking cationic block copolymers with pathogen-Associated carbohydrates as potential vaccine adjuvants. *RSC Adv.* **4**, 15655–15663 (2014).
268. Andrianov, A. K., Marin, A. & Chen, J. Synthesis, Properties, and Biological Activity of Poly[di(sodium carboxylatoethylphenoxy)phosphazene]. *Biomacromolecules* **7**, 394–399 (2006).
269. Andrianov, A. K., Svirkin, Y. Y. & LeGolian, M. P. Synthesis and biologically relevant properties of polyphosphazene polyacids. *Biomacromolecules* **5**, 1999–2006 (2004).
270. Lyu, S. & Untereker, D. Degradability of Polymers for Implantable Biomedical Devices. *Int. J. Mol. Sci.* **10**, 4033–4065 (2009).
271. Wong, D. Y., Hollister, S. J., Krebsbach, P. H. & Nosrat, C. Poly(ϵ -Caprolactone) and Poly (L-Lactic-Co-Glycolic Acid) Degradable Polymer Sponges Attenuate Astrocyte Response and Lesion Growth in Acute Traumatic Brain Injury. *Tissue Eng.* **13**, 2515–2523 (2007).
272. Zolnik, B. S. & Burgess, D. J. Effect of acidic pH on PLGA microsphere degradation and release. *J. Control. Release* **122**, 338–344 (2007).
273. Kipper, M. J. & Narasimhan, B. Molecular Description of Erosion Phenomena in Biodegradable Polymers. *Macromolecules* **38**, 1989–1999 (2005).
274. Ke, Y., Chen, Z. & Yang, R. *Yersinia pestis*: mechanisms of entry into and resistance to the host cell. *Front. Cell. Infect. Microbiol.* **3**, (2013).
275. Hill, J., Leary, S. E. C., Griffin, K. F., Williamson, E. D. & Titball, R. W. Regions of *Yersinia pestis* V antigen that contribute to protection against plague identified by passive and active immunization. *Infect. Immun.* **65**, 4476–82 (1997).
276. Xiao, X. *et al.* Human anti-plague monoclonal antibodies protect mice from *Yersinia pestis* in a bubonic plague model. *PLoS One* **5**, 1–12 (2010).
277. Goodin, J. L. *et al.* Purification and protective efficacy of monomeric and modified *Yersinia pestis* capsular F1-V antigen fusion proteins for vaccination against plague. *Protein Expr. Purif.* **53**, 63–79 (2007).
278. Powell, B. S. *et al.* Design and testing for a nontagged F1-V fusion protein as vaccine antigen against bubonic and pneumonic plague. *Biotechnol. Prog.* **21**, 1490–1510 (2005).
279. Ma, Z. & Damania, B. The cGAS-STING Defense Pathway and Its Counteraction by Viruses. *Cell Host Microbe* **19**, 150–158 (2016).
280. Narasimhan, B., Goodman, J. T. & Vela Ramirez, J. E. Rational Design of Targeted Next-Generation Carriers for Drug and Vaccine Delivery. **18**, 25–49 (2016).

281. Vela Ramirez, J. E. *et al.* Carbohydrate-functionalized nanovaccines preserve HIV-1 antigen stability and activate antigen presenting cells. *J. Biomater. Sci. Polym. Ed.* **25**, 1387–1406 (2014).
282. Tao, P. *et al.* A Bivalent Anthrax–Plague Vaccine That Can Protect against Two Tier-1 Bioterror Pathogens, *Bacillus anthracis* and *Yersinia pestis*. *Front. Immunol.* **8**, (2017).
283. Williamson, E. D. *et al.* A single dose sub-unit vaccine protects against pneumonic plague. *Vaccine* **19**, 566–571 (2000).
284. Williamson, E. D. *et al.* Kinetics of the immune response to the (F1 + V) vaccine in models of bubonic and pneumonic plague. *Vaccine* **25**, 1142–1148 (2007).
285. Anderson, G. W., Heath, D. G., Bolt, C. R., Welkos, S. L. & Friedlander, A. M. Short- and long-term efficacy of single-dose subunit vaccines against *Yersinia pestis* in mice. *Am. J. Trop. Med. Hyg.* **58**, 793–799 (1998).
286. Parent, M. A. *et al.* Cell-Mediated Protection against Pulmonary *Yersinia pestis* Infection. *Infect. Immun.* **73**, 7304–7310 (2005).
287. Lin, J. S. *et al.* TNF α and IFN γ contribute to F1/LcrV-targeted immune defense in mouse models of fully virulent pneumonic plague. *Vaccine* **29**, 357–362 (2010).
288. Huntimer, L. M. *et al.* Polyanhydride nanovaccine platform enhances antigen-specific cytotoxic T cell responses. *TECHNOLOGY* **2**, 171–175 (2014).
289. Li, B. *et al.* Humoral and cellular immune responses to *Yersinia pestis* infection in long-term recovered plague patients. *Clin. Vaccine Immunol.* **19**, 228–234 (2012).
290. Reed, D. S. & Martinez, M. J. Respiratory immunity is an important component of protection elicited by subunit vaccination against pneumonic plague. *Vaccine* **24**, 2283–2289 (2006).
291. Hill, J. *et al.* Administration of antibody to the lung protects mice against pneumonic plague. *Infect. Immun.* **74**, 3068–70 (2006).
292. Glynn, A., Freytag, L. C. & Clements, J. D. Effect of homologous and heterologous prime-boost on the immune response to recombinant plague antigens. *Vaccine* **23**, 1957–1965 (2005).
293. Blaauboer, S. M. *et al.* The mucosal adjuvant cyclic di-GMP enhances antigen uptake and selectively activates pinocytosis-efficient cells in vivo. *Elife* **2015**, 1–25 (2015).
294. Quenee, L. E. *et al.* Amino acid residues 196–225 of LcrV represent a plague protective epitope. *Vaccine* **28**, 1870–1876 (2010).
295. Khan, A. A., Babu, J. P., Gupta, G. & Rao, D. N. Identifying B and T cell epitopes and studying humoral, mucosal and cellular immune responses of peptides derived from V antigen of *Yersinia pestis*. *Vaccine* **26**, 316–332 (2008).

296. Determan, A. S., Graham, J. R., Pfeiffer, K. a & Narasimhan, B. The role of microsphere fabrication methods on the stability and release kinetics of ovalbumin encapsulated in polyanhydride microspheres. *J. Microencapsul.* **23**, 832–43 (2006).
297. Ross, K. A. *et al.* Hemagglutinin-based polyanhydride nanovaccines against H5N1 influenza elicit protective virus neutralizing titers and cell-mediated immunity. *Int. J. Nanomedicine* **10**, 229–243 (2015).
298. Ngundi, M. M., Meade, B. D., Lin, T. L., Tang, W. J. & Burns, D. L. Comparison of three anthrax toxin neutralization assays. *Clin. Vaccine Immunol.* **17**, 895–903 (2010).
299. Hering, D. *et al.* Validation of the anthrax lethal toxin neutralization assay. *Biologicals* **32**, 17–27 (2004).
300. World Health Organization. Health aspects of Chemical and Biological and Weapons: report of a group of consultants. (1970).
301. Brachman, P. S. INHALATION ANTHRAX. *Ann. N. Y. Acad. Sci.* **353**, 83–93 (1980).
302. Adalja, A. A., Toner, E. & Inglesby, T. V. Clinical Management of Potential Bioterrorism-Related Conditions. *N. Engl. J. Med.* **372**, 954–962 (2015).
303. Friedlander, A. M. *et al.* Postexposure Prophylaxis against Experimental Inhalation Anthrax. *J. Infect. Dis.* **167**, 1239–1242 (1993).
304. Bouzianas, D. G. Medical countermeasures to protect humans from anthrax bioterrorism. *Trends Microbiol.* **17**, 522–528 (2009).
305. Shepard, C. W. *et al.* Antimicrobial Postexposure Prophylaxis for Anthrax: Adverse Events and Adherence. *Emerg. Infect. Dis.* **8**, 1124–1132 (2002).
306. Malkevich, N. V *et al.* Efficacy and Safety of AVP-21D9, an Anthrax Monoclonal Antibody, in Animal Models and Humans. *Antimicrob. Agents Chemother.* **58**, 3618–3625 (2014).
307. Rivera, J. *et al.* A Monoclonal Antibody to Bacillus anthracis Protective Antigen Defines a Neutralizing Epitope in Domain 1. *Infect. Immun.* **74**, 4149–4156 (2006).
308. Martin, |, Weiss, M., Weiss, P. D. & Weiss, J. B. Anthrax Vaccine and Public Health Policy. *Am. J. Public Health* **97**, (2007).
309. Fowler, R. A. *et al.* Cost-Effectiveness of Defending against Bioterrorism: A Comparison of Vaccination and Antibiotic Prophylaxis against Anthrax. *Ann. Intern. Med.* **142**, 601 (2005).
310. Oscherwitz, J., Quinn, C. P. & Cease, K. B. Anthrax vaccine recipients lack antibody against the loop neutralizing determinant: A protective neutralizing epitope from Bacillus anthracis protective antigen. *Vaccine* **33**, 2342–2346 (2015).

311. Chi, X. *et al.* Generation and Characterization of Human Monoclonal Antibodies Targeting Anthrax Protective Antigen following Vaccination with a Recombinant Protective Antigen Vaccine. *Clin. Vaccine Immunol.* **22**, 553–560 (2015).
312. Reason, D., Liberato, J., Sun, J., Keitel, W. & Zhou, J. Frequency and Domain Specificity of Toxin-Neutralizing Paratopes in the Human Antibody Response to Anthrax Vaccine Adsorbed. *Infect. Immun.* **77**, 2030–2035 (2009).
313. Reason, D. C. *et al.* Domain specificity of the human antibody response to *Bacillus anthracis* protective antigen. *Vaccine* **26**, 4041–4047 (2008).
314. D'Souza, A. J. M. *et al.* Rapid Deamidation of Recombinant Protective Antigen when Adsorbed on Aluminum Hydroxide Gel Correlates with Reduced Potency of Vaccine. *J. Pharm. Sci.* **102**, 454–461 (2013).
315. Wagner, L. *et al.* Structural and Immunological Analysis of Anthrax Recombinant Protective Antigen Adsorbed to Aluminum Hydroxide Adjuvant. *Clin. Vaccine Immunol.* **19**, 1465–1473 (2012).
316. Nair, H. *et al.* Global burden of acute lower respiratory infections due to respiratory syncytial virus in young children: a systematic review and meta-analysis. *Lancet* **376**, 1074–1084 (2010).
317. Taylor, G. *et al.* Efficacy of a virus-vectored vaccine against human and bovine respiratory syncytial virus infections. *Sci. Transl. Med.* **7**, 300ra127 (2015).
318. Taylor, G. *et al.* Resistance to bovine respiratory syncytial virus (BRSV) induced in calves by a recombinant bovine herpesvirus-1 expressing the attachment glycoprotein of BRSV. *J. Gen. Virol.* **79**, 1759–1767 (1998).
319. Ross, K. A. *et al.* Lung Deposition and Cellular Uptake Behavior of Pathogen-Mimicking Nanovaccines in the First 48 Hours. *Adv. Healthc. Mater.* **3**, 1071–1077 (2014).
320. Vela Ramirez, J. E. *et al.* Polyanhydride Nanovaccines Induce Germinal Center B Cell Formation and Sustained Serum Antibody Responses. *J. Biomed. Nanotechnol.* **12**, 1303–1311 (2016).
321. Dhakal, S. *et al.* Polyanhydride nanovaccine against swine influenza virus in pigs. *Vaccine* **35**, 1124–1131 (2017).
322. Himes, S. R. & Gershwin, L. J. Bovine respiratory syncytial virus fusion protein gene : sequence analysis of cDNA and expression using a baculovirus vector. *J. Gen. Virol.* **73**, 1563–1567 (1992).
323. Wathen, M. W., Brideau, R. J. & Thomsen, D. R. Immunization of cotton rats with the human respiratory syncytial virus f glycoprotein produced using a baculovirus vector. *J. Infect. Dis.* **159**, 255–264 (1989).
324. Pastey, M. K. & Samal, S. K. Baculovirus expression of the fusion protein gene of bovine respiratory syncytial virus and utility of the recombinant protein in a diagnostic enzyme immunoassay. *J Clin Microbiol* **36**, 1105–1108 (1998).

325. Qin, H. *et al.* Construction of a series of vectors for high throughput cloning and expression screening of membrane proteins from *Mycobacterium tuberculosis*. *BMC Biotechnol.* **8**, 51 (2008).
326. Petersen, L. K., Sackett, C. K. & Narasimhan, B. Novel, high throughput method to study in vitro protein release from polymer nanospheres. *J. Comb. Chem.* **12**, 51–56 (2010).
327. McGill, J. L., Rusk, R. A., Guerra-Maupome, M., Briggs, R. E. & Sacco, R. E. Bovine Gamma Delta T Cells Contribute to Exacerbated IL-17 Production in Response to Co-Infection with Bovine RSV and *Mannheimia haemolytica*. *PLoS One* **11**, (2016).
328. Sacco, R. E. *et al.* Differential Expression of Cytokines in Response to Respiratory Syncytial Virus Infection of Calves with High or Low Circulating 25-Hydroxyvitamin D3. *PLoS One* **7**, e33074 (2012).
329. Viuff, B. *et al.* Replication and clearance of respiratory syncytial virus: apoptosis is an important pathway of virus clearance after experimental infection with bovine respiratory syncytial virus. *Am. J. Pathol.* **161**, 2195–2207 (2002).
330. Werling, D., Hope, J. C., Howard, C. J. & Jungi, T. W. Differential production of cytokines, reactive oxygen and nitrogen by bovine macrophages and dendritic cells stimulated with Toll-like receptor agonists. *Immunology* **111**, 41–52 (2004).
331. Livak, K. J. & Schmittgen, T. D. Analysis of Relative Gene Expression Data Using Real-Time Quantitative PCR and the $2^{-\Delta\Delta CT}$ Method. *Methods* **25**, 402–408 (2001).
332. Ross, K. A. *et al.* Structural and antigenic stability of H5N1 hemagglutinin trimer upon release from polyanhydride nanoparticles. *J. Biomed. Mater. Res. - Part A* **102**, 4161–4168 (2014).
333. Torres, M. P., Determan, A. S., Anderson, G. L., Mallapragada, S. K. & Narasimhan, B. Amphiphilic polyanhydrides for protein stabilization and release. *Biomaterials* **28**, 108–116 (2007).
334. Determan, A. S., Trewyn, B. G., Lin, V. S. Y., Nilsen-Hamilton, M. & Narasimhan, B. Encapsulation, stabilization, and release of BSA-FITC from polyanhydride microspheres. *J. Control. Release* **100**, 97–109 (2004).
335. Determan, A. S., Wilson, J. H., Kipper, M. J., Wannemuehler, M. J. & Narasimhan, B. Protein stability in the presence of polymer degradation products: Consequences for controlled release formulations. *Biomaterials* **27**, 3312–3320 (2006).
336. Wegzyn, C. *et al.* Safety and Effectiveness of Palivizumab in Children at High Risk of Serious Disease Due to Respiratory Syncytial Virus Infection: A Systematic Review. *Infect. Dis. Ther.* **3**, 133–158 (2014).

337. McIntosh, K., McQuillin, J. & Gardner, P. S. Cell-Free and Cell-Bound Antibody in Nasal Secretions from Infants with Respiratory Syncytial Virus Infection. *Infect. Immun.* **23**, 276–281 (1979).
338. Zhang, B. *et al.* Protection of calves by a prefusion-stabilized bovine RSV F vaccine. *npj Vaccines* **2**, (2017).
339. Ngwuta, J. O. *et al.* Prefusion F-specific antibodies determine the magnitude of RSV neutralizing activity in human sera. *Sci. Transl. Med.* **7**, 309ra162-309ra162 (2015).
340. McLellan, J. S. *et al.* Structure-Based Design of a Fusion Glycoprotein Vaccine for Respiratory Syncytial Virus. *Science (80-.)*. **342**, 592–598 (2013).
341. McLellan, J. S., Ray, W. C. & Peeples, M. E. Structure and Function of Respiratory Syncytial Virus Surface Glycoproteins. in *Current topics in microbiology and immunology* **372**, 83–104 (2013).
342. Culora, G. a, Ramsay, a D. & Theaker, J. M. Aluminium and injection site reactions. *J. Clin. Pathol.* **49**, 844–847 (1996).
343. Pati, R., Shevtsov, M. & Sonawane, A. Nanoparticle Vaccines Against Infectious Diseases. *Front. Immunol.* **9**, 2224 (2018).
344. Zhang, B. *et al.* Shape dependent cytotoxicity of PLGA-PEG nanoparticles on human cells. *Sci. Rep.* **7**, 7315 (2017).
345. Jiang, H., Wang, Q. & Sun, X. Lymph node targeting strategies to improve vaccination efficacy. *J. Control. Release* **267**, 47–56 (2017).
346. Guarecuco, R. *et al.* Immunogenicity of pulsatile-release PLGA microspheres for single-injection vaccination. *Vaccine* **36**, 3161–3168 (2018).
347. Gutjahr, A. *et al.* Biodegradable Polymeric Nanoparticles-Based Vaccine Adjuvants for Lymph Nodes Targeting. *Vaccines* **4**, 34 (2016).
348. Giteau, A., Venier-Julienne, M. C., Aubert-Pouëssel, A. & Benoit, J. P. How to achieve sustained and complete protein release from PLGA-based microparticles? *Int. J. Pharm.* **350**, 14–26 (2008).
349. Phanse, Y. *et al.* Cellular internalization mechanisms of polyanhydride particles: Implications for rational design of drug delivery vehicles. *J. Biomed. Nanotechnol.* **12**, 1544–1552 (2016).
350. Ross, K. *et al.* Single dose combination nanovaccine provides protection against influenza A virus in young and aged mice. *Biomater. Sci.* **7**, 809–821 (2019).
351. Ron, E., Mathiowitz, E., Mathiowitz, G., Domb, A. & Langer, R. NMR characterization of erodible copolymers. *Macromolecules* **24**, 2278–2282 (1991).
352. Senapati, S. *et al.* Pentablock Copolymer Micelle Nanoadjuvants Enhance Cytosolic Delivery of Antigen and Improve Vaccine Efficacy while Inducing Low Inflammation. *ACS Biomater. Sci. Eng.* **5**, 1332–1342 (2019).

353. Mathiowitz, E., Ron, E., Mathiowitz, G., Amato, C. & Langer, R. Morphological Characterization of Bioerodible Polymers. 1. Crystallinity of Polyanhydride Copolymers. *Macromolecules* **23**, 3212–3218 (1990).
354. Shen, E., Kipper, M. J., Dziadul, B., Lim, M.-K. & Narasimhan, B. Mechanistic relationships between polymer microstructure and drug release kinetics in bioerodible polyanhydrides. *J. Control. Release* **82**, 115–125 (2002).
355. Lueth, P. *et al.* Nanotherapeutic provides dose sparing and improved antimicrobial activity against *Brucella melitensis* infections. *J. Control. Release* **294**, 288–297 (2019).
356. Mckee, A. S. & Marrack, P. Old and new adjuvants. *Curr. Opin. Immunol.* **47**, 44–51 (2017).
357. Del Giudice, G., Rappuoli, R. & Didierlaurent, A. M. Correlates of adjuvanticity: A review on adjuvants in licensed vaccines. *Semin. Immunol.* **39**, 14–21 (2018).
358. Reddy Bonam, S., Partidos, C. D., Kumar, S., Halmuthur, M. & Muller, S. An Overview of Novel Adjuvants Designed for Improving Vaccine Efficacy. *Trends Pharmacol. Sci.* **38**, 771–793 (2017).
359. Petersen, L. K., Sackett, C. K. & Narasimhan, B. High-throughput analysis of protein stability in polyanhydride nanoparticles. *Acta Biomater.* **6**, 3873–3881 (2010).
360. Scheiblhofer, S., Laimer, J., Machado, Y., Weiss, R. & Thalhamer, J. Influence of protein fold stability on immunogenicity and its implications for vaccine design. *Expert Rev. Vaccines* **16**, 479–489 (2017).
361. Shen, E., Pizszczek, R., Dziadul, B. & Narasimhan, B. Microphase separation in bioerodible copolymers for drug delivery. *Biomaterials* **22**, 201–210 (2001).
362. Riedel, S. Plague: From Natural Disease to Bioterrorism. *Baylor Univ. Med. Cent. Proc.* **18**, 116–124 (2005).
363. Sun, W. & Singh, A. K. Plague vaccine: recent progress and prospects. *npj Vaccines* **4**, 1–9 (2019).
364. Taleb, S. A., Al Thani, A. A., Al Ansari, K. & Yassine, H. M. Human respiratory syncytial virus: pathogenesis, immune responses, and current vaccine approaches. *Eur. J. Clin. Microbiol. Infect. Dis.* **37**, 1817–1827 (2018).
365. Philipovskiy, A. V & Smiley, S. T. Vaccination with Live *Yersinia pestis* Primes CD4 and CD8 T Cells That Synergistically Protect against Lethal Pulmonary *Y. pestis* Infection. *Infect. Immun.* **75**, 878–885 (2007).
366. Parent, M. A. *et al.* Cell-mediated protection against pulmonary *Yersinia pestis* infection. *Infect. Immun.* **73**, 7304–7310 (2005).
367. Lin, J. S. *et al.* TNF α and IFN γ contribute to F1/LcrV-targeted immune defense in mouse models of fully virulent pneumonic plague. *Vaccine* **29**, 357–362 (2010).

368. Bashaw, J. *et al.* Development of In Vitro Correlate Assays of Immunity to Infection with *Yersinia pestis*. *Clin. Vaccine Immunol.* **14**, 605–616 (2007).
369. Smiley, S. T. Current challenges in the development of vaccines for pneumonic plague. *Expert Rev Vaccines* **7**, 209–221 (2008).